Rejuvenation of the Aged Stem Cell Niche: Signal Transduction and Reversing the Decline of Adult Hippocampal Neurogenesis and Myogenesis

By

Hanadie Yousef

A dissertation submitted in partial satisfaction of the

requirements for the degree of

Doctor of Philosophy

in

Molecular and Cell Biology

in the

Graduate Division

of the

University of California, Berkeley

Committee in charge:

Professor David Schaffer, Co-Chair
Professor John Ngai, Co-Chair
Professor Michael Rape
Professor Irina Conboy

Fall 2013

Abstract

Rejuvenation of the Aged Stem Cell Niche: Signal Transduction and Reversing the Decline of Adult Hippocampal Neurogenesis and Myogenesis

by

Hanadie Yousef

Doctor of Philosophy in Molecular and Cell Biology

University of California, Berkeley

Professor David Schaffer, Co-Chair

Professor John Ngai, Co-Chair

Although functional organ stem cells persist in the elderly, tissue damage invariably overwhelms tissue repair, ultimately leading to the failure of major organ systems. It has been demonstrated that the microenvironment, or niche in which adult stem cells reside critically influences stem cell function. The delicate balance between positive and negative signaling regulators controls the decision of adult stem cells to remain quiescent, self-renew or differentiate, a crucial balance for the maintenance of tissue homeostasis. In this dissertation, we provide evidence that the same key morphogenic signaling pathways become deregulated with age and contribute to the decline of both hippocampal neurogenesis and skeletal muscle regeneration with aging, leading to the decline in regenerative performance of both brain and muscle tissue stem cells. Furthermore, we demonstrate that the aged tissue niches can be rejuvenated to enhance native stem cell function in muscle and brain by youthful calibration of the intensity of these morphogenic signaling pathways. In particular, local attenuation of BMP signaling in the aged hippocampus, systemic and local attenuation of TGF-β signaling in both the aged hippocampus and aged skeletal muscle, and specific proteins secreted by human embryonic stem cells that act through MAPK and Notch signaling rejuvenate brain and muscle tissue precursor cell function by normalizing the signaling strength of the pathways that are chronically overexpressed or underexpressed with aging. Summarily, by better understanding the age-imposed decline in the regenerative capacity of stem cells, the debilitating lack of organ maintenance in the old, including decline in neurogenesis and skeletal muscle regeneration, can be ameliorated.

Dedication

I would like to dedicate my thesis dissertation first and foremost to my mother and father, Shukria Yousef and Anwar Yousef, for their love and unconditional support throughout my life and my pursuit of higher education and scientific knowledge. I would also like to dedicate my dissertation to my family who mean the world to me: first to my sister Bassema Yousef, and also to my sisters Lubna Zeidan, Rula Yousef, and Noura Yousef, and my brother, Tariq Yousef, for their respect, love, and support.

Table of Contents

List of Figures and Tables

Introduction

Hippocampal neurogenesis and muscle regeneration occur throughout life and are the products of stem cell differentiation. However, the ability of mammalian neural and muscle stem cells to survive and function properly declines with age. Interestingly, evidence suggests that the intrinsic capacity of some tissue stem cells, such as in muscle, for tissue maintenance and repair does not drastically decline with age. Rather, molecular changes in the stem cell microenvironments or niches contribute to or account for diminished stem cell regenerative potential in several tissue types, ultimately leading to tissue aging. Such changes in stem cell microenvironments that negatively regulate stem cell function have been observed in aged skeletal muscle, brain, skin, blood, and bone (Conboy & Rando 2012). In this dissertation, we are interested in understanding how the microenvironments of both brain and muscle tissue change with age and result in the decline of tissue stem cell function.

An adult tissue stem cell has the ability to self-renew or differentiate, and it is the biochemical cues in the microenvironment, or stem cell niche, that influences this decision. For example, a hippocampal adult neural stem cell has the ability to self-renew, or differentiate into a neuron, astrocyte, or oligodendrocyte (Ming & Song 2005). What regulates this decision are the various biochemical cues in the neural stem cell niche, which include juxtacrine or paracrine signaling with other cell types, including astrocytes, microglia, endothelial cells, and mature neurons, morphogenic signaling through these cell-cell interactions which include through Notch, Wnt, transforming growth factor β (TGF-β), fibroblast growth factor (FGF), and Sonic hedgehog (Shh) signaling pathways, endocrine factors and chemokines that influence the local environment, small molecules such as neurotransmitters, and biophysical cues from the extracellular matrix, such as stiffness cues and the presence of various proteoglycans including heparin sulfate (Ming & Song 2005; Schwarz et al. 2012; Basak & Taylor 2009). In this dissertation, we focus on the extrinsic, morphogenic signal transduction pathways that change with age in the neural and muscle stem cell niches and contribute to decline in tissue stem cell function and regeneration.

Considering that the same morphogenic signal transduction pathways – including Notch, Wnt, TGF-β, FGF, Shh, and others – regulate adult stem cell behavior in different tissues (Conboy & Rando 2012), it is possible that age-related changes in these pathways that lead to diminished stem cell regeneration are also conserved among multiple organ systems. Furthermore, complex interplays between systemic and local changes in specific signaling factors with age have been shown to inhibit stem cell mediated tissue regeneration (Loffredo et al. 2013; Villeda et al. 2011; Vukovic et al. 2012; Carlson, Conboy, et al. 2009; Paliwal et al. 2012; Ruckh et al. 2012), and these interactions may also be conserved across tissues. In this dissertation, we assess age-induced changes in extrinsic signaling in both hippocampal neural and muscle stem cell microenvironments that lead to diminished tissue stem cell function and organogenesis. We furthermore assess methods of reversing age-induced signaling changes and thus methods to rejuvenate tissue regeneration in the aged.

Neurogenesis occurs throughout our lifetime within the central nervous system (CNS), in the subgranular zone (SGZ) of the dentate gyrus of the hippocampus and the subventricular zone (SVZ) of the lateral ventricles, via differentiation of adult neural stem cells (NSCs) into excitatory granule neurons and inhibitory olfactory bulb interneurons, respectively (Ming & Song 2005). Hippocampal neurogenesis is believed to aid learning and new memory formation,

while SVZ neurogenesis plays a role in maintaining sensory functions. Hippocampal neurogenesis is a result of Type 1 NSCs differentiating into granule neurons in the dentate gyrus through successive stages which are marked by specific protein marker expression (Figure 1), and is regulated by a variety of complex stimuli. Positive regulators of neurogenesis, which are known to either increase proliferating neural precursor cells or to enhance survival of immature neurons include enriched environment, exercise, stroke, epilepsy, and diet (Ming & Song 2005; Gould et al. 2000). Negative regulators of neurogenesis, known to inhibit proliferation or neuronal survival include stress, depression, neurodegeneration, and aging. In this dissertation, we are interested in understanding the mechanistic causes of the decline in hippocampal neurogenesis with aging, as it may have impacts for the effects of aging on human cognitive function.

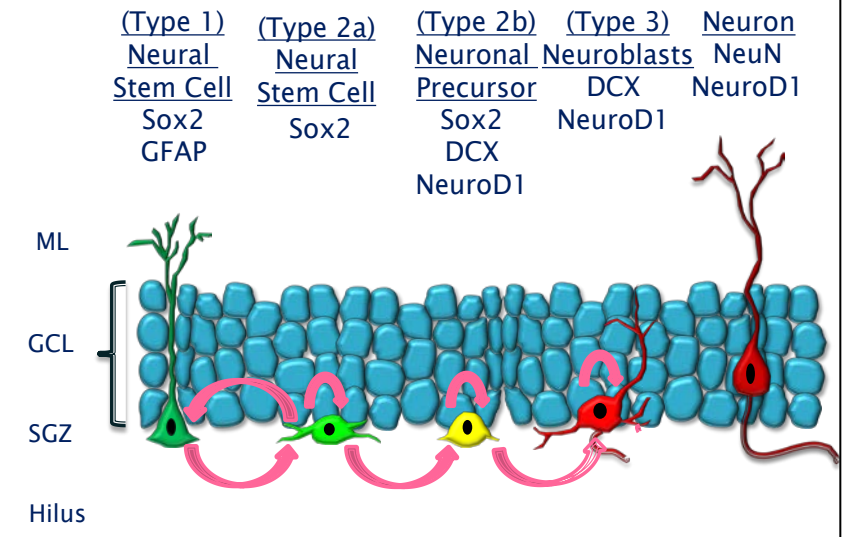

Figure 1. Stages of Hippocampal Neurogenesis.

Likewise, skeletal muscle slowly degenerates with old age, as illustrated by a loss of skeletal muscle mass and strength, a process known as sarcopenia (Le Grand & Rudnicki 2007). Skeletal muscle regeneration and repair also occur throughout our lifetimes, in response to injury and exercise (Kuang et al. 2008). The ability of muscle stem cells (satellite cells) to induce myogenesis also declines with age, leading to increased fibrosis and scar tissue formation in place of regenerated muscle after injury (Conboy & Rando 2005) (Figure 2a). Understanding the causes of muscle degeneration with age may allow us to develop methods of reversing the effects of aging on muscle repair. Furthermore, if we could find similar mechanisms underlying the failure of organ stem cell function with age, this could result in the development of therapies that tackle the aging of multiple organs, and thus aging on an organismal level.

The declines in hippocampal neurogenesis and muscle regeneration are believed to be a result of both a reduction in the number of organ stem cells and in the ability of the remaining stem cells to function properly with age. In particular within the SGZ, type 1 and 2 NSCs and neural progenitor cells (NPCs) significantly decrease in number with increasing age (Maslov et al. 2004; Olariu et al. 2007; Kuhn et al. 1996; Walter et al. 2011), as demonstrated by the 50-70% decline in Sox2+ and Nestin+ cells. Furthermore, there is a significant decrease in the ability of the remaining NPCs to undergo neurogenesis, as demonstrated by the ~90% loss in proliferating BrdU+ and doublecortin (DCX)+ cells in neurogenic regions of aged mice and rats. Satellite cells similarly decrease in number with increasing age (Shefer et al. 2006), as shown by quantifying the number of Pax7+ and PCNA+ cells in freshly isolated young and old myofibers. In addition, the remaining old satellite cells fail to become activated upon injury to enter the cell cycle, and subsequently fail to proliferate as progenitor cells (myoblasts) in order to populate the

injured tissue. Instead, the myoblasts that do manage to proliferate will prematurely fuse into myofibers, leaving the remaining extracellular space in the injury site to be populated by fibroblasts and form scar tissue (Conboy & Rando 2005) (Figure 2b).

Although the phenomena of reduced stem cell numbers and activity with aging has been firmly established, the molecular mechanisms that underlie the loss of organ stem cell numbers and function with age, particularly in brain, are only beginning to be elucidated. In particular, both an elevation in the systemic levels of chemokines and a decrease in hippocampal Wnt signaling with age have been correlated with or demonstrated to hinder hippocampal neurogenesis (Vukovic et al. 2012; Okamoto et al. 2011; Miranda et al. 2012; Seib et al. 2013; Villeda et al. 2011).

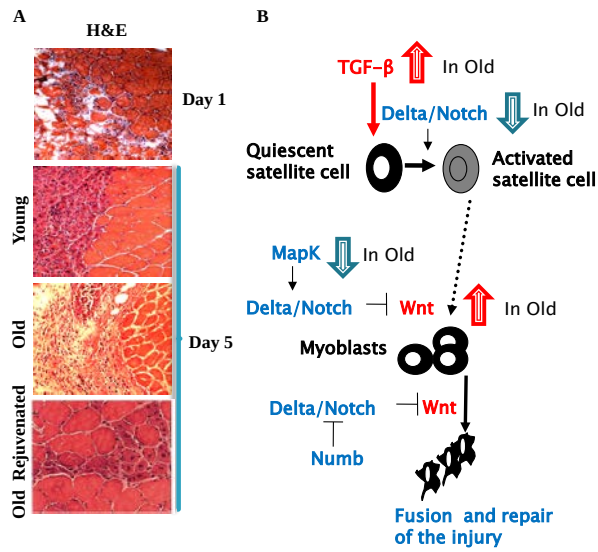

Figure 2. Stages of Young and Old Skeletal Muscle Regeneration. (A) On Day 1 of muscle injury in a mouse model (either via cardiotoxin injection or excessive exercise), in both young (2-4 month) and old (18-24 months) mice there is tissue damage as shown by extracellular space between myofibres. Five days post injury, young skeletal muscle is fully regenerated as shown by new myofibres with centrally located nuclei, while old muscle instead displays fibrosis. Old skeletal muscle, however, can be rejuvenated by modulated various signal transduction pathways known to be deregulated with age. (B) Stages of Myogenesis and the various morphogenic signaling pathways that regulate differentiation and change in intensities with age.

Similarly in muscle, several morphogenic signaling pathways are known to be deregulated with age in the muscle stem cell niche. These include Notch and MAPK signaling, which decreases with age, and Wnt and TGF-β, which increase with age in the muscle stem cell niche and contribute to decline in skeletal muscle regeneration with aging (Conboy et al. 2003; Conboy et al. 2005; Brack et al. 2007; Carlson & Conboy 2007; Carlson et al. 2008; Carlson, Conboy, et al. 2009; Carlson, Suetta, et al. 2009) (Figure 2b). Old skeletal muscle, furthermore, can be rejuvenated through multiple mechanisms, including modulating the signaling intensities of these pathways to mimic the young microenvironment, administering human embryonic stem cell (hESC)-secreted proteins, or through heterochronic parabiosis, the process of linking the blood stream of a young and old animal (Conboy & Rando 2012; Conboy et al. 2011; Yousef et al. 2013). While multiple methods of rejuvenating the aged mouse skeletal muscle regeneration have been established, none of these methods have translated into human therapies, nor has conserved aging between muscle and other tissues been addressed.

In Chapter 1 of this dissertation, we assess the role of TGF-β signaling, in particular the Bone Morphogenic Protein (BMP) branch of signaling, in the decline of hippocampal neurogenesis with aging. In Chapter 2, we determine the conserved role of TGF-β signal deregulation in decline of both hippocampal neurogenesis and skeletal muscle regeneration.

Finally, in Chapter 3, we determine the potent and rejuvenating effects of human embryonic stem cell (hESC)-secreted proteins on enhancement of mouse and human myogenesis, as well as it's proliferative and neuroprotective effects on neuronal precursors and cell types, identifying conserved effects on muscle and brain tissue types. Summarily, the goal of this dissertation is to elucidate conserved, extrinsic morphogenic signaling mechanisms that are deregulated in brain and muscle stem cell niches with aging. In each Chapter, we take additional steps by using our knowledge of signal deregulation to provide multiple methods to rejuvenate aged neural and muscle microenvironments in order to enhance native stem and progenitor cell function.

TGF-β1 is a pleiotropic cytokine that becomes elevated with age both in the circulation and locally in several tissues, including the muscle and brain (Carlson, Conboy, et al. 2009; Doyle et al. 2010). Such changes in the intensity of TGF- β1/pSmad2,3 signaling – with aging, pathology, or experimental induction – have been shown to perturb maintenance and homeostasis of such diverse tissues as muscle, bone and cartilage, the subventricular and subgranular zones of the brain, vasculature, the hematopoietic / immune system, and skin (Allen & Boxhorn 1989; Buckwalter et al. 2006; Carlson, Suetta, et al. 2009; Han et al. 2012; Bohatschek et al. 2004; Rico et al. 2010; Sanjabi et al. 2009; Lan et al. 2013; Pineda et al. 2013). In the Conboy lab in particular, TGF-β/pSmad2,3 signaling pathway has been implicated in the decline of satellite cell function and subsequent skeletal muscle regeneration with age (Carlson et al. 2008). Due to its inhibitory effect on multiple tissues throughout the body, we decided to explore the conserved and endogenous role of TGF-β signaling in decline of both skeletal muscle regeneration and hippocampal neurogenesis with age, with an assessment of its context-dependent, pleiotropic effects.

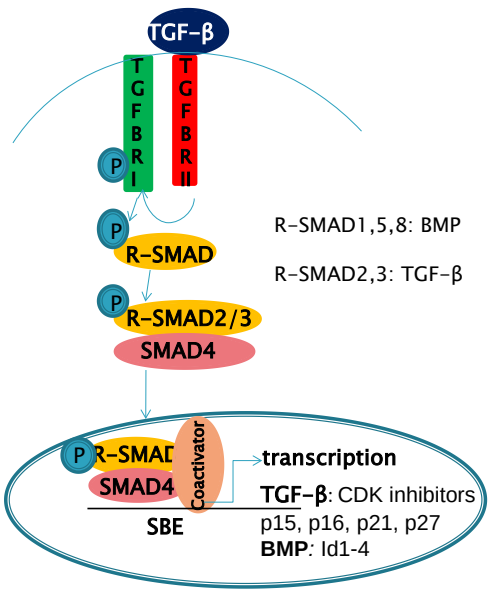

Figure 3. Canonical TGF-β Signal Transduction.

TGF-β ligands bind type II receptors, which then phosphorylate and activate type I serine/threonine kinase receptors. The type I receptors in turn phosphorylate and activate R-Smads(1,2,3,5,8) which then bind with Co-Smad4 and translocate to the nucleus, where they bind coactivators or corepressors to activate or inhibit gene expression (Figure 3). TGF-βs, Activins, Nodal, and some Growth and Differentiation Factors (GDFs) signal through R-Smads 2 and 3, while BMPs and most GDFs signal through R-Smads 1,5, and 8 (Massagué 2012; Oshimori & Fuchs 2012). Of the 100s of known genes regulated by TGF-β signaling, of particular interest in our assessment of regulation of stem cell activity are the transcriptional regulation of various CDK inhibitors including p21 by R-Smad2,3 signaling, and transcriptional regulation of inhibition of differentiation genes (Id1-4) by the R-Smad1,5,8 signaling branch.

Recent work has indicated that the capacity for muscle regeneration decreases with age due to increased TGF-β1 expression, among several other pathways deregulated in the satellite cell microniche (Figure 2B), (Conboy & Rando 2012; Carlson et al. 2008). Normally, TGF-β1

inhibits the proliferation of satellite cells by inducing expression of CDK inhibitors (Allen & Boxhorn 1989). Aged satellite cells overexpress pSmad3, one of the transcription factors activated by TGF-β ligand binding to its receptor, leading to overexpression of CDK inhibitors p15, p16, p21 and p27, and arrest of proliferation and differentiation during skeletal muscle regeneration (Carlson et al. 2008).

TGF-β may similarly regulate the cell fate of adult neural stem cells. TGF-β1 inhibits proliferation of NSCs in the SGZ (Buckwalter et al. 2006; Wachs et al. 2006). TGF-β1 mRNA is highly expressed in the murine hippocampus (Lein et al. 2007) and in the aged brain (Doyle et al. 2010). Furthermore, adult neural stem and progenitor cells express the receptor types I and II, necessary for TGF-β1 signaling (Wachs et al. 2006). In addition, TGF-β1 inhibits proliferation of NSCs in culture, arresting them in the G0/1 phase of the cell cycle. Moreover, TGF-β1 overexpression from a GFAP promoter in transgenic mice results in a dramatic decrease in hippocampal neurogenesis via inhibition of neural progenitor cell proliferation (Buckwalter et al. 2006). Additionally, an increase in TGF-β1 secretion by ECs in the aged SVZ or following irradiation inhibits proliferation and induces apoptosis of neural progenitor cells (Pineda et al. 2013). Lastly, excessive TGF-β1 signaling is associated with multiple neurodegenerative diseases, including Alzheimer's and Huntington's diseases (Apelt & Schliebs 2001; Zetterberg et al. 2004; Kandasamy et al. 2011).

TGF-β's role in aging of several tissues and pathologies, including muscle, led us to explore its role in more depth in skeletal muscle regeneration and importantly, for the first time in hippocampal neurogenesis and to establish a conserved and systemic role for pathological TGF-β signaling in decline of both neural and muscle stem cell homeostasis with aging. Based on the similar role of TGF-β in skeletal muscle regeneration and hippocampal neurogenesis, we hypothesized that this same pathway may be deregulated in the aging hippocampus, thereby resulting in a decline in neurogenesis. We predicted that TGF-β1 is upregulated in the dentate gyrus of the hippocampus leading to inhibition of neurogenesis. Additionally, just like the microenvironment or niche of satellite cells upregulates TGF-β ligand expression with age, resulting in an increase of Smad3 phosphorylation and signaling in satellite cells, we hypothesized that the neural stem cell niche in the dentate gyrus of the hippocampus contributes to decline of both the number of neural stem cells and their ability to differentiate into functional granular neurons with age by similar deregulation of TGF-β1/pSmad3 signaling.

While evidence would suggest that increased TGF-β/pSmad3 may inhibit old neurogenesis similarly to myogenesis inhibition via inhibiting stem cell proliferation, based on the pleiotropic functions of TGF-β signaling which vary depending on the cellular and microenvironmental context (Massagué 2012), we hypothesized that increased TGF-β signaling in the aged hippocampus and skeletal muscle could modulate cellular responses other than proliferation. In support of this notion, TGF-β signaling is upregulated upon CNS damage and in a variety of neurodegenerative diseases (Bohatschek et al. 2004; Apelt & Schliebs 2001; Zetterberg et al. 2004; Kandasamy et al. 2011). Pathologies of CNS damage and neurodegeneration include excessive neuroinflammation (Glass et al. 2010). Additionally, inflammation increases generally in brain and muscle with age (Higuchi et al. 1991; Bohatschek et al. 2004). Finally, TGF-β can be pro-inflammatory depending on the cellular and microenvironmental context (Han et al. 2012; Sanjabi et al. 2009). Based on this information, we decided to assess the effects of TGF-β signaling on inflammation in the aged neural and muscle stem cell niches, in addition to its role on progenitor cell proliferation. Chapter 2 of this

dissertation details the results of our studies on the conserved role of TGF-β signaling in inhibiting proliferation and enhancing inflammation in aged brain and muscle stem cell niches.

Other TGF-β ligands may also play a role in decreased tissue stem cell function with age, namely BMPs. BMPs signal through R-Smads 1,5,8, and induce expression of Id1-4, bHLH repressors that are necessary for progression of cells through the G1 phase of the cell cycle, for inhibiting differentiation inducing factors, and for maintaining motility (Nakashima et al. 2001). BMP signaling results in a variety of biological functions in various organ systems and during development, including in the central nervous system (CNS).

While BMP signaling has been extensively studied in the maintenance and differentiation of embryonic pluripotent and neural stem cells (Oshimori & Fuchs 2012; Bond et al. 2012), its roles within the adult CNS are only beginning to be elucidated. BMP inhibits neurogenesis and promotes NSC glial differentiation in the adult SVZ (Lim et al. 2000), resulting in a depletion of the stem cell pool (Porlan et al. 2013). BMP mRNA is highly expressed in the murine hippocampus (Lein et al. 2007). Importantly for the SGZ, it was demonstrated that BMP signaling through BMPRIA inhibits proliferation and promotes the maintenance of NSCs in an undifferentiated and quiescent state (Mira et al. 2010). Additionally, inhibiting BMP signaling through transgenic overexpression of the antagonist Noggin induced proliferation of hippocampal stem cells and enhanced the self-renewal of these cells, thereby expanded the pool (Bonaguidi et al. 2008). Furthermore, BMP4 inhibition has been implicated in exercise-induced hippocampal neurogenesis and hippocampal dependent learning (Gobeske et al. 2009; Fan et al. 2003). Finally, various BMPs increase in human Alzheimer's disease brains and its mouse models, which is also correlated with a decrease in neurogenesis (Crews et al. 2010; Li et al. 2008). Interestingly, BMP involvement in the decline of adult stem cell function with age has not been investigated for any tissue in mammals, including brain. In Chapter 1 of this dissertation, we assess the role of BMP signaling in decline of hippocampal neurogenesis with aging.

While methods of enhancing neurogenesis and myogenesis have been developed in aged mouse models by reversing age-induced changes in key morphogenic signaling pathways including TGF-β, Notch and MAPK, these niche rejuvenation techniques are not translational for human therapies. This is because achieving precisely "young" levels of TGF-β, Wnt, Notch and MAPK signaling, among other signaling pathways, is critically important, since these pathways generally regulate cell growth and differentiation and control p53, p21 and other CDK inhibitors, as well as cMyc and other pro-oncogenes (Rizzo et al. 2008; Lea et al. 2007; Meloche & Pouyssegur 2007; Cooper 2006). Thus, deviation from the physiologic levels of signaling strength in these pathways

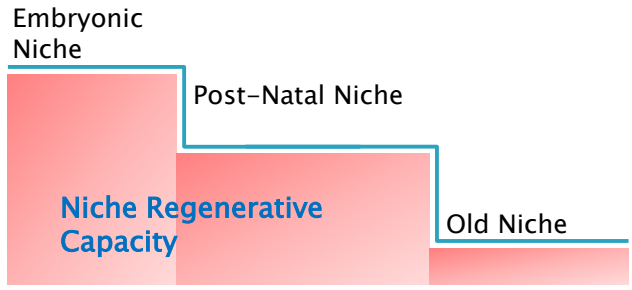

Figure 4. hESCs have an unlimited regenerative capacity and ability to form every tissue of the body. As we go through postnatal development, the regenerative capacity of tissue stem cells becomes more limited, even inhibitory by old age. In this dissertation, we ask the question: Will the embryonic niche be supportive of old post natal tissue repair? Will it rejuvenate the old niche, in turn, by modulating multiple signaling pathways known to be deregulated with age in the adult stem cell niche?

is very likely to cause undesired changes in multiple tissues, including but not limited to oncogenic transformation. In practical terms, not enough is known about the identity and the expression profile of natural agonists and antagonists that modulate the signaling strength of TGF-β, Wnt, Notch, MAPK and other age-specific regulators of stem cells in embryonic, versus adult and old mammals. Hence, approaches for boosting tissue repair are not based on a clear understanding of the physiologic regulation, where robust formation of embryonic tissues is followed by less efficient, but still good, tissue regeneration in adults, and deteriorates into poor tissue repair in the old due to an increasingly limited niche regenerative capacity (Figure 4). A better characterization of the transition from inductive to inhibitory modes of stem cell regulation during the progression from embryo to young, adult and aged mammal might help to uncover the key physiological molecules that modulate the age-specific rate of regeneration. Ultimately, this would lead to novel clinical applications for safely enhancing tissue regeneration in the old without the side effects associated with non-physiological disruption in signal transduction.

As an initial step in this direction, in Chapter 3 we assess the ability of hESCs to combat the inhibition of aged adult tissue regeneration via production of soluble secreted proteins and show that such a youthful barrier to aging is lost when hESCs differentiate.

hESCs have an infinite capacity to self-renew and to differentiate into every cell type in the body (Levi & Morrison 2008; Conboy & Rando 2012; He et al. 2009). The tremendous potential of hESCs for organogenesis has created great interest in understanding and deliberately controlling their cell fate determination, and significant progress was made in recent years in directed differentiation (Wobus & Boheler 2005). At the same time, much less is known about the properties of self-renewing, undifferentiated hESCs that do not directly relate to developmental lineage progression, but that might indirectly influence the regenerative capacity of post-natal tissues through secretion of proregenerative proteins in order to maintain the embryonic niche. In this respect, previous research in the Conboy lab uncovered that in co-cultures with mouse muscle precursor cells, hESCs dramatically enhanced myogenesis in vitro. Moreover, hESCs rejuvenated the repair of injured muscle in old mice when injected intramuscularly into immunocompromised animals, even though the hESCs themselves did not contribute to new muscle tissue (Carlson & Conboy 2007). The same work hinted that the positive regulation of mouse myogenesis by hESCs might be due to soluble factors (be they protein, lipid, sugar or other macromolecules), and that human mesenchymal stem cells lack this pro-regenerative activity (Carlson & Conboy 2007). The data and discussion in Chapter 3 of this dissertation introduces evidence that self-renewing hESCs, but not differentiated hESCs (hESCs vs. dhESCs), secrete proteins that counteract the oppressive biochemical milieu of aged muscle, aged brain and old circulation.

Furthermore, we show that this embryonic proregenerative activity requires intact MAPK, Notch, and BMP signaling, and importantly, that it is conserved in mouse and human myogenesis, which would suggest promising translational therapies for enhanced tissue regeneration in the aged. Finally, we uncover the shared characteristics of the proregenerative secreted proteins, and identify some of the key proteins in the hESC-secreted mixture.

In conclusion, the role of TGF-β/pSmad2,3 signaling in decline of muscle precursor cell function with age has been elucidated, but further insights into the multi-functional role of this pleiotropic signaling pathway in the muscle stem cell niche, as well as if it is deregulated similarly in hippocampal neural stem cell niche with age was assessed in this dissertation. In regards to hippocampal neurogenesis, the other canonical branch of TGF-β family growth factor

signaling, BMP/pSmad1,5,8, and its deregulation in the neural stem cell niche during aging was also assessed. Thirdly, with the goal of identifying human proteins that may enhance tissue stem cell-mediated regeneration, this dissertation details our discovery of specific hESC-secreted proteins that enhance tissue regeneration by mimicking the embryonic stem cell niche and modulating multiple biochemical signaling pathways known to be deregulated with age.

The central goal of my thesis is to investigate the conserved molecular mechanisms underlying stem cell dysfunction in brain and muscle microenvironments with age. By identifying and understanding the conserved, extrinsic molecular mechanisms that lead to diminished tissue stem cell function with aging, we can ultimately develop therapies to rejuvenate aged microenvironments to enhance native stem cell function, tackling multiple organ systems through conserved deregulation and rejuvenation mechanisms.

References – Introduction

Allen, R.E. & Boxhorn, L.K., 1989. Regulation of skeletal muscle satellite cell proliferation and differentiation by transforming growth factor-beta, insulin-like growth factor I, and fibroblast growth factor. *J Cell Physiol*, 138(2), pp.311–315.

Apelt, J. & Schliebs, R., 2001. Beta-amyloid-induced glial expression of both pro- and anti-inflammatory cytokines in cerebral cortex of aged transgenic Tg2576 mice with Alzheimer plaque pathology. *Brain research*, 894(1), pp.21–30. Available at: http://www.ncbi.nlm.nih.gov/pubmed/11245811.

Basak, O. & Taylor, V., 2009. Stem cells of the adult mammalian brain and their niche. *Cellular and molecular life sciences : CMLS*, 66(6), pp.1057–72. Available at: http://www.ncbi.nlm.nih.gov/pubmed/19011753 [Accessed December 1, 2013].

Bohatschek, M. et al., 2004. Microglial major histocompatibility complex glycoprotein-1 in the axotomized facial motor nucleus: regulation and role of tumor necrosis factor receptors 1 and 2. *J Comp Neurol*, 470(4), pp.382–399. Available at: http://www.ncbi.nlm.nih.gov/pubmed/14961564.

Bonaguidi, M. a et al., 2008. Noggin expands neural stem cells in the adult hippocampus. *The Journal of neuroscience : the official journal of the Society for Neuroscience*, 28(37), pp.9194–204. Available at: http://www.pubmedcentral.nih.gov/articlerender.fcgi?artid=3651371&tool=pmcentrez&rendertype=abstract [Accessed October 28, 2013].

Bond, A.M., Bhalala, O.G. & Kessler, J. a, 2012. The dynamic role of bone morphogenetic proteins in neural stem cell fate and maturation. *Developmental neurobiology*, 72(7), pp.1068–84. Available at: http://www.pubmedcentral.nih.gov/articlerender.fcgi?artid=3773925&tool=pmcentrez&rendertype=abstract [Accessed October 22, 2013].

Brack, A.S. et al., 2007. Increased Wnt signaling during aging alters muscle stem cell fate and increases fibrosis. *Science*, 317(5839), pp.807–810. Available at: http://www.ncbi.nlm.nih.gov/entrez/query.fcgi?cmd=Retrieve&db=PubMed&dopt=Citation&list_uids=17690295.

Buckwalter, M S et al., 2006. Chronically increased transforming growth factor-beta1 strongly inhibits hippocampal neurogenesis in aged mice. *Am J Pathol*, 169(1), pp.154–164. Available at: http://www.ncbi.nlm.nih.gov/pubmed/16816369.

Buckwalter, Marion S. et al., 2006. Chronically Increased Transforming Growth Factor-β1 Strongly Inhibits Hippocampal Neurogenesis in Aged Mice. *The American Journal of Pathology*, 169(1), pp.154–164. Available at: http://linkinghub.elsevier.com/retrieve/pii/S0002944010614393 [Accessed October 26, 2013].

Carlson, M.E., Suetta, C., et al., 2009. Molecular aging and rejuvenation of human muscle stem cells. *EMBO Mol Med*, 1(8-9), pp.381–391. Available at: http://www.ncbi.nlm.nih.gov/entrez/query.fcgi?cmd=Retrieve&db=PubMed&dopt=Citation&list_uids=20049743.

Carlson, M.E., Conboy, M.J., et al., 2009. Relative roles of TGF-beta1 and Wnt in the systemic regulation and aging of satellite cell responses. *Aging Cell*, 8(6), pp.676–689. Available at: http://www.ncbi.nlm.nih.gov/entrez/query.fcgi?cmd=Retrieve&db=PubMed&dopt=Citation&list_uids=19732043.

Carlson, M.E. & Conboy, I.M., 2007. Loss of stem cell regenerative capacity within aged niches. *Aging Cell*, 6(3), pp.371–382.

Carlson, M.E., Hsu, M. & Conboy, I.M., 2008. Imbalance between pSmad3 and Notch induces CDK inhibitors in old muscle stem cells. *Nature*, 454(7203), pp.528–532. Available at: http://www.ncbi.nlm.nih.gov/entrez/query.fcgi?cmd=Retrieve&db=PubMed&dopt=Citation&list_uids=18552838.

Conboy, I.M. et al., 2003. Notch-mediated restoration of regenerative potential to aged muscle. *Science*, 302(5650), pp.1575–1577.

Conboy, I.M. et al., 2005. Rejuvenation of aged progenitor cells by exposure to a young systemic environment. *Nature*, 433(7027), pp.760–764.

Conboy, I.M. & Rando, T.A., 2005. Aging, stem cells and tissue regeneration: lessons from muscle. *Cell Cycle*, 4(3), pp.407–410.

Conboy, I.M. & Rando, T.A., 2012. Heterochronic parabiosis for the study of the effects of aging on stem cells and their niche. *Cell Cycle*, 11(12), pp.2260–2267.

Conboy, I.M., Yousef, H. & Conboy, M.J., 2011. Embryonic anti-aging niche. *Aging*, 3(5), pp.555–63. Available at: http://www.pubmedcentral.nih.gov/articlerender.fcgi?artid=3156606&tool=pmcentrez&rendertype=abstract.

Cooper, K., 2006. Rb, whi it's not just for metazoans anymore. *Oncogene*, 25(38), pp.5228–5232. Available at: http://www.ncbi.nlm.nih.gov/entrez/query.fcgi?cmd=Retrieve&db=PubMed&dopt=Citation&list_uids=16936741.

Crews, L. et al., 2010. Increased BMP6 levels in the brains of Alzheimer's disease patients and APP transgenic mice are accompanied by impaired neurogenesis. *The Journal of neuroscience : the official journal of the Society for Neuroscience*, 30(37), pp.12252–62. Available at: http://www.pubmedcentral.nih.gov/articlerender.fcgi?artid=2978735&tool=pmcentrez&rendertype=abstract [Accessed October 29, 2013].

Doyle, K.P. et al., 2010. TGFβ signaling in the brain increases with aging and signals to astrocytes and innate immune cells in the weeks after stroke. *Journal of neuroinflammation*, 7(1), p.62. Available at: http://www.pubmedcentral.nih.gov/articlerender.fcgi?artid=2958905&tool=pmcentrez&rendertype=abstract [Accessed October 25, 2013].

Fan, X.-T. et al., 2003. Effect of antisense oligonucleotide of noggin on spatial learning and memory of rats. *Acta pharmacologica Sinica*, 24(5), pp.394–7. Available at: http://www.ncbi.nlm.nih.gov/pubmed/12740172.

Glass, C.K. et al., 2010. Mechanisms underlying inflammation in neurodegeneration. *Cell*, 140(6), pp.918–34. Available at: http://www.pubmedcentral.nih.gov/articlerender.fcgi?artid=2873093&tool=pmcentrez&rendertype=abstract [Accessed November 7, 2013].

Gobeske, K.T. et al., 2009. BMP signaling mediates effects of exercise on hippocampal neurogenesis and cognition in mice. *PloS one*, 4(10), p.e7506. Available at: http://www.pubmedcentral.nih.gov/articlerender.fcgi?artid=2759555&tool=pmcentrez&rendertype=abstract [Accessed October 24, 2013].

Gould, E. et al., 2000. Regulation of hippocampal neurogenesis in adulthood. *Biological psychiatry*, 48(8), pp.715–720. Available at: http://linkinghub.elsevier.com/retrieve/pii/S0006322300010210?showall=true.

Le Grand, F. & Rudnicki, M.A., 2007. Skeletal muscle satellite cells and adult myogenesis. *Current Opinion in Cell Biology*, 19(6), pp.628–633. Available at: http://www.sciencedirect.com/science/article/pii/S0955067407001342.

Han, G. et al., 2012. The pro-inflammatory role of TGFbeta1: a paradox? *Int J Biol Sci*, 8(2), pp.228–235. Available at: http://www.ncbi.nlm.nih.gov/pubmed/22253566.

He, S., Nakada, D. & Morrison, S.J., 2009. Mechanisms of stem cell self-renewal. *Annu Rev Cell Dev Biol*, 25, pp.377–406. Available at: http://www.ncbi.nlm.nih.gov/entrez/query.fcgi?cmd=Retrieve&db=PubMed&dopt=Citation&list_uids=19575646.

Higuchi, I. et al., 1991. Vacuolar myositis with expression of both MHC class I and class II antigens on skeletal muscle fibers. *J Neurol Sci*, 106(1), pp.60–66. Available at: http://www.ncbi.nlm.nih.gov/pubmed/1779240.

Kandasamy, M. et al., 2011. Transforming Growth Factor-Beta Signaling in the Neural Stem Cell Niche : A Therapeutic Target for Huntington ' s Disease. , 2011.

Kuang, S., Gillespie, M.A. & Rudnicki, M.A., 2008. Niche regulation of muscle satellite cell self-renewal and differentiation. *Cell Stem Cell*, 2(1), pp.22–31. Available at: http://www.ncbi.nlm.nih.gov/entrez/query.fcgi?cmd=Retrieve&db=PubMed&dopt=Citation&list_uids=18371418.

Kuhn, H.G., Dickinson-Anson, H. & Gage, F.H., 1996. Neurogenesis in the Dentate Gyrus of the Adult Decrease of Neuronal Progenitor Proliferation Rat : Age-Related. , 76(6), pp.2027–2033.

Lan, T.H., Huang, X.Q. & Tan, H.M., 2013. Vascular fibrosis in atherosclerosis. *Cardiovasc Pathol*, 22(5), pp.401–407. Available at: http://www.ncbi.nlm.nih.gov/pubmed/23375582.

Lea, I.A. et al., 2007. Genetic pathways and mutation profiles of human cancers: site- and exposure-specific patterns. *Carcinogenesis*, 28(9), pp.1851–1858. Available at: http://www.ncbi.nlm.nih.gov/entrez/query.fcgi?cmd=Retrieve&db=PubMed&dopt=Citation&list_uids=17693665.

Lein, E.S. et al., 2007. Genome-wide atlas of gene expression in the adult mouse brain. *Nature*, 445(7124), pp.168–176. Available at: http://dx.doi.org/10.1038/nature05453.

Levi, B.P. & Morrison, S.J., 2008. Stem cells use distinct self-renewal programs at different ages. *Cold Spring Harb Symp Quant Biol*, 73, pp.539–553. Available at: http://www.ncbi.nlm.nih.gov/entrez/query.fcgi?cmd=Retrieve&db=PubMed&dopt=Citation&list_uids=19150957.

Li, D. et al., 2008. Decreased hippocampal cell proliferation correlates with increased expression of BMP4 in the APPswe/PS1ΔE9 mouse model of Alzheimer's disease. *Hippocampus*, 18(7), pp.692–698. Available at: http://dx.doi.org/10.1002/hipo.20428.

Lim, D.A. et al., 2000. Noggin Antagonizes BMP Signaling to Create a Niche for Adult Neurogenesis. *Neuron*, 28(3), pp.713–726. Available at: http://linkinghub.elsevier.com/retrieve/pii/S0896627300001483.

Loffredo, F.S. et al., 2013. Growth differentiation factor 11 is a circulating factor that reverses age-related cardiac hypertrophy. *Cell*, 153(4), pp.828–839. Available at: http://www.ncbi.nlm.nih.gov/pubmed/23663781.

Maslov, A.Y. et al., 2004. Neural stem cell detection, characterization, and age-related changes in the subventricular zone of mice. *The Journal of neuroscience : the official journal of the Society for Neuroscience*, 24(7), pp.1726–33. Available at: http://www.ncbi.nlm.nih.gov/pubmed/14973255 [Accessed October 26, 2013].

Massagué, J., 2012. TGFβ signalling in context. *Nature reviews. Molecular cell biology*, 13(10), pp.616–30. Available at: http://www.ncbi.nlm.nih.gov/pubmed/22992590 [Accessed October 17, 2013].

Meloche, S. & Pouyssegur, J., 2007. The ERK1/2 mitogen-activated protein kinase pathway as a master regulator of the G1- to S-phase transition. *Oncogene*, 26(22), pp.3227–3239. Available at: http://www.ncbi.nlm.nih.gov/entrez/query.fcgi?cmd=Retrieve&db=PubMed&dopt=Citation&list_uids=17496918.

Ming, G. & Song, H., 2005. Adult neurogenesis in the mammalian central nervous system. *Annual review of neuroscience*, 28, pp.223–50. Available at: http://www.ncbi.nlm.nih.gov/pubmed/16022595 [Accessed October 17, 2013].

Mira, H. et al., 2010. Signaling through BMPR-IA regulates quiescence and long-term activity of neural stem cells in the adult hippocampus. *Cell stem cell*, 7(1), pp.78–89. Available at: http://www.ncbi.nlm.nih.gov/pubmed/20621052 [Accessed October 25, 2013].

Miranda, C.J. et al., 2012. Aging brain microenvironment decreases hippocampal neurogenesis through Wnt-mediated survivin signaling. *Aging cell*, 11(3), pp.542–52. Available at: http://www.pubmedcentral.nih.gov/articlerender.fcgi?artid=3350615&tool=pmcentrez&rendertype=abstract [Accessed October 26, 2013].

Nakashima, K. et al., 2001. BMP2-mediated alteration in the developmental pathway of fetal mouse brain cells from neurogenesis to astrocytogenesis. *Proceedings of the National Academy of Sciences of the United States of America*, 98(10), pp.5868–73. Available at: http://www.pubmedcentral.nih.gov/articlerender.fcgi?artid=33305&tool=pmcentrez&rendertype=abstract.

Okamoto, M. et al., 2011. Reduction in paracrine Wnt3 factors during aging causes impaired adult neurogenesis. *FASEB journal : official publication of the Federation of American*

Societies for Experimental Biology, 25(10), pp.3570–82. Available at: http://www.ncbi.nlm.nih.gov/pubmed/21746862 [Accessed October 26, 2013].

Olariu, A.N.A., Cleaver, K.M. & Cameron, H.A., 2007. Decreased Neurogenesis in Aged Rats Results from Loss of Granule Cell Cell Cycle. , 667(October 2006), pp.659–667.

Oshimori, N. & Fuchs, E., 2012. The harmonies played by TGF-β in stem cell biology. *Cell stem cell*, 11(6), pp.751–64. Available at: http://www.ncbi.nlm.nih.gov/pubmed/23217421 [Accessed October 26, 2013].

Paliwal, P. et al., 2012. Age dependent increase in the levels of osteopontin inhibits skeletal muscle regeneration. *Aging (Albany NY)*, 4(8), pp.553–566. Available at: http://www.ncbi.nlm.nih.gov/pubmed/22915705.

Pineda, J.R. et al., 2013. Vascular-derived TGF-β increases in the stem cell niche and perturbs neurogenesis during aging and following irradiation in the adult mouse brain. *EMBO molecular medicine*, 5(4), pp.548–62. Available at: http://www.pubmedcentral.nih.gov/articlerender.fcgi?artid=3628106&tool=pmcentrez&rendertype=abstract [Accessed November 10, 2013].

Porlan, E. et al., 2013. Transcriptional repression of Bmp2 by p21Waf1/Cip1 links quiescence to neural stem cell maintenance. *Nat Neurosci*, 16(11), pp.1567–1575. Available at: http://dx.doi.org/10.1038/nn.3545.

Rico, M.C. et al., 2010. The axis of thrombospondin-1, transforming growth factor beta and connective tissue growth factor: an emerging therapeutic target in rheumatoid arthritis. *Curr Vasc Pharmacol*, 8(3), pp.338–343. Available at: http://www.ncbi.nlm.nih.gov/pubmed/19485899.

Rizzo, P. et al., 2008. Rational targeting of Notch signaling in cancer. *Oncogene*, 27(38), pp.5124–5131. Available at: http://www.ncbi.nlm.nih.gov/entrez/query.fcgi?cmd=Retrieve&db=PubMed&dopt=Citation&list_uids=18758481.

Ruckh, J.M. et al., 2012. Rejuvenation of regeneration in the aging central nervous system. *Cell Stem Cell*, 10(1), pp.96–103. Available at: http://www.ncbi.nlm.nih.gov/pubmed/22226359.

Sanjabi, S. et al., 2009. Anti-inflammatory and pro-inflammatory roles of TGF-beta, IL-10, and IL-22 in immunity and autoimmunity. *Curr Opin Pharmacol*, 9(4), pp.447–453. Available at: http://www.ncbi.nlm.nih.gov/pubmed/19481975.

Schwarz, T.J., Ebert, B. & Lie, D.C., 2012. Stem cell maintenance in the adult mammalian hippocampus: a matter of signal integration? *Developmental neurobiology*, 72(7), pp.1006–15. Available at: http://www.ncbi.nlm.nih.gov/pubmed/22488809 [Accessed November 25, 2013].

Seib, D.R.M. et al., 2013. Loss of Dickkopf-1 restores neurogenesis in old age and counteracts cognitive decline. *Cell stem cell*, 12(2), pp.204–14. Available at: http://www.ncbi.nlm.nih.gov/pubmed/23395445 [Accessed October 24, 2013].

Shefer, G. et al., 2006. Satellite-cell pool size does matter: defining the myogenic potency of aging skeletal muscle. *Dev Biol*, 294(1), pp.50–66. Available at: http://www.ncbi.nlm.nih.gov/entrez/query.fcgi?cmd=Retrieve&db=PubMed&dopt=Citation&list_uids=16554047.

Villeda, S. a et al., 2011. The ageing systemic milieu negatively regulates neurogenesis and cognitive function. *Nature*, 477(7362), pp.90–4. Available at: http://www.pubmedcentral.nih.gov/articlerender.fcgi?artid=3170097&tool=pmcentrez&rendertype=abstract [Accessed October 20, 2013].

Vukovic, J. et al., 2012. Microglia modulate hippocampal neural precursor activity in response to exercise and aging. *The Journal of neuroscience : the official journal of the Society for Neuroscience*, 32(19), pp.6435–43. Available at: http://www.ncbi.nlm.nih.gov/pubmed/22573666 [Accessed October 25, 2013].

Wachs, F.-P. et al., 2006. Transforming growth factor-beta1 is a negative modulator of adult neurogenesis. *Journal of neuropathology and experimental neurology*, 65(4), pp.358–70. Available at: http://www.ncbi.nlm.nih.gov/pubmed/16691117.

Walter, J. et al., 2011. Age-related effects on hippocampal precursor cell subpopulations and neurogenesis. *Neurobiology of aging*, 32(10), pp.1906–14. Available at: http://www.ncbi.nlm.nih.gov/pubmed/20006411 [Accessed October 26, 2013].

Wobus, A.M. & Boheler, K.R., 2005. Embryonic stem cells: prospects for developmental biology and cell therapy. *Physiol Rev.*, 85(2), pp.635–678.

Yousef, H. et al., 2013. hESC-secreted proteins can be enriched for multiple regenerative therapies by heparin-binding. *Aging*, 5(5), pp.357–72. Available at: http://www.pubmedcentral.nih.gov/articlerender.fcgi?artid=3701111&tool=pmcentrez&rendertype=abstract.

Zetterberg, H., Andreasen, N. & Blennow, K., 2004. Increased cerebrospinal fluid levels of transforming growth factor-beta1 in Alzheimer's disease. *Neuroscience letters*, 367(2), pp.194–6. Available at: http://www.ncbi.nlm.nih.gov/pubmed/15331151 [Accessed December 1, 2013].

Acknowledgments

The research detailed in this dissertation was supported by grants from California Institute for Regenerative Medicine, National Institute of Health, and National Institute of Aging to Professors David Schaffer and Irina Conboy, and National Science Foundation Pre-doctoral fellowship to Hanadie Yousef. I thank the CIRM/QB3 Shared Stem Cell Facility at UC Berkeley for use of the Molecular Devices ImageXpress and Prairie 2P/Confocal microscope. I thank my thesis advisors, Professors David Schaffer and Irina Conboy, for mentoring, guiding, and integrating these studies. I thank Dr. Michael Conboy for his collaboration and mentorship on various aspects of the research presented in Chapters 1& 3. I also thank my thesis committee members, Professors John Ngai, Michael Rape, David Schaffer, and Irina Conboy for constructive feedback on my dissertation research. I also thank postdoctoral researchers Drs. Tandis Vazin and Ju Li for collaboration on various aspects of research presented in Chapter 3. Additionally, I thank the undergraduate researchers, honors thesis students and volunteers I have mentored between 2011-2013 during my graduate studies, whose contributions to the research presented in this dissertation have been instrumental: Matthew Zeiderman, Christina Schlesinger, Adam Morganthaler, Hikaru Mamiya, Mustafa Alkhouli, George Sun, Manika Paul, Amir Abbas, and Ashutosh Shrestha. I also thank the Chemical Biology Graduate Program for interdisciplinary training and coursework, and all members of the Schaffer and Conboy labs. Lastly, I thank the journal Impact Aging, for publication of the research perspective (Conboy et al. 2011) and research manuscript (Yousef et al. 2013) presented in Chapter 3 of this dissertation.

Curriculum vitae

Hanadie Yousef

845 46th Street, Oakland, CA 94608
Mobile (914) 560-6536• hyousef@berkeley.edu
Linkedin: http://www.linkedin.com/pub/hanadie-yousef/26/200/a21

Education

2008- Dec 2013 **University of California, Berkeley,** Berkeley, CA
Ph.D. in Molecular and Cell Biology, Chemical Biology Graduate Program

2004 - 2008 **Carnegie Mellon University,** Pittsburgh, PA
Bachelors of Science in Chemistry with High Honors and Spanish Minor;
Conversant in English (first language), Arabic, and Spanish; **GPA: 3.75**

Research Experience

2009- Ongoing **University of California Berkeley,** Berkeley, CA
Graduate Student, Laboratories of Dr. David Schaffer and Dr. Irina Conboy

- Explore TGF-β and BMP signaling in decline of adult hippocampal neurogenesis with age.
- Study mechanisms underlying enhancement of old muscle regeneration and human myogenesis by specific hESC-secreted proteins.
- Managed 9 undergraduates and research assistants; 3 manuscripts submitted; and published 1 manuscript and 1 research perspective.

Summer 2013 **Genentech Inc.**, South San Francisco, CA
Intern, Neuroscience Division

- Studied the role of neuroinflammation in Alzheimer's Disease
- Analyzed inflammatory cytokine signaling in glial and neuronal cell types and studied the ability of these cytokines to cross the blood brain barrier
- Identified specific markers of microglia for cell sorting by flow cytometry from primary murine cortex
- Assessed mass spectrometry and single cell RNA-sequencing technologies for characterization of microglia in animal model of Alzheimer's Disease

2007 – 2008 **University of Pittsburgh Medical Center,** Pittsburgh, PA
Undergraduate Researcher, Division of Pulmonary & Critical Care Medicine

- Transcriptional regulation of the microRNA let-7d by TGF-β in fibrosis, cancer and development.
- Undergraduate Research Honors Thesis and authorship on a manuscript and invention disclosure.

2003 - 2008 **Regeneron Pharmaceuticals Inc.,** Tarrytown, NY

Intern, Oncology and Angiogenesis Group

- Worked for 5 years during winter and summer recesses to develop multiple recombinant adenoviral, AAV and lentiviral vectors for gene transfer or gene silencing via siRNA.
- Modified tumor mammalian cell lines for development of VEGF models.

Publications

- **Yousef H,** Conboy MJ, Li J, Zeiderman M, Vazin T, Schlesinger C, Schaffer D, Conboy IM. hESC-secreted proteins can be enriched for multiple regenerative therapies by heparin-binding. Aging. 2013 May; Online ISSN: 1945-4589.
- Pandit KV, Corcoran D, **Yousef H**, Naftali Kaminski (2010). Inhibition and Role of let-7d in Idiopathic Pulmonary Fibrosis. American Journal of Respiratory and Critical Care Medicine. 2010 July; 182(2):220-9.
- Conboy IM, **Yousef H,** Conboy MJ. Embryonic Anti-Aging Niche. Aging. 2011 May; 3(5):555-63.

Manuscripts Submitted:

- **Yousef H ,** Conboy MJ, Morgenthaler A, Schlesinger C, Bugaj L, Paliwal P, Conboy IM**,** Schaffer D. Systemic attenuation of TGF-β1 pathway in old mice simultaneously rejuvenates neurogenesis and myogenesis by down-modulating MHC I β2 microglobulin. (In Review)
- **Yousef H,** Conboy MJ, Mamiya H, Zeiderman M, Schaffer D, Conboy IM. Molecular Identity and Mechanisms of Action of hESC-secreted Proteins that Enhance Human and Mouse Myogenesis. (In Review)
- **Yousef H ,** Morgenthaler A, Schlesinger C, Bugaj L, Conboy IM**,** Schaffer D. Age-Associated Increase in BMP Signaling inhibits Hippocampal Neurogenesis. (Submitted)

Invention Disclosures:

- **University of California**, Berkeley, CA
  Title: Molecular composition for broadly enhancing and rejuvenating maintenance and repair of mammalian tissues
  Innovators: Irina Conboy; **Hanadie Yousef;** Mike Conboy; David Schaffer

- **University of California**, Berkeley, CA
  Title: Methods and Compositions for Somatic Cell Proliferation and Viability
  Innovators: Irina Conboy; **Hanadie Yousef;** Mike Conboy; David Schaffer

- **University of Pittsburgh Medical Center**, Pittsburgh, PA
  Title: Use of microRNAs to determine and treat the lung phenoptype in Idiopathic Pulmonary Fibrosis
  Innovators: Naftali Kaminski; Panayotis Benos; David Corcoran; Kusum Pandit; Jadranca Miolosevic; **Hanadie Yousef**

Funding and Fellowships

- National Science Foundation Graduate Research Fellowship (2009-2012)
- Ellison Medical Foundation funded Molecular Biology of Aging course at the Marine Biological Laboratories, (July-August 2011).
- Molecular and Cell Biology Department Travel Award, International Society for Stem Cell Research Conference in Boston, Ma (June 2013)
- California Institute of Regenerative Medicine Travel Award, International Society for Stem Cell Research Conference in Toronto, Canada (June 2011)
- Howard Hughes Medical Institute Research fellowship (2004 – 2005)
- Howard Hughes Summer Undergraduate Researcher Grant (2007)
- Mitchell Scholarship in Chemistry (2004-2008)

Scientific Conferences

July 2011 **National Institute of Aging Juvenile Factors Conference,** Bethesda, MD
Speaker: Embryonic Anti-Aging Niche: Understanding the effects of hESC-Secreted Proteins on Muscle Rejuvenation
Authors: Hanadie Yousef, Mike Conboy, Irina Conboy

April 2013 **UC Berkeley Stem Cell Retreat**, Monterey, CA
Speaker: hESC-Secreted Factors Enhance Human Myoblast Proliferation and Muscle Regeneration Through Modulating Multiple Signaling Pathways
Authors: Yousef H, Conboy MJ, Mamiya H, Zeiderman M, Schaffer D, Conboy IM
Poster: Enhancement of Neurogenesis in the Aged Hippocampus Through Inhibition of TGF-β and BMP Signaling Pathways
Authors: Yousef H, Schlesinger C, Morgenthaler A, Conboy IM, Schaffer D

April 2013 **Cal Day,** Berkeley, CA
Speaker: Understanding Neural Stem Cells and the causes and decline of Adult Neurogenesis with Aging
Authors: Yousef H, Conboy IM, Schaffer D

June 2013 **International Society for Stem Cell Research Conference,** Boston, CA
Poster: hESC-secreted proteins can be enriched for multiple regenerative therapies by heparin-binding
Authors: Yousef H, Conboy MJ, Zeiderman M, Vazin T, Schlesinger C, Schaffer D, Conboy IM

May 2013 **UC Santa Cruz Stem Cells and Aging Symposium,** Santa Cruz, CA
Poster: hESC-secreted proteins can be enriched for multiple regenerative therapies by heparin-binding
Authors: Yousef H, Conboy MJ, Zeiderman M, Vazin T, Schlesinger C,

Schaffer D, Conboy IM

April 2011 **UC Berkeley Stem Cell Retreat,** Monterey, CA
Poster: Differences in expression of TGF-β and BMP signaling pathways in the hippocampi of young versus old brains
Authors: Hanadie Yousef, Irina Conboy, David Schaffer

June 2011 **International Society for Stem Cell Research Conference,** Toronto, Canada
Received California Institute of Regenerative Medicine Travel Award to attend. Research presented in Dr. Irina Conboy's plenary symposium oral presentation.

2007 **RECOMB Satellite Conference,** Boston, MA
Poster. Small but essential: let-7d miRNA in a transcriptional regulatory network that determines the fate of epithelial cells
Authors: **Hanadie Yousef**, David L. Corcoran, Daniel Handley, Kusum Pandit, Isidore Rigoutsos, Oliver Eickelberg, Naftali Kaminski, Panayiotis V. Benos

2007 **University of Pittsburgh Science 2007 Conference,** Pittsburgh, PA
Poster Title: Let-7d —A microRNA at the junction of TGF-β signaling and epithelial mesenchymal transition
Authors: **Hanadie Yousef**, David L. Corcoran, Dan Handley, Kusum Pandit, Isidore Rigoutsos, Ahmi Ben-Yehudah, Oliver Eickelberg, Panayiotis V.Benos, Naftali Kaminski

Honors

- 2008 Judith A. Resnik Award, Carnegie Mellon
- 2008 American Institute of Chemists Award
- Carnegie Mellon University Senior Leadership Award
- Phi Beta Kappa Honors Society
- Sigma Xi Scientific Research Society
- University Honors, College Honors, Departmental Honors in Chemistry (2004-2008)
- Mortar Board National Senior Honor Society (2007 – 2008)
- Department of Chemistry Undergraduate Freshman Award, Carnegie Mellon (2005)
- Mellon College of Science Dean's List (Honors: Fall 2004, High Honors: Spring 2005, Fall 2005, Spring 2007, Fall 2007, Spring 2008)

Scientific Services and Professional Experience

Fall 2012 **UC Berkeley,** Berkeley, CA
Graduate Student Instructor
BioE 113: Stem Cells and Technologies
Instructor: Irina Conboy

Spring 2011 MCB 104: Genetics, Genomics, and Cell Biology
Instructors: Rebecca Heald, Sharon Amacher, Daniel Rokhsar

Fall 2009 MCB 32: Intro to Human Physiology
Instructors: Terry Machen, Helen Lew, Andrew Wurmser

May 2012 *Mentor for Honors Thesis Undergraduate Students*
Title: hESC-Secreted Factors Enhance Human Myoblast Myogenesis through the Map Kinase and Notch Signaling Pathways

Dec 2012 **Title:** Enhancement of Hippocampal Neurogenesis in the Aged through Inhibition of TGF-β and BMP Signaling Pathways

Jan 2012-
June 2013 *Personal Tutor*
Math and Science tutor for high school student with severe ADHD

Spring 2009 *Science Writer for Berkeley Science Review*
Feature article on archaeology research conducted by Berkeley researchers in Greece and Hawaii.

Spring 2007 **Carnegie Mellon University—Qatar,** Doha, Qatar
Teaching Assistant
TA for Modern Biology, Physics I for Engineers, and Elementary Spanish II.
Presented Regeneron research at *Meeting of the Minds* 2007 symposium.

2005 – 2008 **Carnegie Mellon University,** Pittsburgh, PA
Department of Academic Development
Supplemental Instruction Leader
Served as Academic support for Modern Chemistry and Modern Biology. Held weekly review sessions and exam review sessions.

2006 – 2008 *Peer Tutor*
Held up to 10 tutor sessions per week with students in chemistry courses.

2008 *Training Assistant*
Trained new SI leaders and Teaching Assistants for the Doha campus

2005 – 2008 **The Tartan Student Newspaper**
Science and Technology Staff Writer
Wrote articles on recent scientific breakthroughs in Pittsburgh.

Spring 2006 *Science and Technology Editor*
Edited science and technology articles for student newspaper. Assigned articles and photograph requests for 4-7 articles weekly. Held weekly staff meetings, and mentored writers. Organized and conducted interviews with professors, graduate

students, and researchers. Aided in layout design. Attended a newspaper conference for student editors, Los Angeles, CA (March 2006).

Relevant Graduate Coursework and Training

Summer 2011 **Marine Biological Laboratories,** Woodshole, MA
Molecular Biology of Aging Course
Three week intensive course on aging with presentation of results at the end. Fully funded by the Ellison Medical Foundation.

2008-2012 **UC Berkeley,** Berkeley, CA
Physical Biochemistry
Advanced Immunology
Advanced Biophysical Chemistry
Chemical Biology
Stem Cells and Directed Organogenesis (Lab training)
Fundamentals of Business
Seminar Courses: Hippo Pathway, Epigenetics and Environment, Cancer and Immunology

2006 **Carnegie Mellon,** Pittsburgh, PA
Bioorganic Chemistry
Advanced Mathematical Methods for Chemists
Spanish Literature

Volunteer Work

2009-2012 **UC Berkeley,** Berkeley, CA
Stem Cell Education Outreach Program
Educational program funded by the California Institute for Regenerative Medicine (CIRM). Gave presentations to high school students on stem cell research. Gave tours of campus stem cell laboratories to visiting high school students.

2009-2010 **UC Berkeley,** Berkeley, CA
Berkeley Edge Program
Advised visiting seniors from underrepresented minority backgrounds whom were interested in applying to science and engineering PhD programs at Berkeley.

2007 **Urban League of Pittsburgh Charter School,** Pittsburgh, PA
Math tutor
Tutored third grade students at the weekend math tutorial program

Spring 2007 **Hamad Hospital,** Doha, Qatar
Volunteer
Shadowed a group of American doctors affiliated with University of Pittsburgh Medical Center in the Emergency Department. Acted as Arabic translator.

2005 - 2006 **Greenfield Elementary School,** Pittsburgh, PA
Tutor
Math and English tutor for kindergarten and first grade English for Second Language students whose first languages were Arabic or Spanish. Math, Spanish, and History tutor for sixth, seventh, eighth grade students in after school program.

References

1. David V. Schaffer, Ph.D. (Doctoral Thesis advisor)
Professor of Chemical and Biomolecular Engineering,
Bioengineering, and the Helen Wills Neuroscience Institute
University of California, Berkeley
274 Stanley Hall
Berkeley, CA 94720
Email: schaffer@berkeley.edu
Phone: (510) 643-5963

2. Irina Conboy, Ph.D. (Doctoral Thesis co-advisor)
Professor of Bioengineering and QB3 Institute
University of California, Berkeley
174 Stanley Hall
Berkeley, CA 94720-3220
Email: iconboy@berkeley.edu
Phone: (510) 666-2792

3. Naftali Kaminski, MD (Undergraduate Honors Thesis Advisor)
Bernigher-Ingelheim Endowed Professor of Internal Medicine
Chief of Pulmonary, Critical Care, and Sleep Medicine
Yale University School of Medicine
330 Cedar St, Boardman 110
New Haven, CT 06520-8056
Email: naftali.kaminski@yale.edu
Phone: (203) 737-4612

4. Ella Ioffe, Ph.D. (Mentor, Regeneron Pharmaceuticals)
Associate Director, Oncology & Angiogenesis and Target Gene Delivery
Regeneron Pharmaceuticals, Inc.
777 Old Saw Mill River Rd

Tarrytown, NY 10591
Email: ella.ioffe@regeneron.com
Phone: (914) 347-7000

5. David Hansen, Ph.D. (Manager, Genentech)
Scientist, Neuroscience
Genentech Inc.
1 DNA Way
South San Francisco, CA 94080
Email: hansen.david@gene.com
Phone: (650) 467-3689

6. Michael Conboy, Ph.D. (Collaborator at UC Berkeley)
Professional Researcher and Instructor
QB3 Institute
University of California, Berkeley
174 Stanley Hall
Berkeley, CA 94720-3220
Email: conboymj@berkeley.edu
Phone: (408) 621-2063

Chapter 1

Age-Associated Increase in BMP Signaling inhibits Hippocampal Neurogenesis

Hanadie Yousef[2], Adam Morgenthaler[1], Christina Schlesinger[1], Lukasz Bugaj[1], Irina Conboy[1] & David Schaffer[1,3,4]*

1 Department of Bioengineering and California Institute for Quantitative Biosciences (QB3), UC Berkeley, Berkeley, CA 94720, USA

2 Department of Molecular and Cellular Biology, UC Berkeley, Berkeley, CA 94720, USA

3 Department of Chemical and Biomolecular Engineering, UC Berkeley, Berkeley, CA 94720 USA

4 Helen Wills Neuroscience Institute, UC Berkeley, Berkeley, CA 94720 USA

* to whom correspondence should be addressed:

Email schaffer@berkeley.edu

Acknowledgments

This work was supported by California Institute for Regenerative Medicine grant RT2-02022 to DVS, grants from the National Institutes of Health R01 AG02725201 and California Institute for Regenerative Medicine RN1-00532-1 to IMC, and NSF Pre-doctoral fellowship to HY. We thank Mary West and the CIRM/QB3 Shared Stem Cell Facility at UC Berkeley for use of the Molecular Devices ImageXpress and Prairie 2P/Confocal microscope and training on these instruments. We thank Drs. John Ngai and Russell Fletcher at UC Berkeley for providing a breeding pair of BMPR1A$^{lox/lox}$ BMPR1B$^{+/-}$ Rosa26lacZ mice, Mustafa Alkhouli for animal care and assistance with brain staining and image processing, Hikaru Mamiya and Matthew Zeiderman for assistance in *in vitro* NPC staining and qPCRs, Manika Paul for her assistance with brain staining and image processing, and George Sun for assistance with qPCRs, and Ashutosh Shrestha for assistance with cell staining and imaging.

Abstract

Hippocampal neurogenesis, the product of resident neural stem cell proliferation and differentiation, persists into adulthood but decreases with organismal aging, which may contribute to the age-related decline in cognitive function. The mechanisms that underlie this decrease in neurogenesis are not well understood, though evidence in general indicates that extrinsic changes in an aged stem cell niche can contribute to functional decline in old stem cells. Bone Morphogenetic Protein (BMP) family members are intercellular signaling proteins that regulate quiescence, proliferation, and differentiation in precursor cells throughout the adult body and are likewise critical regulators of neurogenesis. Here, we establish that BMP signaling increases significantly in old murine hippocampi and inhibits neural progenitor cell proliferation. Furthermore, direct *in vivo* attenuation of BMP signaling via genetic and transgenic perturbations in aged mice led to elevated neural stem cell proliferation, and subsequent neurogenesis, in old hippocampi. Such advances in our understanding of mechanisms underlying decreased hippocampal neurogenesis with age may offer targets for the treatment of age-related cognitive decline.

Introduction

Neurogenesis occurs throughout our lifetime in the subgranular zone (SGZ) of the dentate gyrus (DG) of the hippocampus and the subventricular zone (SVZ) of the lateral ventricles in mammals, via differentiation of adult neural stem cells (NSCs) into excitatory granule neurons and inhibitory olfactory bulb interneurons, respectively (Ming & Song 2005). Hippocampal neurogenesis is believed to aid new memory formation, while SVZ neurogenesis plays a role in sensory functions (Deng et al. 2010; Deng et al. 2009; Oboti et al. 2009).

Neurogenesis, however, significantly declines with age, which is believed to result from both a reduction in the overall number of stem cells and in the ability of the remaining cells to function properly with age (Walter et al. 2011). In particular within the SGZ, type 1 and 2 NSCs and neural progenitor cells (NPCs) significantly decrease in number with increasing age (Maslov et al. 2004; Olariu et al. 2007; Walter et al. 2011; Kuhn et al. 1996), as demonstrated by the two-fold decline in Sox2+ cells and nine-fold decline in proliferating BrdU+ and doublecortin (DCX)+ cells in neurogenic regions of aged animals. SGZ neurogenesis is also very active in humans and exhibits a steady decline with age (Eriksson et al. 1998; Spalding et al. 2013). In addition, the molecular mechanisms that underlie the loss of organ stem cell numbers with age, particularly in brain, are beginning to be elucidated. Both an elevation in the systemic levels of chemokines and a decrease in hippocampal Wnt signaling with age have been correlated with or demonstrated to hinder hippocampal neurogenesis (Vukovic et al. 2012; Okamoto et al. 2011; Miranda et al. 2012; Seib et al. 2013; Villeda et al. 2011). In addition, TGF-β signaling has been implicated in the decline of neurogenesis with age in the subventricular zone (SVZ) (Pineda et al. 2013), the other CNS region that can exhibit adult neurogenesis, though the significance of the SVZ to human biology and health is unclear as this region does not appear to have active neurogenesis in adult humans (Bergmann et al. 2012).

Bone Morphogenic Protein (BMP) family members and most growth and differentiation factor (GDF) ligands bind BMP type II receptors, which then phosphorylate and activate type I receptor serine-threonine kinases. In the canonical pathway, the type I receptors in turn phosphorylate and activate specific R-Smads(1,5,8), which then heterodimerize with Co-Smad4 and translocate to

the nucleus, where they bind coactivators or corepressors to activate or inhibit gene expression (Oshimori & Fuchs 2012; Massagué 2012). In particular, BMP induces expression of Id1 and Id3, bHLH transcriptional repressors that are necessary for progression of cells through the G1 phase of the cell cycle and inhibiting differentiation-inducing factors. (Nakashima et al. 2001). BMP signaling regulates a variety of biological functions in various organ systems and during development, including in the central nervous system (CNS).

While BMP signaling has been extensively studied in embryonic pluripotent stem cells and NSCs (Oshimori & Fuchs 2012; Bond et al. 2012), its roles within the adult CNS are only beginning to be elucidated. BMP inhibits neurogenesis and promotes NSC glial differentiation in the adult SVZ (Lim et al. 2000), resulting in a depletion of the stem cell pool (Porlan et al. 2013). In addition, BMP signaling through BMPRIA inhibits proliferation and promotes the maintenance of SGZ NSCs in an undifferentiated and quiescent state (Mira et al. 2010). Additionally, overexpression of the BMP antagonist Noggin induced proliferation and enhanced the self-renewal of hippocampal stem cells , thereby expanding the pool (Bonaguidi et al. 2008). Furthermore, BMP4 inhibition has been implicated in exercise-induced hippocampal neurogenesis and hippocampal dependent learning (Gobeske et al. 2009; Fan et al. 2003). However, BMP involvement in the decline of adult stem cell function with age has not been investigated for any tissue in mammals. Here, we demonstrate that multiple BMP growth factors and downstream signaling effectors increase in expression with aging in the neural stem cell niche and as a result inhibit neural precursor cell proliferation. Furthermore, we demonstrate a partial rescue of aged hippocampal neurogenesis through *in vivo* genetic and transgenic inhibition of BMP signaling.

Materials and Methods

Animals

Young (2-3 month old) and old (18-24 month old) C57BL6/J male mice were purchased from the Jackson Laboratory and the NIH. A breeding pair of BMPR1A$^{lox/lox}$ BMPR1B$^{+/-}$ Rosa26lacZ were obtained as a gift from the laboratory of Professor John Ngai, UC Berkeley. The mice were bred and aged in house, in accordance with the Guide for Care and Use of Laboratory Animals of the National Institutes of Health.

For each experiment on aged (18-24 month old) mice, an n of at least 7 per group was used initially. If aged mice were lost due to surgery or age-related health issues, a minimum of n=3 remaining mice were analyzed and assessed for statistical significance (described in statistical analysis below). Mice of the same genetic strain and age were assigned to groups at random. The animal experimental procedures were performed in accordance with the Guide for Care and Use of Laboratory Animals of the National Institutes of Health, and approved by the Office of Laboratory Animal Care, UC Berkeley.

Cell Culture

Primary rat neural progenitor cells isolated from the hippocampi of 6-week-old female Fisher 344 rats (Charles River) were cultured in growth medium (DMEM/F12 (Life Technologies) containing N2 supplement (Life Technologies) and 10 ng/mL FGF-2 (PeproTech)) on laminin (Roche) and polyornithine (Sigma) coated tissue culture plates, with subculturing on reaching

80% confluency using Accutase (Phoenix Flow Systems), as previously described (Ashton et al. 2012).

Primary mouse neural progenitor cells were isolated form C57BL6/J mice (Charles River) as previously described (Babu et al. 2011). Cells were cultures in growth medium (Neurobasal A (Gibco) containing B27 supplement (Gibco), Glutamax-1 supplement (Gibco), 20 ng/mL FGF-2 (Peprotech), and 20 ng/mL EGF (PeproTech)) on Poly-d-Lysine (Sigma) and Laminin (Roche) coated tissue culture plate, with subculturing on reaching 80% confluency using Accutase (Phoenix Flow Systems). Progenitor cells were tested for mycoplasma contamination at the UC Berkeley Stem Cell Core Facility and using Hoechst DNA stain.

In vitro validation of BMP Signaling and Proliferation Assay

Rat NPCs were cultured in growth medium (DMF12 + N2 + 10 ng/mL FGF-2) as described above. Cells were cultured at a density of 200,000 cells per well of a 6-well culture slide in the presence/absence of BMP4 (50 ng/mL) (R&D) for 30 minutes, followed by a PBS wash and cell scraping into RIPA buffer for Western blot analysis as described below. Rat hippocampal-derived NPCs were also cultured at a density of 80,000 cells per well of an 8-well chamber slide in growth medium plus the presence/absence of BMP4 (100 ng/mL) for 24 hours. NPCs were pulsed for 2 hours with 10 µM BrdU (Sigma Aldrich) before cell fixation with 70% cold ethanol for immunocytochemistry analysis as described below.

Dissection and Preparation of Murine Hippocampi for RNA or Protein Analysis

Young or old mice were anesthetized and perfused with 20 mL saline, followed by dissection and isolation of hippocampi. For RNA extraction, tissue was placed in 1 mL Trizol (Life Technologies) and homogenized, followed by chloroform extraction as previously described (Ashton et al. 2012). For protein extraction, hippocampi tissue was homogenized in RIPA buffer (50 mM Tris, 150 mM NaCl, 1% NP40, 0.25% sodium deoxycholate and 1 mM EDTA, pH 7.4) containing 1X protease inhibitor (Roche), 1 mM Phenylmethylsulfonyl fluoride (PMSF), 1 mM sodium fluoride, and 1 mM sodium orthovanadate. Lysates were spun at 10K rpm for 5 min at 4ºC to remove debris, and supernatant containing protein extract was snap frozen with dry ice.

RNA extraction, RT-PCR and real-time PCR

Total RNA was extracted from primary neural progenitor cells or young and old murine hippocampi using Trizol reagent (Life Technologies) according to manufacturer's instructions. 1 ug of total RNA was used for cDNA synthesis with oligo dT primers (Life Technologies). For real-time PCR amplification and quantification of genes of interest, an initial amplification using specific primers to each gene of interest (realtimeprimers.com) was conducted with a denaturation step at 95°C for 5 min, followed by 40 cycles of denaturation at 95°C for 1 min, primer annealing at 55°C for 30 s, and primer extension at 72°C for 30 s. Real-time PCR was performed using SYBR and an ABI PRISM 7500 Sequence Detection System (Applied Biosystems). Reactions were run in triplicate in three independent experiments. The geometric mean of housekeeping gene *GAPDH* was used as an internal control to normalize the variability in expression levels, which were analyzed using the $2^{-\Delta\Delta CT}$ method described (Livak & Schmittgen 2001).

ELISA

The concentration of active BMP4 in hippocampal tissue protein lysate was determined using enzyme-linked immunoabsorbent assay (ELISA)-based cytokine antibody array (R&D), according to manufacturer instructions.

Immunocytochemistry

Mice were anesthetized and perfused with saline and 4% PFA. Brains were collected and placed in 4% PFA overnight for post-fixation, followed by dehydration in 30% sucrose/PBS at 4°C for 2 days. Brains were then sectioned at 40 µM using a sliding microtome and stored in a glycerol-based cryoprotectant at -20°C until further analysis by immunostaining.

For BrdU *in vivo* labeling of mitotic cells, mice were intraperitoneally injected with BrdU (50 mg/kg of body weight, Sigma Aldrich) dissolved in saline to label mitotic cells, as previously described (Lai et al. 2003). Sections were incubated in SSC/formamide at 65°C water for 2 hours, washed in TBS, followed by 2N HCl for 15 minutes. They were then placed in 2X Saline-Sodium Citrate (SSC) for 30 minutes, .1 mM Borate Buffer for 15 minutes, followed by 6, 15 minute washes in TBS, then blocked in a permeabilization/staining buffer, TBS++ (3% Donkey Serum and .25% Triton-X-100) for 2 hours. Sections were then incubated with αRat-BrdU (Abcam Inc. ab6326) and other antibodies (see Antibodies below) in TBS++ at 4°C for 72 hours. Secondary staining was done as described below.

For EdU *in vivo* labeling of mitotic cells, mice were intraperitoneally injected with EdU (50 mg/kg of body weight, Life Technologies) dissolved in phosphate-buffered saline. Brain sections were post-fixed with 4% PFA for 30 minutes after primary and secondary staining, and treated for EdU visualization using the Click-iT EdU kit (Life Technologies), as per the manual's instructions.

For non-BrdU/EdU staining, sections were washed 3 times for 15 minutes in TBS, followed by one hour blocking in a permeabilization/staining buffer, TBS++ (3% Donkey Serum and .25% Triton-X-100 in TBS), then incubated with primary antibodies of interest (see Antibodies) for 72 hours. For secondary staining, sections were washed 3 times, 15 minutes each in TBS, followed by 2 hour incubation in donkey raised, fluorophore-conjugated, species-specific secondary antibodies (Jackson Immunoresearch) at 1:250 dilution in TBS++. Following secondary staining, sections underwent 3, 15 minute washes in TBS, with 4 µM Hoechst in the second wash. Finally, the sections were mounted on positively charged frosted slides, dried overnight and imaged with a prairie confocal microscope.

Antibodies

αRabbit-pSmad1/5/8 (Cell Signaling #9511), αRabbit-βactin (Cell Signaling #4967), αMouse-BMP6 (Chemicon International MAB1048), αRabbit-BMP4 (Abcam ab39973), αMouse-β-galactosidase (MP Biomedicals 08633651), αMouse-mCherry (Novus Biologicals 1C51), EdU Click-it kit (Life Technologies C10337 and C10338), αGuineyPig-DCX (Millipore AB2253), αGoat-Sox2 (Santa Cruz SC-17320), αChicken-GFP (Abcam ab13970), αRat-BrdU (Abcam ab6326), BMP4 ELISA kit (R&D DY314)

Western Blot Analysis

Neural progenitor cells were lysed in RIPA buffer (50 mM Tris, 150 mM NaCl, 1% NP40, 0.25% sodium deoxycholate and 1 mM EDTA, pH 7.4) containing 1X protease inhibitor (Roche), 1 mM Phenylmethylsulfonyl fluoride (PMSF), 1 mM sodium fluoride and 1 mM sodium orthovanadate. The protein concentration was determined by a Bradford assay (Bio-Rad). Lysates were resuspended in 1X Laemmli buffer (Bio-Rad), boiled for 5 minutes, and separated on precast 7.5% or 4-15% TGX gels (Bio-Rad). Primary antibodies were diluted in 5% non-fat milk in TBS + 0.1% Tween-20, and nitrocellulose membranes were incubated with antibody mixtures overnight at 4°C. HRP-conjugated secondary antibodies (Santa Cruz Biotech) were diluted 1:500 in 5% non-fat milk in TBS + 0.1% Tween-20 and incubated for 1 hour at room temperature. Blots were developed using Western Lightning ECL reagent (Perkin Elmer), and analyzed with Bio-Rad Gel Doc/Chemi Doc Imaging System and Quantity One software. Results of multiple assays were quantified using Applied Biosystems of Image J software. Pixel intensity of bands of interest were normalized with the corresponding pixel intensities of glyceraldehydes-3-phosphate dehydrogenase or β-actin.

Lentiviral Vector Construction, Packaging, and Purification

A DNA cassette encoding human U6 promoter-driven expression of shRNA against mouse SMAD3 (Gene ID: 17127) was constructed by PCR with flanking *PacI* sites and, following restriction digestion and phenol/chloroform purification, ligated into the *PacI* site of the pFUGW lentiviral vector (Lois et al. 2002). Five candidate sequences were tested for knockdown efficiency, and the most effective sequence (shSMAD 1.3 in **Table 1**) was selected for experimental studies. Sequences for all shRNAs tested are provided in **Table 1**. The control shRNA vector against *LacZ* was constructed previously (Ashton et al. 2012). PCR was performed with Phusion DNA Polymerase (New England Biolabs) under the following conditions: 98°C for 2 min, 30 cycles of 12 s at 95°C, 30 s at 65°C, and 25 s at 72°C, with a final extension step of 2 min at 72°C. Lentiviral and retroviral vectors were packaged and purified using standard methods as described (Yu & Schaffer 2006; Peltier & Schaffer 2010).

Cre lentiviral plasmids were obtained (Addgene http://www.addgene.org/20781/ and http://www.addgene.org/27546/), packaged, and purified as previously described (Yu & Schaffer 2006; Peltier & Schaffer 2010). The control GFP vector was constructed previously (Lois et al. 2002).

In vitro validation of Smad1 shRNA Vector

Mouse neural progenitor cells (NPCs) were plated at 200,000 cells per well of a 6 well tissue culture plate in growth medium, transduced with lentivirus encoding shRNA to *Smad1* or *lacZ* at a multiplicity of infection (MOI) of 5, and cultured for two weeks. RNA was extracted with Trizol (Life Technologies), followed by qPCR to assess levels of *Smad1* (see **Table 1** for sequences).

To assess shRNA functionality, rNPCs were plated at 200,000 cells per well of a 6 well tissue culture plate in growth medium, transduced with lentivirus encoding shRNA to *Smad1* or *lacZ* at a multiplicity of infection (MOI) of 10, and cultured for 72 hours. Cells were then plated at 10^5 cells per well of 8 well chamber slides and cultured for 16 hours in growth medium in the presence or absence of 200 ng/mL BMP4. A 4 hour EdU (30 μM) pulse was performed before cell fixation in 4% PFA to label proliferating cells. Quantification described below.

In vivo loss of function via lentiviral vector stereotaxic injections to hippocampus

Aged (18 month) C57BL6/J male mice received lateral intrahippocampal injections of equal volume and similar titer of lentiviral solutions (1 µl of LV-shRNA-Smad1-GFP or LV-shRNA-lacZ-GFP, 1-3 x 10^8 IU/mL) in PBS on day -14, on the right hemisphere hippocampus, at 0.25 uL per minute. The injection coordinates with respect to bregma were -2.12 mm anteriorposterior, -1.55 mm dorsoventral (from dura), and 1.5 mm mediolateral (refer to **Figure 4a**). Mice were allowed to recover 14 days, followed by BrdU intraperitoneal (IP) injections (50 mg/kg bodyweight) 1 times daily for 5 days. One day after receiving the fifth BrdU IP injection, mice were saline and 4% PFA perfused. Immunostaining and quantification described in immunocytochemistry section and quantification and statistical analysis section.

Aged (18 month) C57BL6/J male mice received lateral intrahippocampal injections of equal volume and similar titer of lentiviral solutions (1 µl of LV-shRNA-Smad1-GFP or LV-shRNA-lacZ-GFP, 1-3 x 10^8 IU/mL) in PBS on day -14, on the right hemisphere hippocampus, at 0.25 uL per minute. The injection coordinates with respect to bregma were -2.12 mm anteriorposterior, -1.55 mm dorsoventral (from dura), and 1.5 mm mediolateral (refer to **Figure 5a**). Mice were allowed to recover 14 days, followed by EdU IP injections (50 mg/kg bodyweight) 1 times daily for 5 days. Five days after receiving the fifth IP injection, mice were saline and 4% PFA perfused. Immunostaining and quantification described in quantification and statistical analysis section.

Aged (18 month) $BMPR1A^{lox/lox}$ $BMPR1B^{+/-}$ Rosa26lacZ male mice received lateral intrahippocampal injections of equal volume and similar titer of lentiviral solutions (1 µl of LV-Cre-mCherry or LV-FUGW (LV-GFP), 1-3 x 10^7 IU/mL) in PBS on day -14, on the right hemisphere hippocampus, at 0.25 uL per minute. The injection coordinates with respect to bregma were -2.12 mm anteriorposterior, -1.55 mm dorsoventral (from dura), and 1.5 mm mediolateral (refer to **Figure 6a**). Mice were allowed to recover 14 days, followed by BrdU IP injections (50 mg/kg bodyweight) 1 times daily for 5 days. One day after receiving the fifth BrdU IP injection, mice were saline and 4% PFA perfused. Immunostaining and Quantification described elsewhere.

Aged (18 month) C57BL6/J male mice received lateral intrahippocampal injections of equal volume and similar titer of lentiviral solutions (1 µl of LV-Cre-GFP or LV-FUGW (LV-GFP), 1-3 x 10^7 IU/mL) in PBS on day -14, on the right hemisphere hippocampus, at 0.25 uL per minute. The injection coordinates with respect to bregma were -2.12 mm anteriorposterior, -1.55 mm dorsoventral (from dura), and 1.5 mm mediolateral (refer to **Figure 7a**). Mice were allowed to recover 14 days, followed by EdU IP injections (50 mg/kg bodyweight) 1 times daily for 5 days. Five days after receiving the fifth EdU IP injection, mice were saline and 4% PFA perfused. Immunostaining and quantification described in Quantification and Statistical Analysis section.

Quantification and Statistical Analysis

For quantification of immunofluorescent images for BrdU or EdU incorporation, 25 20x images per replicate were taken on the Molecular Devices ImageXpress Micro automated epifluorescence imager, followed by automated cell quantification using the multiwavelength cell scoring module within the MetaXpress analysis software. Data was analyzed using ANOVA,

and P values equal or lower than 0.05 were considered statistically significant. Sample sizes of n=3 or greater were used for each experiment based on previously published experimental group numbers (Miranda et al. 2012; Ashton et al. 2012) and assessed for significance based on P values and heteroscedastic variance between groups that are statistically compared. For pixel intensity quantifications of immunofluorescent images, ImageJ was used to determine integrated pixel intensity of thresholded images, with n=3 young or old brain tissue sections, and 2 images (right and left hippocampi) per section assessed.

For quantification of the number of BrdU+Sox2+ or EdU+DCX+ cells in shRNA or Cre injected mice, confocal stacks of 8 coronal GFP+ or mCherry+ brain sections spanning the hippocampus (40 microns thick, 200 microns apart) were acquired on a Prairie confocal microscope, and cells were counted. Cell numbers were normalized to the volume of the DG granule cell layer using ImageJ as previously described (Seib et al. 2013). Briefly, volume was calculated based on a threshold of the granule layer of each image as determined with Hoechst staining, then calculating the volumetric fraction based on the thickness of the brain slice (40 μM) and the interval at which hippocampi sections were analyzed (every 6^{th} section).

Only aged mice that were lost during the study due to health reasons were excluded from analysis. For automated cell counting using MetaXpress analysis software, only sites that were blurry with indistinguishable colors (such as occasional areas on the slide with bubbles or rare images acquired with incorrect focus by the Molecular Devices ImageXpress Micro automated epifluorescence imager), or in the case of cell culture occasional areas with large cell clumps, were excluded from the cell quantification analysis. These criteria were pre-established.

When performing *in vivo* experiments, there was no blinding as to experimental groups. For quantification and analysis, researchers were blinded to the group allocation when performing cell counts.

Results

BMP signaling increases in the aged murine hippocampus

Consistent with prior reports (Maslov et al. 2004; Olariu et al. 2007; Walter et al. 2011; Kuhn et al. 1996), we found that Sox2+BrdU+ proliferating hippocampal cells, which include type 1 and 2a neural stem and progenitor cells, significantly decline with age (Figure 1A). To correlate this decrease in proliferating neural stem and progenitor cells with levels of BMPs, known negative regulators of cell proliferation and differentiation in the young dentate gyrus (Mira et al. 2010), we isolated hippocampi from young (2-4 mo) and old (22-24 mo) male C57BL6/J mice and analyzed mRNA and protein levels of various BMP family members. We observed an increase in BMP2 and BMP6 mRNA expression levels with age as assessed by qRT-PCR (Figure 1B,C), as well as an increase in BMP6 protein expression as assessed by immunofluorescence (Figure 1D,E). BMP4 protein levels were analyzed both by immunofluorescence in whole tissue sections and via ELISA in tissue lysates and found to increase with age (Figure 1F,G). Consistent with the vascular-like staining observed in young and old hippocampi, BMPs are known to be expressed in endothelial cells and regulate angiogenesis (Beets et al. 2013). Accordingly, BMP4 was shown to colocalize with CD31+ endothelium in young and old dentate gyri (Supplementary

1A,B). BMP6, interestingly, is primarily expressed by microglia and is not expressed by the endothelium (Supplementary 2A-C).

To confirm and build upon these results, we analyzed downstream SMAD signaling in young versus aged neural stem cells *in vivo*. qRT-PCR revealed that *in vivo* hippocampal expression of total *Smad1*, a transcription factor activated by BMP signaling (Massagué 2012), was elevated with age (Figure 2A). In addition, though active, phosphorylated SMAD1/5/8 protein levels did not appear to change across the hippocampus as a whole with age (Figure 2B), the percentage of Sox2+ cells that were also pSmad1/5/8+ in the SGZ increased substantially (Figure 2C, quantified in D). Furthermore, Id1, a known down-stream target of the BMP/pSmad pathway (Nakashima et al. 2001; Ross et al. 2003) that inhibits the function of proneural transcription factors and thereby inhibits neurogenic differentiation (Ross et al. 2003), was elevated with age (Figure 2E). These data are the first to demonstrate that in the hippocampus BMP transcript and protein levels and Id1 transcript levels increase with age, and that in hippocampal Sox2+ neural stem and progenitor cells SMAD1/5/8 phosphorylation is correspondingly elevated with age.

Partial rescue of neurogenesis in aged hippocampi by *in vivo* genetic inhibition of BMP/pSmad1 signaling

To probe whether an increase in BMP may be functionally relevant for neurogenesis, BMP4 was added to hippocampal-derived Sox2+ NPC cultures. After 30 minutes, it was found to upregulate pSmad1/5/8 (Figure 3A), and after 24 hours it decreased cell proliferation, as assayed by reduced BrdU uptake (Figure 3 B, quantified in C). To further assess the importance of downstream BMP signaling in regulating NPC proliferation, we genetically perturbed BMP signaling using a lentivirally-encoded shRNA we developed against *Smad1* plus a GFP reporter, and RNAi efficacy was confirmed in mouse neural progenitor cells *in vitro* via qRT-PCR (Figure 3D). As shown and quantified in Figures 3E and F, *Smad1* shRNA but not control shRNA prevented the BMP4-induced decrease in proliferation. Collectively, these results indicate that BMP/pSmad1 signaling inhibits NPC proliferation.

To further build upon these findings, the function of elevated BMP/pSmad1 signaling in the aged hippocampus was assessed *in vivo* via genetic perturbation of this pathway. After a single stereotaxic hippocampal injection of equal titers of either a lentiviral vector encoding GFP plus the shRNA against *Smad1* – or a control shRNA against *LacZ* – into 18 month old mice, animals were allowed to recover for 2 weeks, followed by five consecutive days of IP BrdU administration (Figure 4A). As shown in Figure 4B-C, the numbers of Sox2+ proliferating cells (quantified in the GFP+ region of tissue sections throughout the entire hippocampus) were significantly increased after a single injection of shRNA to *Smad1*, compared to the control shRNA. Furthermore, there was a significantly higher proportion of GFP+Sox2+ cells that were also BrdU+ in *Smad1* shRNA injected mice (Figure 4D). Neurogenesis was thus significantly enhanced by the inhibition of pSmad1 in the local niche of neural stem cells in 18 month old mice (analogous to 80 year old humans).

To analyze subsequent effects on type 2b doublecortin (DCX) + transit amplifying cells, a second cohort of animals was injected with the shRNA lentiviral vectors, mitotically labeled 2 weeks later with EdU, and investigated 5 days after the last EdU injection to enable cells to progress towards neuronal commitment (Ming & Song 2005) (Figure 5A). There was a substantial increase in the total number of EdU+DCX+GFP+ type 2b transit amplifying cells

(Figure 5B-C). Thus, the *in vivo* delivery of lentiviral shRNA to *Smad1* partially rejuvenated neural stem cell function and confirmed that canonical BMP/pSmad1 signaling is involved in the age-imposed inhibition of neurogenesis.

Partial rescue of neurogenesis in aged hippocampi by *in vivo* transgenic inhibition of BMP signaling

To further investigate the finding that attenuation of BMP signaling enhances neurogenesis, we directly perturbed BMP signaling through Cre-mediated deletion of BMPR1A in aged (18-22 month old) $BMPR1A^{lox/lox}$ $BMPR1B^{+/-}$ Rosa26lacZ mice. It has been demonstrated that type 1 and 2a cells specifically express BMPR1A in the SGZ, whereas granule neurons express BMPR1B (Mira et al. 2010). After a single stereotaxic hippocampal injection of equal titer of either a lentiviral vector encoding mCherry as well as Cre recombinase – or control vector encoding GFP only – into 18-22 month aged mice, animals were allowed to recover for 2 weeks, followed by five consecutive days of IP BrdU administration (Figure 6A). Cre recombination was evident by β-galactosidase immunoreactivity in animals administered with the Cre, but not the control, virus (Figure 6B). Furthermore, the number of Sox2+ proliferating cells (quantified in the mCherry+ or GFP+ region of tissue sections throughout the entire hippocampus) was significantly increased after a single injection of Cre recombinase, as compared with control GFP lentivirus (Figure 6C-E). Finally, there was a significantly higher proportion of mCherry+Sox2+ cells that were also BrdU+ (Figure 6F). Proliferation was thus significantly enhanced by the inhibition of BMP signaling through the BMPR1A receptor in NSCs of 18-22 month old mice.

To analyze effects on downstream type 2b transit amplifying cells, additional aged, BMPR1A floxed animals were injected with equal titer of a lentiviral vector encoding GFP and Cre, or control vector encoding GFP. Two weeks after the injection, cells were mitotically labeled with EdU, then investigated 5 days after the last EdU injection (Figure 7A). There was a substantial increase in the number of EdU+/DCX+ type 2b cells (quantified in the GFP+ region of tissue sections throughout the entire hippocampus) (Figure 7B-C). This was confirmed to be a direct result of the lentiviral delivery of Cre and subsequent BMPR1A deletion, since there were a significantly higher proportion of GFP+DCX+ cells that were also EdU+ (Figure 7D). Thus, inhibition of BMP signaling via Cre-induced deletion of BMPR1A *in vivo* further established that canonical BMP/pSmad signaling is involved in the age-imposed inhibition of neurogenesis.

Discussion

Collectively, our data indicate that BMP signaling reversibly inhibits the capacity of stem cells in the aged brain to contribute to neurogenesis. Specifically, an age-imposed increase of BMP/pSmad1,5,8 signaling in the neural stem cell niche was identified and shown to inhibit neural progenitor cell proliferation. Importantly, genetic inhibition of BMP signaling partially rescued neural stem and progenitor cell proliferation and neuronally committed transit amplifying type 2b cells in aged mice. This ability to rapidly enhance neurogenesis via modulating the levels of signaling pathways in the stem cell microenvironment suggests promising strategies for combatting the loss of cognitive function and memory with aging.

In humans, there are 20 known BMP family members (Chen et al. 2004). BMPs and many GDFs signal through SMAD1/5/8 (Oshimori & Fuchs 2012). Specifically, BMPs bind type 2 receptors (BMPR2 or ACVR2) and type 1 receptors (BMPR1A (ALK3),BMPR1B (ALK6), ALK2, or

ALK1) to induce downstream SMAD1/5/8 signaling. BMPs thereby induce or repress numerous target genes that vary with the microenvironmental, transcriptional, and epigenetic landscapes during which they act during development and during tissue homeostasis (Oshimori & Fuchs 2012; Massagué 2012). Here, we show an increase in expression of BMPs 2, 4, and 6 with age. All three are known to bind BMPR2, BMPR1A, and BMPR1B, and to act through SMAD1,5,8 (Chen et al. 2004). It will be interesting to determine if there are differences in receptor binding affinity and downstream target genes amongst these 3 BMPs..

Within the developing CNS, several downstream BMP targets act to embryonic neurogenesis and promotes glial differentiation (Nakashima et al. 2001). For example, Id1 and Id3 prevent the activity of transcription factors that promote neuronal differentiation, including Neurogenin, Ascl1, and NeuroD1 (Nakashima et al. 2001; Ross et al. 2003). BMPs also induces expression of Hes genes, which are known to prevent neuronal differentiation (Bond et al. 2012). Finally, BMP can promote astrocytic differentiation during embryonic development in part by inducing expression of glial fibrillary acidic protein (GFAP) (Bonaguidi et al. 2005). It would be interesting to determine whether analogous modulators function during adult neurogenesis, and thus may thus change with aging.

Within the SVZ, BMP is secreted by neural stem and progenitor cells (i.e. resident radial glial-like cells and transient amplifying cells), while the ependymal cells in this neurogenic niche secrete Noggin, an inhibitor of BMP (Bond et al. 2012). By comparison, although BMP4 is known to be expressed in the young murine hippocampus (Lein et al. 2007), in general the sources of BMP ligand secretion in the dentate gyrus remains to be determined. These may include several cell types with which hippocampal NSCs are known to interact, including astrocytes, microglia, endothelial cells and neurons (Basak & Taylor 2009). In particular, the vascular endothelium may play a role analogous to its secretion of BMPs to regulate angiogenesis (Beets et al. 2013), consistent the vascular immunostaining we observe (Figure 1).

While BMPs have been implicated in age-associated CNS pathologies, their role in the aging of the hippocampal stem cell niche and decline of neurogenesis has not previously been elucidated. Specifically, an increase in BMP6 and BMP4 and associated decreased neurogenesis was shown for such age-associated pathologies as human Alzheimer's Disease and corresponding mouse models (Crews et al. 2010; Li et al. 2008). Interestingly, neurogenesis is rescued by inhibiting BMP signaling with Noggin in AD models (Tang et al. 2009). It has also been demonstrated that increased BMP signaling results in cognitive impairments, whereas its inhibition improves cognition in hippocampus-dependent learning (Fan et al. 2003; Gobeske et al. 2009).

It will be interesting to assess if inhibiting excessive BMP signaling in aged mice improves cognitive functions that are dependent on hippocampal neurogenesis. It may in general prove beneficial to inhibit BMP signaling in the elderly to enhance neurogenesis and potentially reverse age-induced brain pathologies, for example through systemic administration of small molecule inhibitors. However, the role of systemic BMP inhibition on various aged tissues will need consideration. Furthermore, while inhibiting excessive BMP signaling may promote neurogenesis in the aged, it may prove important to tune the level of signaling in old to that seen in the young, in order to rejuvenate the stem cell niche while preserving the crucial role of BMP signaling in maintaining the stem cell pool. That is, over-inhibition of BMP signaling that was already at physiological young levels has proven detrimental to long-term neurogenesis in young

mice (Mira et al. 2010). In particular, while inhibiting BMP signaling via BMPR1A led to a transient increase in proliferating progenitors in the SGZ of young mice, after a period of time this proliferation decreased due to a depletion of the stem cell pool (Mira et al. 2010).

In addition to BMP signaling, it may be necessary to retune multiple signaling pathways to rescue aged neurogenesis. Several studies have demonstrated that not just one signaling pathway, but a network of highly interactive morphogenic signaling pathways become affected by the aging process in various tissue stem cell compartments, including the brain (Seib et al. 2013; Conboy & Rando 2012; Okamoto et al. 2011; Silva & Conboy 2008). Multiple steps of hippocampal neurogenesis are regulated by many of these same signaling pathways, including Notch, Wnt, Shh, and TGF-β/BMP signaling (Suh et al. 2009; Schwarz et al. 2012). Of these pathways, Wnt signaling, important for neurogenic differentiation (Pozniak & Pleasure 2006), has been demonstrated to decrease with aging in the hippocampus (Okamoto et al. 2011; Miranda et al. 2012; Seib et al. 2013). When upstream or downstream Wnt pathway regulators are modulated, there is a 2 to 3 fold increase in neurogenesis (Seib et al. 2013), similar to the level of increase found in this study upon inhibiting BMP signaling. Therefore, it may be beneficial to simultaneously modulate multiple signaling pathways that are deregulated with age in order to obtain an enhancement of neurogenesis to levels seen in the young.

In summary, this work improves our understanding of the aging of neural stem cells by revealing a key signaling pathway, BMP that becomes deregulated with age. Partial rescue of neurogenesis through acute inhibition of this pathway demonstrates that decline in functionality of neuronal stem cells with age is reversible and can be rescued by the modulation of regulatory signaling in the stem cell microenvironment.

Figure Legends

Figure 1. BMPs Increase with Age Locally in Mice Hippocampi (A) Young (2 month) and old (24 month) mice (n=3) were given daily IP injections of BrdU for 5 days, followed by perfusion and PFA fixation. Immunofluorescence (IF) was performed for Sox2 (green) and BrdU (red), with Dapi (blue) labeling all nuclei. Representative images are shown. Scale bar = 100 μM (B) Quantification of *Bmp2* mRNA expression by qRT-PCR performed on RNA extracted from young and old hippocampi. The relative expression levels were normalized to *GAPDH* and presented relative to that of young hippocampi. Significant differences were identified by Student's t-tests (*$p<0.008$). Error bars indicate standard error of the mean (n=4). (C) qRT-PCR quantification of *Bmp6* mRNA was performed on RNA extracted from young and old hippocampi. The expression levels were normalized to *GAPDH* and presented relative to that of young hippocampi. Significant differences were identified by Student's t-tests (*$p<0.05$). Error bars indicate standard error of the mean (n=5 young, 4 old). (D) Integrated pixel intensity of BMP6 immunofluorescence in young and old dentate gyri tissue sections was calculated using ImageJ. Pixel intensities are presented relative to young dentate gyri. Significant differences were identified by Student's t-tests (*$p<0.003$). Error bars indicate standard error of the mean (n=3 young, 3 old). (E) Immunofluorescence was performed on perfused young and old brain tissue sections (n=3) for Sox2 (green) and BMP6 (red), with Hoechst (blue) labeling all nuclei. Representative low and high magnification images are shown. Scale bar = 50 μM (F) Immunofluorescence was performed on perfused young and old brain tissue sections (n=3), for Sox2 (green) and BMP4 (red), with DAPI (blue) labeling all nuclei. Representative images are shown. Scale bar = 50 μM (G) An ELISA was performed on young and old hippocampal protein

lysate to assess the level of BMP4. Significant differences were identified by Student's t-tests (*$p<0.05$), and error bars indicate standard error of the mean (n=5 young, 5 old).

Figure2. Downstream effectors of BMP Signaling increase with Age in Mice Hippocampi. (A) qRT-PCR quantification of *Smad1* mRNA expression in young and old hippocampi. The relative expression levels were normalized to GAPDH and presented relative to that of young hippocampi. Significant differences were identified by Student's t-tests (*$p<0.01$), and error bars indicate the standard error of the mean (n=3). (B) Immunofluorescence was performed on young and old brain tissue sections (n=4) for pSmad1/5/8 (green) and Sox2 (red), with DAPI (blue) labeling all nuclei. Representative images are shown. Scale bar = 100 μM (C) Representative high magnification images of brain sections stained for pSmad1/5/8 (green) and Sox2 (red), with DAPI (blue) labeling all nuclei. Scale bar = 50 μM (D) Quantification of the percentage of pSmad1/5/8+ Sox2+ neural stem and progenitor cells in the denate gyrus demonstrates an increase with age in BMP signaling to NPCs. Significant differences were identified by Student's t-tests (*$p<0.01$), and error bars indicate the standard deviation (n=4) (E) qRT-PCR quantification of *Id1* mRNA levels in RNA extracted from young and old hippocampi. The relative expression levels were normalized to *GAPDH* and presented relative to that of young hippocampi. Significant differences were identified by Student's t-tests (*$p<0.02$), and error bars indicate the standard error of the mean (n=4).

Figure 3. BMP inhibits neural progenitor cell proliferation. (A) Immunoblotting analysis shows that BMP4 (50 ng/mL) addition for 30 minutes activated its downstream effectors pSmad1/5/8 in NPCs cultured in growth medium (DMF12 + N2 + 10 ng/mL FGF2). Protein loading was normalized to β-actin (B) Functional validation of increasing BMP4. Primary NPCs were cultured in growth medium in the presence or absence of BMP4 (100 ng/mL) for 24 hrs. A 2 hour BrdU (10 μM) pulse was performed before cell fixation to label proliferating cells. Immunofluorescence was performed for BrdU (green) and Sox2 (red), with Hoechst (blue) labeling all nuclei. Representative images are shown. Scale bar = 100 μM (C) Proliferation of NPCs were quantified by cell scoring in 25 random fields of each condition using an automated imager and MetaXpress cell scoring software. Results are displayed as the mean percent of BrdU+ proliferating NPCs +/-SD, respectively. Significant differences were identified by Student's t-tests (*$p< 0.001$), and error bars indicate the standard deviation (n=4). (D) Quantification of *Smad1* mRNA expression by qRT-PCR was performed on RNA extracted from NPCs transduced with shRNA to *Smad1* or control virus and passaged for 2 weeks. The relative cDNA expression level was normalized to *GAPDH* and presented relative to that of mNPCs transduced with *lacZ* shRNA lentivirus. Significant differences were identified by Student's t-tests (*$p<0.05$). Error bars indicate standard deviation (n=3). (E) NPCs were transduced with control or *Smad1* shRNA lentivirus. 72 hours post transduction, cells were cultured for 16 hours in growth medium (containing FGF2) in the presence or absence of BMP4 (200 ng/mL). A 4 hour EdU (30 μM) pulse was performed before cell fixation to label proliferating cells. Immunofluorescence was performed for GFP (green), EdU (red) and Sox2 (gray), with Hoechst (blue) labeling all nuclei. Representative images are shown. Scale bar = 100 μM. (F) Proliferation of NPCs were quantified by cell scoring in 36 random fields of each condition using an automated imager and MetaXpress cell scoring software. Results are displayed as the mean percent of EdU+ proliferating NPCs +/-SD, respectively. Significant differences were identified by Student's t-tests (*$p< 2 x10^{-34}$), and error bars indicate the standard deviation (n=36 technical replicates, with 4 biological replicates per condition).

Figure 4. Rescue of neurogenesis in aged hippocampi by *in vivo* genetic inhibition of pSmad1. (A) Schematic of stereotaxic lentiviral injection experiment. Aged (18 month old) mice received stereotaxic injections into hippocampi (coordinates from bregma: AP: -2.12, ML: +/-1.5, VD: -1.55) of lentiviral vectors delivering either shRNA against *Smad1* or shRNA against *lacZ*. The mice were allowed to recover for 10 days, followed by daily BrdU (50 mg/kg) intraperitonial injections for 5 days. Mice were perfused the morning after the last BrdU injection (Day 5). (B) Brain sections of *lacZ* or *Smad1* shRNA injected mice (n=5 *lacZ* shRNA, 4 *Smad1* shRNA) spanning the entire hippocampus were immunostained with GFP (green), BrdU (red), and Sox2 (gray), with Hoechst (blue) labeling cell nuclei. Representative images are shown. High magnification of immunostaining of the subgranular zone of the dentate gyrus also shown. Scale bars = 50 μM (C) *Smad1* shRNA increases the number of BrdU+Sox2+ cells per GFP+ aged murine dentate gyrus. Significant differences were identified by Student's t-tests (*$p<0.04$). Error bars indicate standard error of the mean (n=5 *lacZ* shRNA, 4 *Smad1* shRNA brains) (D) Quantification of the mean percentage of BrdU+GFP+Sox2+ proliferating NPCs as compared with total GFP+Sox2+ (BrdU+/-) NPCs in shRNA injected brains demonstrates an increase in proliferating neural progenitor cells due to *Smad1* shRNA transduction as compared with *lacZ* shRNA transduced control mice. Significant differences were identified by Student's t-tests *(*$p< 2 \times 10^{-5}$)*. Error bars indicate standard deviation (n=3 mice, with 5 GFP+ hippocampal sections counted per mouse).

Figure 5. Increase in type 2b cell proliferation in aged hippocampi by *in vivo* genetic inhibition of *Smad1*. (A) Schematic of injection experiment. Aged (18 month old) mice received stereotaxic injections into hippocampi (coordinates from bregma: AP: -2.12, ML: +/-1.5, VD: -1.55) of lentiviral vectors delivering either shRNA against *Smad1* or shRNA against *lacZ*. The mice were allowed to recover for 14 days, followed by daily EdU (50 mg/kg) intraperitonial injections for 5 days. Five days after the last EdU injection, mice were saline and 4% PFA perfused. (B) Brain sections of *lacZ* or *Smad1* shRNA injected mice (n=3 *lacZ* shRNA, 5 *Smad1* shRNA) spanning the entire hippocampus were immunostained with GFP (green), EdU (red) and DCX (gray), with Hoechst (blue) labeling cell nuclei. Representative images are shown, as well as high magnification representative images. Scale bar = 50 μM (C) *Smad1* shRNA increases the number of EdU+DCX+GFP+ cells in aged murine dentate gyri. Significant differences were identified by Student's t-tests (*$p<0.0002$). Error bars indicate standard error of the mean (n=3 *lacZ* shRNA, 5 *Smad1* shRNA).

Figure 6. Rescue of Neurogenesis in aged hippocampi by *in vivo* Cre-mediated BMPR1A deletion. (A) Schematic of stereotaxic lentiviral injection experiment. Aged (18-22 month old) $BMPR1A^{lox/lox}$ $BMPR1B^{+/-}$ Rosa26lacZ mice received stereotaxic injections into hippocampi (coordinates from bregma: AP: -2.12, ML: +/-1.5, VD: -1.55) of lentiviral vectors delivering either Cre-mCherry or GFP. The mice were allowed to recover for 14 days, followed by daily BrdU (50 mg/kg) intraperitonial injections for 5 days. Mice were saline and PFA perfused the morning after the last BrdU injection (Day 5). (B) Brain sections of Cre or GFP injected mice were immunostained with βgal (green), GFP/mCherry (red) and Sox2 (gray), with Hoechst (blue) labeling cell nuclei. βgal is positive only in $BMPR1A^{lox/lox}$ $BMPR1B^{+/-}$ Rosa26lacZ brains injected with Cre, demonstrating BMPR1A deletion. Representative images are shown. Scale bar = 50 μM (C) Brain sections of Cre or GFP injected mice (n=5) spanning the entire hippocampus were immunostained with BrdU (green), GFP/mCherry (red) and Sox2 (gray), with Hoechst (blue) labeling cell nuclei. Representative images are shown. Scale bar = 50 μM (D) High

magnification of immunostaining of the subgranular zone of the dentate gyrus, with GFP/mCherry (green), BrdU (red), and Sox2 (gray), with Hoechst (blue) labeling cell nuclei. Scale bar = 50 μM (E) Cre-mediated BMPR1A deletion increases the number of BrdU+Sox2+ cells in aged murine dentate gyri. Significant differences were identified by Student's t-tests (*$p<0.04$). Error bars indicate standard error of the mean (n=5 per group). (F) Quantification of the mean percentage of BrdU+GFP/mCherry+Sox2+ proliferating NPCs as compared with total GFP+/mCherry+Sox2+ NPCs in shRNA injected brains demonstrates an increase in proliferating neural progenitor cells due to Cre-induced recombination as compared with GFP transduced control mice. Significant differences were identified by Student's t-tests *(*$p< 9 \times 10^{-10}$)*. Error bars indicate standard deviation (n=3 mice, with 5 GFP+ or mCherry+ hippocampal sections counted per mouse).

Figure 7. Increase in type 2b cell proliferation in aged hippocampi by *in vivo* Cre-mediated BMPR1A deletion. (A) Schematic of stereotaxic lentiviral vector injection experiment. Aged (18-22 month old) BMPR1A$^{lox/lox}$ BMPR1B$^{+/-}$ Rosa26lacZ mice received stereotaxic injections into hippocampi (coordinates from bregma: AP: -2.12, ML: +/-1.5, VD: -1.55) of lentiviral vectors encoding either Cre-GFP or GFP. The mice were allowed to recover for 14 days, followed by daily EdU (50 mg/kg) intraperitonial injections for 5 days. Mice were saline and PFA perfused 5 days after the last EdU injection (Day 10). (B) Brain sections of Cre or GFP injected mice (n=5) spanning the entire hippocampus were immunostained with GFP (green), EdU (red), and DCX (gray), with Hoechst (blue) labeling cell nuclei. Representative images are shown alongside high magnification representative images. Scale bars = 50 μM (C) Cre-induced deletion of BMPR1A increases the number of EdU+/DCX+ cells in GFP+ aged murine dentate gyri. Significant differences were identified by Student's t-tests (*$p<0.03$). Error bars indicate standard error of the mean (n=5) (D) Quantification of the mean percentage of EdU+GFP+DCX+ proliferating cells as compared to total GFP+DCX+ cells in Cre-GFP verse GFP injected brains demonstrates an increase in proliferating neuronally committed cells due to Cre-induced deletion of BMPR1A as compared with control mice. Significant differences were identified by Student's t-tests (*$p<0.006$). Error bars indicate standard deviation (n=3 mice per group, with 6 GFP+ hippocampal sections counted per mouse).

Supplementary Figure 1. BMP4 is secreted by endothelial cells. (A) Immunofluorescence was performed on perfused old brain tissue sections for BMP4 (green), CD31 (red), and Iba1 (gray), with Hoechst (blue) labeling all nuclei. Representative low and high magnification images are shown. (B) Immunofluorescence was performed on perfused young brain tissue sections for BMP4 (green), CD31 (red), and Iba1 (gray), with Hoechst (blue) labeling all nuclei. Representative images are shown.

Supplementary Figure 2. BMP6 is secreted by microglia. (A) Immunofluorescence was performed on perfused old brain tissue sections for BMP6 (green), Iba1 (red), and GFAP (gray), with Hoechst (blue) labeling all nuclei. Representative low and high magnification images are shown. (B) Immunofluorescence was performed on perfused young brain tissue sections for BMP6 (green), Iba1 (red), and GFAP (gray), with Hoechst (blue) labeling all nuclei. Representative low and high magnification images are shown. (C) Immunofluorescence was performed on perfused young brain tissue sections for BMP6 (green), and CD31 (red), with Hoechst (blue) labeling all nuclei. Representative low and high magnification images are shown and indicate there is no colocalization of BMP6 with endothelium.

Author Contributions

HY produced and assessed all viral particles, designed, performed and analyzed the experiments for Figures 1-7 and Suppl. 1-2, interpreted these data and co-wrote the manuscript; AM performed and analyzed experiments for Figures 4-7; CS performed and analyzed experiments for Figures 4,6,and 7; LB cloned Smad1 shRNA constructs; IMC participated in the design and interpretation of the experiments and edited the manuscript; DVS designed, directed and integrated the study, interpreted the data and co-wrote the manuscript.

References

Ashton, R.S. et al., 2012. Astrocytes regulate adult hippocampal neurogenesis through ephrin-B signaling. *Nature neuroscience*, 15(10), pp.1399–406. Available at: http://www.pubmedcentral.nih.gov/articlerender.fcgi?artid=3458152&tool=pmcentrez&rendertype=abstract [Accessed October 22, 2013].

Babu, H. et al., 2011. A protocol for isolation and enriched monolayer cultivation of neural precursor cells from mouse dentate gyrus. *Frontiers in neuroscience*, 5(July), p.89. Available at: http://www.pubmedcentral.nih.gov/articlerender.fcgi?artid=3140691&tool=pmcentrez&rendertype=abstract [Accessed October 28, 2013].

Basak, O. & Taylor, V., 2009. Stem cells of the adult mammalian brain and their niche. *Cellular and molecular life sciences : CMLS*, 66(6), pp.1057–72. Available at: http://www.ncbi.nlm.nih.gov/pubmed/19011753 [Accessed December 1, 2013].

Beets, K. et al., 2013. Robustness in angiogenesis: Notch and BMP shaping waves. *Trends in genetics : TIG*, 29(3), pp.140–149. Available at: http://linkinghub.elsevier.com/retrieve/pii/S0168952512001928.

Bergmann, O. et al., 2012. The Age of Olfactory Bulb Neurons in Humans. *Neuron*, 74(4), pp.634–639. Available at: http://linkinghub.elsevier.com/retrieve/pii/S0896627312003418.

Bonaguidi, M. a et al., 2005. LIF and BMP signaling generate separate and discrete types of GFAP-expressing cells. *Development (Cambridge, England)*, 132(24), pp.5503–14. Available at: http://www.ncbi.nlm.nih.gov/pubmed/16314487 [Accessed October 18, 2013].

Bonaguidi, M. a et al., 2008. Noggin expands neural stem cells in the adult hippocampus. *The Journal of neuroscience : the official journal of the Society for Neuroscience*, 28(37), pp.9194–204. Available at: http://www.pubmedcentral.nih.gov/articlerender.fcgi?artid=3651371&tool=pmcentrez&rendertype=abstract [Accessed October 28, 2013].

Bond, A.M., Bhalala, O.G. & Kessler, J. a, 2012. The dynamic role of bone morphogenetic proteins in neural stem cell fate and maturation. *Developmental neurobiology*, 72(7), pp.1068–84. Available at:

http://www.pubmedcentral.nih.gov/articlerender.fcgi?artid=3773925&tool=pmcentrez&rendertype=abstract [Accessed October 22, 2013].

Chen, D., Zhao, M. & Mundy, G.R., 2004. Bone Morphogenetic Proteins. *Growth Factors*, 22(4), pp.233–241. Available at: http://dx.doi.org/10.1080/08977190412331279890.

Conboy, I.M. & Rando, T.A., 2012. Heterochronic parabiosis for the study of the effects of aging on stem cells and their niche. *Cell Cycle*, 11(12), pp.2260–2267.

Crews, L. et al., 2010. Increased BMP6 levels in the brains of Alzheimer's disease patients and APP transgenic mice are accompanied by impaired neurogenesis. *The Journal of neuroscience : the official journal of the Society for Neuroscience*, 30(37), pp.12252–62. Available at: http://www.pubmedcentral.nih.gov/articlerender.fcgi?artid=2978735&tool=pmcentrez&rendertype=abstract [Accessed October 29, 2013].

Deng, W. et al., 2009. Adult-born hippocampal dentate granule cells undergoing maturation modulate learning and memory in the brain. *The Journal of neuroscience : the official journal of the Society for Neuroscience*, 29(43), pp.13532–42. Available at: http://www.pubmedcentral.nih.gov/articlerender.fcgi?artid=2787190&tool=pmcentrez&rendertype=abstract [Accessed October 20, 2013].

Deng, W., Aimone, J.B. & Gage, F.H., 2010. New neurons and new memories: how does adult hippocampal neurogenesis affect learning and memory? *Nat Rev Neurosci*, 11(5), pp.339–350. Available at: http://dx.doi.org/10.1038/nrn2822.

Eriksson, P.S. et al., 1998. Neurogenesis in the adult human hippocampus. *Nature medicine*, 4(11), pp.1313–7. Available at: http://www.ncbi.nlm.nih.gov/pubmed/19714567.

Fan, X.-T. et al., 2003. Effect of antisense oligonucleotide of noggin on spatial learning and memory of rats. *Acta pharmacologica Sinica*, 24(5), pp.394–7. Available at: http://www.ncbi.nlm.nih.gov/pubmed/12740172.

Gobeske, K.T. et al., 2009. BMP signaling mediates effects of exercise on hippocampal neurogenesis and cognition in mice. *PloS one*, 4(10), p.e7506. Available at: http://www.pubmedcentral.nih.gov/articlerender.fcgi?artid=2759555&tool=pmcentrez&rendertype=abstract [Accessed October 24, 2013].

Kuhn, H.G., Dickinson-Anson, H. & Gage, F.H., 1996. Neurogenesis in the Dentate Gyrus of the Adult Decrease of Neuronal Progenitor Proliferation Rat : Age-Related. , 76(6), pp.2027–2033.

Lai, K. et al., 2003. Sonic hedgehog regulates adult neural progenitor proliferation in vitro and in vivo. *Nature neuroscience*, 6(1), pp.21–7. Available at: http://www.ncbi.nlm.nih.gov/pubmed/12469128 [Accessed October 28, 2013].

Lein, E.S. et al., 2007. Genome-wide atlas of gene expression in the adult mouse brain. *Nature*, 445(7124), pp.168–176. Available at: http://dx.doi.org/10.1038/nature05453.

Li, D. et al., 2008. Decreased hippocampal cell proliferation correlates with increased expression of BMP4 in the APPswe/PS1ΔE9 mouse model of Alzheimer's disease. *Hippocampus*, 18(7), pp.692–698. Available at: http://dx.doi.org/10.1002/hipo.20428.

Lim, D.A. et al., 2000. Noggin Antagonizes BMP Signaling to Create a Niche for Adult Neurogenesis. *Neuron*, 28(3), pp.713–726. Available at: http://linkinghub.elsevier.com/retrieve/pii/S0896627300001483.

Livak, K.J. & Schmittgen, T.D., 2001. Analysis of Relative Gene Expression Data Using Real-Time Quantitative PCR and the 2−ΔΔCT Method. *Methods*, 25(4), pp.402–408. Available at: http://www.sciencedirect.com/science/article/pii/S1046202301912629.

Lois, C. et al., 2002. Germline Transmission and Tissue-Specific Expression of Transgenes Delivered by Lentiviral Vectors. *Science* , 295 (5556), pp.868–872. Available at: http://www.sciencemag.org/content/295/5556/868.abstract.

Maslov, A.Y. et al., 2004. Neural stem cell detection, characterization, and age-related changes in the subventricular zone of mice. *The Journal of neuroscience : the official journal of the Society for Neuroscience*, 24(7), pp.1726–33. Available at: http://www.ncbi.nlm.nih.gov/pubmed/14973255 [Accessed October 26, 2013].

Massagué, J., 2012. TGFβ signalling in context. *Nature reviews. Molecular cell biology*, 13(10), pp.616–30. Available at: http://www.ncbi.nlm.nih.gov/pubmed/22992590 [Accessed October 17, 2013].

Ming, G. & Song, H., 2005. Adult neurogenesis in the mammalian central nervous system. *Annual review of neuroscience*, 28, pp.223–50. Available at: http://www.ncbi.nlm.nih.gov/pubmed/16022595 [Accessed October 17, 2013].

Mira, H. et al., 2010. Signaling through BMPR-IA regulates quiescence and long-term activity of neural stem cells in the adult hippocampus. *Cell stem cell*, 7(1), pp.78–89. Available at: http://www.ncbi.nlm.nih.gov/pubmed/20621052 [Accessed October 25, 2013].

Miranda, C.J. et al., 2012. Aging brain microenvironment decreases hippocampal neurogenesis through Wnt-mediated survivin signaling. *Aging cell*, 11(3), pp.542–52. Available at: http://www.pubmedcentral.nih.gov/articlerender.fcgi?artid=3350615&tool=pmcentrez&rendertype=abstract [Accessed October 26, 2013].

Nakashima, K. et al., 2001. BMP2-mediated alteration in the developmental pathway of fetal mouse brain cells from neurogenesis to astrocytogenesis. *Proceedings of the National Academy of Sciences of the United States of America*, 98(10), pp.5868–73. Available at: http://www.pubmedcentral.nih.gov/articlerender.fcgi?artid=33305&tool=pmcentrez&rendertype=abstract.

Oboti, L. et al., 2009. Integration and sensory experience-dependent survival of newly-generated neurons in the accessory olfactory bulb of female mice. *European Journal of Neuroscience*, 29(4), pp.679–692. Available at: http://dx.doi.org/10.1111/j.1460-9568.2009.06614.x.

Okamoto, M. et al., 2011. Reduction in paracrine Wnt3 factors during aging causes impaired adult neurogenesis. *FASEB journal : official publication of the Federation of American Societies for Experimental Biology*, 25(10), pp.3570–82. Available at: http://www.ncbi.nlm.nih.gov/pubmed/21746862 [Accessed October 26, 2013].

Olariu, A.N.A., Cleaver, K.M. & Cameron, H.A., 2007. Decreased Neurogenesis in Aged Rats Results from Loss of Granule Cell Cell Cycle. , 667(October 2006), pp.659–667.

Oshimori, N. & Fuchs, E., 2012. The harmonies played by TGF-β in stem cell biology. *Cell stem cell*, 11(6), pp.751–64. Available at: http://www.ncbi.nlm.nih.gov/pubmed/23217421 [Accessed October 26, 2013].

Peltier, J. & Schaffer, D., 2010. Viral Packaging and Transduction of Adult Hippocampal Neural Progenitors. In I. M. Conboy et al., eds. *Protocols for Adult Stem Cells SE - 7*. Humana Press, pp. 103–116. Available at: http://dx.doi.org/10.1007/978-1-60761-063-2_7.

Pineda, J.R. et al., 2013. Vascular-derived TGF-β increases in the stem cell niche and perturbs neurogenesis during aging and following irradiation in the adult mouse brain. *EMBO molecular medicine*, 5(4), pp.548–62. Available at: http://www.pubmedcentral.nih.gov/articlerender.fcgi?artid=3628106&tool=pmcentrez&rendertype=abstract [Accessed November 10, 2013].

Porlan, E. et al., 2013. Transcriptional repression of Bmp2 by p21Waf1/Cip1 links quiescence to neural stem cell maintenance. *Nat Neurosci*, 16(11), pp.1567–1575. Available at: http://dx.doi.org/10.1038/nn.3545.

Pozniak, C.D. & Pleasure, S.J., 2006. A tale of two signals: Wnt and Hedgehog in dentate neurogenesis. *Science's STKE : signal transduction knowledge environment*, 2006(319), p.pe5. Available at: http://www.ncbi.nlm.nih.gov/pubmed/16434726 [Accessed October 29, 2013].

Ross, S.E., Greenberg, M.E. & Stiles, C.D., 2003. Basic Helix-Loop-Helix Factors in Cortical Development. *Neuron*, 39(1), pp.13–25. Available at: http://linkinghub.elsevier.com/retrieve/pii/S0896627303003659.

Schwarz, T.J., Ebert, B. & Lie, D.C., 2012. Stem cell maintenance in the adult mammalian hippocampus: a matter of signal integration? *Developmental neurobiology*, 72(7), pp.1006–15. Available at: http://www.ncbi.nlm.nih.gov/pubmed/22488809 [Accessed October 29, 2013].

Seib, D.R.M. et al., 2013. Loss of Dickkopf-1 restores neurogenesis in old age and counteracts cognitive decline. *Cell stem cell*, 12(2), pp.204–14. Available at: http://www.ncbi.nlm.nih.gov/pubmed/23395445 [Accessed October 24, 2013].

Silva, H. & Conboy, I.M., 2008. Aging and stem cell renewal. In *StemBook*. pp. 1–14. Available at: http://www.stembook.org/node/459 [Accessed October 29, 2013].

Spalding, K.L. et al., 2013. Dynamics of Hippocampal Neurogenesis in Adult Humans. *Cell*, 153(6), pp.1219–1227. Available at: http://linkinghub.elsevier.com/retrieve/pii/S0092867413005333.

Suh, H., Deng, W. & Gage, F.H., 2009. Signaling in adult neurogenesis. *Annual review of cell and developmental biology*, 25, pp.253–75. Available at: http://www.ncbi.nlm.nih.gov/pubmed/19575663 [Accessed October 29, 2013].

Tang, J. et al., 2009. Noggin and BMP4 co-modulate adult hippocampal neurogenesis in the APPswe/PS1ΔE9 transgenic mouse model of Alzheimer's disease. *Biochemical and Biophysical Research Communications*, 385(3), pp.341–345. Available at: http://www.sciencedirect.com/science/article/pii/S0006291X09009991.

Villeda, S. a et al., 2011. The ageing systemic milieu negatively regulates neurogenesis and cognitive function. *Nature*, 477(7362), pp.90–4. Available at: http://www.pubmedcentral.nih.gov/articlerender.fcgi?artid=3170097&tool=pmcentrez&rendertype=abstract [Accessed October 20, 2013].

Vukovic, J. et al., 2012. Microglia modulate hippocampal neural precursor activity in response to exercise and aging. *The Journal of neuroscience : the official journal of the Society for Neuroscience*, 32(19), pp.6435–43. Available at: http://www.ncbi.nlm.nih.gov/pubmed/22573666 [Accessed October 25, 2013].

Walter, J. et al., 2011. Age-related effects on hippocampal precursor cell subpopulations and neurogenesis. *Neurobiology of aging*, 32(10), pp.1906–14. Available at: http://www.ncbi.nlm.nih.gov/pubmed/20006411 [Accessed October 26, 2013].

Yu, J.H. & Schaffer, D. V, 2006. High-throughput, library-based selection of a murine leukemia virus variant to infect nondividing cells. *Journal of virology*, 80(18), pp.8981–8. Available at: http://www.pubmedcentral.nih.gov/articlerender.fcgi?artid=1563944&tool=pmcentrez&rendertype=abstract [Accessed October 28, 2013].

Table 1

	shRNA and qPCR Primer Sequences
shRNA Smad 1.1	5'-GCCCATTTGGTTCCAAGCAGAACTCTTCAAGAGAGAGTTCTGCTTGGAACCAAATGGGCTTTTT-3'
shRNA Smad 1.2	5'-GTCCTATTTCATCCGTGTCTTACTCTTCAAGAGAGAGTAAGACACGGATGAAATAGGACTTTTT-3'
shRNA Smad 1.3	5'-GTGGTGCTCTATTGTGTACTATCTCTTCAAGAGAGAGATAGTACACAATAGAGCACCACTTTTT-3'
shRNA Smad 1.4	5'-GCATTTGGTTCCAAGCAGAATTCAAGAGATTCTGCTTGGAACCAAATGCTTTTT-3'
shRNA Smad 1.5	5'-GTCCTATTTCATCCGTGTCTTTCAAGAGAAGACACGGATGAAATAGGACTTTTT-3'
shRNA lacZ	Sense: 5'-GGGGTTAATTAAAAGGTCGGGCAGGAAGAGGGC-3' Antisense: 5'-GGGGTTAATTAAAAAAAGTGACCAGCGAATACCTGTTCTC-3'
Bmp6	F: 5'-AAC CTG GTG GAG TAC GAC AA-3'; R: 5'-CGG GTG TCC AAC AAA AAT AG -3'
Bmp2	F: 5'-TTG CAC ACT TGC TGT CTG TT-3'; R: 5'-GTT CTC ACG GAT TGG ACA AC -3'
Id1	F: 5' GTC CAG TGG GTA GAG GGT TT-3'; R: 5-GAG AAG CAC GAA ATG TGA CC-3'
Smad1	F:5'- GAT GGA CAA GTC AGA CAG GAT GG -3'; R: 5'-TGT CCC TGG CTT GGC CAT CTC-3'
GapDH	F: 5'-CTGGAGAAACCTGCCAAGTA-3' R: 5'-TGTTGCTGTAGCCGTATTCA-3'

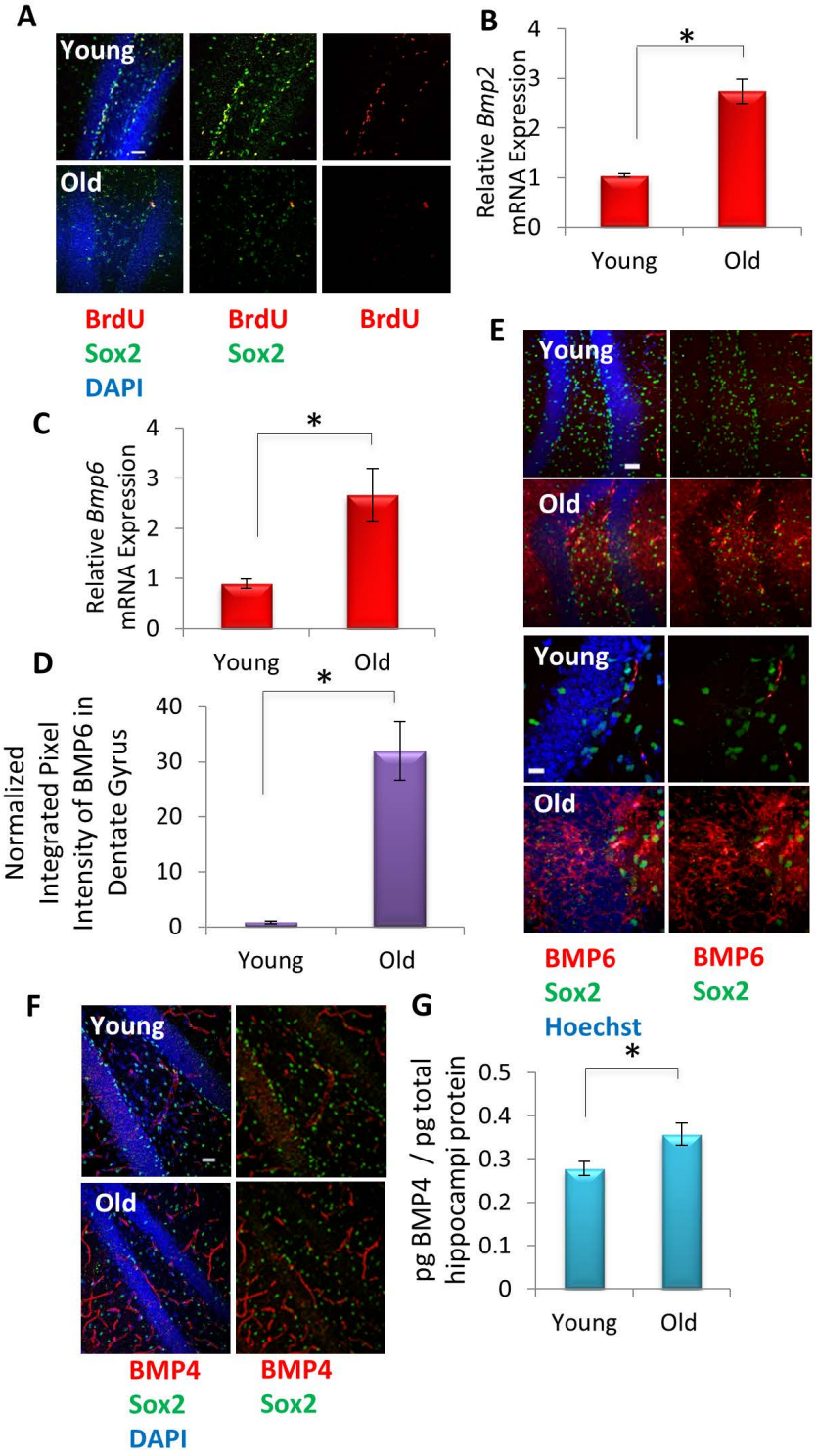
A
Young
Old
BrdU
Sox2
DAPI
BrdU
Sox2
BrdU
B
Relative Bmp2 mRNA Expression
Young
Old
C
Relative Bmp6 mRNA Expression
Young
Old
D
Normalized Integrated Pixel Intensity of BMP6 in Dentate Gyrus
Young
Old
E
Young
Old
Young
Old
BMP6
Sox2
Hoechst
BMP6
Sox2
F
Young
Old
BMP4
Sox2
DAPI
BMP4
Sox2
G
pg BMP4 / pg total hippocampi protein
Young
Old

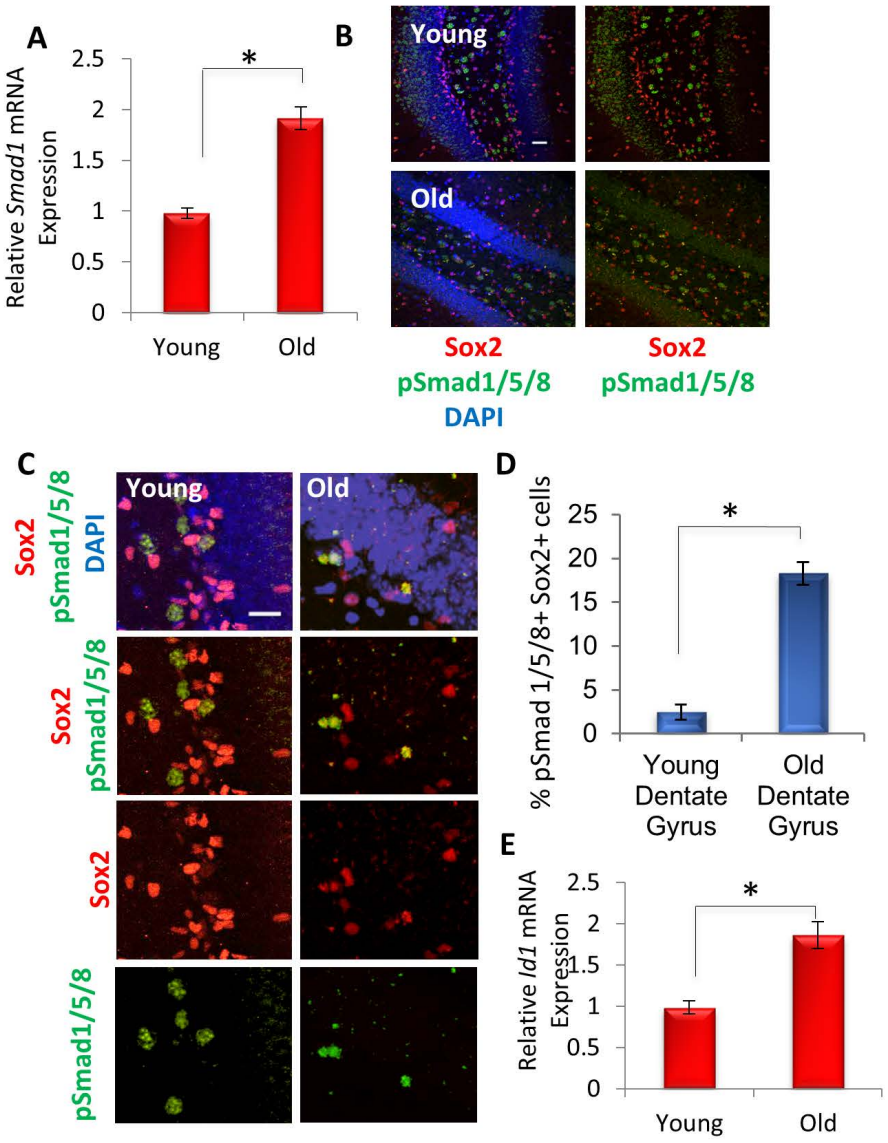
A
B
Relative Smad1 mRNA Expression
2.5
2
1.5
1
0.5
0
*
Young
Old
Young
Old
Sox2
pSmad1/5/8
DAPI
Sox2
pSmad1/5/8
C
D
E
Sox2
pSmad1/5/8
DAPI
Young
Old
Sox2
pSmad1/5/8
Sox2
pSmad1/5/8
% pSmad 1/5/8+ Sox2+ cells
25
20
15
10
5
0
*
Young Dentate Gyrus
Old Dentate Gyrus
Relative Id1 mRNA Expression
2.5
2
1.5
1
0.5
0
*
Young
Old

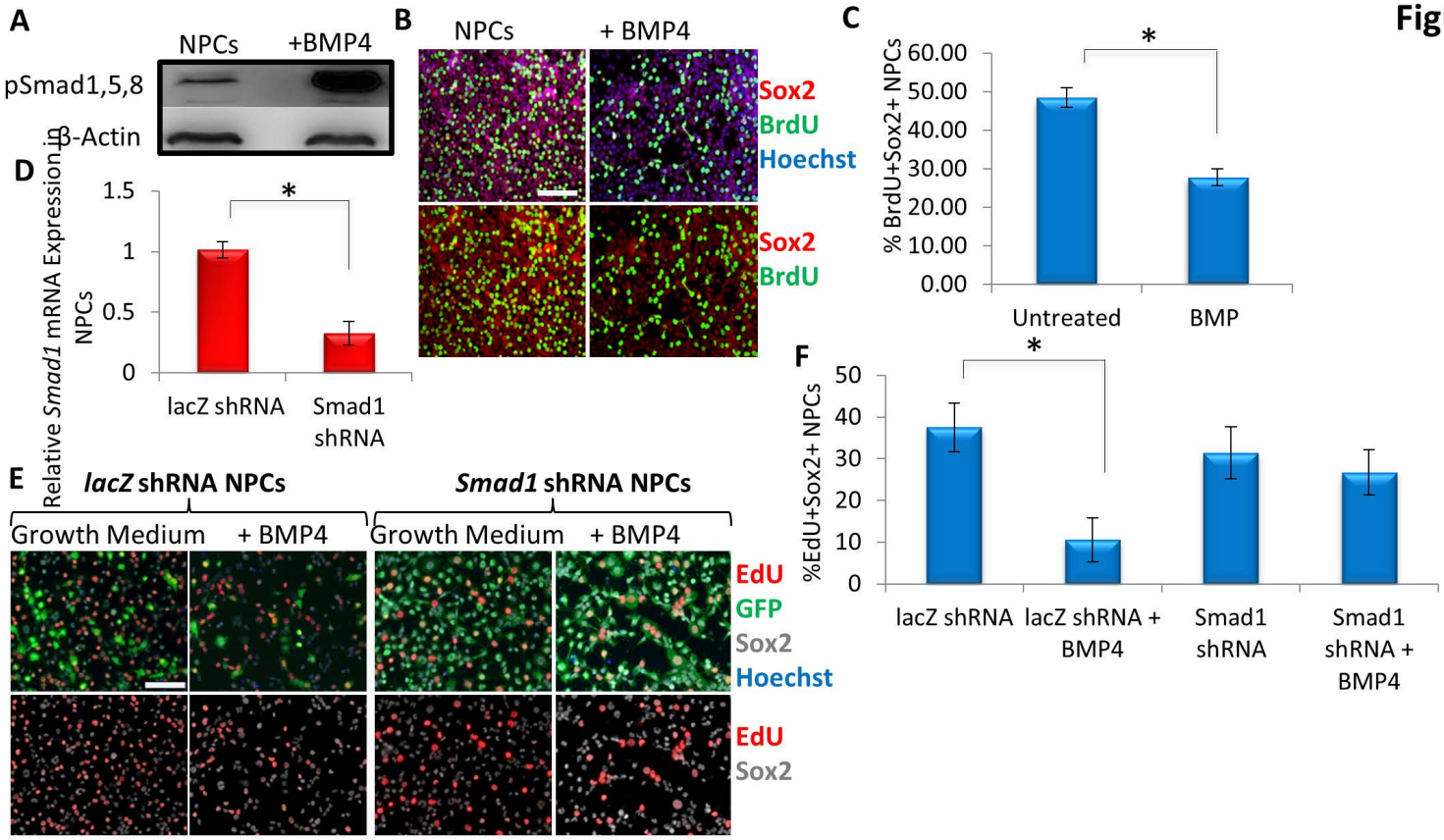
A
NPCs
+BMP4
pSmad1,5,8
β-Actin
B
NPCs
+ BMP4
Sox2
BrdU
Hoechst
Sox2
BrdU
C
% BrdU+Sox2+ NPCs
60.00
50.00
40.00
30.00
20.00
10.00
0.00
*
Untreated
BMP
D
Relative Smad1 mRNA Expression in NPCs
1.5
1
0.5
0
*
lacZ shRNA
Smad1 shRNA
E
lacZ shRNA NPCs
Smad1 shRNA NPCs
Growth Medium
+ BMP4
Growth Medium
+ BMP4
EdU
GFP
Sox2
Hoechst
EdU
Sox2
F
%EdU+Sox2+ NPCs
50
40
30
20
10
0
*
lacZ shRNA
lacZ shRNA + BMP4
Smad1 shRNA
Smad1 shRNA + BMP4

Figure 3

Figure 4

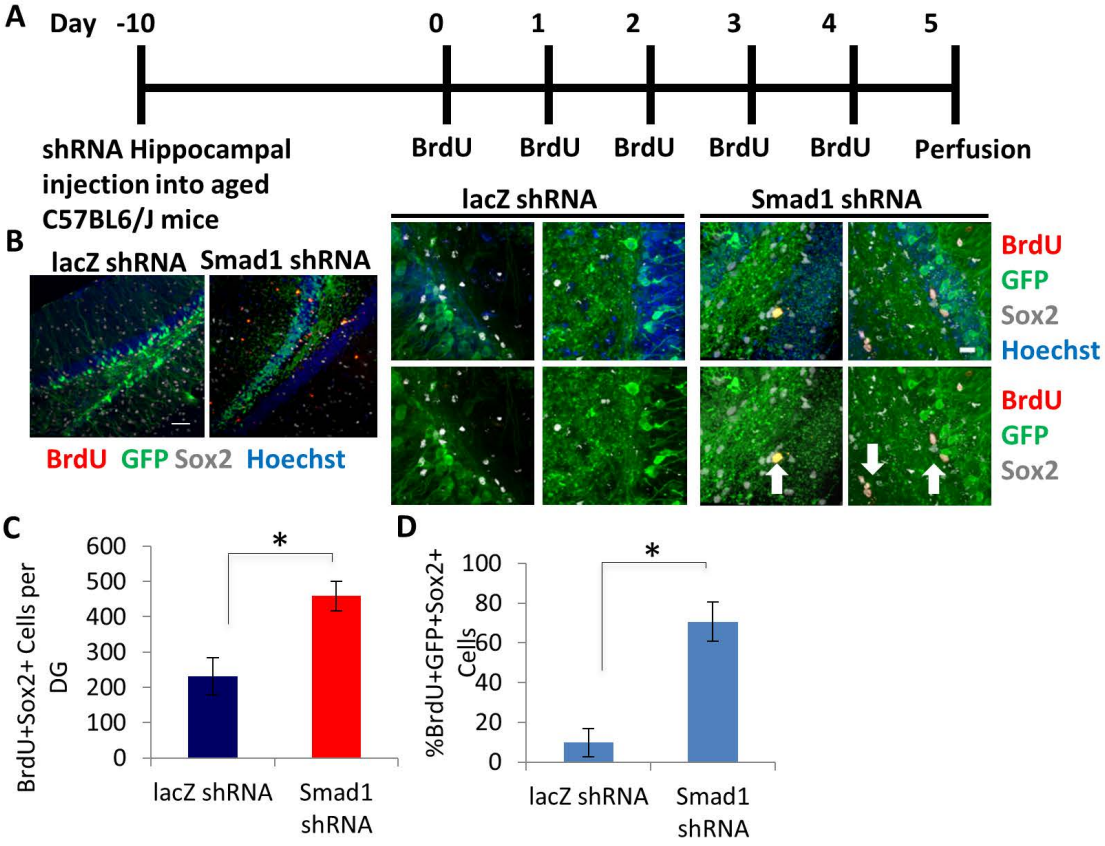
A
Day -10
0
1
2
3
4
5
shRNA Hippocampal injection into aged C57BL6/J mice
BrdU
BrdU
BrdU
BrdU
BrdU
Perfusion
B
lacZ shRNA
Smad1 shRNA
BrdU GFP Sox2 Hoechst
lacZ shRNA
Smad1 shRNA
BrdU
GFP
Sox2
Hoechst
BrdU
GFP
Sox2
C
BrdU+Sox2+ Cells per DG
600
500
400
300
200
100
0
*
lacZ shRNA
Smad1 shRNA
D
%BrdU+GFP+Sox2+ Cells
100
80
60
40
20
0
*
lacZ shRNA
Smad1 shRNA

Figure 5

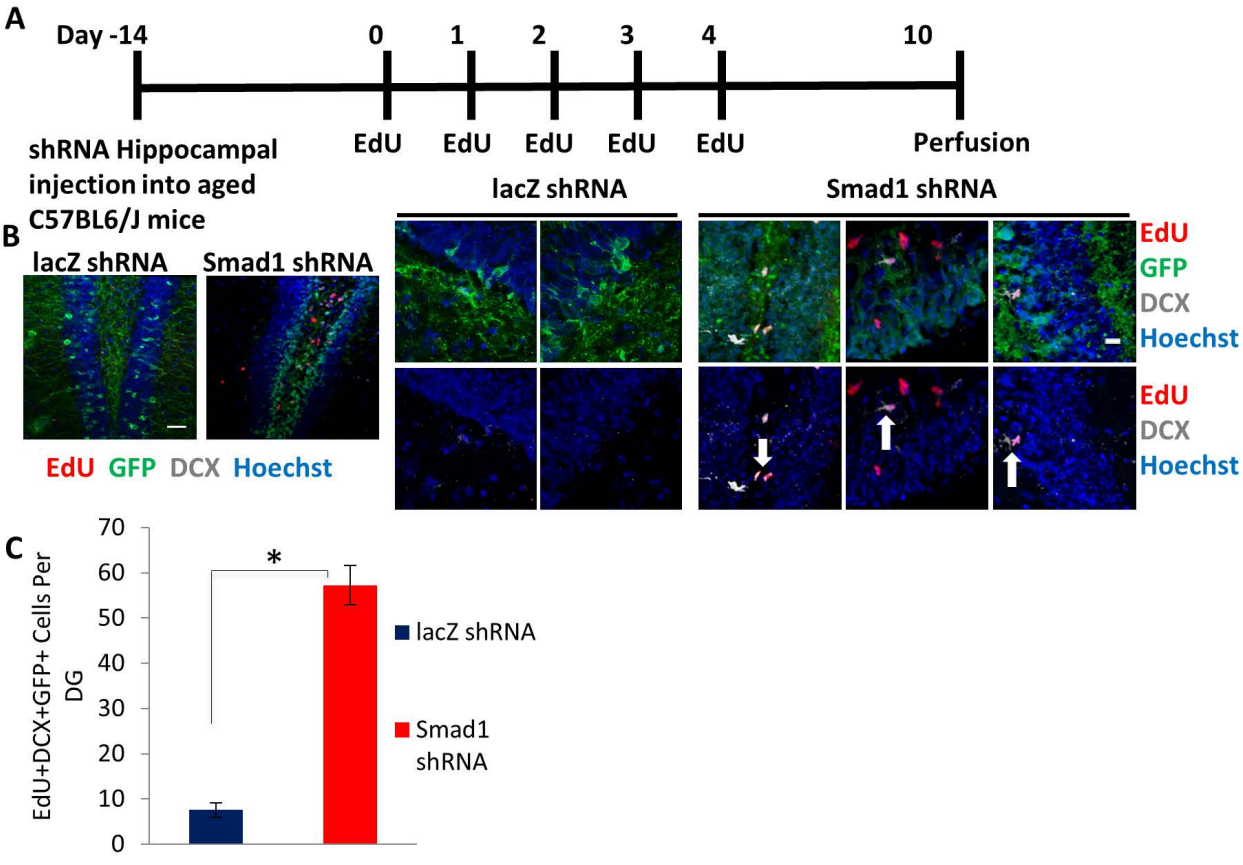
A
Day -14
0
1
2
3
4
10
shRNA Hippocampal injection into aged C57BL6/J mice
EdU
EdU
EdU
EdU
EdU
Perfusion
B
lacZ shRNA
Smad1 shRNA
EdU GFP DCX Hoechst
lacZ shRNA
Smad1 shRNA
EdU
GFP
DCX
Hoechst
EdU
DCX
Hoechst
C
EdU+DCX+GFP+ Cells Per DG
70
60
50
40
30
20
10
0
*
lacZ shRNA
Smad1 shRNA

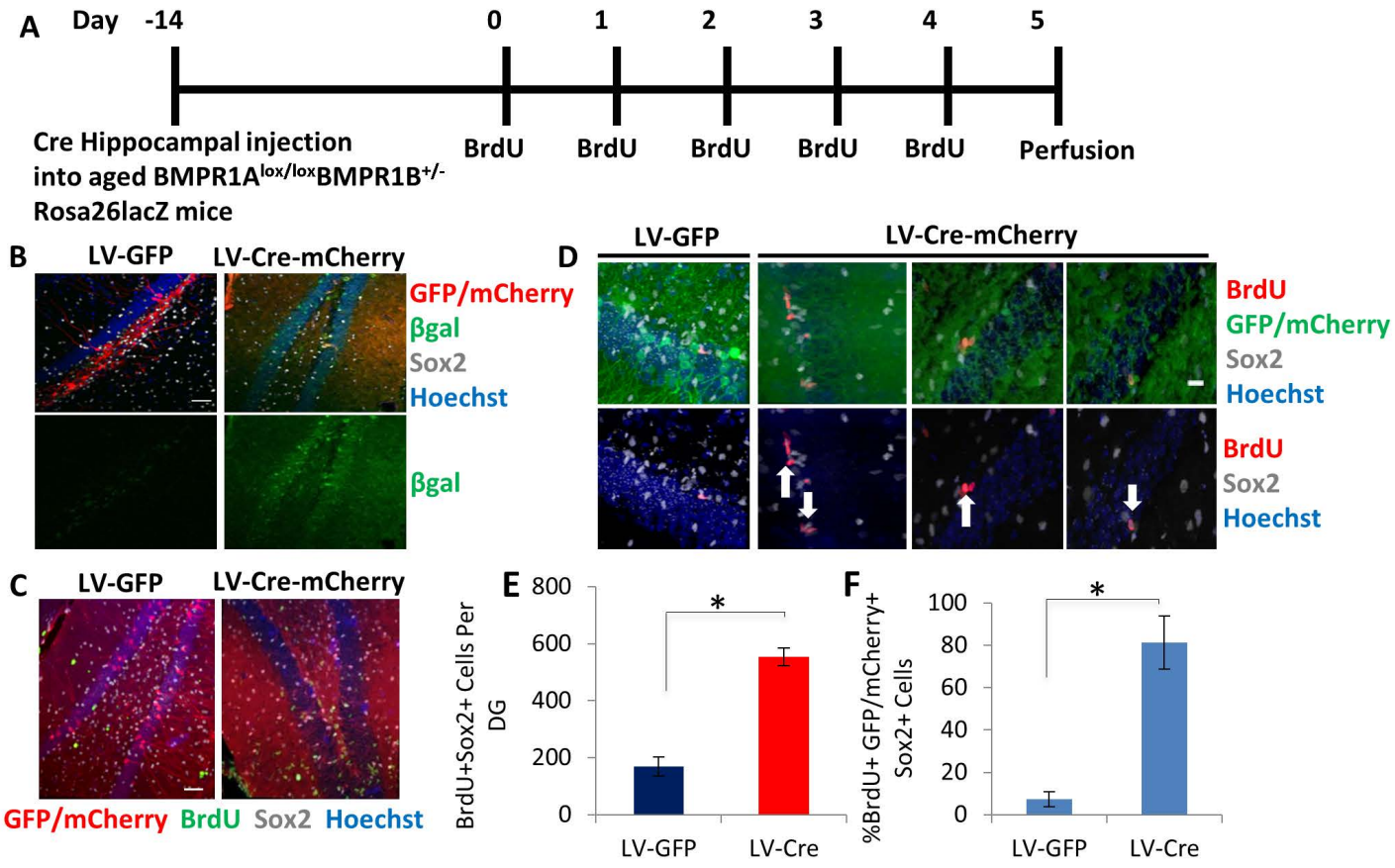
A
Day -14
0
1
2
3
4
5
Cre Hippocampal injection into aged BMPR1A$^{lox/lox}$BMPR1B$^{+/-}$ Rosa26lacZ mice
BrdU
BrdU
BrdU
BrdU
BrdU
Perfusion
B
LV-GFP
LV-Cre-mCherry
GFP/mCherry
βgal
Sox2
Hoechst
βgal
C
LV-GFP
LV-Cre-mCherry
GFP/mCherry BrdU Sox2 Hoechst
D
LV-GFP
LV-Cre-mCherry
BrdU
GFP/mCherry
Sox2
Hoechst
BrdU
Sox2
Hoechst
E
BrdU+Sox2+ Cells Per DG
800
600
400
200
0
*
LV-GFP
LV-Cre
F
%BrdU+ GFP/mCherry+ Sox2+ Cells
100
80
60
40
20
0
*
LV-GFP
LV-Cre

Figure 7

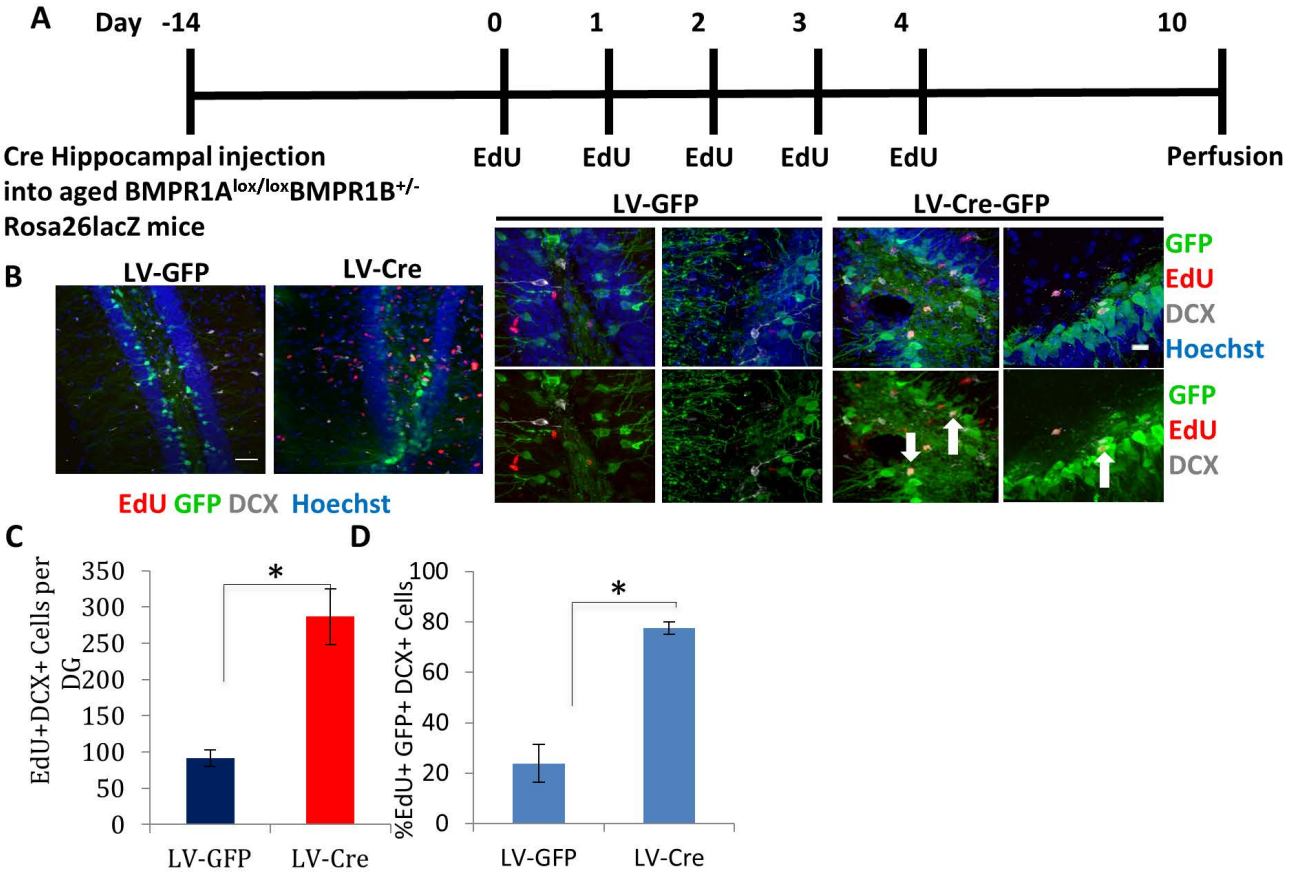
A
Day -14
0
1
2
3
4
10
Cre Hippocampal injection into aged BMPR1A lox/lox BMPR1B +/- Rosa26lacZ mice
EdU
EdU
EdU
EdU
EdU
Perfusion
B
LV-GFP
LV-Cre
EdU GFP DCX Hoechst
LV-GFP
LV-Cre-GFP
GFP
EdU
DCX
Hoechst
GFP
EdU
DCX
C
EdU+DCX+ Cells per DG
350
300
250
200
150
100
50
0
*
LV-GFP
LV-Cre
D
%EdU+ GFP+ DCX+ Cells
100
80
60
40
20
0
*
LV-GFP
LV-Cre

Source of BMP4 secretion

A

Endothelial Cells

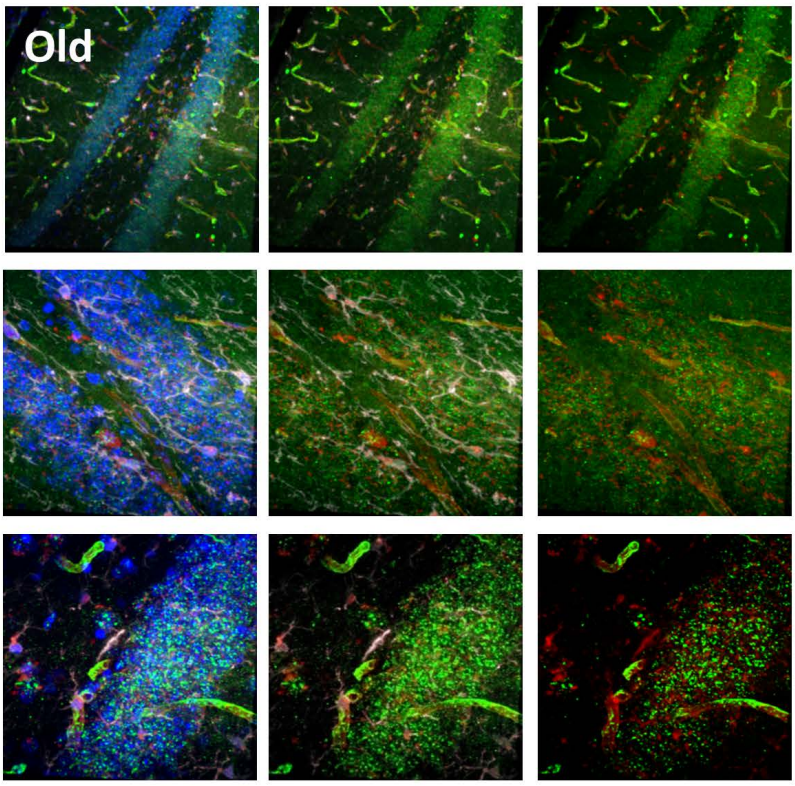

B

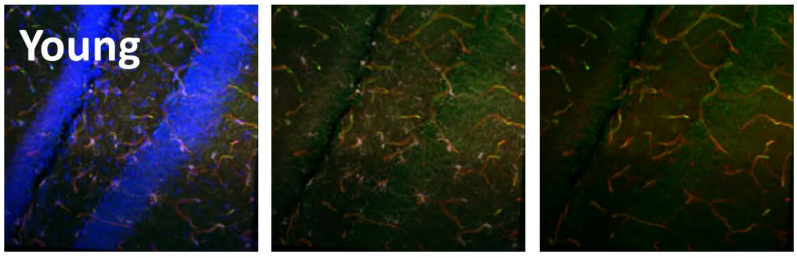

Source of BMP6 secretion

Supplementary Figure 2

Microglia

A

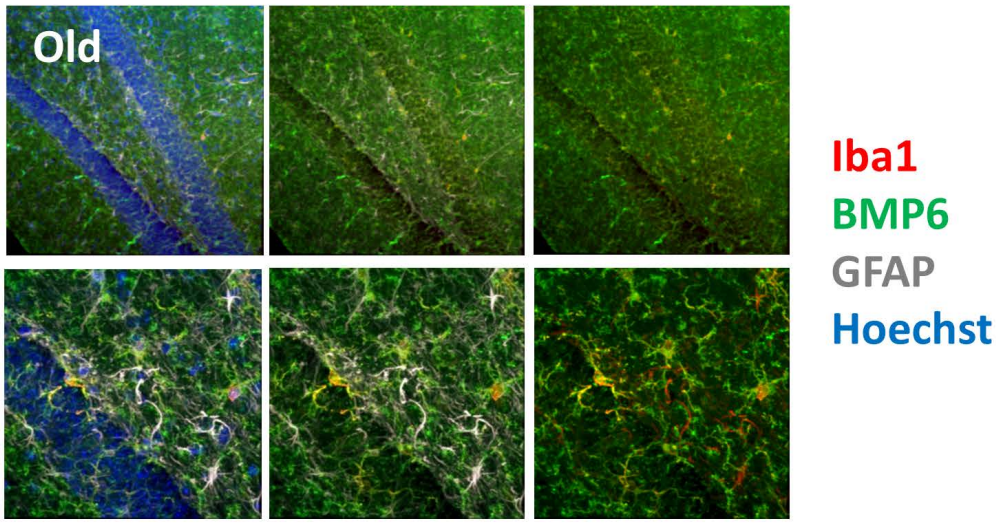

B

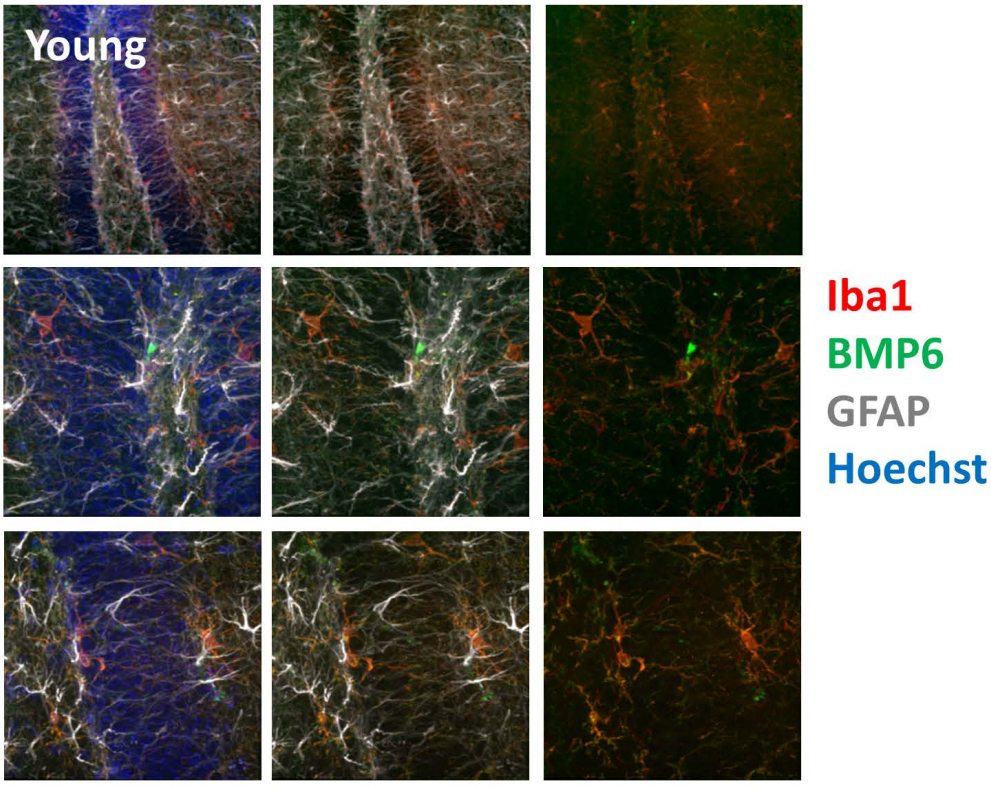

C

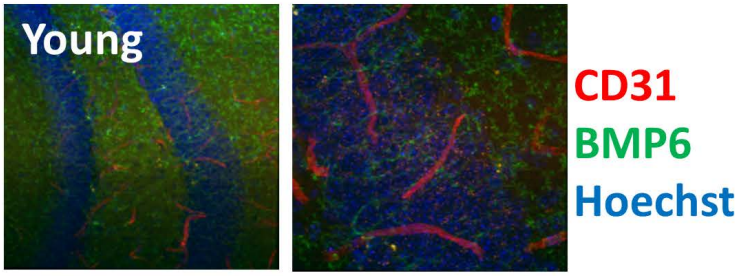

Chapter 2

Systemic attenuation of TGF-β1 pathway in old mice simultaneously rejuvenates neurogenesis and myogenesis by down-modulating MHC I β2 microglobulin.

Hanadie Yousef[2], Michael Conboy[1], Adam Morgenthaler[1], Christina Schlesinger[1], Lukasz Bugaj[1], Preeti Paliwal[1], Christopher Greer[1], Irina Conboy[1*] & David Schaffer[1,3,4*]

1 Department of Bioengineering and California Institute for Quantitative Biosciences (QB3), UC Berkeley, Berkeley, CA 94720, USA
2 Department of Molecular and Cellular Biology, UC Berkeley, Berkeley, CA 94720, USA
3 Department of Chemical and Biomolecular Engineering, UC Berkeley, Berkeley, CA 94720 USA
4 Helen Wills Neuroscience Institute, UC Berkeley, Berkeley, CA 94720 USA

* equal contribution co-authors to whom correspondence should be addressed:
Email schaffer@berkeley.edu & iconboy@berkeley.edu

Abstract

An emerging paradigm proposes that aging of multiple tissues is greatly influenced by the diminished function of their resident stem cells, and that molecular changes in the stem cell microenvironments contribute to or account for diminished stem cell regenerative potential, ultimately leading to tissue aging. To address the hypothesis that cross-tissue conservation in the aging of signal transduction may exist, we investigated and found common age-specific changes in the transforming growth factor β1 (TGF-β1)/pSmad2,3 signaling pathway in the neurogenic niche of the hippocampus and the myogenic niche of skeletal muscle. Furthermore, we show that systemically attenuating TGF-β1 signaling *in vivo* in old mice with a small molecule inhibitor simultaneously enhances neurogenesis and muscle regeneration. These findings are further substantiated via genetic perturbations. Importantly, we demonstrate that the age-induced increase in TGF-β1 in the stem cell niches of aged hippocampus and skeletal muscle is pro-inflammatory as it results in elevated expression of β2 microglobulin (B2M), a component of MHC class I molecules, and that inhibition of TGF-β1 signaling normalizes the B2M to its young levels in old neurogenic and myogenic niches. Summarily, our work uncovers a new phenomenon of broad, age-specific regulation of tissue stem cells by TGF-β1 / B2M signaling cross-talk within their niches.

Introduction

Interestingly, evidence suggests that the intrinsic capacity of some tissue stem cells, such as in muscle, for tissue maintenance and repair does not drastically decline with age. Rather, molecular changes in the stem cell microenvironments or niches contribute to or account for diminished stem cell regenerative potential in several tissue types, ultimately leading to tissue aging. Such changes in stem cell microenvironments that negatively regulate stem cell function have been observed in aged skeletal muscle, brain, skin, blood, and bone [1]. Considering that the same morphogenic signal transduction pathways – including Notch, Wnt, transforming growth factor β (TGF-β), fibroblast growth factor (FGF), Sonic hedgehog (Shh), and others – regulate adult stem cell behavior in different tissues [1-4], it is possible that age-related changes in these pathways that lead to diminished stem cell regeneration are also conserved among multiple organ systems. Furthermore, complex interplays between systemic and local changes in specific signaling factors with age have been shown to inhibit stem cell mediated tissue regeneration [5-10], and these interactions may also be conserved across tissues. This work is the first to demonstrate that there is cross-tissue conservation in the aging of TGF-β1 signal transduction in the skeletal muscle and neural stem cell microenvironments, and that one of the mechanisms by which TGF-β1 exerts it pro-aging affects involves the upregulation of β2 microglobulin (B2M), a component of MHC class I molecules. Furthermore, youthful calibration of TGF-β1/pSmad2,3 pathway by a systemically administered small molecule normalizes the levels of B2M and robustly rejuvenates hippocampal neurogenesis and skeletal myogenesis in the same old animal.

TGF-β1 is a multi-functional cytokine that becomes elevated with age both in circulation and locally in several tissues, including the muscle and brain [8,11]. Such changes in the intensity of TGF-β1/pSmad2,3 signaling – with aging, pathology, or experimental induction – have been shown to perturb homeostasis of such diverse tissues as muscle, bone and cartilage, the subventricular zone of the brain, vasculature, the hematopoietic / immune system, and skin [12-19,24].

TGF-β1 can inhibit cell proliferation by upregulating the expression of several CDK inhibitors, including p21 [13,20-22], and it may thereby directly inhibit the proliferation of tissue stem and progenitor cells. However, it may also modulate tissue inflammation, as TGF-β1 can be either anti- or pro-

inflammatory depending on the levels of this morphogen and the gene expression landscape of the responding tissue [15,18]. For example, young and healthy levels of TGF-β1 are known to down-modulate the immune response, and accordingly the complete absence of TGF-β1 or its downstream signaling causes multifocal inflammation in young mammals (reviewed in [18]). In contrast, when present at high or pathological levels, TGF-β1 has been shown to promote massive inflammation in a variety of systems [15,18]. While inflammatory responses, which in general include induction of MHC class I and class II genes and the production of multiple inflammatory cytokines including TGF-β1, are needed for productive regeneration of tissues including skeletal muscle and brain, prolonged and excessive inflammation is known to interfere with tissue maintenance and repair [9,15,18].

Circulating TGF-β1 is unlikely to reach the neurogenic niche (due to the blood-brain barrier), but local overproduction of TGF-β1 by aged microglia and by endothelial cells has been reported in the subventricular zone of the forebrain [23,24]. However, despite the importance of hippocampal neurogenesis for learning and memory [25], and the contribution that age-imposed deterioration of this brain region may make to declines in cognition [26], it is unknown whether levels of local TGF-β1 and the strength of TGF-β1/pSmad2,3 signaling rise with age in the hippocampal niche of neural stem cells and contribute to this age-specific decline in neurogenesis.

TGF-β1/pSmad signaling increases in aged neural and muscle stem cell niches

Consistent with previously published results [26-28], we found that Sox2+BrdU+ proliferating Type 1 and 2a hippocampal neural stem and progenitor cells significantly decline with age (Figure 1a). To correlate this decrease in proliferating neural stem and progenitor cells with levels of TGF-β1, we isolated hippocampi from young (2-4 mo) and old (22-24 mo) male C57BL6/J mice. TGF-β1 mRNA expression was examined by qRT-PCR, and protein levels were analyzed both by ELISA in tissue lysates and via immunofluorescence in whole tissue sections. As shown in Figure 1b-e, TGF-β1 became elevated with age in the murine hippocampus. Confirming a broad age-related increase of TGF-β1, this cytokine also became elevated in old blood serum (Extended Data Figure 1a and [8]) and skeletal muscle (Extended Data Figure 1b, c and [20]). Additional immunostaining was performed in order to assess the course of TGF-β secretion. As shown in Extended Data Figure 6a-d, microglia and endothelial cells, but not astrocytes, secrete TGF-β.

To confirm and build upon these results, we analyzed downstream pSmad signaling in young versus aged neural stem cells *in vivo*. As shown in Figure 2a (quantified in b), the levels of pSmad3 were up-regulated in aged compared to young Sox2+ neural stem and progenitor cells in the subgranular zone (SGZ) of the dentate gyrus of the hippocampus. Furthermore, TGF-□1 is a known inhibitor of cell proliferation [13,20,22,29], and accordingly qRT-PCR revealed that *in vivo* hippocampal expression of p21, a known down-stream target of TGF-β1/pSmad pathway that inhibits cell cycle progression [22,30], was elevated with age (Figure 2c). To initially investigate whether this age-associated increase in TGF-β1 may be functionally important for neurogenesis, TGF-β1 ligand was added to hippocampal-derived Sox2+ neural progenitor cell (NPCs) cultures and observed to both upregulate pSmad3 (Figure 3a) and decrease cell proliferation, as assayed by reduced BrdU uptake (Figure 3b-c). These data are the first to demonstrate that the levels of TGF-β1 transcript and protein and p21 transcript increase with age in the hippocampus, and that Smad3 phosphorylation increases in resident Sox2+ neural stem and progenitor cells of the old hippocampus.

Simultaneous systemic enhancement of hippocampal neurogenesis and myogenesis in old mice

The conserved increase in TGF-β1/pSmad signaling within muscle and brain stem cell niches with age suggested that stem cell responses could be enhanced in both tissues by attenuating the intensity of this pathway, which would both validate our conclusions and offer translational potential for rejuvenating multiple tissues in the same organism with a single therapeutic intervention. Accordingly, a small molecule pharmacological inhibitor of the TGF-β1 receptor I kinase (Alk5) was added to cultured NPCs, where it was found to down-modulate pSmad2 and pSmad3 levels (Extended Data Figure 2a, quantified in b). *In vivo*, this molecule was administered systemically via intraperitoneal (IP) injection into aged mice (24-26 mo) once daily for 11 days. In mice perfused on day 12, a robust decrease in pSmad2/3 levels was observed in the hippocampus, validating both activity and blood brain barrier transport of the inhibitor (Extended Data Figure 2c-f). To assess the ability of the Alk5 inhibitor to enhance regeneration of multiple tissues in the same animal, muscle was injured by cardiotoxin one week after the start of Alk5 inhibitor administration (day 0 of schematic Figure 4a), and tissue regeneration was analyzed at 5 days post-injury (Figure 4a). In parallel, we quantified hippocampal neurogenesis – i.e. the numbers of BrdU+Sox2+ cells in tissue sections across the hippocampus – in the same animal cohorts (Figure 4b-c). Very interestingly, both neurogenesis and myogenesis were significantly enhanced in the aged mice treated with Alk5 inhibitor, compared to the animals receiving control buffer (Figure 4b-e). In brain this was evident from a two-fold increase in the numbers of Sox2+ proliferating neural stem and progenitor cells within the hippocampal dentate gyrus (Figure 4b-c). In muscle we observed enhanced de novo myofiber formation 5 days post-injury as assayed by quantifying the numbers of eMyHC+ fibers with centrally located nuclei (Figure 4d, e). These results confirm the pro-myogenic effects of Alk5 inhibitor [8,31] and reveal that systemic administration of an attenuator of the TGF-β1/pSmad pathway simultaneously rejuvenates skeletal myogenesis and hippocampal neurogenesis in the same old animal.

Rejuvenation of myogenesis and neurogenesis by genetic attenuation of TGF-β1 signaling

To confirm these findings in independent experimental approaches, we genetically inhibited TGF-β1 signaling using a lentivirally-encoded shRNA we developed against Smad3. The efficacy of this shRNA was confirmed in transduced mouse muscle progenitor cells *in vitro* via western blotting and in mouse neural progenitor cells *in vitro* via qRT-PCR (Extended Data Figure 3a-b). After a single stereotaxic hippocampal injection of a lentiviral vector encoding GFP plus the shRNA against Smad3 – or control shRNA against LacZ – into 24 month old mice, animals were allowed to recover for 2 weeks, followed by five consecutive days of BrdU administration (Figure 5a). As shown in Figure 5b-d, the numbers of Sox2+ proliferating cells (quantified in the GFP+ region of tissue sections throughout the entire hippocampus) were significantly increased after a single injection of shRNA to Smad3, as compared with control shRNA lentiviral transduction. This was confirmed to be a direct result of the lentiviral delivery of shRNA against Smad3, since there was a significantly higher proportion of GFP+ and of GFP+Sox2+ cells that were also BrdU+ (Figure 5e, f). Neurogenesis was thus significantly enhanced by the inhibition of Smad3 signaling in the local niche of neural stem cells in 2 year old mice (analogous to 80 year old humans), demonstrating progress in rejuvenating neurogenesis in very old mice and complementing reports on the enhancement of neurogenesis through increase of Wnt-mediated survivin signaling in 13 month old mice [2]. To analyze analogous effects on type 2b Doublecortin expressing (DCX+) transit amplifying cells, another cohort of animals were mitotically labeled (with EdU) for 5 consecutive days and studied 5 days after the last injection to detect the cells that had progressed towards neuronal commitment [25]. There was a substantial increase in the total number of EdU+DCX+GFP+ type 2b cells (Extended Data Figure 4a-c), demonstrating that not only the proliferation of neural stem cells but the formation of new neurons is rejuvenated in old mice administered with Alk5 inhibitor.

To further compare molecular conservation of tissue aging between brain and muscle, we also administered the lentiviral vector encoding shRNA against Smad3 into injured hind leg muscle of 24 month old mice, simultaneously with cardiotoxin to induce muscle injury [32,33]. Significant enhancement of old muscle repair, based on the numbers of de-novo formed muscle fibers that were quantified throughout the entire injury site [32,34], was observed in the 24 month old mice injected just once with the shRNA to Smad3, compared to the control shRNA (Extended Data Figure 4d,e). This is consistent with previously published results using shRNA to Smad3 to enhance old muscle regeneration, though several injections were administered [20].

We further corroborated our findings by introducing a dominant negative form of the TGF-β1 receptor (dnTGFBR2, known to inhibit pSmad2/3 levels [35]). Expression of the dnTGFBR2 in neural progenitor cells and downstream inhibition of pSmad3 were confirmed by western blotting (Extended Data Figure 5a, b). Retroviral vectors encoding dnTGFBR2 or GFP as a control were injected into CTX injured muscle one day after injury, when resident muscle stem cells are breaking quiescence and entering the cell cycle [1,32] (Figure 6a). Three days after injury, muscle was harvested and assayed for proliferating (EdU+) myogenic cells. Compared to the aged tissue injected with control vector, in old muscle administered with dnTGFBR2 retroviral vector there was a marked increase in the percentage of desmin+ muscle precursor cells (Figure 6b,c) and a significant increase in proliferating desmin+EdU+ myogenic cells (Figure 6d,e). We also examined tissue 5 days after injury and observed that repair of old damaged muscle *in vivo* was robustly enhanced by dnTGFBR2, as assayed by the replacement of the injury with the newly formed myofibers and reduction in scarring (Figure 6f, g). These results agree with our prior work in muscle [20]. Thus, *in vivo* retroviral delivery of dnTGFBR2 rejuvenated the myogenic capacity of muscle stem cells responding to tissue injury, suggesting that old muscle repair can be enhanced after the time of breakage of quiescence (e.g. by enhancing the proliferation of the few old muscle stem cells that have entered cell cycle) and confirming that canonical TGF-β1/pSmad signaling is involved in the age-imposed inhibition of myogenesis.

To further validate the cross-tissue conservation of TGF-β1 signaling with aging, hippocampal neural progenitor cells were transduced with dnTGFBR2 encoding retrovirus and assessed for proliferation. As shown in Figure 6h-i, dnTGFBR2 increased neural progenitor proliferation in their (FGF-2-rich) growth medium as compared to GFP control, based on EdU incorporation. Western blotting analysis showed that there was relatively high pSmad3 signaling in NPCs in growth medium even in the absence of exogenous TGF-β1, which was diminished upon dnTGFBR2 retroviral transduction (Extended Data Figure 5a). Furthermore, TGF-β1 (10 ng/mL) addition to growth medium overnight inhibited proliferation of GFP+ NPCs, but did not affect dnTGBR2+ NPCs (Figure 6h,i). Collectively, these results including both pharmacological and genetic intervention suggest that TGF-□1/pSmad2/3 signaling increases with age in both myogenic and neurogenic niches of tissue stem cells and that attenuation of this pathway partially rescues myogenesis and neurogenesis.

TGF- β increases B2M expression in aged neural and muscle stem cell niches

The developmental origins, as well as properties of muscle and brain (and their respective stem cells), are quite different, and we therefore next focused on potential underlying molecular mechanisms that may be regulated by the pleiotropic TGF-□□/pSmad pathway and thus shared between such adult organ systems. The TGF-β1/pSmad pathway exerts complex and sometimes reciprocal effects on cellular and tissue responses, including the rate of cell cycle progression and the anti- versus pro-inflammatory role in regulating immune responses [15]. Thus, we next examined the effects of the age-

specific elevated TGF-β1 on MHC class I gene expression, which when deregulated is known to promote tissue inflammation and associate with brain pathologies [23,36,37]. B2M is the invariant chain of the MHC class I protein complex, and its expression is regulated similarly to the variable / polymorphic MHC class I and class II genes [38-40]. In general, MHCI molecules are involved in a variety of processes that regulate brain development and plasticity, including neurite outgrowth, the establishment and function of cortical connections, activity-dependent refinement in the visual system, and long-term and homeostatic plasticity [41,42]. Many MHCI molecules, including B2M, have been shown to be expressed in the brain and limit synaptic plasticity in healthy neurons [42,43]. Additionally, transgenic mice mutant for MHCI have a striking ability to form new synapses and recover from brain injury such as stroke, suggesting that overexpression of MHCI may be inhibitory to healthy brain function and processes such as learning and memory [44]. In muscle and other tissues, persistently elevated MHC class I frequently signifies inflammation and pathology [45,46]. To analyze whether B2M may be involved in the effects of TGF-β1 signaling in muscle and brain (Figure 4), we compared the B2M expression levels between young and old mice treated with vehicle control, and old mice treated with the Alk5 inhibitor. B2M levels were extremely low in young brain and muscle, consistent with prior work [16], but increased significantly with aging (Figure 7a-d). Importantly, when TGF-β1 signaling was attenuated in vivo by the Alk5 inhibitor, B2M levels were significantly diminished both in old brain (Figure 7a,b) and old muscle (Figure 7c,d). These results demonstrate that MHC class I becomes upregulated with aging in multiple tissues (demonstrating a propensity for inflammation) and that down-modulation of TGF-β1 signaling, which rejuvenates myogenesis and neurogenesis, normalizes the MHCI protein complex levels in myogenic and neurogenic regions to their young levels. As further support of this conclusion, the levels of B2M were also significantly reduced in regenerating regions of the old muscle administered with the dnTGFBR2, as compared to tissue administered with control GFP virus (Figure 7e, f).

Conclusion

Comprehensively, these data suggest that similar molecular mechanisms acutely yet reversibly inhibit the capacity of stem cells in old muscle and in the aged brain to contribute to differentiated tissue. This study specifically focused on age-imposed de-regulation of the TGF-β1/pSmad2,3 signaling pathway, and a clear cross-tissue conservation was identified. Specifically, systemic administration of an Alk5 Type I receptor kinase inhibitor simultaneously improved repair of skeletal muscle and enhanced hippocampal neurogenesis in 2-year old mice, suggesting promising strategies for combating multiple age-related degenerative disorders, which are known to contribute to the loss of a person's agility, mobility, memory, learning, and independence.

Independent genetic and pharmacological approaches to attenuate TGF-β1/pSmad signaling drove parallel enhancements of neurogenesis and myogenesis, thus providing important cross-validation of these results and conclusions. While local tissue delivery of shRNA against Smad3 most likely inhibited TGF-β1/pSmad2,3 signaling directly in muscle or brain, the systemic administration of Alk5 inhibitor could function both directly and potentially indirectly through attenuation of TGF-β1 pathway signaling in multiple tissues.

Various studies have demonstrated that not just one signaling pathway, but a network of highly interactive pathways – including Notch, Wnt, BMP, Shh, TNF-α, IGF, and IL-6 – become affected by the aging process [1,33,47]. For example, *in vivo* TGF-β1 signal inhibition not only enhanced neurogenesis and myogenesis by increasing cell proliferation but may also have worked through inhibiting inflammation, as seen by the decrease in expression of MHCI class molecule B2M. With potential

significance to aging, TGF-β1 is known to be up regulated upon central nervous system damage, and such elevation is concurrent with the dramatic induction of MHC class I gene expression, as well as with such known phenotypes of the aged brain as activation of microglia and neuronal apoptosis [16]. One of the known inflammatory cytokines that becomes prevalent in the old, particularly at the sites of tissue damage, is IL-6 [48], which is known to promote inflammation in part via support of Th17 cells and up-regulation of MHC class I and class II gene expression [18,49]. Therefore, it is possible that the age-specific increase in TGF-β1 signaling may contribute to the excess of IL-6 or other inflammatory cytokines such as IL-17, and consequentially experimental attenuation of TGF-β1 may result in lower levels of inflammatory cytokines and normalized levels of MHCI proteins. In support of the pro-aging role of excessive MHC class I, work by Smith *et al*. demonstrates that (1) B2M levels increase with age in the brain, (2) attenuation of B2M results in the enhanced neurogenesis and better memory and cognition of the old mice, and (3) antigen presentation by MHC class I is required for the age-imposed inhibition of neurogenesis and diminished brain function caused by elevated B2M. In this regard, our study provides a mechanism for the age-specific elevation in B2M, by demonstrating a role of TGF-β1/pSmad2/3 and further suggesting that attenuation of TGF-β1 signaling results in the normalization of B2M and thereby promotes effective myogenesis and neurogenesis in the old.

In summary, this work improves our understanding of the aging of tissue stem cells, reveals a molecular conservation of the aging process between muscle and brain, and suggests novel clinical strategies for the simultaneous rejuvenation of myogenesis and neurogenesis in old mammals.

Figure Legends

Figure 1. TGF-β1 Increases with Age Locally in Mice Hippocampi (a) Young (2 month) and old (24 month) mice (n=3) were administered daily with BrdU for 5 days, followed by perfusion and PFA fixation. Immunofluorescence (IF) was performed for Sox2 (green) and BrdU (red), with DAPI (blue) labeling all nuclei. Representative images are shown. Scale bar = 100 μM. (b) qRT-PCR quantification of *Tgfb1* mRNA expression from young and old hippocampi. The relative average expression level was normalized to *GAPDH* and presented as the average expression level relative to that of young hippocampi. Significant differences were identified by Student's t-tests (two-tailed) (*$p<0.003$). Error bars indicate standard deviation (n=4 biological replicates). (c) Immunofluorescence was performed on perfused and PFA fixed young and old brain tissue sections (n=3), for Sox2 (green) and TGF-β1,2,3 (red), with Hoechst (blue) labeling all nuclei. Representative low and high magnification images are shown. Scale bars = 50 μM. (d) Integrated pixel intensity of TGF-β1,2,3 immunofluorescence in young and old dentate gyri tissue sections was calculated using ImageJ. Pixel intensities are presented relative to young dentate gyri. Significant differences were identified by Student's t-tests (*$p<0.003$). Error bars indicate standard error of the mean (n=3 young, 3 old). (e) An ELISA was performed on young and old hippocampal protein extract to assess the level of local TGF-β1 and represented as the averages of the pg TGF-β1 normalized to pg total hippocampal protein lysate. Significant differences were identified by Student's t-tests (two-tailed) (*$p<0.008$). Error bars indicate standard deviation (n=3 biological replicates).

Figure 2. Downstream effectors of TGF-β1 Signaling increase with Age in Mice Hippocampi. (a) Immunofluorescence staining for Sox2 (green) and pSmad3 (red) was performed on young and old brain tissue sections (n=4 young, 6 old), with DAPI (blue) labeling all nuclei. Representative images are shown. Scale bar = 50 μM. (b) MetaXpress image quantification was developed to calculate the average pixel intensity specifically in Sox2+ neural stem and progenitor cells in the SGZ of the dentate gyrus. Significant differences were identified by Student's t-tests (two-tailed) (*$p<0.001$). Error bars

indicate standard error (n=4 young, 6 old). (c) qRT-PCR quantification of *p21* mRNA expression from young and old hippocampi (n=3 biological replicates). The relative average expression level was normalized by *GAPDH* and presented relative to young hippocampi. Significant differences were identified by Student's t-tests (two-tailed) (*p<0.003), and error bars indicate standard deviation (n=3).

Figure 3. TGF-β1 inhibits Neural Progenitor Cell Proliferation. (a) Immunoblotting analysis of a downstream effector of TGF-β1, pSmad3, from NPCs cultured in growth medium in the presence or absence of TGF-β1 (50 ng/mL) for 30 minutes. pSmad3 signaling is induced through TGF-β1, as compared with levels of total Smad2/3. (b) Functional validation of increasing TGF-β1. NPCs were cultured in growth medium (DMF12 + N2 + 10 ng/mL FGF-2) in the presence or absence of TGF-β1 (100 ng/mL) for 24 hrs. A 2 hour BrdU (10 μM) pulse was performed before cell fixation to label proliferating cells. Staining was conducted for BrdU (green) and Sox2 (red), with Hoechst (blue) labeling all nuclei. Representative images are shown. Scale bar = 100 μM. (c) Proliferation of NPCs was quantified by cell scoring in 25 random fields of each condition using an automated imager and MetaXpress cell scoring software. Results are displayed as the mean percent of BrdU+ proliferating NPCs +/-SD, respectively. Significant differences were identified by Student's t-tests (two-tailed) (*p< 0.0003), and error bars indicate standard deviation (n=5 biological replicates). The experiment was replicated 4 times.

Figure 4. Simultaneous Partial Rescue of Hippocampal Neurogenesis and Myogenesis in Aged Mice through Systemic *In vivo* inhibition of TGF-β1 (a) Schematic of Alk5 inhibitor administration. Aged (2 year old) mice received IP injections of TGF-β1 type I receptor kinase Alk5 inhibitor (Alk5i), or vehicle control, once daily for 11 days (Day -6 through Day 4) and were sacrificed on Day 5. Tibialis anteriors (TAs) were injured with cardiotoxin on Day 0, and mice began receiving daily IP injections of BrdU through Day 4. TAs were collected on Day 5, 5 days post injury (5 dpi). (b) Following perfusion and PFA fixation, brain sections of Alk5 inhibitor or vehicle treated mice (n=4 per group) spanning the entire hippocampus were immunostained for BrdU (red) and Sox2 (green), with Hoechst (blue) labeling cell nuclei. Representative images are shown. Scale bar = 50 μM. (c) Quantification by stereology of BrdU+Sox2+ cells per dentate gyrus. As shown, Alk5 type I receptor kinase inhibitor increases the average number of BrdU+Sox2+ cells in the dentate gyrus. Significant differences were identified by Student's t-tests (two-tailed) (*$p<5x10^{-7}$). Error bars indicate standard deviation (n=4 biological replicates) (d) TA muscle sections collected 5 days post injury were immunostained for eMyHC (green), with Hoechst (blue) labeling cell nuclei. Representative images show newly regenerating myofibers in injured muscle sections. Hematoxylin and eosin staining of injury sites also shown. Scale bars = 100 μM. (e) Regenerative index quantifies the number of newly formed eMyHC+ myofibers per square millimeter in the injured area. Systemic administration of the Alk5 inhibitor enhances old muscle regeneration after injury, as displayed by the mean regenerative index per group. Significant differences were identified by Student's t-tests (two-tailed) (*p<0.0002), and error bars indicate standard error of the mean (n=4 biological replicates). The experiment was replicated 3 times.

Figure 5. Rescue of Neurogenesis in Aged Hippocampi by *in vivo* Genetic Inhibition of pSmad3. (a) Schematic of stereotaxic lentiviral injection experiment. Aged (18 month old) mice received stereotaxic injections into hippocampi (coordinates from bregma: AP: -2.12, ML: +/-1.5, VD: -1.55) of lentiviral vectors encoding shRNA against either Smad3 or lacZ. Mice were allowed to recover for 14 days, followed by daily BrdU (50 mg/kg) intraperitonial injections for 5 days, then analysis. (b) Brain sections of lacZ or Smad3 shRNA injected mice (n=5 lacZ shRNA lentivirus, 4 Smad3 shRNA) spanning the entire hippocampus were immunostained with GFP (green), BrdU (red), and Sox2 (gray), with Hoechst (blue) labeling cell nuclei. Representative images are shown. Scale bar = 50 μM. (c) High

magnification of immunostaining of the subgranular zone of the dentate gyrus, as described in (b). Scale bar = 50 μM. (d) Quantification of the mean number of BrdU+Sox2+ cells per dentate gyrus shows an increase in proliferating NPCs in aged animals expressing anti-Smad3 shRNA. Significant differences were identified by Student's t-tests (two-tailed) (*$p<0.05$). Error bars indicate standard error of the mean (n=5 lacZ shRNA, 4 Smad3 shRNA brains). (e) Quantification of the mean percentage of GFP+ cells that are also BrdU+/proliferating in shRNA injected brains demonstrates an increase in proliferation due to shRNA-Smad3 transduction as compared with shRNA-lacZ control mice. Significant differences were identified by Student's t-tests (two-tailed) (*$p<0.05$). Error bars indicate standard deviation (n=3 biological replicates). (f) Quantification of the mean percentage of BrdU+GFP+Sox2+ proliferating NPCs as compared with BrdU-GFP+Sox2+ NPCs in shRNA injected brains demonstrates an increase in proliferating neural progenitor cells due to shRNA-Smad3 transduction as compared with shRNA-lacZ control mice. Significant differences were identified by Student's t-tests (two-tailed) (*$p< 4 \times 10^{-7}$), and error bars indicate standard deviation (n=3). The stereotaxic shRNA brain injection experiment was replicated 3 times.

Figure 6. Rescue of Myogenesis in Aged Muscle by *in vivo* Genetic Inhibition of TGF-β1 Receptor II (a) Schematic. Aged (18 month old) mice TA muscle was injured with cardiotoxin on Day 0, followed by injection of dnTGFBR2 retrovirus into injury sites 36 hours later, on Day 1.5. On Day 2 gastrocnemius muscle were injured, followed by injection of dnTGFBR2 retrovirus at sites of injury 36 hours later, on Day 3.5. Mice received IP injection of EdU 12 hours before muscle tissue was harvested. (b) Myogenic precursor cells isolated 3 days post-injury from gastrocnemius muscle were stained for Desmin (red), with Hoechst (blue) labeling all cell nuclei. Representative images are shown. Scale bar = 50 μM. (c) Quantification of the mean percentage of Desmin+ precursor cells. Significant differences were identified by Student's t-tests (two-tailed) (*$p<0.03$). Error bars indicate standard error of the mean (n=3 biological replicates). (d) Myogenic precursor cells isolated 3 days post-injury from gastrocnemius muscle were stained for Desmin (red) and EdU (green), with Hoechst (blue) labeling all cell nuclei. Representative images are shown. Scale bar = 50 μM. (e) Quantification of the mean percentage of proliferating myogenic precursor cells isolated from muscle that received dnTGBR2 or GFP. Significant differences were identified by Student's t-tests (two-tailed) (*$p<0.02$), and error bars indicate standard deviation (n=3 biological replicates) (f) Hematoxylin and eosin of muscle TAs isolated 5 days post-injury and sectioned in a cryostat at 10 μM. Representative images shown. Scale bar = 100 μM. (g) Five days post-injury regeneration of old mice tibialis anterior muscle, which received dnTGFBR2 or GFP retrovirus, was quantified from muscle sections (10 μM sections throughout sites of injury) and is presented as the mean number of newly regenerated myofibers per square millimeter of injury site. Error bars indicate standard error of the mean, (n=3 mice per group). Significant differences were identified by Student's t-tests (two-tailed) (*$p <0.01$). (h) NPCs were transduced with dnTGFBR2 or GFP and cultured for one week, followed by 16 hour incubation in growth medium in the presence/absence of 10 ng/mL TGF-β1. Cells were pulsed with EdU (30 μM) for 4 hours before fixation to label proliferating cells. Cells were stained for GFP or FLAG (green), EdU (red), and Sox2 (gray), with Hoechst (blue) labeling cell nuclei. Representative images are shown. Scale bar = 100 μM. (i) Proliferation of NPCs was quantified by cell scoring in 36 random fields of each condition using an automated imager and MetaXpress cell scoring software. Results are displayed as the mean percent of EdU+Sox2+ proliferating NPCs +/-SD, respectively. Significant differences were identified by Student's t-tests (two-tailed) (*$p<9\times10^{-10}$,**$p<3\times10^{-24}$,***$p<4\times10^{-16}$). Error bars indicate standard deviation (n=36 technical replicates). The experiment was replicated 4 times.

Figure 7. B2M Levels Decrease in Muscle and Brain When TGF-β1 is Attenuated Systemically or Locally. (a) Brain sections spanning the hippocampus from young mice (2 month), as well as Alk5

inhibitor or vehicle treated old (24 month) mice, were immunostained for B2M (red), with Hoechst (blue) labeling all cell nuclei. Representative images are shown. Scale bar = 50 μM. (b) Average B2M pixel intensity was quantified using MetaXpress software, and significant differences were identified by Student's t-tests (two-tailed) (*$p < 3 \times 10^{-6}$, **$p<0.0001$). Error bars indicate standard error of the mean (n=5 young, 3 old + Alk5i, 3 old + vehicle biological replicates (mice), with n=12 technical replicates per mouse) (c) Tibialis anterior muscle collected 5 days post-injury were immunostained for B2M (red), with Hoechst (blue) labeling all cell nuclei. Representative images are shown. Scale bar = 100 μM. (d) Average B2M pixel intensity of 10 μM tibialis anterior muscle sections throughout sites of injury were quantified using MetaXpress software. Significant differences were identified by Student's t-tests (two-tailed) (*$p<7\times10^{-7}$, **$p<5\times10^{-5}$), and error bars indicate standard error of the mean (n=3 biological replicates per group (mice), with n=12 technical replicates per mouse (e) TA muscles collected 5 days post injury were immunostained for B2M (red), with Hoechst (blue) labeling all cell nuclei. Representative images are shown. Scale bar = 100 μM. (f) Average B2M pixel intensity of TA muscle sections throughout sites of injury were quantified using MetaXpress software. Significant differences were identified by Student's t-tests (two-tailed) (*$p<0.002$). Error bars indicate standard error of the mean (n=3 biological replicates per group (mice), with n=12 technical replicates per mouse).

Extended Data Figure 1. TGF-β1 Levels are Increased Systemically in Serum and Old Muscle. (a) An ELISA was performed on young and old serum to assess the average level of systemic TGF-β1, represented as pg/mL. Significant differences were identified by Student's t-tests (two-tailed) (*$p<0.003$). Error bars indicate standard deviation (n=3 biological replicates per group). (b) Whole muscle from young and old resting TA and resting TA adjacent to cardiotoxin injured gastrocnemius muscle was isolated and western blotting against TGF-β1 antibody was performed on muscle samples. GAPDH served as control. No differences were observed between the levels of TGF-β1 in the TA from completely non-injured leg and those levels in non-injured TA adjacent to injured gastrocnemius. As shown, aged muscle had significantly more TGF-β1 as compared to young. (c) TGF-β1 quantification graph. TGF-β1 levels from panel A were quantified and relative fold induction after GAPDH normalization was plotted as a histogram (Young=1) (n=4 biological replicates, *$p\leq0.05$).

Extended Data Figure 2. Alk5 Inhibitor Reduces the Levels of pSmad2/3 in Primary Neural Progenitor Cells *in vitro* and in the Murine Dentate Gyrus after Systemic Administration *in vivo*. (a) NPCs were incubated in basal medium (DMF12 + N2 but no FGF-2) for 1 hour, then either untreated, or treated with TGF-β1 (1 ng/mL) for 1 hour +/- 5 uM Alk5 inhibitor. Representative western blotting for pSmad2 and 3 is shown and quantified in (b), represented as the mean pixel intensity of pSmad2 or pSmad3 normalized to total Smad2/3 (n=2 biological replicates). (c) Following systemic delivery of Alk5 inhibitor or control vehicle, immunofluorescence was performed on brain sections spanning the hippocampus for pSmad3 (red), with hoechst (blue) labeling cell nuclei. Representative images are shown. Scale bar = 50 μM. (d) pSmad3 integrated fluorescence intensity was quantified in brain sections using MetaXpress software. Significant differences were identified by Student's t-tests (two-tailed) (*$p<0.05$). Error bars indicate standard deviation (n=4 biological replicates (mice), with n=6 technical replicates per mouse). (e) pSmad2 (red) immunofluorescence was performed on brain sections spanning the hippocampus following systemic delivery of Alk5 inhibitor or control, with hoechst (blue) labeling cell nuclei. Representative images are shown. Scale bar = 50 μM. (f) pSmad2 integrated fluorescence intensity was quantified in brain sections using MetaXpress software. Significant differences were identified by Student's t-tests (two-tailed) (*$p<0.05$). Error bars indicate standard deviation (n=4 biological replicates (mice), with n=6 technical replicates per mouse).

Extended Data Figure 3. *In vitro* Validation of shRNA- Smad3. (a) Mouse muscle progenitor cells were transduced with 1 µl of concentrated Smad3 shRNA or lacZ shRNA lentiviruses and cultured for 72 hours, followed by western blot analysis of pSmad3 expression and total Smad2/3. Smad3 shRNA inhibited expression of Smad3. β-actin was used as a loading control. (b) Quantification of *Smad3* mRNA expression by qRT-PCR was performed on RNA extracted from mouse NPCs transduced with shRNA to Smad3 or control virus and passaged for 2 weeks. The relative expression level was normalized to *GAPDH* and presented as the expression level relative to that of NPCs transduced with lacZ shRNA lentivirus. Significant differences were identified by Student's t-tests (two-tailed) (*$p<0.04$). Error bars indicate standard deviation (n=3 biological replicates).

Extended Data Figure 4. *Smad3* Inhibition via *Smad3* shRNA Enhances Neurogenesis and Myogenesis of Old Tissue. (a) Aged (18 month old) mice received stereotaxic injections into hippocampi (coordinates from bregma: AP: -2.12, ML: +/-1.5, VD: -1.55) of lentiviral vectors encoding either shRNA against Smad3 or shRNA against lacZ. The mice were allowed to recover for 14 days, followed by daily EdU (50 mg/kg) intraperitonial injections for 5 days. Five days after the last EdU injection, mice were saline and 4% PFA perfused. Brain sections of lacZ or Smad3 shRNA injected mice (n=3 lacZ shRNA, 5 Smad3 shRNA) spanning the entire hippocampus were immunostained with GFP (green), EdU (red), and Doublecortin (DCX) (gray), with Hoechst (blue) labeling cell nuclei. Representative images are shown. Scale bar = 50 µM. (b) High magnification representative images as described in (a). Scale bar = 100 µM. (c) Quantification of the mean number of EdU+DCX+GFP+ cells per dentate gyrus shows an increase in proliferating cells in Smad3 shRNA injected aged murine hippocampi. Significant differences were identified by Student's t-tests (two-tailed) (*$p<0.03$). Error bars indicate standard error of the mean (n=3 lacZ shRNA, 5 smad3 shRNA). (d) Representative hematoxylin and eosin stained 10-µm cross-sections of tibialis anterior muscle 5 days after cardiotoxin induced injury in the presence of shRNA to Smad3 or control lentiviral particles. (e) Quantitative analysis of the number of newly formed fibers normalized to cross-sectional area of regenerating tissue in control transduced and Smad3 shRNA-transduced tibialis anterior muscle 5 days after injury. Centrally nucleated myofibers were scored from hematoxylin and eosin stained cryosections (10 µM sections throughout the site of injury) (n=3 mice per group, with n=3 technical replicates per mouse, mean $\pm$ SEM) (*$p < 0.0001$).

Extended Data Figure 5. Expression of dnTGFBR2 in Neural Progenitor Cells. (a) Neural progenitor cells were transduced with retrovirus delivering dnTGFBR2-FLAG or GFP. After 72 hours in growth (FGF-2 rich) medium, cells were lysed. Western blotting was performed with an anti-FLAG antibody specific for the C-terminal fusion of the dnTGFBR2, GFP, pSmad3, Smad2/3, and β-actin as a loading control. As shown, the 22 kDa FLAG/dnTGFBR2 band was detected in RV-dnTGBR2 transduced cells, and GFP was detected in RV-GFP transduced neural progenitor cells. dnTGFBR2 expression resulted in downregulation of pSmad3, as well as total Smad2/3 after 72 hours. (b) Neural progenitor cells were cultured for one week post retroviral transduction, then incubated for four hours in basal (DMF12+N2, no FGF-2) medium after splitting. Cells were then either treated or not with 1 or 12.5 ng/mL TGF-β1 for 45 minutes. pSmad3, Smad2/3, and βactin were assessed via western blot. pSmad3 pixel intensity relative to β-actin was quantified with Bio-Rad imaging software.

Extended Data Figure 6. TGF-β is secreted by microglia and endothelial cells. (a) Immunofluorescence was performed on perfused old brain tissue sections for TGF-β (green), Iba1 (red), and GFAP (gray), with Hoechst (blue) labeling all nuclei. Representative low and high magnification images are shown. (b) Immunofluorescence was performed on perfused old brain tissue sections for TGF-β (green), CD31 (red), and Sox2 (gray), with Hoechst (blue) labeling all nuclei.

Representative low and high magnification images are shown. (c) Immunofluorescence was performed on perfused young brain tissue sections for TGF-β (green), Iba1 (red), and GFAP (gray), with Hoechst (blue) labeling all nuclei. Representative low and high magnification images are shown. (d) Immunofluorescence was performed on perfused young brain tissue sections for TGF-β (green), CD31 (red), and Sox2 (gray), with Hoechst (blue) labeling all nuclei. Representative low and high magnification images are shown.

Methods

Animals

Young (2-3 month old) and old (18-24 month old) C57BL6/J male mice were purchased from the Jackson Laboratory and the NIH. The animal experimental procedures were performed in accordance with the Guide for Care and Use of Laboratory Animals of the National Institutes of Health, and approved by the Office of Laboratory Animal Care, UC Berkeley.

For each experiment on aged (18-24 month old) mice, an n of at least 7 per group would be used initially. If aged mice died due to surgery or age-related health issues, a minimum of n=3 remaining mice were analyzed and assessed for statistical significance (described in statistical analysis below). Mice of the same genetic strain and age were assigned to groups at random.

Cell Culture

Primary rat neural progenitor cells isolated from the hippocampi of female Fisher 344 rats (Charles River) were cultured in growth medium (DMEM/F12 (Life Technologies) containing N2 supplement (Life Technologies) and 10 ng/mL FGF-2 (PeproTech)) on laminin (Roche) and polyornithine (Sigma) coated tissue culture plates, with subculturing on reaching 80% confluency using Accutase (Phoenix Flow Systems), as previously described [50].

Primary mouse neural progenitor cells were isolated froom C57BL6/J male mice (Charles River) as previously described [51]. Cells were cultured in growth medium (Neurobasal A (Gibco) containing B27 supplement (Gibco), Glutamax-1 supplement (Gibco), 20 ng/mL FGF-2 (Peprotech), and 20 ng/mL EGF (PeproTech)) on Poly-d-Lysine (Sigma) and Laminin (Roche) coated tissue culture plates, with subculturing on reaching 80% confluency using Accutase (Phoenix Flow Systems).

Primary mouse muscle progenitor cells (myoblasts) were isolated as previously described [52] and cultured and expanded in growth medium containing: Ham's F-10 (Gibco), 20% Bovine Growth Serum (Hyclone), 5 ng/mL FGF-2 (PeproTech) and 1% penicillin-streptomycin on Matrigel (BD Biosciences) coated plates (1:300 Matrigel: PBS), with subculturing on reaching 80% confluency using 0.5% Trypsin (Sigma Aldrich) diluted in PBS.

Progenitor cells were tested for miscroplasma contamination at the UC Berkeley Stem Cell Core Facility and using Hoechst DNA stain.

Primary Muscle stem cells were isolated from male C57BL6/J mice as described below and cultured in DMEM (Life Technologies) with 5% serum from the same age mouse on Matrigel (BD Biosciences) coated plates (1:100 Matrigel:PBS) overnight before cell fixation with 70% cold ethanol.

In vitro Validation of TGF-β1 Signaling and Proliferation Assay

Primary rat NPCs were cultured in growth medium (DMF12 + N2 + 10 ng/mL FGF-2) as described above. Cells were cultured at a density of 200,000 cells per well of a 6-well culture slide in the presence/absence of TGF-β1 (50 ng/mL) (HumanZyme, Inc.) for 30 minutes, followed by a PBS wash and cell scraping into RIPA buffer for western blot analysis as described below. rNPCs were also cultured at a density of 80,000 cells per well of an 8-well chamber slide in growth medium plus the presence/absence of TGF-β1 (100 ng/mL) for 24 hours. NPCs were pulsed for 2 hours with 10 μM BrdU (Sigma Aldrich) before cell fixation with 70% cold ethanol for immunocytochemistry analysis as described below.

Dissection and Preparation of Murine Hippocampi for RNA or Protein Analysis

Young or old mice were anesthetized and perfused with 20 mL saline, followed by dissection of hippocampi. For RNA extraction, tissue was placed in 1 mL Trizol (Invitrogen) and homogenized, followed by chloroform extraction as previously described [50]. For protein extraction, hippocampi tissue was homogenized in RIPA buffer (50 mM Tris, 150 mM NaCl, 1% NP40, 0.25% sodium deoxycholate and 1 mM EDTA, pH 7.4) containing 1X protease inhibitor (Roche), 1 mM Phenylmethylsulfonyl fluoride (PMSF), 1 mM sodium fluoride and 1 mM sodium orthovanadate. The tissue debris was spun at 10K rpm for 5 min at 4C, and supernatant containing protein extract snap frozen with dry ice.

RNA Extraction, RT-PCR and real-time PCR

Total RNA was extracted from primary neural progenitor cells or young and old murine hippocampi using Trizol reagent (Invitrogen) according to manufacturer's instructions. 1 ug of total RNA was used for cDNA synthesis with Olig D_t primers (Invitrogen). For real-time PCR amplification and quantification of genes of interest, an initial amplification using specific primers to each gene of interest (realtimeprimers.com) was done with a denaturation step at 95°C for 5 min, followed by 40 cycles of denaturation at 95°C for 1 min, primer annealing at 55°C for 30 s, and primer extension at 72°C for 30 s. Real-time PCR was performed using SYBR and an ABI PRISM 7500 Sequence Detection System (Applied Biosystems). Reactions were run in triplicate in three independent experiments. The geometric mean of housekeeping gene *GAPDH* was used as an internal control to normalize the variability in expression levels and were analyzed using the $2^{-\Delta\Delta CT}$ method described [53].

ELISA

The concentration of active TGF-β1 in blood serum or tissue protein lysate was determined using enzyme-linked immunoabsorbent assay (ELISA)-based cytokine antibody array (R&D), according to manual instructions.

Immunocytochemistry

Mice were anesthetized and perfused with saline and 4% PFA. Brains were collected and placed in 4% PFA overnight for a post fixation, followed by dehydration in 30% sucrose/PBS at 4^0C for 2 days. Brains were then sectioned at 40 μM using a vibratome and stored in a glycerol-based cryoprotectant at -20^0C until further analysis by immunostaining. For non-BrdU/EdU staining, sections were washed 3 times for 15 minutes in TBS, followed by one hour blocking in a permeabilization/staining buffer, TBS++ (3% Donkey Serum and 0.25% Tween X-100 in TBS), then incubated with primary antibodies of interest (see Antibodies) for 72 hours. For secondary staining, sections were washed 3 times, 15

minutes each in TBS, followed by 2 hour incubation in donkey raised, fluorophore-conjugated, species-specific secondary antibodies (Jackson Immunoresearch) at 1:250 dilution in TBS++. Following secondary staining, sections underwent 3, 15 minute washes in TBS, with 4 µM Hoechst in the second wash. Finally, the sections were mounted on positively charged frosted slides, dried overnight and imaged with a prairie confocal microscope.

BrdU In vivo Labeling and Immunostaining
Mice were intraperitoneally injected with BrdU (50 mg/kg of body weight, Sigma Aldrich) dissolved in saline to label mitotic cells. Sections were incubated in SSC/formamide at 65^0C water for 2 hours, washed in TBS, followed by 2N HCl for 15 minutes. They were then placed in 2X Saline-Sodium Citrate (SSC) for 30 minutes, .1 mM Borate Buffer for 15 minutes, followed by 6, 15 minute washes in TBS, then blocked in a permeabilization/staining buffer, TBS++ for 2 hours. Sections were then incubated with αRat-BrdU (Abcam Inc. ab6326) and other antibodies (see Antibodies section) in TBS++ at 4^0C for 72 hours. Secondary staining was done as described above.

EdU In vivo Labeling and Immunostaining
Mice were intraperitoneally injected with EdU (50 mg/kg of body weight, Invitrogen) dissolved in phosphate-buffered saline to label mitotic cells. Brain sections were post-fixed with 4% PFA for 30 minutes after primary and secondary staining, and treated for EdU visualization using the Click-iT EdU kit (Invitrogen), as per the manual's instructions.

Muscle progenitor cells were fixed with cold, 70% ethanol and stained for αRabbit-Desmin and secondary staining as described below under muscle methods. Following secondary staining, cells were treated for EdU visualization using the Click-iT EdU kit (Invitrogen), as per the manual's instructions.

Western Blot Analysis

Primary neural or muscle progenitor cells, or whole muscle tissue were lysed in RIPA buffer (50 mM Tris, 150 mM NaCl, 1% NP40, 0.25% sodium deoxycholate and 1 mM EDTA, pH 7.4) containing 1X protease inhibitor (Roche), 1 mM Phenylmethylsulfonyl fluoride (PMSF), 1 mM sodium fluoride and 1 mM sodium orthovanadate. The protein concentration was determined by Bradford assay (Bio-Rad). Lysates were resuspended in 1X Laemmli buffer (Bio-Rad), boiled for 5 minutes and separated on precast 7.5% or 4-15% TGX gels (Biorad). Primary antibodies were diluted in 5% non-fat milk in TBS + 0.1% Tween-20, and nitrocellulose membranes were incubated with antibody mixtures overnight at 4 °C. HRP-conjugated secondary antibodies (Santa Cruz Biotech) were diluted 1:500 in 5% non-fat milk in TBS + 0.1% Tween-20 and incubated for 1 hour at room temperature. Blots were developed using Western Lightning ECL reagent (Perkin Elmer), and analyzed with Bio-Rad Gel Doc/Chemi Doc Imaging System and Quantity One software. Results of multiple assays were quantified using Applied Biosystems of Image J software. Pixel Intensity of bands of interest were normalized with pixel intensity of glyceraldehydes-3-phosphate dehydrogenase or β-actin.

In vitro validation of Alk5 inhibitor in rNPCs

Following overnight rNPC culturing in growth medium at a density of 300,000 cells per well of a 6 well tissue culture plate, rNPCs were starved in a basal medium (lacking FGF-2) for 1 hour, then untreated, or treated with 1 ng/mL TGF-β1 for 1 hour in the presence/absence of 5 uM of Alk5 inhibitor, followed by a PBS wash and cell scraping to collect cells into RIPA buffer for western blot analysis.

In vivo Validation of Alk5 inhibitor

Aged (24 month old) C57BL6/J male mice were injected intraperitonially (IP) with TGF-β1 Type I Receptor Kinase Alk5 inhibitor 2-(3-(6-Methylpyridin-2-yl)-1*H*-pyrazol-4-yl)-1,5-naphthyridine (Enzo Life Sciences) diluted in sunflower seed oil to a concentration of 57.4 µM. Mice (n=4) received 100 uL IP injections of the Alk5 inhibitor or vehicle control once daily for 11 days, and were perfused on the 12th day. Tibialis Anterior muscle was injured with cardiotoxin after one week of IP injections, on day 7 (as described below in muscle methods). Additionally, on day 7 we began daily IP BrdU injections (50 mg/kg body weight). Four hours after receiving the fifth BrdU IP injection, the mice were perfused (on Day 12), and brains and TAs were collected for analysis.

Lentiviral and Retroviral Vector Construction, Packaging, and Purification

A DNA cassette encoding human U6 promoter-driven expression of shRNA against mouse SMAD3 (Gene ID: 17127) was constructed by PCR with flanking *Pac I* sites and, following restriction digestion and phenol/chloroform purification, ligated into the *Pac I* site of the pFUGW lentiviral vector. Five candidate sequences were tested for knockdown efficiency, and the most effective sequence (shSMAD 3.4 in **Extended Table 1**) was selected for experimental studies. Sequences for all shRNAs tested are provided in **Extended Table 1**. The control shRNA vector against *LacZ* was constructed previously [50]. PCR was performed with Phusion DNA Polymerase (New England Biolabs) under the following conditions: 98 °C for 2 min, 30 cycles of 12 s at 95 °C, 30 s at 65 °C, and 25 s at 72 °C, with a final extension step of 2 min at 72 °C. Lentiviral and retroviral vectors were packaged and purified using standard methods as described [54].

A dominant negative TGFBR2 retroviral plasmid was obtained (Addgene, Cambridge, MA, http://www.addgene.org/12640/) and packaged and purified as previously described [55].

In vitro Validation of Smad3 shRNA Vector

Mouse myoblasts were cultured for 24 hours at a density of 100,000 cells per well of a 6 well tissue culture plate in 50% growth medium and 50% lentiviral supernatant (in DMEM + 10%FBS), packaged as previously described [55], followed by culturing in growth medium for a total of 72 hours. Cells were then washed once with PBS, scraped and collected into RIPA for western blot analysis.

mNPCs were plated at 200,000 cells per well of a 6 well tissue culture plate in growth medium, and transduced with lentivirus encoding shRNA to Smad3 or lacZ at a multiplicity of infection (MOI) of 5 and cultured for two weeks. RNA was extracted with Trizol (Invitrogen) followed by qPCR to assess levels of Smad3 (see **Extended Table 1** for sequences).

In vivo Loss of Function with shRNA

Aged (18 month) C57BL6/J male mice received lateral intrahippocampal injections of 1 µl of lentiviral solutions (LV-shRNA-Smad3-GFP or LV-shRNA-lacZ-GFP, 1-3 x 10^8 IU/mL) in PBS on day -14, on the right hemisphere hippocampus, at 0.25 uL per minute. The injection coordinates with respect to bregma were -2.12 anteriorposterior, -1.55 dorsoventral (from the dura), and 1.5 mediolateral (refer to **Figure 5a**). Mice were allowed to recover 14 days, followed by BrdU IP injections (50 mg/kg

bodyweight) 1X daily for 5 days. One day after receiving the fifth BrdU IP injection, mice were saline and 4% PFA perfused. Immunostaining and Quantification described elsewhere.

Aged (18 month) C57BL6/J male mice received lateral intrahippocampal injections of 1 µl of lentiviral solutions (LV-shRNA-Smad3-GFP or LV-shRNA-lacZ-GFP, 1-3 x 10^8 IU/mL) in PBS on day -14, on the right hemisphere hippocampus, at 0.25 uL per minute. The injection coordinates with respect to bregma were -2.12 anteriorposterior, -1.55 dorsoventral (from the dura), and 1.5 mediolateral (refer to **Extended Data Figure 4**). Mice were allowed to recover 14 days, followed by EdU IP injections (50 mg/kg bodyweight) 1X daily for 5 days. Five days after receiving the fifth EdU IP injection, mice were saline and 4% PFA perfused. Immunostaining and Quantification described elsewhere.

shRNA Muscle Injection
Aged (24 month) C57BL6/J male mice were injured with CTX in the tibialis anterior (TA) muscle in two sites as described below, and on the following day 5 µl of concentrated lentiviruses carrying Smad3 shRNA or LacZ shRNA were injected to the injury sites using a 30 gauge needle. Mice TAs were harvested 5 days post injury, as described below.

In vitro Validation of dnTGFBR2 Vector

Neural progenitor cells (NPCs) were transduced with retroviruses carrying dominant negative TGFBR2 (Addgene, Cambridge, MA, http://www.addgene.org/12640/) which has a cytoplasmic truncation and a FLAG tag, or GFP control and cultured for 72 hours. GFP and dnTGFBR2-transduced cell lysates were prepared as described in western blotting methods, and probed on western blots for the FLAG-tagged dnTGFBR2 using anti-FLAG antibody (Santa Cruz), GFP (Abcam), pSmad3 (Epitomics), Smad2/3 (Santa Cruz), and βactin (Cell Signaling). Transduced NPCs were also plated at 300,000 cells per well of a 6-well tissue culture plate and cultured in basal medium (DMF12 + N2) after cell splitting for 4 hours, followed by 45 minute treatment with 0,1, or 12.5 ng/mL TGF-β1 . Cell pellets were lysed in 100 uL RIPA buffer, and probed on western blots for pSmad3, Smad2/3, and βactin.

For proliferation assay, NPCs were transduced with 3µL concentrated retroviruses per $3x10^5$ cells, delivering dnTGFBR2 or GFP and cultured for one week. Transduced NPCs were then split at 80,000 cells per well into 8-well chamber slides and cultured overnight in growth medium (DMF12 + N2 + 10 ng/mL FGF-2) in the presence/absence of 10 ng/mL TGF-β1. 16 hours post addition of TGF-β1, cells were pulsed for 4 hours with EdU (30µM). Cells were fixed with 4%PFA for 20 minutes, and immunostained for FLAG (Abcam), GFP (Abcam), EdU (Invitrogen), and Sox2 (Santa Cruz), as described in immunocytochemistry methods.

In vivo Muscle Injection of dnTGFBR2 Retrovirus

Aged (18 month) C57BL6/J male mice were injured with CTX in the tibialis anterior muscle in two sites and in the gastrocnemius muscle in four sites as described below, and 5 µl of concentrated retroviruses carrying dnTGFBR2 or GFP control were injected to the injury sites using a 30 gauge needle at different time points (see figure 6 for details). Mice received EdU IP injection (50 mg/kg) 12 hours before muscle harvest at 5 days post injury.

Muscle Injury

Isoflurane was used to anesthetize the animal during the muscle injury procedure. For bulk myofiber

satellite cell activation, gastrocnemius muscles were injected with cardiotoxin 1 (Sigma) dissolved at 100 micrograms per milliliter in PBS, at 4 sites of 5 microliters each for each muscle. Muscles were harvested 3 days later. For focal injury to assay regeneration by immunoanalysis and histology, 5 microliters of 0.5 milligram per milliliter CTX was injected to two sites at the middle of the tibialis anterior muscle, and muscle harvested 5 days later.

Muscle Fibers and Muscle Progenitor Cell Isolation

Injured gastrocnemius muscle was dissected from old mice and incubated at 37°C in digestion medium (150 U/mL Collagenase type II in DMEM medium, buffered with 30 mM HEPES) for 2 hours. Digested muscle was gently triturated and myofibers were collected. Myofibers were further digested with 1 U/mL Dispase and 40 U/mL Collagenase type II to liberate muscle stem cells [52]. Muscle stem cells were cultured in DMEM (Life Sciences) with 5% serum from the same age mouse.

Muscle Tissue Immunofluorescence and Histological Analysis

Muscle tissue was dissected, flash frozen in OCT compound (Tissue Tek; Sakura) and cryo-sectioned at 10 micrometers. Cryo-sectioning was performed through the entire volume of muscle (50–70 sections total, done at 200 μm intervals), thereby serially sampling the entire tissue. Muscle sections were stained with aqueous hematoxylin and eosin (H&E), as per the manufacturer's instructions (Sigma-Aldrich). Regeneration and myogenic potential was quantified by examining injury sites from representative sections along the muscle spanning the injury, then by measuring the injured area using Adobe Photoshop Elements. Myofiber regeneration was quantified by counting total newly regenerated fibers and dividing by the regeneration area. Immunostaining was performed as described [56]. Briefly, after permeabilization in PBS + 1% FBS + 0.25% Triton-X-100, tissues and cells were incubated with primary antibodies in staining buffer (PBS + 1% FBS) for 1 h at room temperature, followed by 1 h incubation fluorochrome-labeled secondary antibodies (ALEXA at 1:1000). BrdU-specific immunostaining required an extra step of 2 M HCl treatment before permeablization.

Whole Muscle Tissue Analysis

Whole muscle from young and old resting TA and TA adjacent to cardiotoxin injured gastrocnemius muscle was isolated and lysed as described earlier [9]. In brief, muscles were lysed using Miltenyi Biotec Tissue Dissociator in tissue lysate buffer and lysates were run on 7.5% Criterion gel (BioRad) and western blotted against TGF-β1 (R&D, mouse monoclonal antibody) and GAPDH (Abcam, goat polyclonal) antibody. The images were quantified using Image J software and P values calculated using student's t-test.

Quantification and Statistical Analysis

For quantification of immunofluorescent images for BrdU incorporation, 25 20x images per replicate were taken on the Molecular Devices ImageXpress Micro automated epifluorescence imager, followed by automated cell quantification using the multiwavelength cell scoring module within the MetaXpress analysis software. Data was analyzed using Anova and P values equal or lower than 0.05 were considered statistically significant. Sample sizes of n=3 or greater were determined for each experiment based on previously published experimental group numbers [2,32,50] and assessed for significance based on p values and heteroscedastic variance between groups that were statistically compared.

For quantification of the number of BrdU+ or BrdU+Sox2+ cells in Alk5 inhibitor treated mice, unbiased stereology (Zeiss Axio Imager, software by MicroBrightfield) using the optical fractionator method was performed on 8 vibratome coronal brain slices spanning the hippocampus (40 microns thick, 200 microns apart), and the number of selected cells was normalized by the volume of hippocampal tissue analyzed. For quantification in shRNA viral vector injected brains, confocal stacks of 8 vibratome coronal GFP+ brain slices spanning the hippocampus (40 microns thick, 200 microns apart) were acquired on a Prairie confocal microscope and cells were counted. Cell numbers were normalized to the volume of the DG granule cell layer measured by ImageJ and as previously described [4].

Inclusion/Exclusion Criteria
Only aged mice that died during the study due to health reasons were excluded from analysis. In terms of automated counting of cells using MetaXpress analysis software, only sites that were blurry with indistinguishable colors (such as areas on the slide with bubbles or sites imaged with incorrect focus by the Molecular Devices ImageXpress Micro automated epifluorescence imager), or areas with large cell clumps were excluded from the cell quantification analysis. These criteria were pre-established.

When performing in vivo experiments, such as Alk5 inhibitor injections or shRNA steretaxic brain injections, there was no blinding. For quantification and analysis, researchers were blinded to the group allocation, specifically when doing regenerative index calculations, stereology and cell counts.

Antibodies

αRabbit-pSmad2 (Millipore AB3849), αRabbit-βactin (Cell Signaling #4967), αMouse-TGFβ1 (R&D MAB240), αMouse-TGFβ1,2,3 (R&D MAB1835), EdU Click-it kit (Invitrogen C10337 and C10338), αGuineyPig-DCX (Millipore AB2253), αGoat-Sox2 (Santa Cruz SC-17320), αRabbit-Desmin (Abcam ab32362), αMouse-embryonic myosin heavey chain (eMyHC) (Hybridoma Bank, clone F1.652), αChicken-GFP (Abcam ab13970), αRabbit-FLAG (Santa Cruz sc-807), αMouse-FLAG (Abcam ab18230),αRabbit-pSmad3 (Epitomics #1880-1), αRat-BrdU (Abcam ab6326), TGF-β1 ELISA kit (R&D DY1679), αMouse-Smad2/3 (Santa Cruz sc-133098), αRabbit-B2M (Abcam ab75853), αGoat-GapDH (Abcam ab9483)

Acknowledgements
This work was supported by grants from the National Institutes of Health R01 AG02725201 and California Institute for Regenerative Medicine RN1-00532-1 to IMC, CIRM grant RT2-02022 to DVS, and NSF Pre-doctoral fellowship to HY. We thank Mary West and the CIRM/QB3 Shared Stem Cell Facility at UC Berkeley for designing the MetaXpress journal for quantification of pSmad3 pixel intensity in Sox2+ cells, for use of the Molecular Devices ImageXpress and Prairie 2P/Confocal microscope and training on these instruments. We thank Mustafa Alkhouli for assisting with animal injections and care, cell counts, brain staining and image processing; Pamela Rios for assistance in histology staining and RI calculations of dnTGFBR2 injected muscle TAs; Hikaru Mamiya and Matthew Zeiderman for assistance in *in vitro* rNPC staining, qPCRs and westerns to test for shRNA-Smad3 efficacy; Eric Jabart for the dnTGFBR2 plasmid and reagents and thoughtful discussion; Manika Paul for her assistance with brain staining and image processing, acquisition of pSmad3 pixel intensity, and cell counts; and Ashutosh Shrestha for assistance with cell staining and imaging.

Author contributions
HY produced and assessed all viral particles, designed, performed and analyzed the experiments for

Figures 1-6, Extended Data Figures 1a, 2, 3, 4 a-c, 5, and 6, designed and analyzed experiments for Figure 7, interpreted these data and co-wrote the manuscript. MJC designed and performed experiments for Figures 4d-e, 6a-g, Extended Data Figure 4d-e, designed experiments for Figure 7, interpreted these data and edited the manuscript. AM performed and analyzed experiments for Figures 5-7 and Extended Data Figures 4a-c; CS performed and analyzed experiments for Figures 4,5, and Extended Data Figure 2a-b. LB designed and cloned Smad3 shRNA constructs. PP provided data for Extended Data Figure 1b-c. CG performed and analyzed experiments for Extended Data Figure 4d-e. IMC and DVS designed, directed and integrated the study, interpreted the data, and co-wrote the manuscript.

Extended Table 1

	shRNA and qPCR Primer Sequences
shRNA Smad 3.1	5'-GCCCATGTTTCTGCATGGATTTCTCTTCAAGAGAGAGAAATCCATGCAGAAACATGGGCTTTTT-3'
shRNA Smad 3.2	5'-GCTGTCCAATGTCAACCGGAATCTCTTCAAGAGAGAGATTCCGGTTGACATTGGACAGCTTTTT-3'
shRNA Smad 3.3	5'-GCATCCGTATGAGCTTCGTCAACTCTTCAAGAGAGAGTTGACGAAGCTCATACGGATGCTTTTT-3'
shRNA Smad 3.4	5'-GGACCTGAGTGAAGATGGAGATTCAAGAGATCTCCATCTTCACTCAGGTCTTTTT-3'
shRNA Smad 3.5	5'-GGGTCCAATGTCAACCGGAATTTCAAGAGAATTCCGGTTGACATTGGACCTTTTT-3'
shRNA lacZ	Sense: 5'-GGGGTTAATTAAAAGGTCGGGCAGGAAGAGGGC-3' Antisense: 5'-GGGGTTAATTAAAAAAAGTGACCAGCGAATACCTGTTCTC-3'
Tgfb1	F: 5'-GCT ACC ATG CCA ACT TCT GT -3'; R: 5'-CGT AGT AGA CGA TGG GCA GT-3'
p21	F: 5'-CCG CGG TGT CAG AGT CTA-3'; R: 5'-CAT GAG CGC ATC GCA ATC-3'
Smad3	F: 5'-ACC AAG TGC ATT ACC ATCC-3'; R: 5'-CAG TAG ATA ACG TGA GGG AGC CC-3'
GapDH	F: 5'-CTGGAGAAACCTGCCAAGTA-3' R: 5'-TGTTGCTGTAGCCGTATTCA-3'

References

1 Conboy, I. M. & Rando, T. A. Heterochronic parabiosis for the study of the effects of aging on stem cells and their niches. *Cell cycle (Georgetown, Tex* 11, 2260-2267 (2012).

2 Miranda, C. J. *et al.* Aging brain microenvironment decreases hippocampal neurogenesis through Wnt-mediated survivin signaling. *Aging cell* 11, 542-552, doi:10.1111/j.1474-9726.2012.00816.x (2012).

3 Okamoto, M. *et al.* Reduction in paracrine Wnt3 factors during aging causes impaired adult neurogenesis. *FASEB J* 25, 3570-3582, doi:10.1096/fj.11-184697 (2011).

4 Seib, D. R. *et al.* Loss of Dickkopf-1 restores neurogenesis in old age and counteracts cognitive decline. *Cell stem cell* 12, 204-214, doi:10.1016/j.stem.2012.11.010 (2013).

5 Loffredo, F. S. *et al.* Growth differentiation factor 11 is a circulating factor that reverses age-related cardiac hypertrophy. *Cell* 153, 828-839, doi:10.1016/j.cell.2013.04.015 (2013).

6 Villeda, S. A. *et al.* The ageing systemic milieu negatively regulates neurogenesis and cognitive function. *Nature* 477, 90-94 (2011).

7 Vukovic, J., Colditz, M. J., Blackmore, D. G., Ruitenberg, M. J. & Bartlett, P. F. Microglia modulate hippocampal neural precursor activity in response to exercise and aging. *J Neurosci* 32, 6435-6443, doi:10.1523/JNEUROSCI.5925-11.2012 (2012).

8 Carlson, M. E. *et al.* Relative roles of TGF-beta1 and Wnt in the systemic regulation and aging of satellite cell responses. *Aging cell* 8, 676-689 (2009).

9 Paliwal, P., Pishesha, N., Wijaya, D. & Conboy, I. M. Age dependent increase in the levels of osteopontin inhibits skeletal muscle regeneration. *Aging* 4, 553-566 (2012).

10 Ruckh, J. M. *et al.* Rejuvenation of regeneration in the aging central nervous system. *Cell stem cell* 10, 96-103, doi:10.1016/j.stem.2011.11.019 (2012).

11 Doyle, K. P., Cekanaviciute, E., Mamer, L. E. & Buckwalter, M. S. TGFbeta signaling in the brain increases with aging and signals to astrocytes and innate immune cells in the weeks after stroke. *Journal of neuroinflammation* 7, 62, doi:10.1186/1742-2094-7-62 (2010).

12 Allen, R. E. & Boxhorn, L. K. Regulation of skeletal muscle satellite cell proliferation and differentiation by transforming growth factor-beta, insulin-like growth factor I, and fibroblast growth factor. *Journal of cellular physiology* 138, 311-315, doi:10.1002/jcp.1041380213 (1989).

13 Buckwalter, M. S. *et al.* Chronically increased transforming growth factor-beta1 strongly inhibits hippocampal neurogenesis in aged mice. *Am J Pathol* 169, 154-164 (2006).

14 Carlson, M. E. *et al.* Molecular aging and rejuvenation of human muscle stem cells. *EMBO molecular medicine* 1, 381-391 (2009).

15 Han, G., Li, F., Singh, T. P., Wolf, P. & Wang, X. J. The pro-inflammatory role of TGFbeta1: a paradox? *International journal of biological sciences* 8, 228-235 (2012).

16 Bohatschek, M., Kloss, C. U., Hristova, M., Pfeffer, K. & Raivich, G. Microglial major histocompatibility complex glycoprotein-1 in the axotomized facial motor nucleus: regulation and role of tumor necrosis factor receptors 1 and 2. *The Journal of comparative neurology* 470, 382-399, doi:10.1002/cne.20017 (2004).

17 Rico, M. C., Rough, J. J., Del Carpio-Cano, F. E., Kunapuli, S. P. & DeLa Cadena, R. A. The axis of thrombospondin-1, transforming growth factor beta and connective tissue growth factor: an emerging therapeutic target in rheumatoid arthritis. *Current vascular pharmacology* 8, 338-343 (2010).

18 Sanjabi, S., Zenewicz, L. A., Kamanaka, M. & Flavell, R. A. Anti-inflammatory and pro-inflammatory roles of TGF-beta, IL-10, and IL-22 in immunity and autoimmunity. *Current opinion in pharmacology* 9, 447-453, doi:10.1016/j.coph.2009.04.008 (2009).

19 Lan, T. H., Huang, X. Q. & Tan, H. M. Vascular fibrosis in atherosclerosis. *Cardiovascular pathology : the official journal of the Society for Cardiovascular Pathology* 22, 401-407, doi:10.1016/j.carpath.2013.01.003 (2013).
20 Carlson, M. E., Hsu, M. & Conboy, I. M. Imbalance between pSmad3 and Notch induces CDK inhibitors in old muscle stem cells. *Nature* 454, 528-532 (2008).
21 Inman, G. J. Switching TGFbeta from a tumor suppressor to a tumor promoter. *Current opinion in genetics & development* 21, 93-99, doi:10.1016/j.gde.2010.12.004 (2011).
22 Yoo, Y. D. *et al.* TGF-beta-induced cell-cycle arrest through the p21(WAF1/CIP1)-G1 cyclin/Cdks-p130 pathway in gastric-carcinoma cells. *International journal of cancer. Journal international du cancer* 83, 512-517 (1999).
23 Harry, G. J. Microglia during development and aging. *Pharmacology & therapeutics* 139, 313-326, doi:10.1016/j.pharmthera.2013.04.013 (2013).
24 Pineda JR, Daynac M, Chicheportiche A, Cebrian-Silla A, Sii Felice K, Garcia-Verdugo JM, Boussin FD, Mouthon M-A (2013) Vascular-derived TGF-β increases in the stem cell niche and perturbs neurogenesis during aging and following irradiation in the adult mouse brain. *EMBO Mol Med 5*:548–562 (2013).
25 Ming, G. L. & Song, H. Adult neurogenesis in the mammalian central nervous system. *Annual review of neuroscience* 28, 223-250, doi:10.1146/annurev.neuro.28.051804.101459 (2005).
26 Walter, J., Keiner, S., Witte, O. W. & Redecker, C. Age-related effects on hippocampal precursor cell subpopulations and neurogenesis. *Neurobiology of aging* 32, 1906-1914, doi:10.1016/j.neurobiolaging.2009.11.011 (2011).
27 Maslov, A. Y., Barone, T. A., Plunkett, R. J. & Pruitt, S. C. Neural stem cell detection, characterization, and age-related changes in the subventricular zone of mice. *J Neurosci* 24, 1726-1733, doi:10.1523/JNEUROSCI.4608-03.2004 (2004).
28 Olariu, A., Cleaver, K. M. & Cameron, H. A. Decreased neurogenesis in aged rats results from loss of granule cell precursors without lengthening of the cell cycle. *The Journal of comparative neurology* 501, 659-667, doi:10.1002/cne.21268 (2007).
29 Allen, R. E. & Boxhorn, L. K. Regulation of skeletal muscle satellite cell proliferation and differentiation by transforming growth factor-beta, insulin-like growth factor I, and fibroblast growth factor. *Journal of cellular physiology* 138, 311-315 (1989).
30 Gartel, A. L. & Radhakrishnan, S. K. Lost in transcription: p21 repression, mechanisms, and consequences. *Cancer research* 65, 3980-3985, doi:10.1158/0008-5472.CAN-04-3995 (2005).
31 Jeong, J., Conboy, M. J. & Conboy, I. M. Pharmacological inhibition of myostatin/TGF-beta receptor/pSmad3 signaling rescues muscle regenerative responses in mouse model of type 1 diabetes. *Acta pharmacologica Sinica* 34, 1052-1060, doi:10.1038/aps.2013.67 (2013).
32 Conboy, I. M., Conboy, M. J., Smythe, G. M. & Rando, T. A. Notch-mediated restoration of regenerative potential to aged muscle. *Science (New York, N.Y* 302, 1575-1577 (2003).
33 Conboy, I. M. & Rando, T. A. Aging, stem cells and tissue regeneration: lessons from muscle. *Cell cycle (Georgetown, Tex* 4, 407-410 (2005).
34 Conboy, I. M. *et al.* Rejuvenation of aged progenitor cells by exposure to a young systemic environment. *Nature* 433, 760-764 (2005).
35 Dumont, N. & Arteaga, C. L. A kinase-inactive type II TGFbeta receptor impairs BMP signaling in human breast cancer cells. *Biochem Biophys Res Commun* 301, 108-112 (2003).
36 Hanisch, U. K. Proteins in microglial activation--inputs and outputs by subsets. *Current protein & peptide science* 14, 3-15 (2013).
37 Knight, J. C. Genomic modulators of the immune response. *Trends in genetics : TIG* 29, 74-83, doi:10.1016/j.tig.2012.10.006 (2013).
38 van den Elsen, P. J. & Gobin, S. J. The common regulatory pathway of MHC class I and class II

transactivation. *Microbes and infection / Institut Pasteur* 1, 887-892 (1999).
39 Solheim, J. C. Class I MHC molecules: assembly and antigen presentation. *Immunological reviews* 172, 11-19 (1999).
40 Neefjes, J. J. & Momburg, F. Cell biology of antigen presentation. *Current opinion in immunology* 5, 27-34 (1993).
41 Elmer, B. M. & McAllister, A. K. Major histocompatibility complex class I proteins in brain development and plasticity. *Trends in neurosciences* 35, 660-670, doi:10.1016/j.tins.2012.08.001 (2012).
42 Shatz, C. J. MHC class I: an unexpected role in neuronal plasticity. *Neuron* 64, 40-45, doi:10.1016/j.neuron.2009.09.044 (2009).
43 Huh, G. S. *et al.* Functional requirement for class I MHC in CNS development and plasticity. *Science (New York, N.Y* 290, 2155-2159 (2000).
44 Adelson, J. D. *et al.* Neuroprotection from stroke in the absence of MHCI or PirB. *Neuron* 73, 1100-1107, doi:10.1016/j.neuron.2012.01.020 (2012).
45 Higuchi, I. *et al.* Vacuolar myositis with expression of both MHC class I and class II antigens on skeletal muscle fibers. *Journal of the neurological sciences* 106, 60-66 (1991).
46 Munz, C., Lunemann, J. D., Getts, M. T. & Miller, S. D. Antiviral immune responses: triggers of or triggered by autoimmunity? *Nature reviews. Immunology* 9, 246-258, doi:10.1038/nri2527 (2009).
47 Silva, H. S., Conboy, I. M. & Gilliland, G. in *StemBook* (The Stem Cell Research Community, 2008).
48 Singh, T. & Newman, A. B. Inflammatory markers in population studies of aging. *Ageing research reviews* 10, 319-329, doi:10.1016/j.arr.2010.11.002 (2011).
49 Torchinsky, M. B. & Blander, J. M. T helper 17 cells: discovery, function, and physiological trigger. *Cellular and molecular life sciences : CMLS* 67, 1407-1421, doi:10.1007/s00018-009-0248-3 (2010).
50 Ashton, R. S. *et al.* Astrocytes regulate adult hippocampal neurogenesis through ephrin-B signaling. *Nature neuroscience* 15, 1399-1406, doi:10.1038/nn.3212 (2012).
51 Babu, H. *et al.* A protocol for isolation and enriched monolayer cultivation of neural precursor cells from mouse dentate gyrus. *Frontiers in neuroscience* 5, 89, doi:10.3389/fnins.2011.00089 (2011).
52 Conboy, M. J. & Conboy, I. M. Preparation of adult muscle fiber-associated stem/precursor cells. *Methods in molecular biology (Clifton, N.J* 621, 149-163 (2010).
53 Livak, K. J. & Schmittgen, T. D. Analysis of relative gene expression data using real-time quantitative PCR and the 2(-Delta Delta C(T)) Method. *Methods* 25, 402-408, doi:10.1006/meth.2001.1262 (2001).
54 Peltier, J. & Schaffer, D. V. Viral packaging and transduction of adult hippocampal neural progenitors. *Methods in molecular biology (Clifton, N.J* 621, 103-116, doi:10.1007/978-1-60761-063-2_7 (2010).
55 Yu, J. H. & Schaffer, D. V. High-throughput, library-based selection of a murine leukemia virus variant to infect nondividing cells. *J Virol* 80, 8981-8988 (2006).
56 Conboy, M. J., Cerletti, M., Wagers, A. J. & Conboy, I. M. Immuno-analysis and FACS sorting of adult muscle fiber-associated stem/precursor cells. *Methods in molecular biology (Clifton, N.J* 621, 165-173 (2010).

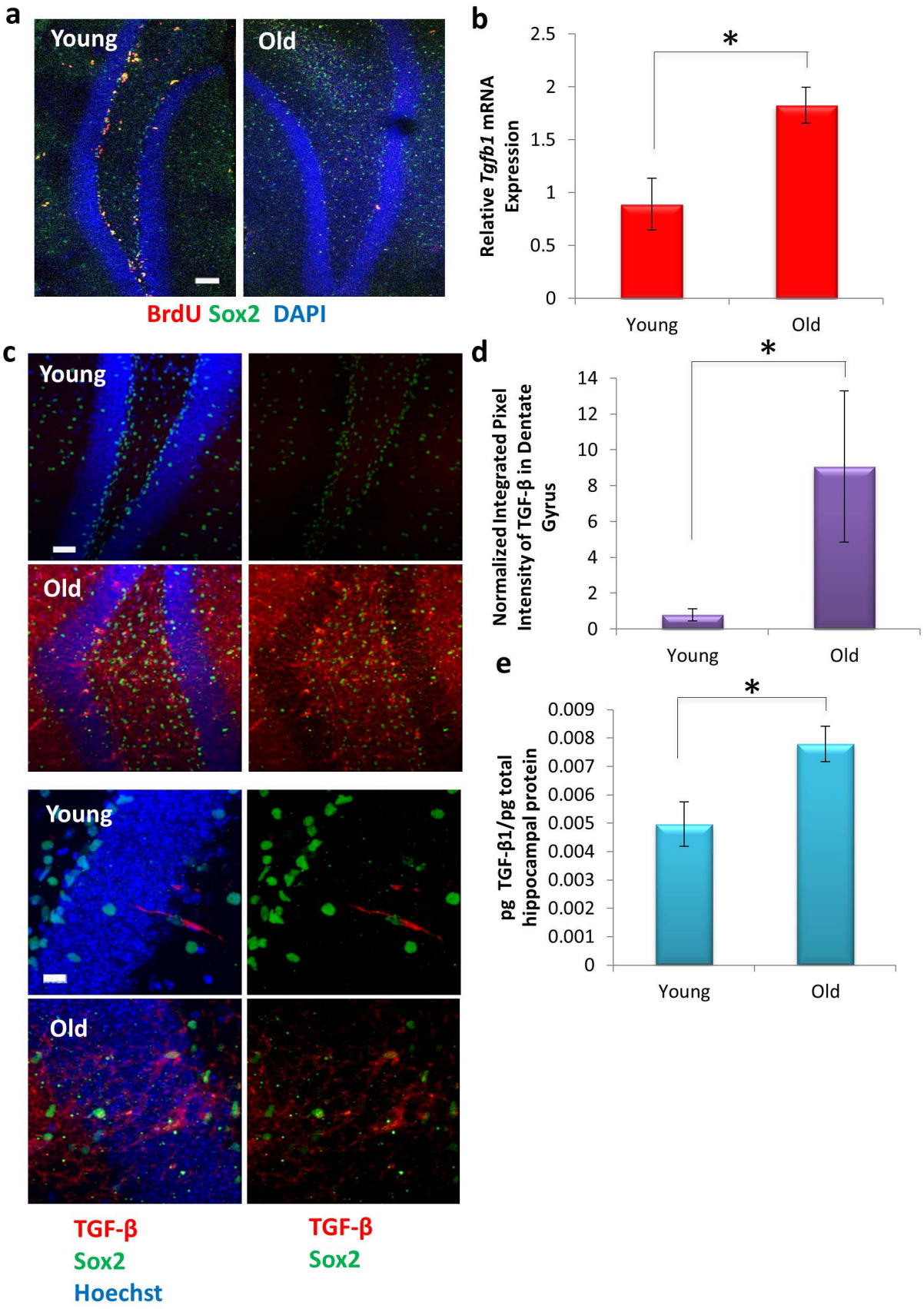
a
Young
Old
BrdU Sox2 DAPI
b
Relative Tgfb1 mRNA Expression
2.5
2
1.5
1
0.5
0
*
Young
Old
c
Young
Old
Young
Old
TGF-β
Sox2
Hoechst
TGF-β
Sox2
d
Normalized Integrated Pixel Intensity of TGF-β in Dentate Gyrus
14
12
10
8
6
4
2
0
*
Young
Old
e
pg TGF-β1/pg total hippocampal protein
0.009
0.008
0.007
0.006
0.005
0.004
0.003
0.002
0.001
0
*
Young
Old

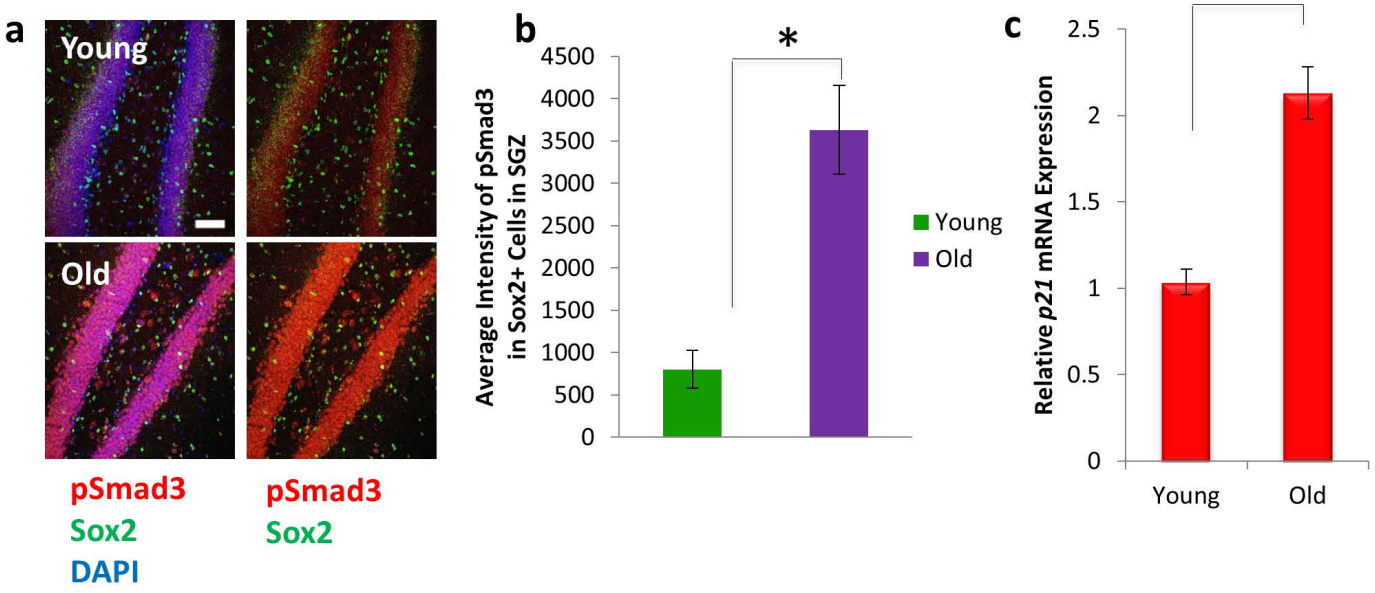
a
Young
Old
pSmad3
Sox2
DAPI
pSmad3
Sox2
b
Average Intensity of pSmad3 in Sox2+ Cells in SGZ
4500
4000
3500
3000
2500
2000
1500
1000
500
0
*
Young
Old
c
Relative p21 mRNA Expression
2.5
2
1.5
1
0.5
0
*
Young
Old

Figure 3

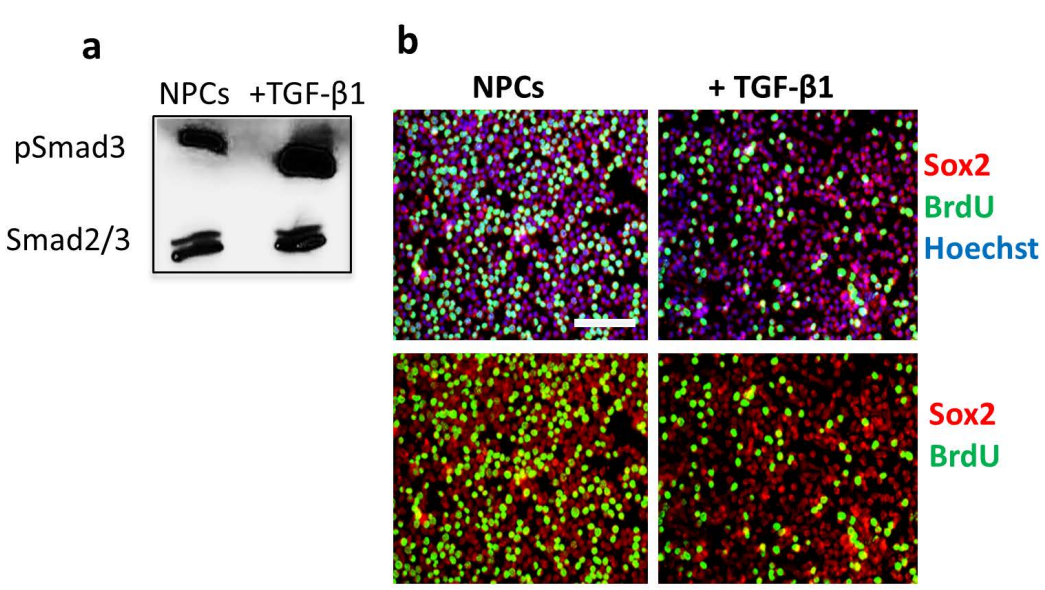
a
NPCs
+TGF-β1
pSmad3
Smad2/3
b
NPCs
+ TGF-β1
Sox2
BrdU
Hoechst
Sox2
BrdU
c
*
60.00
50.00
40.00
30.00
20.00
10.00
0.00
%BrdU+ rNPCs
Untreated
TGF-β

Figure 4

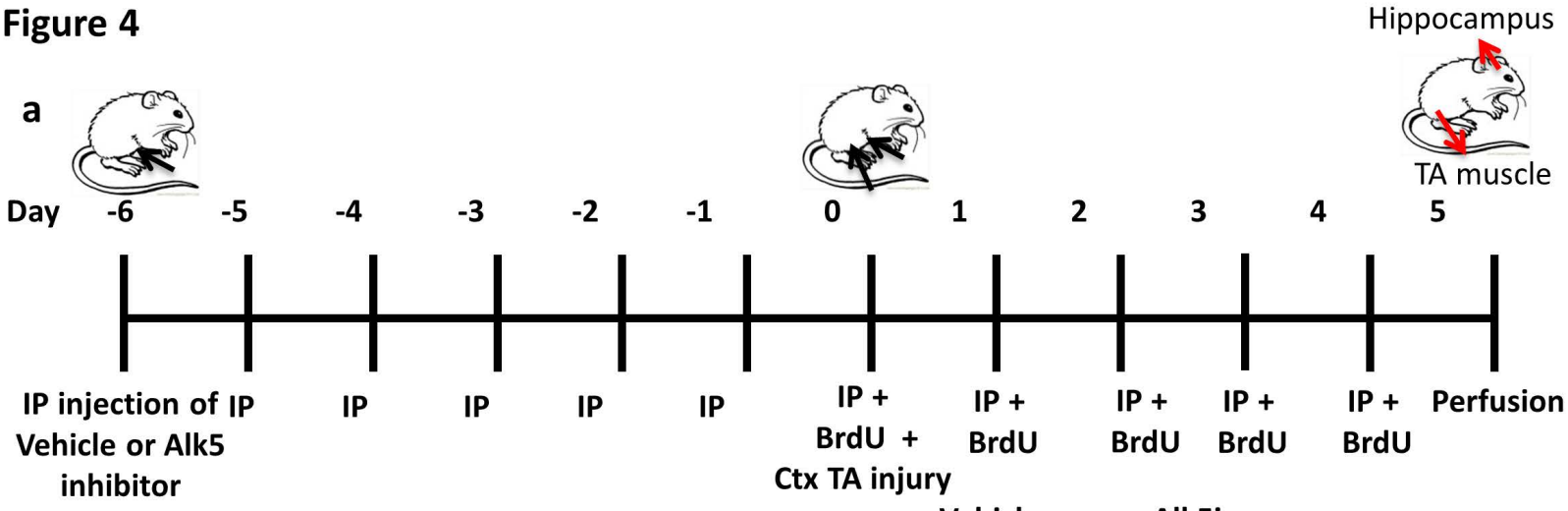
a
Hippocampus
TA muscle
Day -6 -5 -4 -3 -2 -1 0 1 2 3 4 5
IP injection of Vehicle or Alk5 inhibitor
IP
IP
IP
IP
IP
IP + BrdU + Ctx TA injury
IP + BrdU
IP + BrdU
IP + BrdU
IP + BrdU
Perfusion

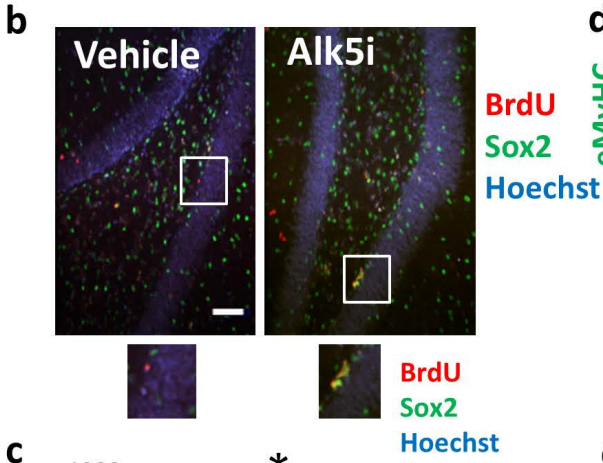
b
Vehicle
Alk5i
BrdU
Sox2
Hoechst
BrdU
Sox2
Hoechst

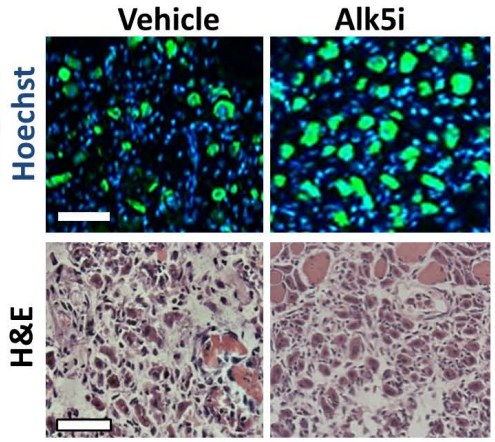
d
Vehicle
Alk5i
eMyHC
Hoechst
H&E

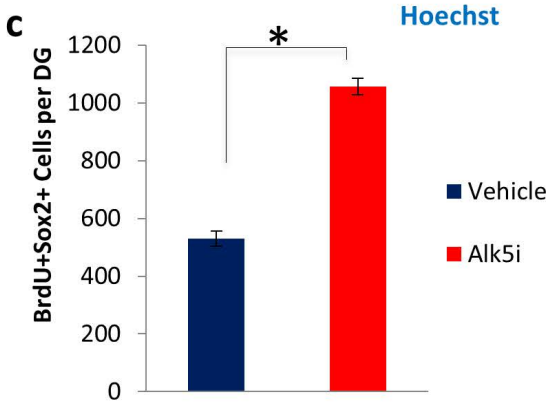
c
BrdU+Sox2+ Cells per DG
1200
1000
800
600
400
200
0
*
Vehicle
Alk5i

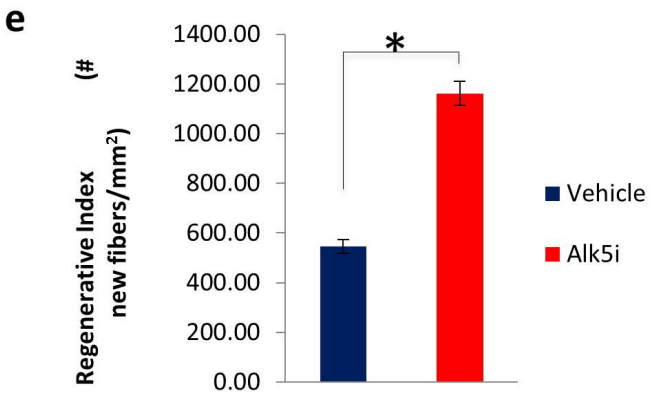
e
Regenerative Index (# new fibers/mm²)
1400.00
1200.00
1000.00
800.00
600.00
400.00
200.00
0.00
*
Vehicle
Alk5i

Figure 5

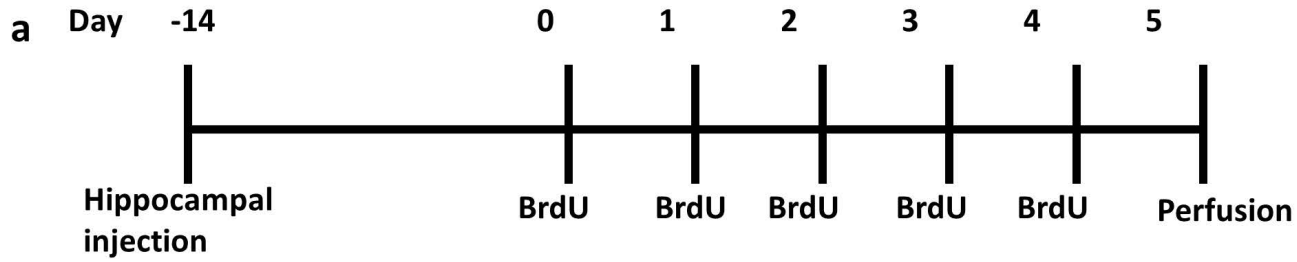
a
Day -14 0 1 2 3 4 5
Hippocampal injection
BrdU BrdU BrdU BrdU BrdU Perfusion

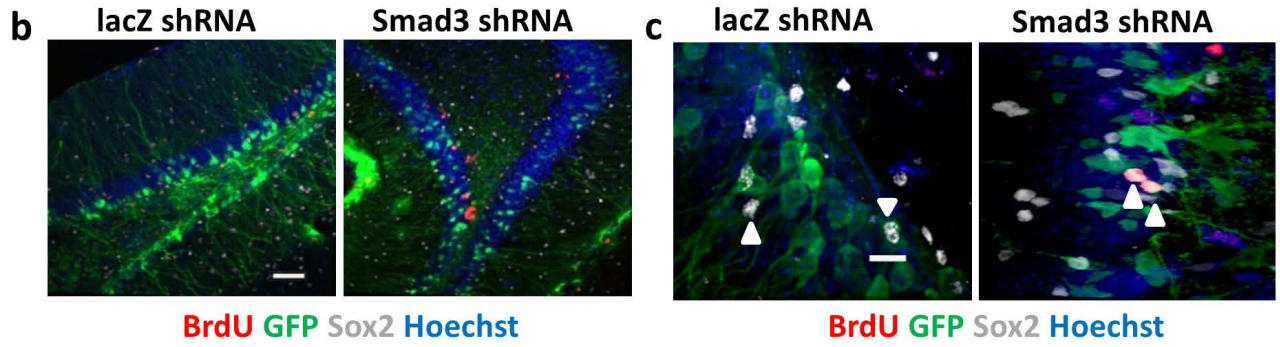
b
lacZ shRNA
Smad3 shRNA
c
lacZ shRNA
Smad3 shRNA
BrdU GFP Sox2 Hoechst
BrdU GFP Sox2 Hoechst

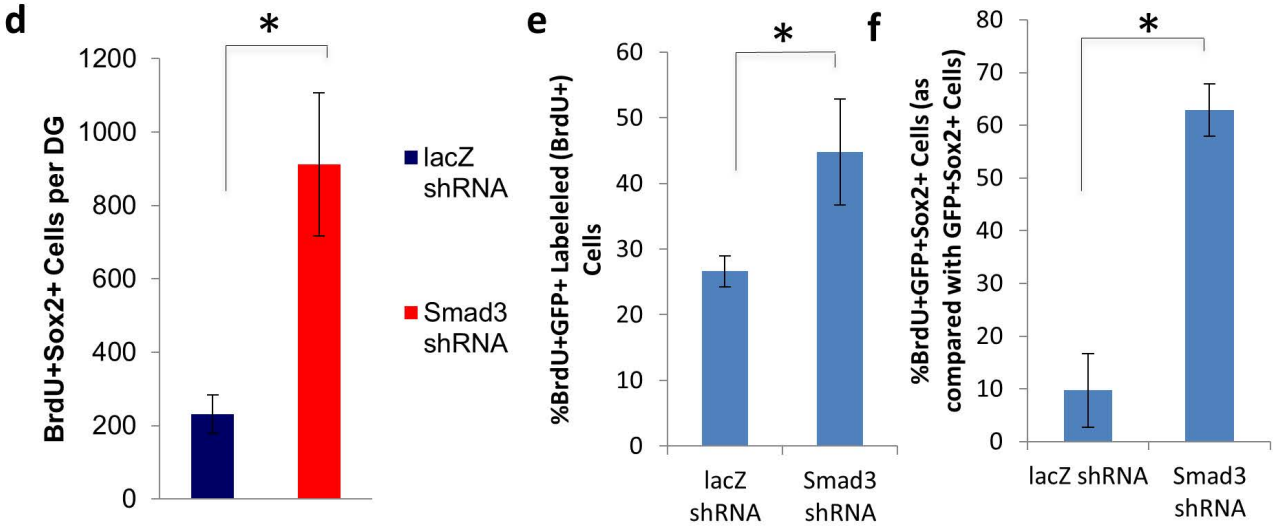
d
BrdU+Sox2+ Cells per DG
1200
1000
800
600
400
200
0
*
lacZ shRNA
Smad3 shRNA
e
%BrdU+GFP+ Labeleled (BrdU+) Cells
60
50
40
30
20
10
0
*
lacZ shRNA
Smad3 shRNA
f
%BrdU+GFP+Sox2+ Cells (as compared with GFP+Sox2+ Cells)
80
70
60
50
40
30
20
10
0
*
lacZ shRNA
Smad3 shRNA

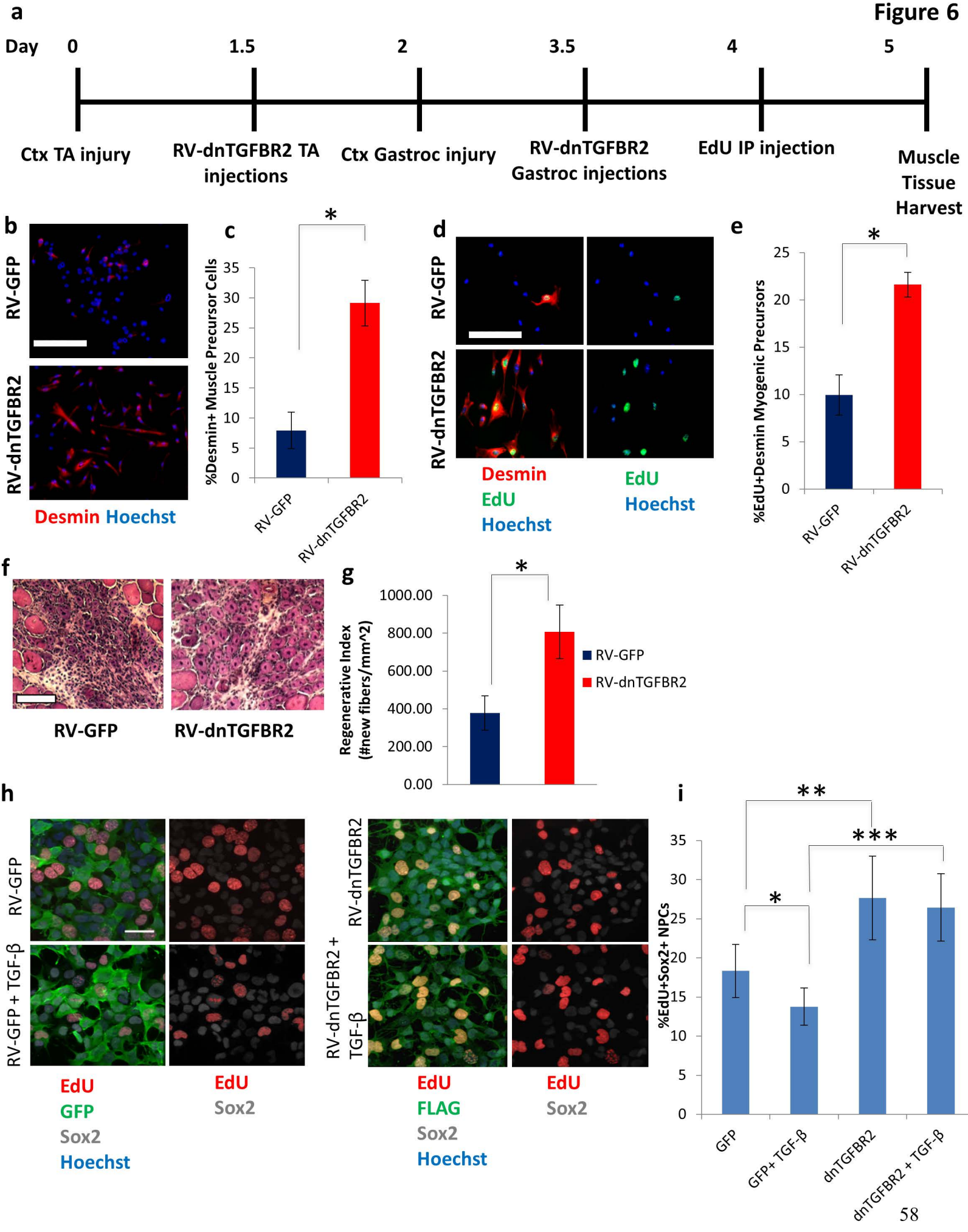
a
Day 0
1.5
2
3.5
4
5
Ctx TA injury
RV-dnTGFBR2 TA injections
Ctx Gastroc injury
RV-dnTGFBR2 Gastroc injections
EdU IP injection
Muscle Tissue Harvest
b
RV-GFP
RV-dnTGFBR2
Desmin Hoechst
c
%Desmin+ Muscle Precursor Cells
RV-GFP
RV-dnTGFBR2
d
RV-GFP
RV-dnTGFBR2
Desmin
EdU
Hoechst
EdU
Hoechst
e
%EdU+Desmin Myogenic Precursors
RV-GFP
RV-dnTGFBR2
f
RV-GFP
RV-dnTGFBR2
g
Regenerative Index (#new fibers/mm^2)
RV-GFP
RV-dnTGFBR2
h
RV-GFP
RV-GFP + TGF-β
RV-dnTGFBR2
RV-dnTGFBR2 + TGF-β
EdU
GFP
Sox2
Hoechst
EdU
Sox2
EdU
FLAG
Sox2
Hoechst
EdU
Sox2
i
%EdU+Sox2+ NPCs
GFP
GFP+ TGF-β
dnTGFBR2
dnTGFBR2 + TGF-β

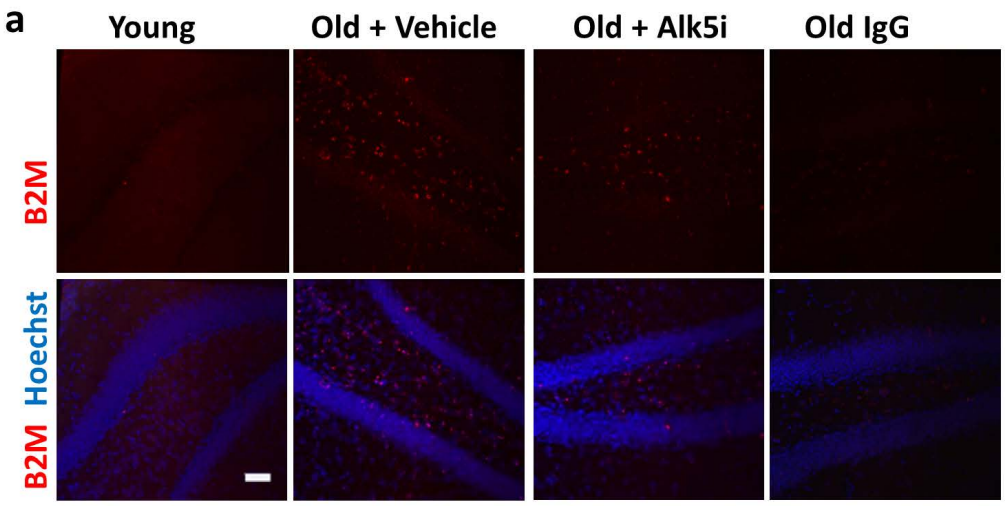
a
Young
Old + Vehicle
Old + Alk5i
Old IgG
B2M
B2M Hoechst

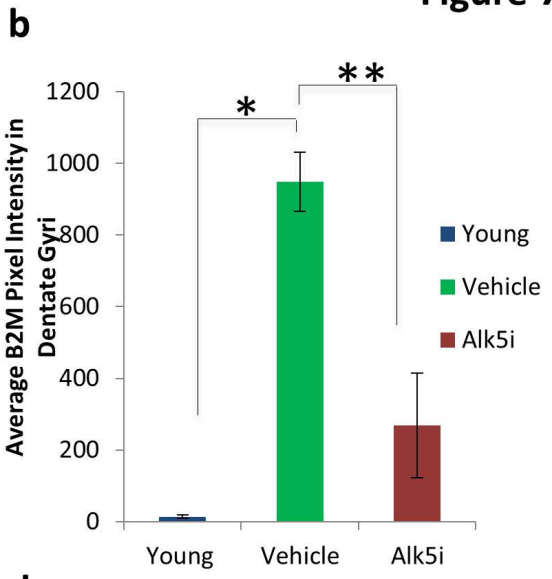
b
Average B2M Pixel Intensity in Dentate Gyri
1200
1000
800
600
400
200
0
*
**
Young
Vehicle
Alk5i
Young
Vehicle
Alk5i

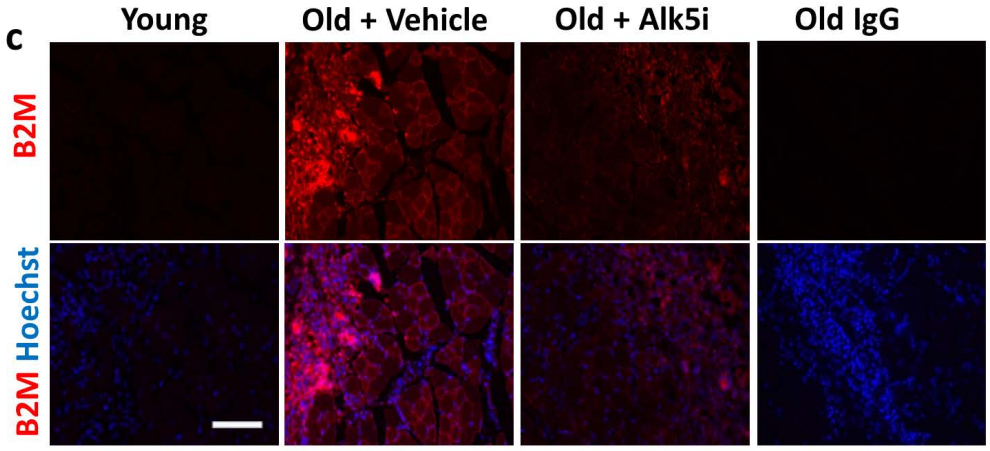
c
Young
Old + Vehicle
Old + Alk5i
Old IgG
B2M
B2M Hoechst

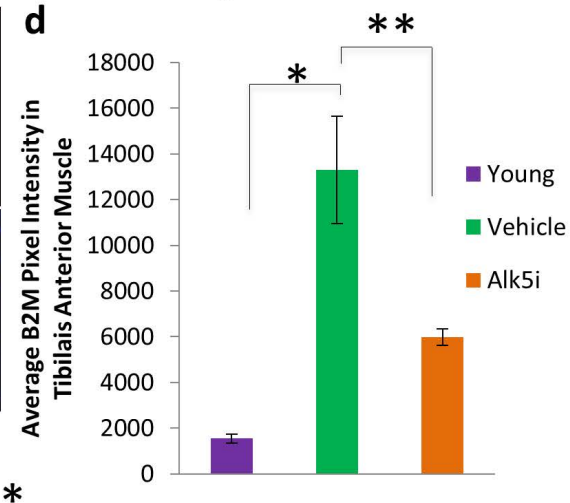
d
Average B2M Pixel Intensity in Tibialis Anterior Muscle
18000
16000
14000
12000
10000
8000
6000
4000
2000
0
*
**
Young
Vehicle
Alk5i

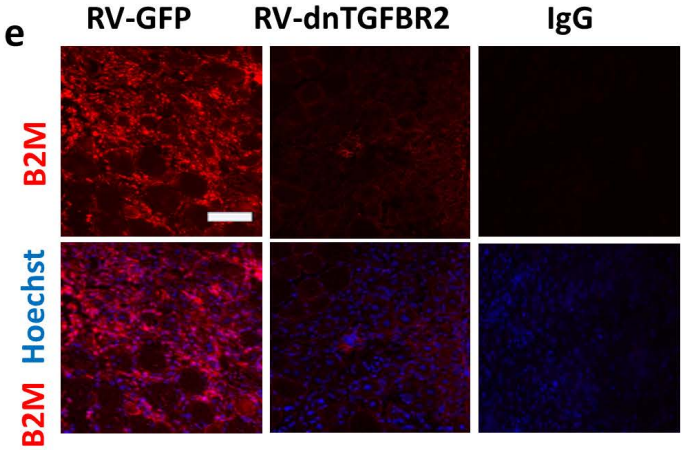
e
RV-GFP
RV-dnTGFBR2
IgG
B2M
B2M Hoechst

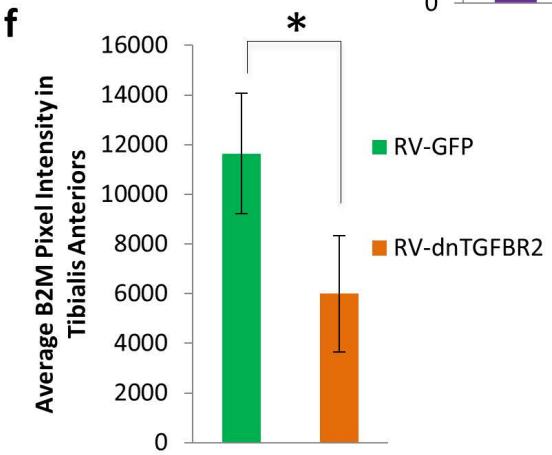
f
Average B2M Pixel Intensity in Tibialis Anteriors
16000
14000
12000
10000
8000
6000
4000
2000
0
*
RV-GFP
RV-dnTGFBR2

Extended Figure 1

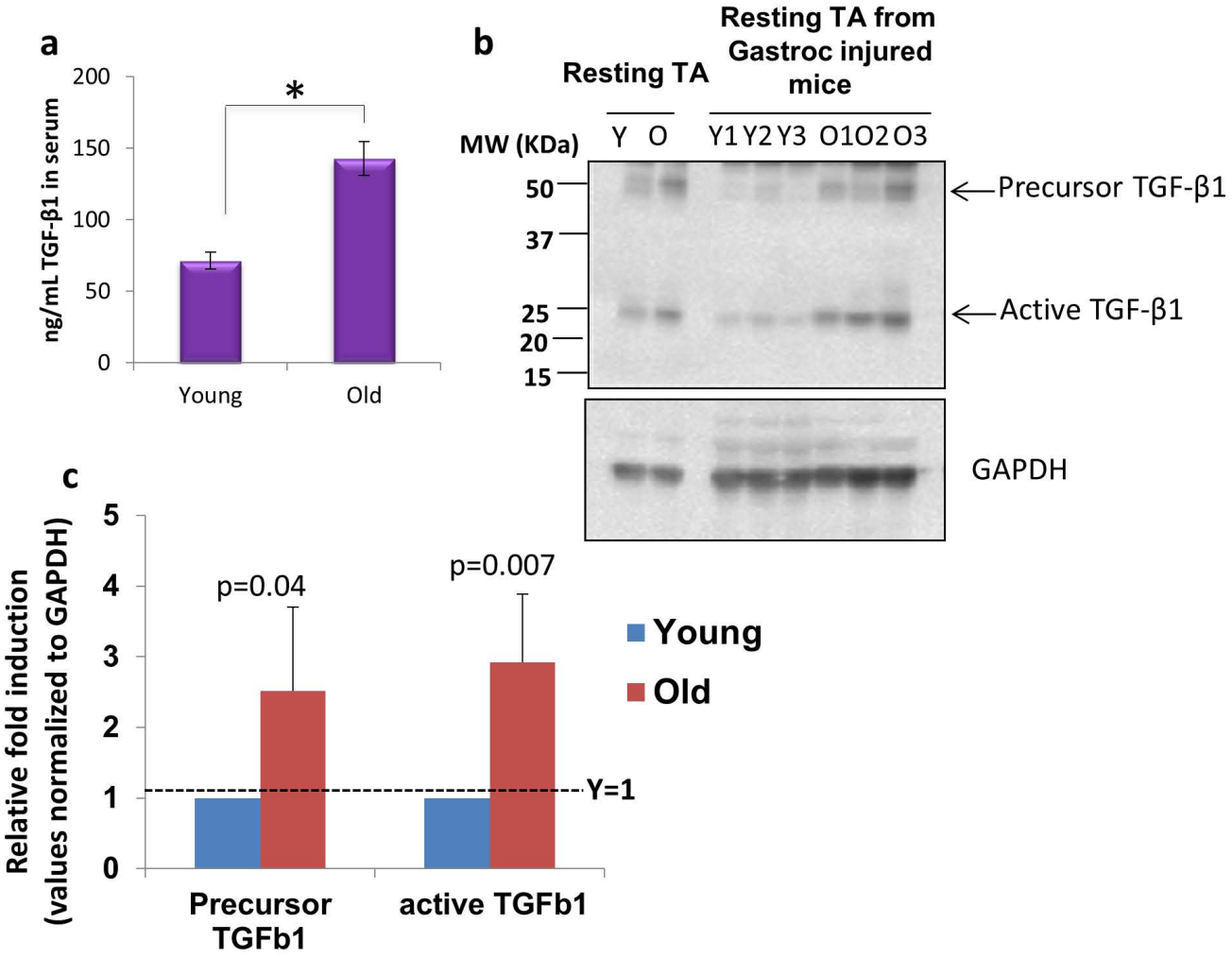

Extended Figure 2

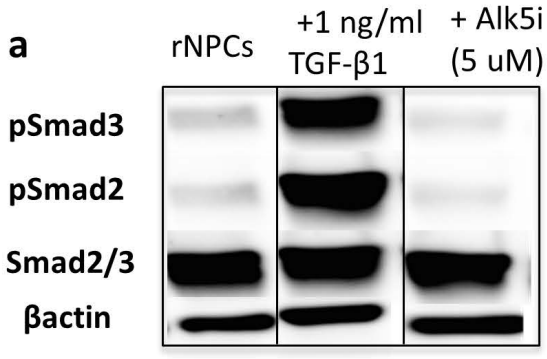

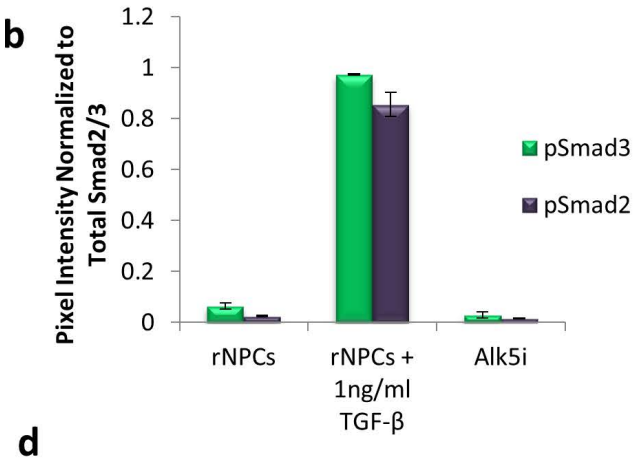

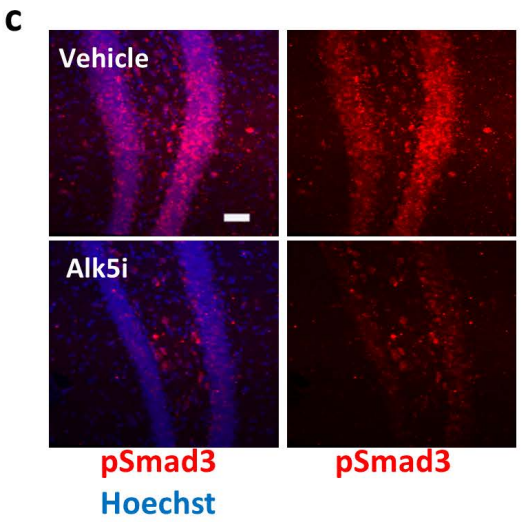

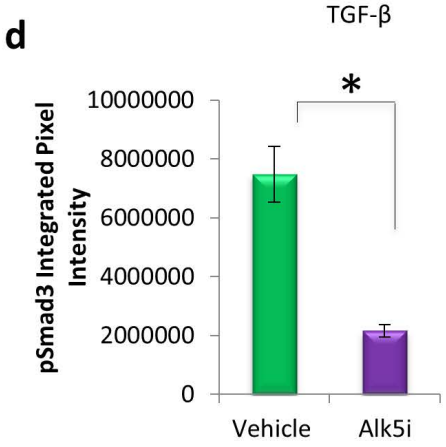

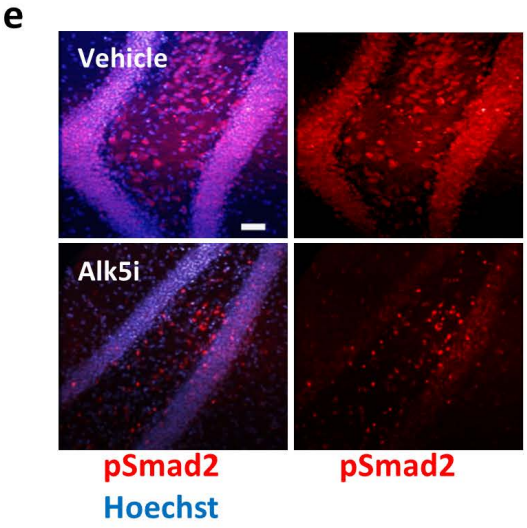

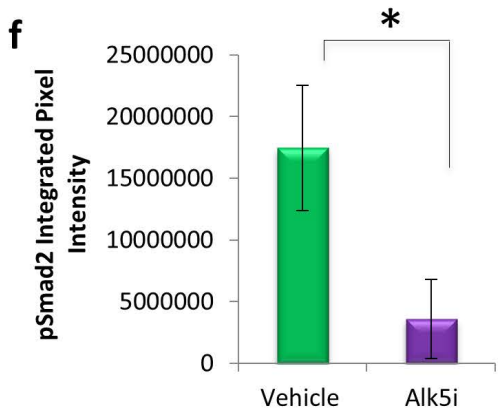

shRNA inhibits Smad3 in mNPCs

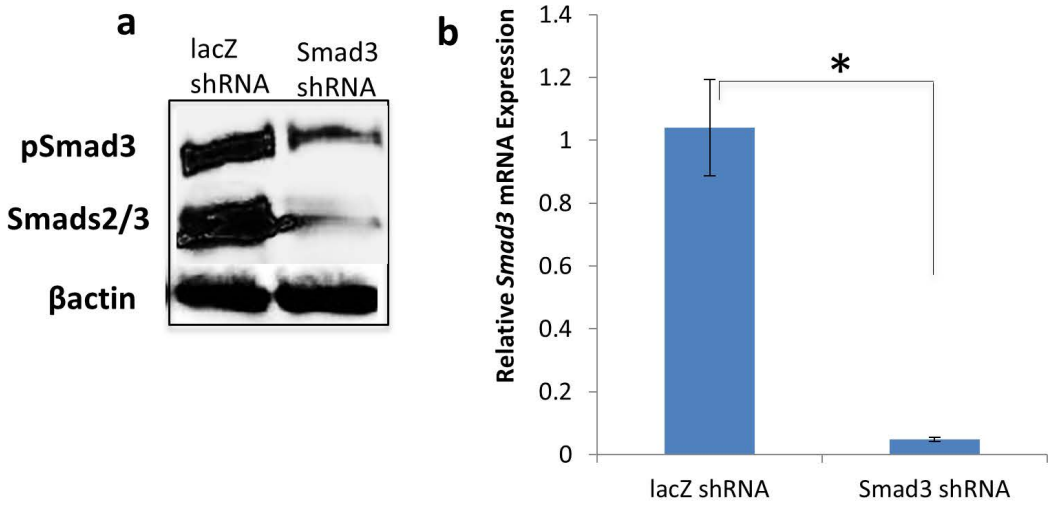

Extended Figure 4

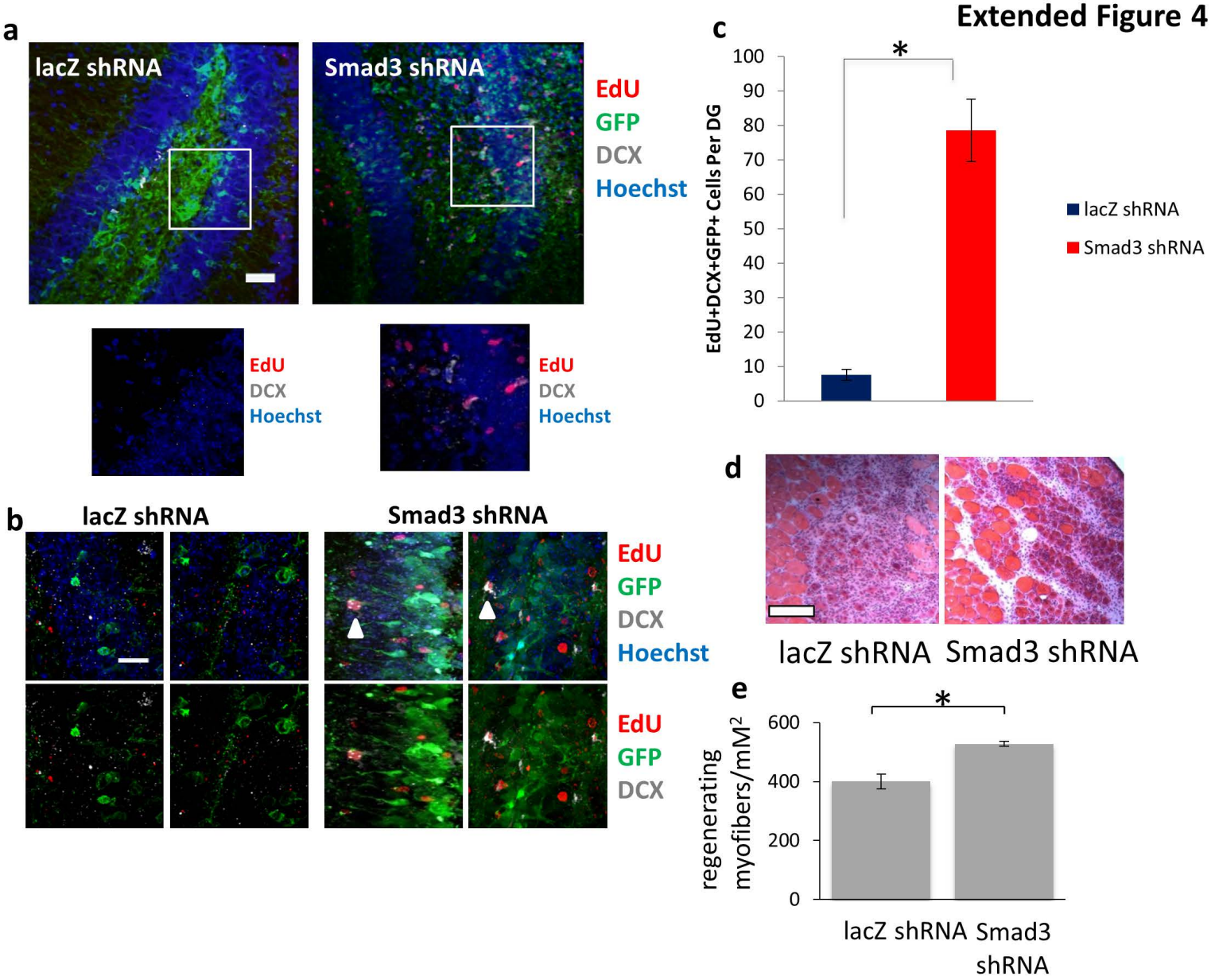

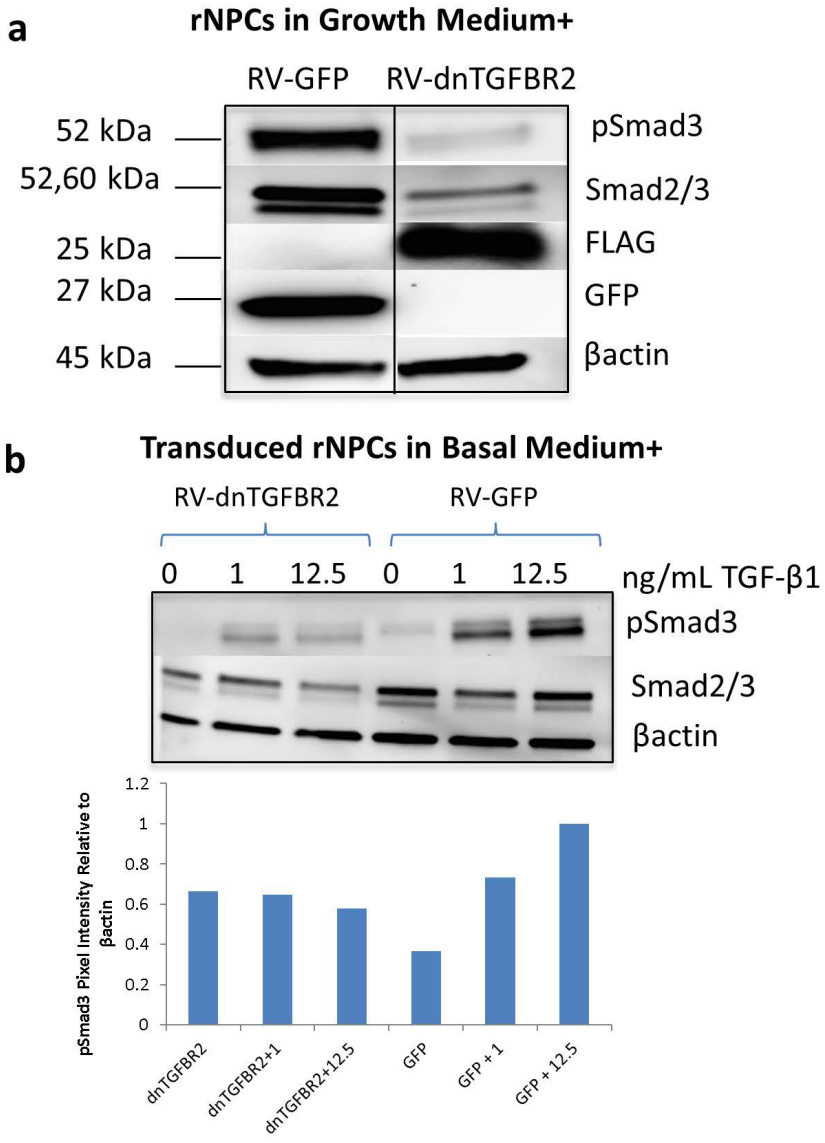
a
rNPCs in Growth Medium+
RV-GFP
RV-dnTGFBR2
52 kDa
52,60 kDa
25 kDa
27 kDa
45 kDa
pSmad3
Smad2/3
FLAG
GFP
βactin
b
Transduced rNPCs in Basal Medium+
RV-dnTGFBR2
RV-GFP
0 1 12.5 0 1 12.5
ng/mL TGF-β1
pSmad3
Smad2/3
βactin
pSmad3 Pixel Intensity Relative to βactin
1.2
1
0.8
0.6
0.4
0.2
0
dnTGFBR2
dnTGFBR2+1
dnTGFBR2+12.5
GFP
GFP + 1
GFP + 12.5

Source of TGF-β secretion

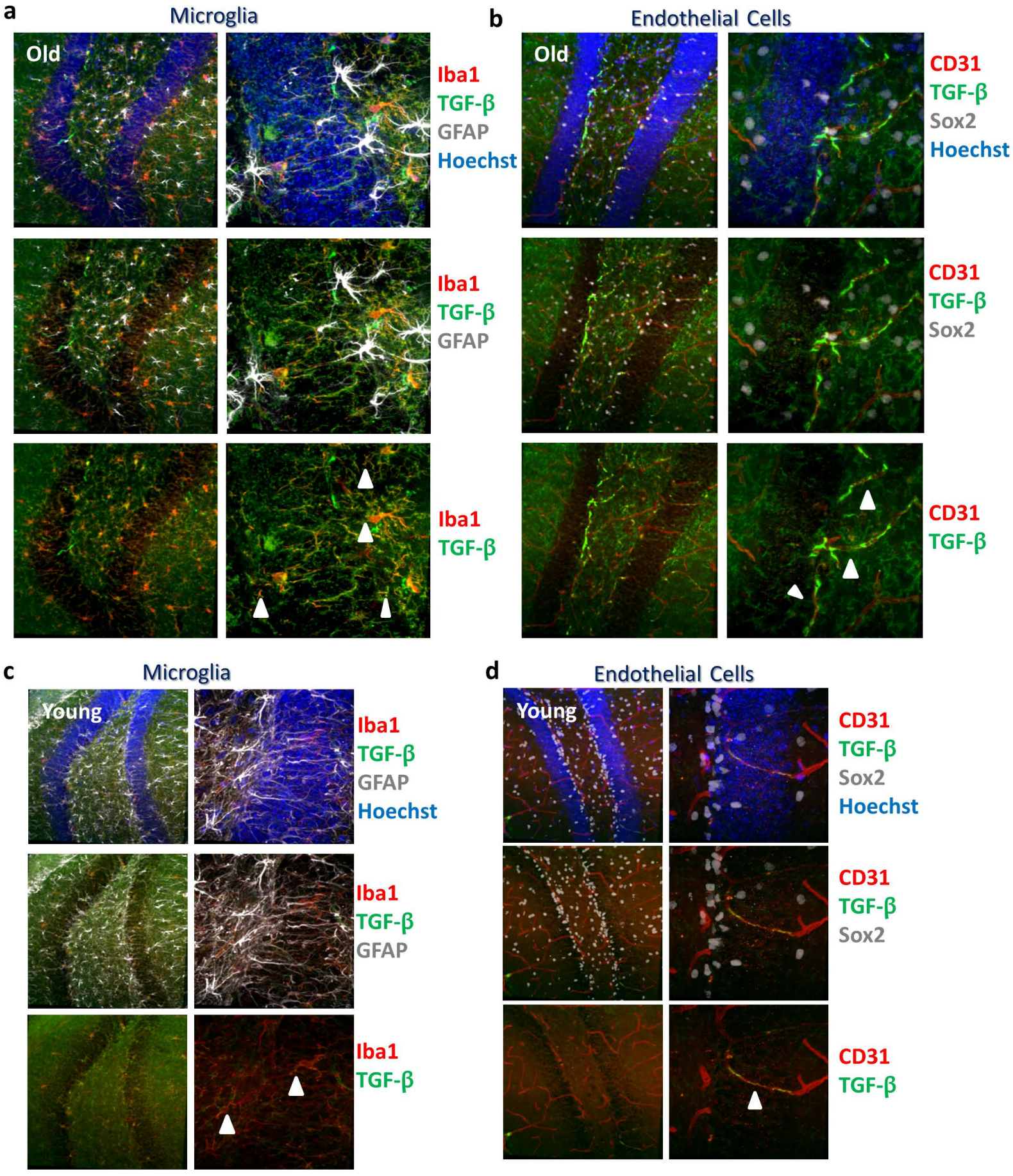

Chapter 3

Embryonic Anti-Aging Niche

A. Embryonic Anti-Aging Niche

Irina M. Conboy[1], Hanadie Yousef[2], and Michael J. Conboy[1]

1 Department of Bioengineering and QB3 Institute, UC Berkeley, Berkeley, CA 94720-3220, USA

2 Department of Molecular and Cellular Biology, UC Berkeley, Berkeley, CA 94720-3200, USA

Key words: stem cell aging, regeneration, niche, senescent, cell cycle, Notch, TGF-β, MAPK, muscle, hESC

Received: 5/24/11; Accepted: 5/28/11; Published: 5/31/11

Corresponding authors: Irina Conboy, PhD; **E-mail:** iconboy@berkeley.edu

Source: Impact Aging Journal (Conboy et al., 2011)

Abstract

Although functional organ stem cells persist in the old, tissue damage invariably overwhelms tissue repair, ultimately causing the demise of an organism. The poor performance of stem cells in an aged organ, such as skeletal muscle, is caused by the changes in regulatory pathways such as Notch, MAPK and TGF-β, where old differentiated tissue actually inhibits its own regeneration. This perspective analyzes the current literature on regulation of organ stem cells by their young versus old niches and suggests that determinants of healthy and prolonged life might be under a combinatorial control of cell cycle check point proteins and mitogens, which need to be tightly balanced in order to promote tissue regeneration without tumor formation. While responses of adult stem cells are regulated extrinsically and age-specifically, we put forward experimental evidence suggesting that embryonic cells have an intrinsic youthful barrier to aging and produce soluble pro-regenerative proteins that signal the MAPK pathway for rejuvenating myogenesis. Future identification of this activity will improve our understanding of embryonic versus adult regulation of tissue regeneration suggesting novel strategies for organ rejuvenation. Comprehensively, the current intersection of aging and stem cell science indicates that if the age-imposed decline in the regenerative capacity of stem cells was understood, the debilitating lack of organ maintenance in the old could be ameliorated and perhaps, even reversed.

Summary and Key Figures

Embryonic stem cells (ESCs) have a virtually infinite capacity to self-renew (e.g. to give rise to another embryonic stem cell), and to be pluripotent (e.g. to differentiate into virtually every cell type in the mammalian organism) (Levi and Morrison, 2008; He et al., 2009). The tremendous potential of ESCs for organogenesis, including those of human origin (hESCs), has created great interest in understanding and deliberately controlling their cell fate determination, and tremendous progress was made in recent years in this field (Wobus and Boheler, 2005; Boyer et al., 2006). At the same time, much less is known about the properties of selfrenewing, undifferentiated hESCs that do not directly relate to developmental lineage progression, but that might indirectly influence the regenerative capacity of post-natal tissues. In this respect, our work uncovered that in co-cultures with mouse muscle precursor cells, hESCs dramatically enhanced myogenesis in vitro, and moreover, rejuvenated the repair of injured muscle in old mice when injected intramuscularly into immunocompromised animals, even though the hES cells themselves did not contribute to new muscle tissue (Carlson and Conboy, 2007). The same work hinted that the positive regulation of mouse myogenesis by hESCs might be due to the soluble factors (be they protein, lipid, sugar or other macromolecules), and that human mesenchymal stem cells lack this pro-regenerative activity (Carlson and Conboy, 2007). The data and discussion below introduce evidence that selfrenewing human embryonic stem cells, but not differentiated hESCs (hESCs vs. dhESCs), secrete *proteins* that counteract the oppressive biochemical milieu of aged muscle and old circulation, and restore efficient myogenesis to old satellite cells that associate with old myofibers and are exposed to old blood serum. Furthermore, we show that this embryonic activity requires an intact MAPK pathway, because the proregenerative effects of hESC- secreted factors become abolished in the presence of a MEK inhibitor. Interestingly, hESC-secreted factors also promote proliferation and delay differentiation of primary myoblasts, which is a typical effect of other molecules known to

enhance adult myogenesis, such as Notch (Conboy and Rando, 2002; Conboy et al., 2003; Brack et al., 2008).

An experimental system that successfully mimics the in vivo myogenesis and is particularly suitable for comparing young and aged mammals (Conboy and Rando, 2002, 2005; Conboy et al., 2005), has been tailored here for characterizing the influence of embryonic and neonatal factors on regenerative capacity of satellite cells and for determining whether the activity is associated with proteins. Specifically, young and old satellite cells activated by muscle injury were cultured in association with their own myofibers in medium with 10% blood serum of their own age. These satellite cell cultures were maintained for 24 hours in HAM's F10 supplemented with 50% OPTI MEM (control medium), or 50% OPTI MEM-conditioned medium from hESCs or dhESCs. Exogenous MEK inhibitor was added to some samples to test the reliance of the system on MAPK pathway. BrdU was added to the cell cultures for the last 2 hours to label cells in S phase of the cell cycle. The myogenic proliferative response of satellite cells was determined based on the percentage of proliferating myoblasts generated by the satellite cells (desmin+ve/BrdU+ve cells) (Conboy et al., 2005; Carlson et al., 2008). The enhancement of myogenic capacity was also determined by measuring continuous proliferation and delayed differentiation of myoblasts in standard differentiation promoting medium, by quantifying the percent of multinucleated terminally differentiated eMyHC+ myotubes vs. BrdU+ mono-nucleated cells. Typically, more than 50% of primary myoblasts fuse into post-mitotic multinucleated myotubes in the low mitogen differentiation medium (DMEM+2%horse serum), however, factors known to boost the regenerative capacity of muscle, such as active Notch, can delay this terminal differentiation in favour of continuous progenitor cell proliferation (Conboy and Rando, 2002; Brack et al., 2008).

These experiments demonstrated that secreted protein(s) in conditioned culture supernatants from hESCs manifested a pro-regenerative activity that enhanced and importantly, rejuvenated the regenerative capacity of satellite cells (Figure 1 A**)** and promoted the proliferation of myoblasts (Figure 1 B). Interestingly, differentiated progeny of hESCs do not possess this proregenerative anti-aging activity, as myogenic responses in supernatants from differentiated hESCs were no higher than that in control medium. The proregenerative activity was also tested and not found in embryoid bodies, suggesting that it is general differentiation and not commitment to a particular lineage that abrogates the production of the anti-aging factor(s). The pro-myogenic effects of hESC supernatants were significantly reduced upon protease treatment (Proteinase K conjugated to agarose beads following by the removal of the beads), indicating a protein source of this activity. The rapid loss of the proregenerative activity of hESC supernatant upon repeated freezing-thawing also indicates that the factors are labile proteins.

Quite interestingly, the pro-regenerative activity was found to be dependent on intact MAPK signaling as there was no enhancement of myogenesis in the presence of a MEK inhibitor (Figure 1 A and B). For satellite cells, inhibition of the MAPK pathway reduced the pro-regenerative effects of hESC supernatants on old satellite cells and slightly diminished the proliferation of young satellite cells (Figure 1A). The attenuation of satellite cell proliferation by MEK inhibitor was partial suggesting that additional positive regulators of cell proliferation (for example, active Notch) might play a role in the studied experimental system. For myoblasts, the inhibition of MAPK signaling prevented both proliferation and differentiation of the majority

(~88%) of cells cultured with hESC supernatants (Figure 1 B), while a few cells (~12%) differentiated into multinucleated myotubes with BrdU-low nuclei. It has been shown that MAPK signalling is important for the G1 to S transition, but once cells enter S phase, they complete cell cycle independently of this pathway (Jones and Kazlauskas, 2001). Hence, it is possible that some myoblasts in the G1 phase of the cell cycle failed to enter the S phase in the presence of MEK inhibitor, even though the hESC supernatant was present, while myoblasts that were already in S or G2/M phases completed the cell cycle and differentiated into myotubes instead of entering into another G1 phase. While two different phenotypes were observed, in both cases the hESC-derived proregenerative factors were not capable to promote proliferation or delay differentiation of primary myoblasts when the MAPK pathway was experimentally inactivated.

Summarily, these results suggest that self-renewing human embryonic stem cells, but not their immediately differentiated progeny, produce soluble proregenerative protein(s) with anti-aging activity, which require an intact MAPK pathway for their positive effects on adult myogenesis. The identification of the pro-regenerative protein(s) is to follow, and the reliance of adult myogenesis on MAPK signalling suggest some interesting candidate gene approaches for uncovering natural molecules that counter the effects of aged niches on organ stem cells. Molecular identification of this activity will broaden our knowledge of embryonic, adult and aged regulation of tissue regeneration and will point toward novel clinical strategies for organ rejuvenation and for improving outcomes of degenerative disorders where endogenous progenitor cells are overwhelmed by continuous tissue death. Since the activity is produced by human cells and manifests in mouse cells, it is likely that the secreted proteins are evolutionarily conserved.

Figures

Figure 1A. Young and old myofibers were isolated from hind leg mouse muscle at 3 days post injury by cardiotoxin and were cultured for 24 hours in Ham's F10 supplemented with 10% young or old mouse serum and 50% of the supernatant specified. 10 μM of MEK inhibitor was added to some wells, as indicated. Proliferating muscle progenitor cells that were generated by the activated satellite cells were immunodetected with anti-desmin(green) and anti-BrdU (red) antibodies; Hoechst (blue) was used to label all nuclei. Percent of proliferating myogenic cells was determined by CellProfiler. Typically poor myogenicity of old satellite cells cultured with old serum was rescued by hESC supernatant in a MAPK-dependent manner.

Figure 1B. Primary myoblasts were cultured for 24 hours in DMEM + 2% Horse Serum and 50% of the supernatant specified. 10 μM of MEK inhibitor was added to some wells, as indicated. At 24 hours, cells were pulsed with 10 μM BrdU for 2 hours and fixed with 70% ethanol. Cells were immuno-stained for eMyHC (green) and BrdU (red); Hoechst (blue) was used to label all nuclei Automated imaging of these cells was done using ImageXpress and automated counting of percent of eMyHC+ and BrdU+ cells was performed by quantifying at least 100 sites per experimental sample by MetaExpress. hESC supernatant enhanced myoblast proliferation in a MAPK-dependent manner and diminished differentiation into myotubes.

References

Boyer LA, Mathur D, Jaenisch R (2006) Molecular control of pluripotency. Curr Opin Genet Dev 16:455–462 Available at: http://www.ncbi.nlm.nih.gov/entrez/query.fcgi?cmd=Retrieve&db=PubMed&dopt=Citation&list_uids=16920351.

Brack AS, Conboy IM, Conboy MJ, Shen J, Rando TA (2008) A temporal switch from notch to Wnt signaling in muscle stem cells is necessary for normal adult myogenesis. Cell Stem Cell 2:50–59 Available at: http://www.ncbi.nlm.nih.gov/entrez/query.fcgi?cmd=Retrieve&db=PubMed&dopt=Citation&list_uids=18371421.

Carlson ME, Conboy IM (2007) Loss of stem cell regenerative capacity within aged niches. Aging Cell 6:371–382.

Carlson ME, Hsu M, Conboy IM (2008) Imbalance between pSmad3 and Notch induces CDK inhibitors in old muscle stem cells. Nature 454:528–532 Available at: http://www.ncbi.nlm.nih.gov/entrez/query.fcgi?cmd=Retrieve&db=PubMed&dopt=Citation&list_uids=18552838.

Conboy IM, Conboy MJ, Smythe GM, Rando TA (2003) Notch-mediated restoration of regenerative potential to aged muscle. Science (80-) 302:1575–1577.

Conboy IM, Conboy MJ, Wagers AJ, Girma ER, Weissman IL, Rando TA (2005) Rejuvenation of aged progenitor cells by exposure to a young systemic environment. Nature 433:760–764.

Conboy IM, Rando TA (2002) The regulation of Notch signaling controls satellite cell activation and cell fate determination in postnatal myogenesis. DevCell 3:397–409.

Conboy IM, Rando TA (2005) Aging, stem cells and tissue regeneration: lessons from muscle. Cell Cycle 4:407–410.

Conboy IM, Yousef H, Conboy MJ (2011) Embryonic anti-aging niche. Aging (Albany NY) 3:555–563 Available at: http://www.pubmedcentral.nih.gov/articlerender.fcgi?artid=3156606&tool=pmcentrez&rendertype=abstract.

He S, Nakada D, Morrison SJ (2009) Mechanisms of stem cell self-renewal. Annu Rev Cell Dev Biol 25:377–406 Available at: http://www.ncbi.nlm.nih.gov/entrez/query.fcgi?cmd=Retrieve&db=PubMed&dopt=Citation&list_uids=19575646.

Jones NC, Fedorov Y V, Rosenthal RS, Olwin BB (2001) ERK1/2 is required for myoblast proliferation but is dispensable for muscle gene expression and cell fusion. J Cell Physiol 186:104–115 Available at:

http://www.ncbi.nlm.nih.gov/entrez/query.fcgi?cmd=Retrieve&db=PubMed&dopt=Citation&list_uids=11147804.

Jones SM, Kazlauskas A (2001) Growth-factor-dependent mitogenesis requires two distinct phases of signalling. Nat Cell Biol 3:165–172 Available at: http://www.ncbi.nlm.nih.gov/entrez/query.fcgi?cmd=Retrieve&db=PubMed&dopt=Citation&list_uids=11175749.

Levi BP, Morrison SJ (2008) Stem cells use distinct self-renewal programs at different ages. Cold Spring Harb Symp Quant Biol 73:539–553 Available at: http://www.ncbi.nlm.nih.gov/entrez/query.fcgi?cmd=Retrieve&db=PubMed&dopt=Citation&list_uids=19150957.

Wobus AM, Boheler KR (2005) Embryonic stem cells: prospects for developmental biology and cell therapy. Physiol Rev 85:635–678.

Figure 1A

hESCs secrete proteins that induce muscle rejuvenation via MAPK signaling

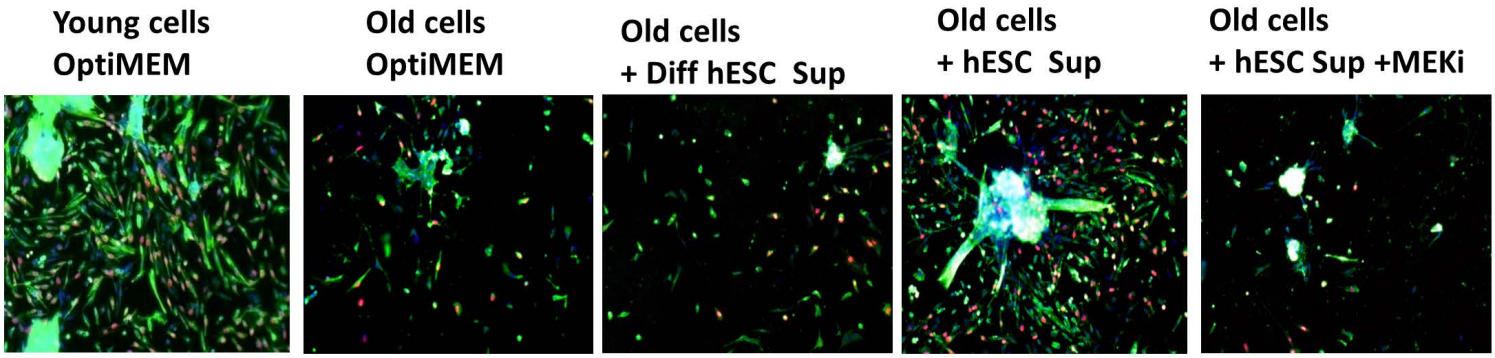

Desmin BrdU Hoechst

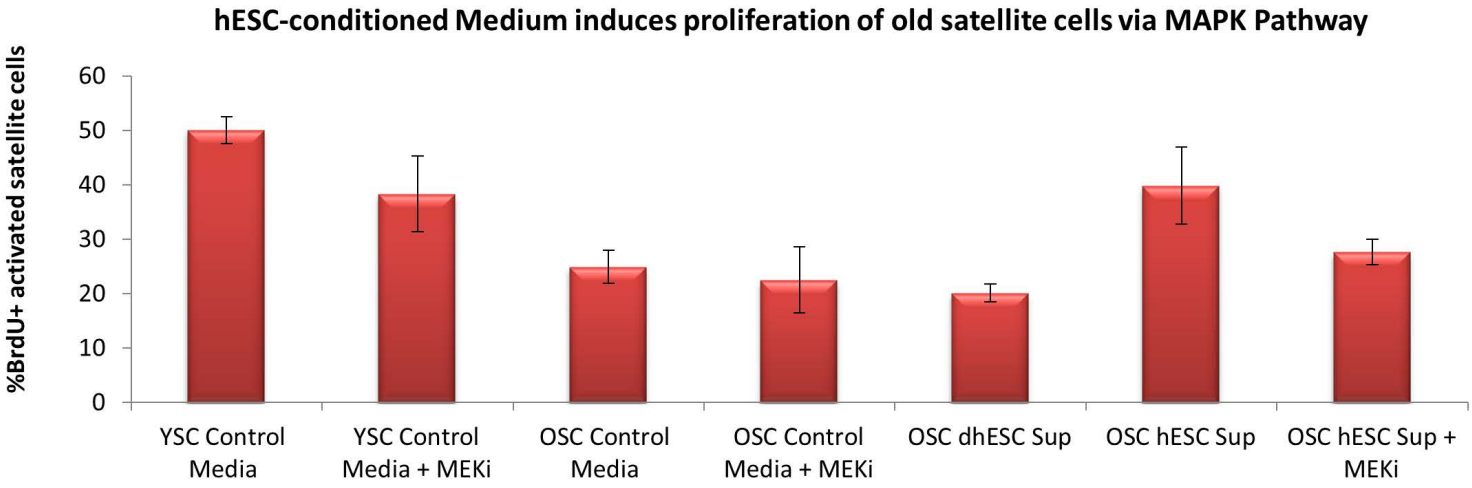

Figure 1B

hESCs secrete proteins that increase myogenesis via MAPK signaling

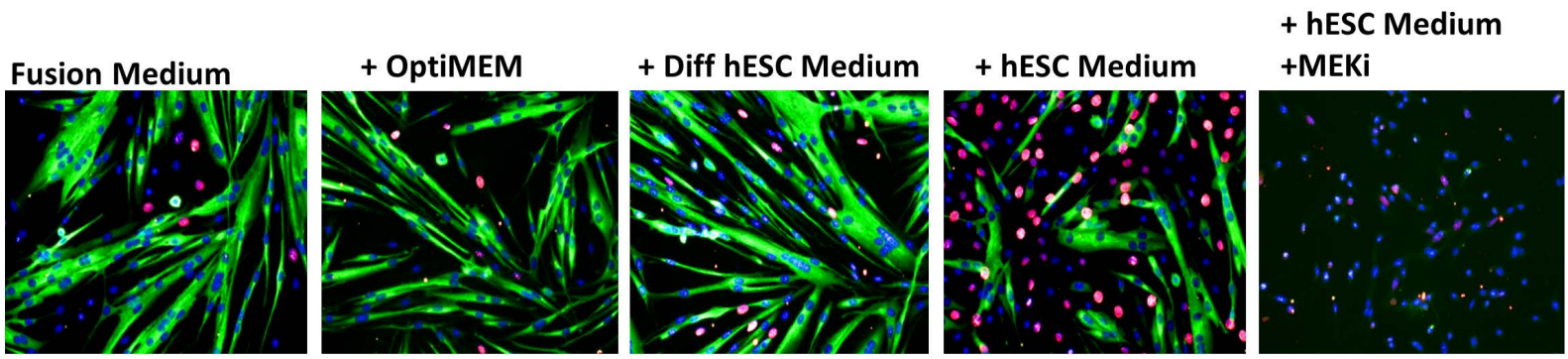

eMyHC BrdU Hoechst

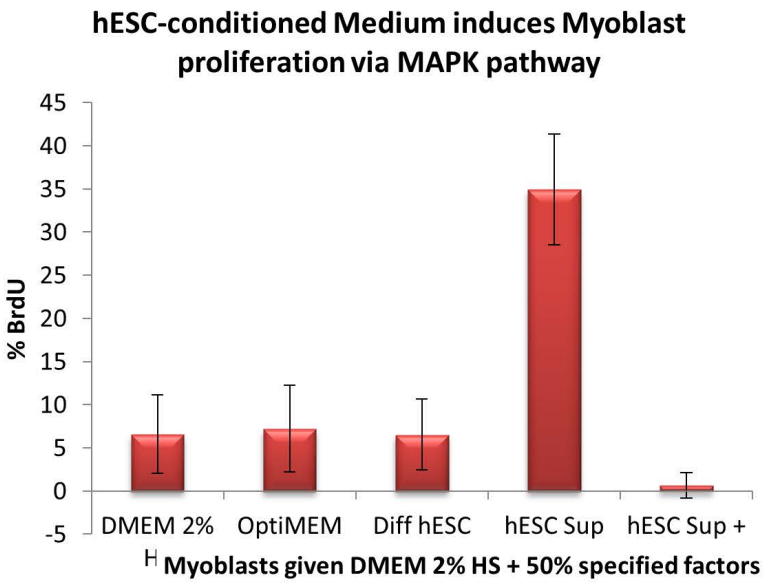

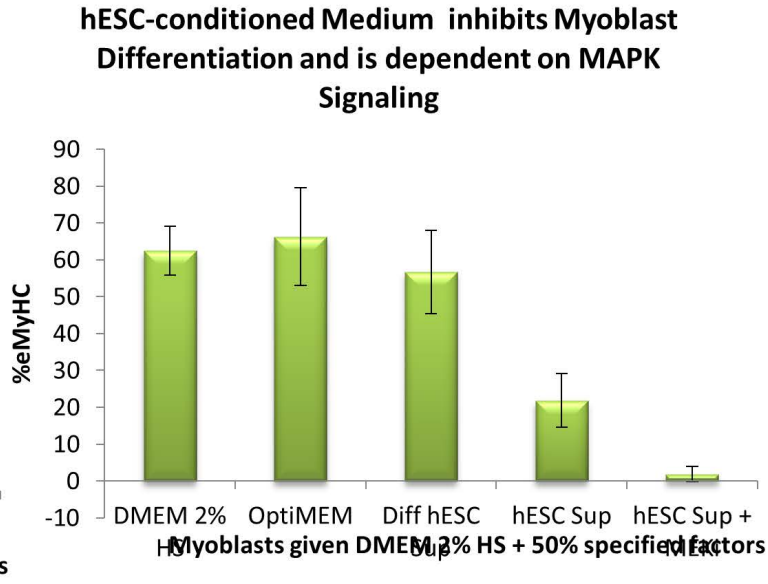

B. hESC-secreted proteins can be enriched for multiple regenerative therapies by heparin-binding

Hanadie Yousef[2], Michael J. Conboy[1],Ju Li[1], Matthew Zeiderman[2], Tandis Vazin[1,3], Christina Schlesinger[1], David V. Schaffer[1,3] and Irina M. Conboy[1]*

1 Department of Bioengineering and California Institute for Quantitative Biosciences (QB3), UC Berkeley, Berkeley, CA 94720, USA

2 Department of Molecular and Cellular Biology, UC Berkeley, Berkeley, CA 94720, USA

3 Department of Chemical Engineering and Helen Wills Neuroscience Institute, UC Berkeley, Berkeley, CA 94720 USA

Key words: rejuvenation, embryonic stem cell, myoblast, satellite cell

Received: 5/13/13; Accepted: 5/21/13; Published: 5/23/13

Correspondence to: Irina M. Conboy, PhD; **E-mail:** iconboy@berkeley.edu

Source: Impact Aging Journal (Yousef et al., 2013)

Abstract

This work builds upon our findings that proteins secreted by hESCs exhibit pro-regenerative activity, and determines that hESC-conditioned medium robustly enhances the proliferation of both muscle and neural progenitor cells. Importantly, this work establishes that it is the proteins that bind heparin which are responsible for the pro-myogenic effects of hESC-conditioned medium, and indicates that this strategy is suitable for enriching the potentially therapeutic factors. Additionally, this work shows that hESC-secreted proteins act independently of the mitogen FGF-2, and suggests that FGF-2 is unlikely to be a pro-aging molecule in the physiological decline of old muscle repair. Moreover, hESC-secreted factors improve the viability of human cortical neurons in an Alzheimer's disease (AD) model, suggesting that these factors can enhance the maintenance and regeneration of multiple tissues in the aging body.

Introduction

Tissue regeneration and maintenance dramatically and invariably decline with age, eventually causing failure of multiple organ systems in all mammals. In muscle, the loss of tissue regeneration with age is thought to be imposed by signaling changes in the satellite stem cell niche, and interestingly, the aging of stem cell niches is to some extent similar between muscle, brain, blood, and other tissues [1-3]. Our previous work found that human embryonic stem cells (hESCs) produce soluble secreted molecules that can counteract the age-imposed inhibition of muscle regeneration, an “anti-aging” activity that is lost when the hESCs differentiate [4, 5].

Numerous mitogenic proteins are expressed by hESCs [6] and are known to act through TGF-beta/BMP, Jak-Stat, MAPK, and other key regulatory signaling pathways, all of which have been implicated in the control of adult tissue regeneration. The precise identity of the pro-myogenic factors that are secreted by hESCs and the molecular mechanism of their action in muscle stem and progenitor cells is still work in progress; however, the effects of one of these molecules, FGF-2, was studied here in detail. FGF-2 is known to be secreted by hESCs and is also contained in the growth/expansion medium of embryonic stem cells [7-9]. FGF-2 does not have a signal peptide and is not secreted through the ER-Golgi pathway [10, 11], and the mechanisms of FGF-2 transport or export from cells in skeletal muscle are not well defined. FGF-2 ligand acts by binding to promiscuous receptor complexes to activate the MAPK/PERK pathway, which is well known to exert strong mitogenic effects and to be necessary for the establishment and maintenance of primary cultures of muscle progenitor cells [12, 13]. With age, the activation and proliferation response of aged muscle stem cells after injury declines as compared to young [14]. Consequentially, the generation of fusion-competent muscle progenitor cells, or myoblasts, that co-express desmin, Myf5, MyoD and Pax-7, incorporate BrdU, and terminally differentiate into myotubes or myofibers that express eMyHC, becomes deficient in poorly regenerating old tissue [1]. Controversially, a recent report [15] suggested that FGF-2 is overproduced by aged myofibers and subsequently induces proliferation and exhaustion of the old satellite cells that are typically quiescent. The age-specific role of FGF-2 was examined here with respect to its localization and signaling in muscle stem cells.

The age-imposed decline in stem cell responses is caused by the aging of the niche, not only in muscle, but also in brain. Thus, we tested whether the enhancement of stem and progenitor proliferation and tissue maintenance by hESC-secreted proteins is conserved between muscle and brain. The brain undergoes many changes with aging, including neuronal cell death,

thinning of the cortex and loss of brain plasticity, and the accumulation of plaques and neurofibrillary tangles [16-19]. Additionally, two regions of the adult brain – the dentate gyrus of the hippocampus and the subventricular zone of the forebrain – harbor neural stem cells (NSCs) that express the marker Sox-2 and are able to give rise to neurons and glia in vivo and in culture. During the natural aging process, similarly to muscle function, cognitive function declines, which may be in part due to the diminished ability of the neural stem cells in the subgranular zone of the dentate gyrus to proliferate and give rise to new neurons [2, 3].

In addition to decrease in neurogenesis observed with aging, the central nervous system can suffer from a number of age-associated neurodegenerative disorders. We have developed an *in vitro* Alzheimer's disease model in which hESC-derived cortical neurons are exposed to a very toxic form of Amyloid beta (Aβ) (Vazin et al., submitted), soluble oligomeric forms of Aβ known as "globulomers", which have shown a stronger clinical correlation with the cognitive deficit than the overall plaque load [20, 21]. Exposure of hESC-derived glutamatergic neurons to such Aβ oligomers induces signs of the disease, including age-dependent binding of Aβ and cell death.

In investigating the pro-myogenic properties of hESC-secreted proteins, we explored a hypothesis that key factors may contain heparin-binding domains, as many proteins known to be key mitogenic regulators of cell-fate specification and secreted by embryonic cells bind heparin or act in complex with heparin-bound proteins [22, 23]. Consistent with this hypothesis, we establish that that depletion of the heparin-binding proteins abrogates, while the enrichment for these proteins robustly manifests, the pro-regenerative activity of the hESC-conditioned medium. In addition to providing a novel method for enrichment of the therapeutic factors that are secreted by the hESCs, this study demonstrates the positive effect of these molecules on tissue regeneration and maintenance not only in muscle, but also in brain. Namely, hESC-secreted proteins robustly enhanced the proliferation of adult NSCs, suggesting a promising application for both the enhancement of cognitive function and improved outcome of NPCs transplantation; and notably, proteins secreted by hESCs had significant neuroprotective, anti-apoptotic effect on human cortical neurons exposed to□□, demonstrating a potential novel therapy for combating AD. Importantly, f this work establishes that hESC-secreted proteins act independently of recombinant FGF-2 that is contained in their growth medium. Interestingly, we also show that mTeSR-1 hESC-conditioned medium exhibits potent pro-myogenic properties due to the high levels of FGF-2. In FGF-2 is not a pro-aging molecule, our work demonstrates that FGF-2 does not signal in the aged muscle stem cells and uncovers an interesting, age-specific mis-localization of the FGF-2 ligand, which may reflect a fundamental difference not only in the permissiveness of FGF-2 signaling in young vs. old muscle, but also in the ability of old differentiated muscle cells to secrete this mitogen.

Results and Discussion

mTeSR-1 growth medium has pro-myogenic activity, which is due to the high levels of FGF-2, and hESC-secreted factors act independently of recombinant FGF-2

Our previous work established that injection of hESCs – which were cultured on mouse embryonic fibroblasts (MEF) and in standard, highly mitogenic, embryonic cell growth medium – enhanced old muscle regeneration [4]. In our more recent work, the hESCs have been cultured in mTeSR-1 (Stem Cell Technologies), a defined feeder-free medium which is also highly

mitogenic [9], and we investigated whether and to what degree the pro-myogenic effects of hESC-conditioned medium was due to the residual activity of the hESC growth/expansion medium. Primary muscle progenitor cells (myoblasts) were cultured overnight in a mitogen-low fusion medium that typically induces differentiation of myoblasts into multinucleated eMyHC+ myotubes. The enhancement of myogenic cell proliferation and inhibition of differentiation was assayed by BrdU uptake for the last 2 hours of culture, after which cells were fixed and used for immunofluorescence with anti-BrdU and anti-MyHC specific antibodies. When primary myoblasts were cultured in 50% fusion medium plus 50% hESC-conditioned mTeSR-1 or 50% unconditioned mTeSR-1, both media compositions induced proliferation and inhibited differentiation of these myogenic cells, though medium containing hESC-conditioned mTeSR-1 inhibited differentiation more significantly (Figure 1A, quantified in B and C). To confirm these data with muscle stem cells, injury-activated satellite cells associated with myofibers were isolated from old muscle and cultured overnight in a 50/50 mix of Opti-MEM containing 5% old mouse serum and hESC-conditioned mTeSR-1 or mTeSR-1. Both conditioned and not-conditioned mTeSR-1 media enhanced the regenerative capacity of satellite cells that were isolated from injured old muscle, based on the numbers of de-novo generated BrdU+/Desmin+ muscle progenitor cells (Figure 1D, quantified in E). These results demonstrate that embryonic stem cell culture medium itself has pro-myogenic effects. To investigate whether hESC-conditioned Opti-MEM exhibits pro-regenerative effects due to the hESC-secreted proteins, and not because of residual mTeSR-1, we washed the hESC culture wells multiple times with Opti-MEM prior to incubation for conditioning the Opti-MEM, and found that even after 3 washes, hESC conditioned the Opti-MEM to yield the same potent pro-regenerative effect on myoblasts (Figure 1F). These results demonstrate that while mTeSR-1 supplementation promotes myoblast proliferation, other factor(s) produced by hESCs independently enhance the regenerative capacity of muscle stem and progenitor cells.

To understand the pro-myogenic effects of mTeSR-1 in greater detail, we addressed the role of FGF-2, which is present at high concentration in mTeSR-1 (over 50 nanograms per milliliter, ~10 times higher than the doses used in conventional culture of muscle progenitor cells). Our hypothesis was that the FGF-2 in mTeSR-1 enhances myoblast and satellite cell proliferation, partially masking the effects of the hESC-produced factors in hESC-conditioned mTeSR-1. To test this hypothesis, we incubated hESCs in a basal medium that had the other growth and signaling factors present in mTeSR-1 (TGF-beta, GABA, pipecolic acid and Lithium Chloride, [9]), but lacked FGF2, and compared the pro-myogenic effects of this FGF-free hESC-conditioned mTeSR-1 analog with the effects of the same mTeSR-1 analog that was not conditioned by the hESCs. Without FGF-2, the mTeSR-1 analog lacked pro-regenerative effects on myoblasts (Figure 2A, quantified in 2B). On the other hand the very same mTeSR-1 analog lacking FGF-2, but conditioned by hESCs, significantly enhanced myoblast proliferation and inhibited differentiation, while conditioning of this mTeSR-1 analog lacking FGF-2 by differentiated hESC derived cells resulted in the absence of pro-myogenic properties (Figure 2A, quantified in 2B). These data demonstrate that the pro-myogenic effects of mTeSR-1 are due to the high concentration of FGF-2, and that it is not simply residual FGF-2 from mTeSR-1 that is responsible for the enhancement of myogenesis by the hESC-conditioned medium.

FGF-2 signaling and satellite cell proliferation are not increased with age.

FGF-2, which often functions as a mitogen, was recently reported to contribute to the aging and depletion of mouse satellite cells. However, the canonical model of muscle stem cell aging postulates that a decline in such mitogens over time leads to reduced activation of satellite cells that are resident to old tissue [1, 24, 25], so we explored these phenomena in more detail. The levels of FGF-2 were determined by Western Blotting in muscle fibers that were derived from Tibialis Anterior (TA) and Gastrocnemius (Gastroc) muscle of young and old mice. As shown in Figure 3A (quantified in 3B), a significant increase in FGF-2 protein was observed with age in myofibers, consistent with Chakkalakal et al. FGF-2 signals through the MAPK/pERK pathway, so we analyzed the levels of pERK in myofibers derived from young and old uninjured muscle. Interestingly, as shown in Figure 3 A (quantified in 3B), no age-specific increase in pERK was found, and the levels of this key effector were very low in cells from both ages, despite the high levels of FGF-2 in protein lysates derived from old muscle fibers. Also, a myoblast control indicates that pERK detection was sensitive (Figure 3A). To understand these data, we examined the presence and localization of FGF-2 in the intact young and old muscle, using 10 micron cryosections. FGF-2 and laminin were detected with specific antibodies and resolved by immunofluorescence. As shown in Figure 3 C (quantified in 3D), FGF-2 was localized in the basement membrane of young muscle, while in the old muscle, FGF-2 was present less in the basement membrane and more in the cytoplasm of the myofibers (e.g. away from its receptors in muscle stem cells). These data suggest that the relatively higher levels of FGF-2 in old muscle do not necessarily represent ligand that is available for signaling in satellite cells. Additionally, these results indicate that detection of elevated FGF-2 in the old muscle might be due to its over-expression within the old muscle fiber itself, or alternatively, due to "washing" of extracellular FGF-2 from young muscle during tissue dissociation when the basement membrane is digested with collagenase and dispase, and tissue integrity is perturbed [26].

To confirm and extend upon these findings, we isolated muscle stem cells from uninjured young and old TA and Gastroc muscle and treated them with FGF-2 for 30 minutes, after which the levels of FGF-2, pERK, and total ERK were determined in these freshly isolated stem cells. As shown in Figure 4 A, B, endogenous FGF-2 was undetectable in either young or old muscle stem cells upon isolation, but the added FGF-2 was clearly present in these satellite cells after 30 minutes. Young and old satellite cells were harvested after just 30 minutes of culture, thus, the FGF-2 protein detected in cultures, which were treated with recombinant FGF-2 is unlikely to represent de-novo expression. Satellite cells were lifted from the plates with PBS and washed prior to their lysing for Western Blotting, and it was thus unlikely that any residual, non-cell associated recombinant FGF-2 from media or plates would contaminate cell lysates. To test this directly and definitively, we performed a control with a matrix-coated but cell-free plate that was identically treated with FGF-2, and found no detectable recombinant FGF-2 in the solution (Figure 4A). Hence, the FGF-2 detected in protein lysates of young and old satellite cells incubated with this growth factor likely reflects ligand that is bound to its specific receptors. In support of this conclusion, recombinant FGF-2 induced pERK in both young and old satellite cells (Figure 4 A and C). In agreement with non-detectable endogenous FGF-2 in both young and old satellite cells, very low levels of pERK that did not differ with age were observed in these muscle stem cells resident to tissue that was neither injured nor treated with recombinant FGF-2 (Figure 4 A and C). To determine whether low levels (as opposed to none) of FGF-2 can be detected in the muscle stem cells, another independent experiment was performed with a prolonged enhanced chemiluminescence exposure of the Western Blots. As shown in

Supplementary Figure 1, low levels of FGF-2 could be indeed detected in muscle stem cells after a 30 minute exposure, but once again, there was no age-specific difference in either FGF-2 or in pERK. These results suggest that FGF-2 does not signal in either young or old satellite cells that reside in non-injured skeletal muscle.

To directly examine cell proliferation, satellite cells were isolated from non-injured young and old tissue and were cultured with or without FGF-2 overnight, after which the levels of the proliferation marker Ki67 were determined in Pax7+ satellite cells. Muscle stem cells for this and other experiments were isolated with high and equal purity from young and old mice, as shown in Supplementary Figure 2. Neither young nor old cells were lost during overnight culturing, as the numbers were similar to initial plating, and no age-specific loss was observed, based on the cell counts. As shown in Figure 4 D and E, no increase in proliferation of aged muscle stem cells was detected, as compared to young, and as expected from previous literature, the majority of both young and old satellite cells were quiescent [14, 26, 27]. When added, FGF-2 significantly enhanced the proliferation of quiescent muscle stem cells that were isolated from uninjured muscle (both young and old), as shown in Figure 4 D and E, which is consistent with the induction of pERK that is shown in Figure 4 A, C. However, very interestingly, 90-95% of muscle stem cells derived from uninjured young and old tissue were not proliferating even in the presence of added FGF-2, suggesting that other mitogens and / or cell-fate changes are needed to induce the robust entry of quiescent satellite cells into the cell cycle, also as published [13]. These data demonstrate that the localization of FGF-2 within the skeletal muscle compartment changes with age and question whether endogenous FGF-2 is likely to exhaust the pool of aged quiescent satellite cells, since it does not induce significant signaling in these cells.

The pro-regenerative activity of hESC-secreted factors is contained in proteins with heparin binding domains.

Based on the fact that many growth factors that are known to enhance cell proliferation contain heparin binding domains, or act by association with heparin binding proteins as co-activators of signal transduction [22, 23], we hypothesized that hESC-secreted factors that have pro-regenerative activity may be proteins that might bind heparin, and furthermore postulated that hESC-conditioned medium depleted of heparin-binding proteins would lose the ability to enhance myoblast proliferation. To confirm that the factors in hESC conditioned medium were proteins, hESC conditioned Opti-MEM was treated with proteinase-K agarose beads, and the beads were removed before mixing 50/50 with Opti-MEM and 5% mouse serum, for culture with injury-activated satellite cells with associated fibers from old muscle, as above. All proliferative activity of the conditioned medium was lost after proteinase treatment, indicating that protein(s) conferred the pro-regenerative activity (Supplemental Figure 3).

To deplete heparin-binding proteins, hESC-conditioned medium was incubated with heparin binding domain - coated acrylic beads. Muscle progenitor cells were then cultured in this heparin-depleted hESC-conditioned medium, hESC-conditioned medium, or controls (medium alone and medium conditioned by differentiated cells that lack the pro-regenerative activity). Proliferation of primary muscle progenitor cells was assayed by BrdU uptake for 2 hours, and cell differentiation was assayed by the expression of eMyHC. Interestingly, hESC-conditioned medium depleted of heparin binding proteins completely lost its pro-regenerative activity on muscle progenitor cells (Figure 5 A, quantified in B). Even more importantly, the pro-regenerative activity of in the hESC-secreted proteins could be eluted from the heparin-coated

beads (Figure 5 A, quantified in B), hence confirming that these factors have heparin-binding domains and suggesting novel strategies for purification of these clinically relevant molecules. Excitingly, when these heparin-binding eluted embryonic proteins were injected at Day 0 and Day 2 into injured muscle (e.g., at the time of the injury and when muscle stem cells become activated for regeneration) old muscle repair became rejuvenated, based on increased formation of de-novo myofibers with centrally located BrdU+ nuclei (Figure 5C, quantified in D). These data reveal the pro-myogenic proteins that are secreted by the hESCs contain heparin-binding domains.

hESC-conditioned Opti-MEM has Pro-Survival and Pro-Mitogenic effects on Neuronal Cell Types

To assess the potential positive effect of hESC-secreted proteins on other cell types, specifically neural cells, we cultured rat neural progenitor cells in the presence of hESC-conditioned medium, or in a control medium conditioned by differentiated hESC-derived cells. Specifically, cells were cultured in the 50/50 mix of neural differentiation medium (see Methods) and Opti-MEM, which was conditioned either by the self-renewing hESCs or by the negative control, differentiated hESC-derived cells. The goal was to determine if hESC-secreted factors can enhance proliferation and inhibit differentiation of NPCs, in parallel to our studies demonstrating these embryonic factors enhance muscle precursor proliferation and inhibit their differentiation in a 50/50 mix of fusion medium [5]. Very interestingly, a significant increase in proliferation of Sox-2+ neural progenitors was observed in cultures exposed to the hESC-produced proteins, an effect that was lost when NPCs were cultured in control medium from differentiated cells (Figure 6 A, quantified in B). As this effect was similar to what we previously reported for muscle stem/progenitor cells, in that we observe an enhancement of proliferation and inhibition of differentiation of precursor cells by hESC-secreted factors [5], it suggests that hESC-secreted proteins enhance the proliferative capacity of progenitor cells in multiple tissue types, and similarly to the situation in muscle, the pro-mitogenic activity is lost when hESCs differentiate.

We next sought to examine whether not only cell proliferation, but cell viability might be enhanced by the hESC-secreted proteins, particularly under pathological conditions. Likewise, we wished to investigate whether the effects of the pro-mitogenic factors would manifest not only on progenitors, but also on terminally differentiated neurons. To answer these questions, we generated human cortical glutamatergic neurons by directed differentiation of embryonic stem cells (see Methods). Specifically, dorsal telencephalic progenitors expressing glutamate and VgluT1 were generated by using Shh and FGF-2. This protocol induced the differentiation of human embryonic stem cells (hESCs) into cultures with up to 74% of neurons expressing glutamate and VgluT1. As an *in vitro* model of AD, soluble oligomeric forms of Aβ known as "globulomers," which have been implicated in the pathology of Alzheimer's disease [20, 21], were added to these cultures of human glutamatergic neurons. They bound Aβ, which led to cell death as measured by the presence of cleaved caspase 3 (Figure 6C, quantified in D).

To examine whether hESC-secreted factors have neuroprotective effects in this *in vitro* human AD model, Aβ globulomers were added to cortical cultures primarily comprised of glutamatergic neurons in the presence or absence of hESC-conditioned medium. The neurons were pre-incubated with hESC-conditioned Opti-MEM for 1 hr prior to treatment with Aβ globulomers, or alternatively, hESC-conditioned medium was added at 50% to neuron medium,

simultaneously with the Aβ globulomers. Analysis with cleaved caspase-3 as an apoptotic marker and MAP2 as neuron marker showed a significant decrease in cell death when neurons were pre-incubated with hESC-secreted factors, as compared to cultures treated with Aβ globulomers alone (Figure 6 C, quantified in D). A noticeable but not statistically significant decrease of apoptosis was observed in neuron cultures that were administered with Aβ and hESC-secreted proteins simultaneously (Figure 6 C, D). These data suggest that hESC-secreted factors exert a protective (anti-apoptotic) effect on human cortical neurons in this AD model.

Conclusions

Since the comprehensive molecular identity of the specific proteins that are responsible for the pro-regenerative effects of the hESC-conditioned medium is a work in progress, we report here the ability to enrich these proteins using the heparin binding domains, and thus to provide a novel approach to study these clinically relevant molecules. Our ability to enrich the pro-regenerative activity of the hESC-secreted proteins is particularly important, because these embryonic factors improved the regenerative capacity of not only muscle, but also enhanced proliferation of neural progenitor cells, suggesting their possible ability to combat tissue degenerative disorders in multiple organ systems. Furthermore, hESC-secreted proteins exhibited not only proliferative effects on different progenitor cell types, but also neuroprotective effects on human cortical neurons in an *in vitro* model of Alzheimer's disease. These results suggests that hESC-produced molecules either prevent the death of human cortical neurons in an Aβ induced neurotoxic environment or are able to reduce the effect of Aβ toxicity by preventing the interaction of such toxic species with neuronal phenotypes that highly susceptible to Aβ, both possibilities that are clinically relevant outcomes and would be very interesting to study further.

With respect to the enhancement of myogenesis, this work revealed a pro-myogenic effect of mTeSR-1, which was linked to the high levels of FGF-2, a known inducer of proliferation in multiple cell types. Importantly, we show that the pro-myogenic activity of the hESC-secreted proteins manifests without added FGF-2 and that the hESC-conditioned Opti-MEM, which we typically use, does not contain any residual activity that is derived from mTeSR1.

While we found that the levels of FGF-2 protein are indeed elevated in old myofibers (in agreement with Chakkalakal et al.), signaling downstream of FGF signaling, namely pERK, was low and not different between the young and aged muscle stem cells or muscle fibers. In resolution of this interesting conundrum, we found that while in the old muscle this protein is localized intracellularly within the myofibers (away from its receptors and from satellite cells), in the young muscle, FGF-2 is located mostly extracellularly in the basement membrane, which is the niche of muscle stem cells. As such, this work suggests that much more FGF-2 ligand is available for signaling to young muscle stem cells than in old muscle, but it is still unclear why FGF-2 does not induce proliferation of quiescent satellite cells in uninjured *young* muscle. Potentially, the disruption of the basement membrane due to the injury or attrition of the myofibers, differentiation of satellite cells along myogenic lineage, and/or extracellular matrix – based activation of FGF-2 for binding to its receptors might be required for the induction of FGF-2 signaling in the muscle stem cells responding to tissue damage. In support of this conclusion, FGF-2 had a weak effect on the proliferation of quiescent muscle stem cells derived from non-injured mice (both, young and old); and thus, not FGF-2 alone but other factors and signaling pathways are likely required for the breakage of satellite cell quiescence [5]. Low

numbers (~3-4%) of proliferating Ki67+ young satellite cells are explained by the fact that these cells (expected to be 99.1% quiescent) were cultured overnight in their own young serum that is known to be pro-proliferative [28]; proliferation of the aged quiescent satellite cells derived from uninjured muscle and cultured with old serum was very low, which is consistent with the fact that old satellite cells divide very poorly in the presence of aged serum [14, 29-31].

FGF-2 does not have a signal peptide, and the mechanisms of FGF-2 activation are not well described in general or in skeletal muscle [26, 28]; therefore, further work is required to understand the age-dependent defect in the localization and activation of FGF-2 signal transduction in muscle stem and progenitor cells. Notably, differential localization of FGF-2 might introduce experimental artifacts into its detection, since the basement membranes of myofibers typically become digested during muscle dissociation, and the plasma membrane may be damaged [26, 28]; thus, the identification of the precise levels of FGF-2 in sub-cellular compartments of skeletal muscle is not an easy task.

Importantly, our data directly demonstrate that the numbers of proliferating (Ki67+Pax7+) muscle stem cells do not increase with age, which is further corroborated by the lack of age-specific increase of BrdU+ muscle stem cells after 4-6 weeks of *in vivo* delivery of BrdU to young and old mice (Amy Wagers, personal communications). Summarily, it is inconsistent with our data that FGF-2 promotes proliferation of quiescent muscle stem cells in old mice, though it still may be possible that old satellite cells are lost through an indirect and MAPK-independent activity of FGF-2.

As well established, in response to injury or attrition of myofibers, quiescent muscle stem cells activate to divide, form myogenic lineage, and regenerate the tissue; and this process becomes inefficient with age. The work presented here introduces novel strategies for the purification and clinical use of the proteins that are able to rejuvenate the aged niches of organ stem cells and uncovers that the viability of differentiated cells in pathological tissues might be also enhanced by these clinically-relevant molecules.

Figure Legends

Figure 1. Both mTeSR-1 and hESC-Conditioned mTeSR-1 increase primary myoblast and satellite cell Proliferation and inhibit Differentiation. (A) Primary Mouse Myoblasts were cultured for 24 hours in 50% fusion/differentiation medium (DMEM, 2% horse serum) plus 50% of the specified medium. A 2 hour BrdU pulse was performed before cell fixation to label proliferating cells. Immunofluorescence was performed for eMyHC (green) and BrdU (red), with Hoechst (blue) labeling all nuclei. Representative images are shown. Proliferation and differentiation of fusion-competent myoblasts were quantified by cell scoring in 25 random fields of each condition using a Molecular Devices automated imager and MetaXpress cell scoring software. Results are displayed as the mean percent of BrdU+ (B) or eMyHC+ (C) proliferating or differentiating cells +/-SD, respectively. N=4 $*P < 4X10^{-10}$ for BrdU+ myoblasts incubated in 50% mTeSR-1 as compared to myoblasts incubated in just fusion medium, or 50% hESC-conditioned mTeSR-1 as compared to myoblasts incubated in just fusion medium. $*P < 0.005$ for eMyHC+ fusing myoblasts in 50% mTeSR-1 as compared to myoblasts incubated in fusion medium alone, and $*P < 9X10^{-5}$ for eMyHC+ fusing myoblasts in 50% hESC-conditioned mTeSR-1 as compared to myoblasts incubated in just fusion medium. (D) Old injury activated myofiber-associated satellite cells were isolated at 3 days post cardiotoxin-induced

muscle injury, and cultured overnight in 50% DMEM/F12 with 10% old serum, and 50% of the medium specified, followed by a 2 hour BrdU pulse to label proliferating cells before cell fixation. Immunofluorescence was performed with Desmin (green) and BrdU (red), with Hoechst (blue) labeling all cell nuclei. Representative images are shown and demonstrate that both hESC-conditioned mTeSR-1 and mTeSR-1 have a pro-myogenic effect on activated satellite cells. (E) Proliferating Desmin+/BrdU+ satellite cells were quantified by cell scoring in multiple random fields of each condition. Results are displayed as the mean percent of BrdU+/Desmin+ proliferating satellite cell cells +/-SD. N=3, $*P< 0.05$ for satellite cells in 50% mTeSR-1 as compared to satellite cells incubated in just basal medium with old serum, and $*P< 0.001$ for satellite cells in 50% hESC-conditioned mTeSR-1 as compared to satellite cells incubated in just basal medium with old serum. (F) Undifferentiated hESCs that were grown in mTeSR-1 medium were washed 0-3 times with Opti-MEM, followed by overnight incubation in Opti-MEM and collection of the resulting conditioned Opti-MEM. The hESC-conditioned Opti-MEM was spun down to remove cell debris, before addition to myoblasts as a 50/50 mix with myogenic fusion medium for culture overnight. A 2 hour BrdU pulse was performed to label proliferating cells prior to cell fixation and immunofluorescence was performed with eMyHC and BrdU, with Hoechst labeling all cell nuclei (images not shown). Proliferating and differentiating cells were quantified by cell scoring 25 random fields of each condition using an automated imager and MetaXpress cell scoring software. Results are displayed as the mean percent of BrdU+ or eMyHC+ proliferating or differentiating cells +/-SD, respectively and n=2.

Figure 2. hESC-conditioned medium enhances myogenic proliferation in the absence of FGF2 in mTeSR-1 growth medium. (A) Primary myoblasts were cultured for 16 hours in 50% fusion/differentiation Medium + 50% of the specified medium. A 2 hour BrdU pulse was performed before cell fixation to label proliferating cells. Immunofluorescence was performed for eMyHC (green) and BrdU (red), with Hoechst (blue) labeling all nuclei. Representative images demonstrate that hESC-conditioned medium lacking FGF2 increases myoblast proliferation and inhibits differentiation. (B) Proliferation and differentiation of fusion-competent myoblasts were quantified by cell scoring in 50 random fields of each condition using an automated imager and MetaXpress cell scoring software. Results are displayed as the mean percent of BrdU+ or eMyHC+ proliferating or differentiating cells +/-SD, respectively. N=4, $*P< 2X10^{-12}$ for hESC-conditioned basal medium with 4 mTeSR-1 ingredient components (lacking FGF2) as compared to differentiation hESC-conditioned basal medium with 4 mTeSR-1 ingredient components (also lacking FGF2), and for hESC-conditioned basal medium with 4 mTeSR-1 ingredient components (lacking FGF2) as compared to myoblasts incubated in basal medium with 4 mTeSR-1 ingredient components (lacking FGF2).

Figure 3. Age-dependent comparison of FGF2 and pERK levels and localization in muscle fibers. (A) Protein was isolated from freshly-derived uninjured myofibers of young and old mice and the levels of FGF2 and phospho-ERK1/2; total ERK1/2 and cytoplasmic beta-actin were analyzed by Western blotting, using specific antibodies. Representative data are shown. (B) Relative protein expression was quantified in 3 young and 3 old mice by normalization of FGF-2 to beta-actin and normalization of pERK to total ERK; significantly higher levels of FGF-2, but not of pERK were detected in the old myofibers, as compared to young (n=3, * P<0.05). (C) Tibialis anterior (TA) muscle from 2 young and 2 old mice were sectioned and immunostained for laminin (green) and FGF2 (red). Hoechst (blue) labels all nuclei. Representative images demonstrate the presence of FGF-2 and laminin in muscle compartments, as compared to the

negative IgG control and higher FGF-2 levels seem to be present in the laminin+ basement membranes of the young myofibers, as compared to old. (D). The pixel density of FGF-2 that co-localizes with laminin+ basement membrane vs. the internal regions of the myofibers was determined in 30-40 areas of each cryosection of 3 muscle tissue slides from young and old muscle, using Image J software. Preferential localization of FGF-2 in the basement membrane was identified in young muscle, while in the old tissue, FGF-2 was mis-localized to the center of the myofibers and away from the basement membrane, n=3, * P<0.05.

Figure 4. Age-related comparison of FGF2 and pERK levels in muscle stem cells derived from uninjured tissue and of proliferation of these cells. (A) Quiescent muscle stem cells were isolated from uninjured young and old muscle as described in Methods. The cells were treated (or not) with FGF2 (10ng/ml) for 30 minutes before being lysed and analyzed for the levels of FGF2, phospho-ERK1/2, total ERK1/2 and beta actin by Western Blotting. Representative images are shown. (B) Relative protein expression of FGF-2, pERK and total ERK were quantified from 3 young and 3 old mice, using beta-actin for normalization. The levels of FGF-2 were equally undetectable in young and old satellite cells, however, added FGF-2 was clearly detected in the cells of both ages after ~2min exposure (but was not detected in accelular samples even after 10min exposure); the levels of pERK and total were equally low in young and old satellite cells and pERK, but not total ERK was, as expected, induced by added FGF-2. n=3, * P<0.05. (C) Muscle stem cells from resting muscle were treated (or not) with FGF2 (10ng/ml) for 24 hours before immunostaining for Ki67 and Pax7. Percent of Ki67+/Pax7+ proliferating myogenic cells were quantified. No age-specific increase in cell proliferation was detected in satellite cells isolated from old uninjured muscle, and in contrast, more proliferating satellite cells were observed in the cultures derived from young muscle. Added FGF-2 enhanced the proliferation of both young and old muscle stem cells in these overnight cultures. n=3, * P<0.05.

Figure 5. Pro-regenerative Embryonic Factors Contain Heparin Binding Domains. (A) Primary Mouse Myoblasts were cultured for 24 hours in 50% fusion/differentiation medium + 50% of the specified medium. A 2 hour BrdU pulse was performed before cell fixation to label proliferating cells. Immunofluorescence was performed for eMyHC (green) and BrdU (red), with Hoechst (blue) labeling all nuclei. Representative images are shown. (B) Proliferation and differentiation of fusion-competent myoblasts were quantified by cell scoring in 25-100 random fields of each condition using an automated imager and MetaXpress cell scoring software. Results are displayed as the mean percent of BrdU+ or eMyHC+ proliferating or differentiating cells +/-SD, respectively. N=6 $*P< 3X10^{\wedge-45}$ for hESC-conditioned Opti-MEM compared to differentiated hESC-conditioned Opti-MEM, and hESC-conditioned Opti-MEM compared to Opti-MEM. *$P<0.005$* for hESC-conditioned Opti-MEM compared to heparin depleted hESC-conditioned Opti-MEM, and hESC-conditioned Opti-MEM compared to differentiated hESC-conditioned OptiMEM. $*P< 5X10^{\wedge-7}$ for hESC-conditioned Opti-MEM compared to Opti-MEM, and Eluted Proteins compared to Opti-MEM. (C) Old Tibialis Anterior muscles were injured with cardiotoxin (see Methods). Heparin bound and eluted protein or vehicle control (Opti-MEM) were injected into sites of injury on Day 0 and Day 2. BrdU was injected (intraperitoneal) at 3 days post injury to label proliferating, fusion-competent myoblasts. Animals were sacrificed and muscle was collected 5 days post injury. Cryosections (10 μm) were analyzed by hematoxylin/eosin (H&E) staining and immunostaining for embryonic myosin heavy chain (eMyHC, shown in green) and BrdU incorporation (shown in red). Hoechst stains nuclei (blue).

As shown by representative images, the regenerative outcome of old muscle given eluted factors was significantly improved as compared to old muscle given Opti-MEM vehicle control, based on significantly diminished scar tissue formation, larger and more dense *de novo* myofibers and an increase in the numbers of eMyHC+ myofibers with centrally-located BrdU+ nuclei that replaced the damaged tissue. (D) Regeneration of old mouse Tibialis Anterior 5 days post injury, that received eluted factors or vehicle, was quantified from muscle sections, and is presented as the number of newly regenerated myofibers per square millimeter of injury site. Error bars indicate SD, n=3 mice per group. *$P < 0.02$ between old given eluted factors and old given vehicle control.

Figure 6. hESC-secreted Factors Enhance NPC Proliferation and are Neuroprotective. (A) Rat Neural Progenitor Cells (rNPCs) were cultured overnight in 50% differentiation medium (DMF12 + N2) and 50% specified medium followed by a 4 hour BrdU pulse to label proliferating cells prior to fixation. Immunofluorescence was performed for Sox2 (red) and BrdU (green), with Hoechst (blue) labeling cell nuclei. Representative images are shown. (B) Quantification of BrdU+/Sox2+ proliferating cells was performed by cell scoring in 100 random fields of each condition using an automated imager and MetaXpress cell scoring software. Results are displayed as the mean percent of BrdU+/Sox2+ proliferating cells +/-SD; N=4, *$P< 2X10^{-15}$ for rNPCs incubated in hESC-conditioned Opti-MEM as compared to rNPCs incubated in differentiated hESC-conditioned Opti-MEM, and *$P< 0.0002$ for rNPCs incubated in hESC-conditioned Opti-MEM as compared to rNPCs incubated in Opti-MEM. (C) Pre-incubation of Aβ globulomers with hESC –conditioned Opti-MEM before incubation with mature cortical neurons prevents neuron cell death and exhibits a neurotrophic effect, as shown via decreased immunofluorescence staining of cleaved caspase3 (red) and increased Map2 + (green) neurons. Hoechst (blue) labels all nuclei. Representative images are shown. (D) Total number of Map2+ neurons and the amount of apoptosis was quantified by cell scoring of random fields taken by an automated imager of each condition in the above assay performed in replicates. Results are displayed as the mean percent of caspase + or Map2+ (C) proliferating or differentiating cells +/-SD, respectively. N=4, *$P< 0.02$ for Map2+ cortical neurons treated with Aβ globulomers preincubated in hESC-conditioned Opti-MEM, as compared to treatment with Aβ globulomers in OptiMEM, and *$P< 0.05$ for the level of caspase3 in cortical neurons treated with Aβ globulomers preincubated in hESC-conditioned Opti-MEM, as compared to treatment with Aβ globulomers in Opti-MEM.

Supplementary Figure 1. Expression of FGF2 in quiescent muscle stem cells from young and old mice. Muscle stem cells were isolated from young and old uninjured muscle, as described in Methods. The cells were immediately lysed for Western blotting without culturing and the expression of FGF2, phosphor-ERK1/2, ERK1/2 and β-actin were analyzed. 30 minutes of enhanced chemiluminescence exposure was used for detection of FGF-2, while pERK, total ERK and actin were detected after 2min, 30 sec and 30 sec exposure, respectively. Low and age-independent levels of FGF-2 and pERK were detected in satellite cells that were derived from uninjured young and old TA muscle.

Supplementary Figure 2. Myogenic marker expression in young and old muscle stem cells. Muscle stem cell isolated from young and old mice were cultured for 24 hours and then immunostained for myogenic markers Pax7 and Myf-5. ~95% of isolated young and old satellite cells expressed these myogenic markers, demonstrating high and age-independent purity.

Supplementary Figure 3. Proteinase K treatement abolishes proliferative hESC factors.

Old injury-activated satellite cells with associated myofibers were cultured overnight in 50% Opti-MEM with 10% old serum and 50% hESC conditioned Opti-MEM that was treated with pre-washed Proteinase K agarose beads (Sigma-Aldrich), for 1 hour at 37C followed by bead removal, or mock-treated hESC conditioned Opti-MEM. Cells received a 2 hour BrdU pulse to label proliferating cells before cell fixation. Immunofluorescence was performed for Desmin (green) and BrdU (red), with Hoechst (blue) labeling all cell nuclei. Proliferating, desmin+ve cells were quantified by imaging and scoring multiple random microscopic fields of each condition. Results are displayed as the mean percent of BrdU+,Desmin+ proliferating satellite cell cells +/-SEM, $p<0.005$, n=3 replicate experiments.

Methods

Animals

Young (2-3 month old) and old (22-24 month old) C57BL6/J mice were purchased from the Jackson Laboratory and the NIH. The animal experimental procedures were performed in accordance with the Guide for Care and Use of Laboratory Animals of the National Institutes of Health, and approved by the Office of Laboratory Animal Care, UC Berkeley.

Antibodies

Antibodies for phospho-ERK1/2, ERK1/2, and cleaved caspase 3 were purchased from Cell Signaling. Laminin and Actin antibodies were from Sigma. FGF2 antibody was from Santa Cruz, Pax7 and eMyHC antibodies were from Hybridoma Bank, BrdU was from Abcam, and Map2 antibody was from BD Biosciences.

Muscle fibers and muscle stem cell isolation

Uninjured TA muscle was dissected from healthy young and old mice and incubated at 37C in digestion medium (250 U/mL Collagenase type II in DMEM medium, buffered with 30 mM HEPES) for 1 hour [26]. Digested muscle was gently triturated and myofibers were collected. Myofibers were further digested with 1 U/mL Dispase and 40 U/mL Collagenase type II to liberate muscle stem cells [28]. Muscle stem cells were cultured in DMEM with serum from the same age mouse.

Immunofluorescence analysis

Cells were fixed with 4% PFA for 10 minutes before permeablization with 0.1% Triton-X 100 for 30 minutes. Then cells were then immunostained for Pax7 (Hybridoma Bank) and ki67 (Abcam). Primary antibodies used for staining cortical human neurons were: mouse anti-MAP2 (1:500, BD Biosciences), rabbit anti-cleaved caspase 3 (1:100, Cell Signaling). For muscle section immunostaining, an uninjured TA muscle was sectioned at 10 um and stained for FGF2 (Santa Cruz) and laminin (Sigma).

Western blotting

Muscle stem cells or myofibers were lysed in RIPA buffer containing 1X protease inhibitor (Roche). The protein concentration was determined by Bradford assay (Bio-Rad). Cell or fiber lysates were resuspended in 1X Laemmli buffer (Rio-rad), boiled for 5 minutes and separated on precast TGX gels from Biorad. The proteins were then transferred to PVDF membrane (Millipore) and blotted with the desired antibodies.

Cell Culture

Rat NPCs were cultured in DMF12 (Gibco) with 5% N2 and 10 ng/mL FGF2, on laminin and polyornithine coated plates. For experimental conditions, cells were plated at 40,000 cells/well in coated 8-well chamber slides and cultured for 12-16 hours at 37C in 10% CO2 incubator prior to fixation with 70% ethanol at 4C. Adult human myoblasts were cultured and expanded in human growth medium (Ham's F-10 (Gibco), 10% Bovine Growth Serum (Hyclone), 30 ng/mL FGF2, and 1% penicillin–streptomycin on Matrigel (BD Biosciences) coated plates (1:100

matrigel:PBS), at 37C and 5% CO2. For experimental conditions, cells were plated at 10,000 cells/well in Matrigel coated 8-well chamber slides (1:100 Matrigel: PBS), and cultured for 72 hours with daily re-feedings at 37C in 10% CO2 incubator prior to fixation with 70% ethanol at 4C. Mouse myoblasts were cultured and expanded in mouse growth medium: Ham's F-10 (Gibco), 20% Bovine Growth Serum (Hyclone), 5 ng/mL FGF2 and 1% penicillin–streptomycin on Matrigel coated plates (1:300 matrigel: PBS), at 37C and 5% CO2. For experimental conditions, cells were plated at 40,000 cells/well on Matrigel coated 8-well chamber slides (1:100 matrigel: PBS) and cultured for 24 hours at 37C in 10% CO2 incubator prior to fixation with 70% ethanol at 4C.

Human embryonic stem cells (H9 and H7 lines), were cultured on diluted Matrigel (1:30), in mTeSR-1 (Stem Cell Technologies), according to manufacturer's recommendations. hESCs were differentiated after plating in mTeSR-1 by changing the medium to DMEM/F12 with 10% Bovine Growth Serum (Hyclone), and culturing for an additional 6-8 days. Cells were washed with Opti-MEM (Gibco) and then cultured in Opti-MEM for 18 hours prior to collection as hESC-Conditioned Opti-MEM (hESC-Conditioned Medium) and stored at -80C.

All experiments using a MEK inhibitor were treated with 10 micromolar MEK1/2 Inhibitor (U0126, Cell Signaling Technologies).

Cell culture and cortical differentiation of human pluripotent stem cells

The H1 (WiCell) and hESC line was cultured on Matrigel-coated cell culture plates (BD) in mTeSR-1 maintenance medium (Stem Cell Technologies). In adherent conditions, hPSCs were seeded at a density of 5×104 cells/cm2 in growth medium. At 50% confluence, the medium was gradually changed to neural basal medium (Invitrogen) containing N2 and B27 (Invitrogen). SMAD signaling inhibitors LDN193189 (Stemgent, 1 µM) and SB432542 (Tocris Biosciences, 10 µM) were added from day 1 to day 7 of neural induction. Cyclopamine (Calbiochem, 400 ng/ml) and FGF-2 (Peprotech, 10 ng/ml) were added from days 3-14 of differentiation. After 12-14 days, cells were mechanically passaged into poly-L-ornithine (Sigma Aldrich) and laminin (Invitrogen, 20µg/ml) coated plates and allowed to undergo maturation for 3-6 weeks. BDNF (10 ng/ml, Peprotech) was added to cultures one week after initiation of neuronal maturation. For EB mediated neural differentiation, PSCs were aggregated for 4 days in ultra low-attachment plates (Corning) and then seeded on Matrigel-coated plates. Cyclopamine (5 µM) and FGF-2 (10 ng/ml) were added to the cultures the following day until day 12 of neural induction. At day 14, structures with a rosette-like morphology were mechanically isolated and plated on poly-L-ornithine and laminin coated plates and allowed to undergo neuronal maturation for 4 weeks. BDNF (10 ng/ml) was added to the cultures one week after rosette isolation.

Globulomer Preparation

The A-beta42 globulomer was prepared as described [32, 33]. Alkaline pretreatment of A-beta42 and preparation of low molecular weight A-beta by filtration protocols were used before beginning the globulomer preparation. After the 18-20 h incubation, the globulomer sample were concentrated to ~500 M via centrifugation and dialyzed into PBS before centrifuging the sample at 10,000 g for 10 min to remove aggregates in the pellet. The supernatant was saved, and the absorbance was measured at 276 nm wavelength to measure the concentration (extinction coefficient = 1390 M-1 cm-1).

Immunocytochemistry

For immunoflourescence assays, mouse myoblasts were given a 2 hour 300μM BrdU pulse, respectively. Cells were then permeabilized in PBS + 0.25% Triton X-100 and incubated with primary antibodies overnight at 4C in PBS +2%FBS. Antigen retrieval was performed via a 10 minute 4 N HCl treatment followed by PBS washes. Primary staining was performed overnight with species-specific monoclonal antibodies for mouse anti-embryonic Myosin Heavy Chain (eMyHC, hybridoma clone 1.652, Developmental Studies Hybridoma Bank) and Rat-BrdU (Abcam Inc. ab6326), and desmin (Sigma-Aldrich DE-U-10 used at 1:300 for best discrimination of myogenic cells), for myoblasts and satellite progenitor cells, and Goat-Sox2 (Santa Cruz) for rNPCs. Secondary staining with fluorophore-conjugated, species-specific antibodies (Donkey anti-Rat-488, #712-485-150; Donkey anti-Mouse-488, #715-485-150; Donkey anti-Rat-Cy3 #712-165-150; or donkey anti-Mouse-Cy3 #715-165-150; all secondary antibodies from Jackson ImmunoResearch) was performed for 1 hour at room temperature at a 1:500 dilution in PBS +2%FBS. Nuclei were visualized by Hoechst staining, and samples were analyzed at room temperature with a Zeiss Axio Imager A1, and imaged with an Axiocam MRC camera and AxioVision software. Mouse myoblasts were imaged at 10X and 20X magnification, respectively. For cell quantification, 25-50 20x images per replicate were taken on the Molecular Devices ImageXpress Micro automated epifluorescence imager, followed by automated cell quantification using the multiwavelength cell scoring module within the MetaXpress analysis software.

Heparin Binding of hESC-Secreted Proteins from hESC-Conditioned Medium
Heparin-Agarose Type I Beads (H 6508, Sigma Aldrich) were washed with molecular grade water and preconditioned in 1mL Opti-MEM as recommended by manufacturer. hESC-conditioned medium was incubated with Heparin-Agarose Beads for 2 hours shaking at 4C. Beads and all medium were separated by centrifugation. Myoblasts were treated with depleted medium after two rounds of centrifugation and separation of beads and medium so as to remove all residual beads from depleted hESC-conditioned medium.

After depleting hESC-Conditioned Opti-MEM, the protein bound heparin beads were washed two times for 10 minutes at 4C in 1ml PBS + .05% Tween-20. Proteins were eluted twice for 15 minutes at 4C in 400μl of elution buffer (.01M Tris-HCl pH 7.5 +1.5M NaCl + 0.1%BSA) to collect proteins in a total of 800μl of elution buffer. The proteins were purified by dialysis for 2 hours shaking at 4C in 500ml McCoy's 5A Medium (Gibco) followed by overnight dialysis shaking at 4C in 200ml Opti-MEM (Gibco). The eluted heparin beads were re-suspended in 800μl Opti-MEM and stored overnight at 4C. One hour after plating, mouse myoblasts were treated with respective mediums for 24 hours prior to 2 hour BrdU pulse and fixation in 70% ethanol.

Muscle Injury

Isoflurane was used to anesthetize the animal during the muscle injury procedure. For bulk myofiber satellite cell activation, gastrocnemius muscles were injected with cardiotoxin 1 (Sigma) dissolved at 100 micrograms per milliliter in PBS, at 4 sites of 10 microliters each for

each muscle. Muscles were harvested 3 days later. For focal injury, to assay regeneration *in vivo*, 5 microliters of 0.5 milligram per milliliter CTX was injected at two sites to the middle of the tibialis anterior, and muscle harvested 5 days later.

Tissue Immunofluorescence and Histological Analysis

Muscle tissue was dissected, flash frozen in OCT compound (Tissue Tek; Sakura) and cryo-sectioned at 10 micrometers, as previously described (Conboy et al., 2003). Cryo-sectioning was performed through the entire volume of muscle (typically 50–70 sections total, done at 200 μm intervals), thereby serially reconstituting the entire tissue, ex vivo. Muscle sections were stained with aqueous hematoxylin and eosin (H&E), as per the manufacturer's instructions (Sigma-Aldrich). Regeneration and myogenic potential was quantified by examining injury sites from representative sections along the muscle (spanning the volume of injury), then by measuring the injured/regenerating area using Adobe Photoshop Elements. Myofiber regeneration was quantified by counting total newly regenerated fibers and dividing by the regeneration area. Immunostaining was performed as described [34]. Briefly, after permeabilization in PBS + 1% FBS + 0.25% Triton-X-100, tissues and cells were incubated with primary antibodies in staining buffer (PBS + 1% FBS) for 1 h at room temperature, followed by 1 h incubation fluorochrome-labeled secondary antibodies (ALEXA at 1:1000). BrdU-specific immunostaining required an extra step of 2 M HCl treatment before permeablization.

Quantification and Statistical Analysis

For quantification of immuno-fluorescent images, 25-100 20x images per replicate were taken on the Molecular Devices ImageXpress Micro automated epifluorescence imager, followed by automated cell quantification using the multiwavelength cell scoring module within the MetaXpress analysis software. Data was analyzed, using Anova and P values equal or lower than 0.05 were considered statistically significant.

Acknowledgements

This work was supported by grants from the National Institutes of Health R01 AG02725201 and California Institute for Regenerative Medicine RN1-00532-1 to IMC, CIRM grant RT2-02022 to DVS, and NSF Pre-doctoral fellowship to HY. We thank Mary West and the CIRM/QB3 Shared Stem Cell Facility at UC Berkeley for use of the Molecular Devices ImageExpress. Hikaru Mamiya and George Sun provided technical assistance with this work, and Aradhana Verma provided cortical neuron cell quantification.

Authors' contributions:

HY performed and analyzed experiments for Figures 1, 2, 5 and 6, participated in the design and interpretation of these data and co-wrote the manuscript; MJC performed experiments for Figures 1, 2, 5, 6 and S3, participated in the design and interpretation of these data and co-wrote the manuscript; JL performed and analyzed experiments for Figures 3, 4, S1 and S2, participated in their design and data interpretation and in writing of the manuscript; MZ performed the experiments for Figure 5 (A, B) and participated in the writing of the manuscript; TV performed

and analyzed the experiments for Figures 6 (C and D) and participated in their design and interpretation, and in writing of the manuscript; CS performed the experiments for Figure 5 (C and D); DVS participated in the design and interpretation of the experiments and edited the manuscript; IMC guided and integrated the study, participated in the design of the experiments, interpreted the data and wrote the manuscript.

References:

1. Conboy, I.M. and T.A. Rando, *Heterochronic parabiosis for the study of the effects of aging on stem cells and their niches.* Cell Cycle, 2012. **11**(12): p. 2260-7.
2. Kuhn, H.G., H. Dickinson-Anson, and F.H. Gage, *Neurogenesis in the dentate gyrus of the adult rat: age-related decrease of neuronal progenitor proliferation.* J Neurosci, 1996. **16**(6): p. 2027-33.
3. Maslov, A.Y., et al., *Neural stem cell detection, characterization, and age-related changes in the subventricular zone of mice.* J Neurosci, 2004. **24**(7): p. 1726-33.
4. Carlson, M.E. and I.M. Conboy, *Loss of stem cell regenerative capacity within aged niches.* Aging Cell, 2007. **6**(3): p. 371-82.
5. Conboy, I.M., H. Yousef, and M.J. Conboy, *Embryonic anti-aging niche.* Aging (Albany NY), 2011. **3**(5): p. 555-63.
6. Bendall, S.C., et al., *An enhanced mass spectrometry approach reveals human embryonic stem cell growth factors in culture.* Mol Cell Proteomics, 2009. **8**(3): p. 421-32.
7. Resnick, J.L., et al., *Long-term proliferation of mouse primordial germ cells in culture.* Nature, 1992. **359**(6395): p. 550-1.
8. Matsui, Y., K. Zsebo, and B.L. Hogan, *Derivation of pluripotential embryonic stem cells from murine primordial germ cells in culture.* Cell, 1992. **70**(5): p. 841-7.
9. Ludwig, T.E., et al., *Feeder-independent culture of human embryonic stem cells.* Nat Methods, 2006. **3**(8): p. 637-646.
10. Beenken, A. and M. Mohammadi, *The FGF family: biology, pathophysiology and therapy.* Nat Rev Drug Discov, 2009. **8**(3): p. 235-53.
11. Nickel, W., *Unconventional secretory routes: direct protein export across the plasma membrane of mammalian cells.* Traffic, 2005. **6**(8): p. 607-14.
12. Rando, T.A. and H.M. Blau, *Primary mouse myoblast purification, characterization, and transplantation for cell-mediated gene therapy.* J Cell Biol, 1994. **125**(6): p. 1275-87.
13. Bischoff, R., *Cell cycle commitment of rat muscle satellite cells.* J Cell Biol, 1990. **111**(1): p. 201-7.
14. Conboy, I.M., et al., *Notch-mediated restoration of regenerative potential to aged muscle.* Science, 2003. **302**(5650): p. 1575-1577.
15. Chakkalakal, J.V., et al., *The aged niche disrupts muscle stem cell quiescence.* Nature, 2012. **490**(7420): p. 355-60.
16. Raz, N., et al., *Regional brain changes in aging healthy adults: general trends, individual differences and modifiers.* Cereb Cortex, 2005. **15**(11): p. 1676-89.
17. Hof, P.R. and J.H. Morrison, *The aging brain: morphomolecular senescence of cortical circuits.* Trends Neurosci, 2004. **27**(10): p. 607-13.
18. Price, J.L., et al., *The distribution of tangles, plaques and related immunohistochemical markers in healthy aging and Alzheimer's disease.* Neurobiol Aging, 1991. **12**(4): p. 295-312.

19. Sowell, E.R., et al., *Mapping cortical change across the human life span.* Nat Neurosci, 2003. **6**(3): p. 309-15.
20. Kuo, Y.M., et al., *Water-soluble Abeta (N-40, N-42) oligomers in normal and Alzheimer disease brains.* J Biol Chem, 1996. **271**(8): p. 4077-81.
21. Jensen, M., et al., *Quantification of Alzheimer amyloid beta peptides ending at residues 40 and 42 by novel ELISA systems.* Mol Med, 2000. **6**(4): p. 291-302.
22. van Zoelen, E.J., et al., *Identification and characterization of polypeptide growth factors secreted by murine embryonal carcinoma cells.* Dev Biol, 1989. **133**(1): p. 272-83.
23. Nurcombe, V., et al., *MK: a pluripotential embryonic stem-cell-derived neuroregulatory factor.* Development, 1992. **116**(4): p. 1175-83.
24. Grounds, M.D., *Age-associated changes in the response of skeletal muscle cells to exercise and regeneration.* Ann.N.Y.Acad.Sci., 1998. **854**: p. 78-91.
25. Conboy, I.M. and T.A. Rando, *Aging, stem cells and tissue regeneration: lessons from muscle.* Cell Cycle, 2005. **4**(3): p. 407-410.
26. Bischoff, R., *Proliferation of muscle satellite cells on intact myofibers in culture.* Developmental biology, 1986. **115**(1): p. 129-139.
27. Conboy, I.M. and T.A. Rando, *The regulation of Notch signaling controls satellite cell activation and cell fate determination in postnatal myogenesis.* Dev.Cell, 2002. **3**(3): p. 397-409.
28. Conboy, M.J. and I.M. Conboy, *Preparation of adult muscle fiber-associated stem/precursor cells.* Methods Mol Biol, 2010. **621**: p. 149-63.
29. Carlson, M.E., et al., *Relative roles of TGF-beta1 and Wnt in the systemic regulation and aging of satellite cell responses.* Aging Cell, 2009. **8**(6): p. 676-89.
30. Carlson, M.E., et al., *Molecular aging and rejuvenation of human muscle stem cells.* EMBO Mol Med, 2009. **1**(8-9): p. 381-91.
31. Paliwal, P., et al., *Age dependent increase in the levels of osteopontin inhibits skeletal muscle regeneration.* Aging (Albany NY), 2012. **4**(8): p. 553-66.
32. Barghorn, S., et al., *Globular amyloid beta-peptide oligomer - a homogenous and stable neuropathological protein in Alzheimer's disease.* J Neurochem, 2005. **95**(3): p. 834-47.
33. Yu, L., et al., *Structural characterization of a soluble amyloid beta-peptide oligomer.* Biochemistry, 2009. **48**(9): p. 1870-7.
34. Conboy, M.J., et al., *Immuno-analysis and FACS sorting of adult muscle fiber-associated stem/precursor cells.* Methods Mol Biol, 2010. **621**: p. 165-73.

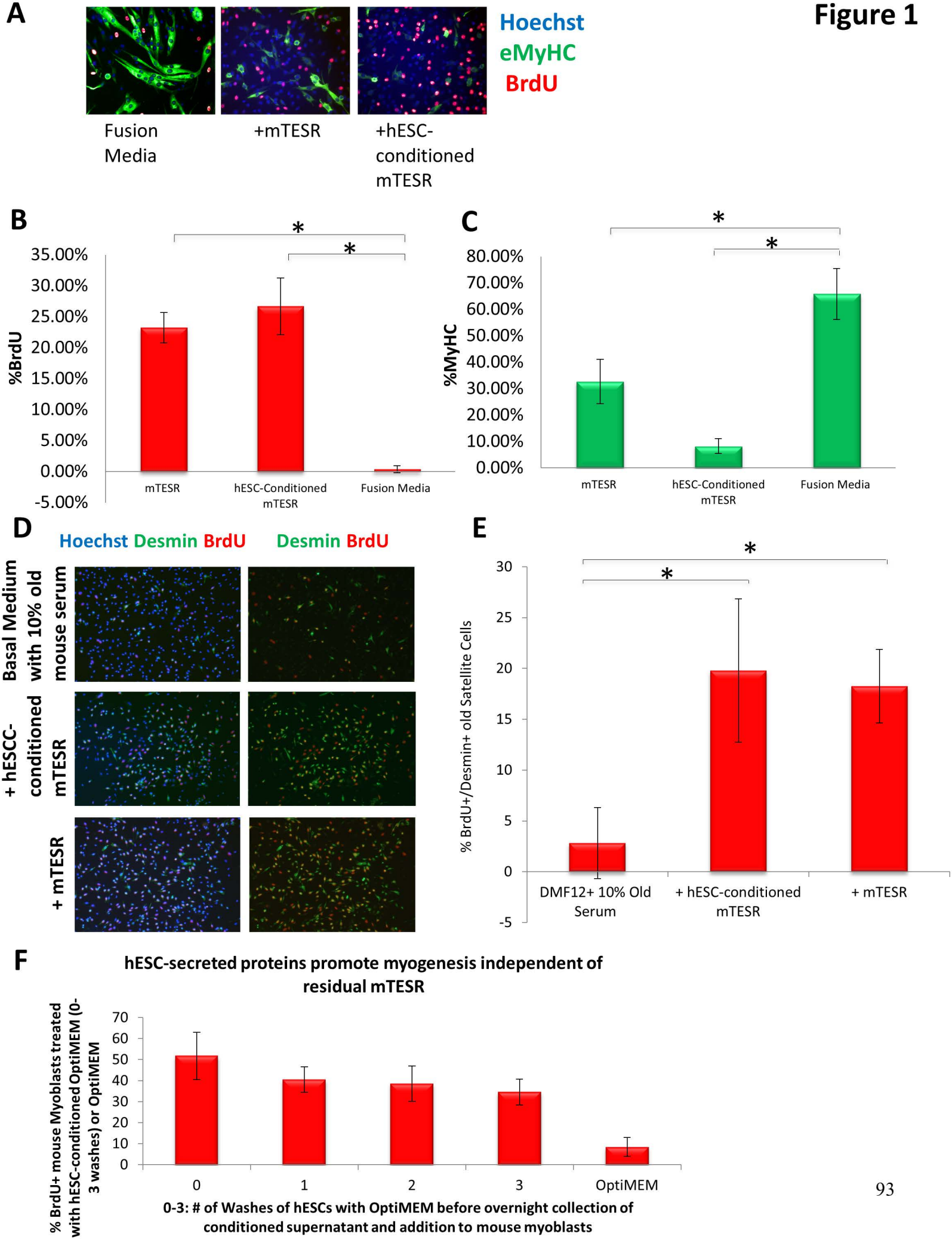
A
Hoechst
eMyHC
BrdU
Fusion Media
+mTESR
+hESC-conditioned mTESR
B
%BrdU
35.00%
30.00%
25.00%
20.00%
15.00%
10.00%
5.00%
0.00%
-5.00%
mTESR
hESC-Conditioned mTESR
Fusion Media
C
%MyHC
80.00%
70.00%
60.00%
50.00%
40.00%
30.00%
20.00%
10.00%
0.00%
mTESR
hESC-Conditioned mTESR
Fusion Media
D
Hoechst Desmin BrdU
Desmin BrdU
Basal Medium with 10% old mouse serum
+ hESCC-conditioned mTESR
+ mTESR
E
% BrdU+/Desmin+ old Satellite Cells
30
25
20
15
10
5
0
-5
DMF12+ 10% Old Serum
+ hESC-conditioned mTESR
+ mTESR
F
hESC-secreted proteins promote myogenesis independent of residual mTESR
% BrdU+ mouse Myoblasts treated with hESC-conditioned OptiMEM (0-3 washes) or OptiMEM
70
60
50
40
30
20
10
0
0
1
2
3
OptiMEM
0-3: # of Washes of hESCs with OptiMEM before overnight collection of conditioned supernatant and addition to mouse myoblasts

Figure 2

A

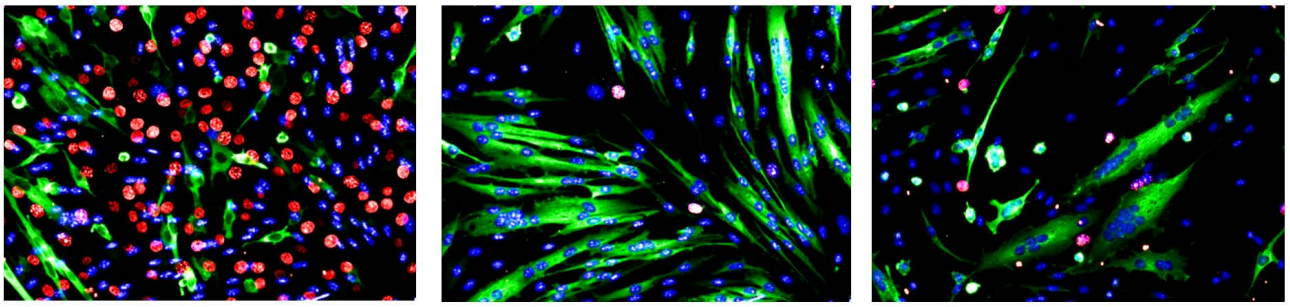

hESC – conditioned Basal Medium + 4 Factors (-FGF2)

Diff hESC–conditioned Basal Medium + 4Factors (-FGF2)

Basal Medium + 4 Factors (-FGF2)

B

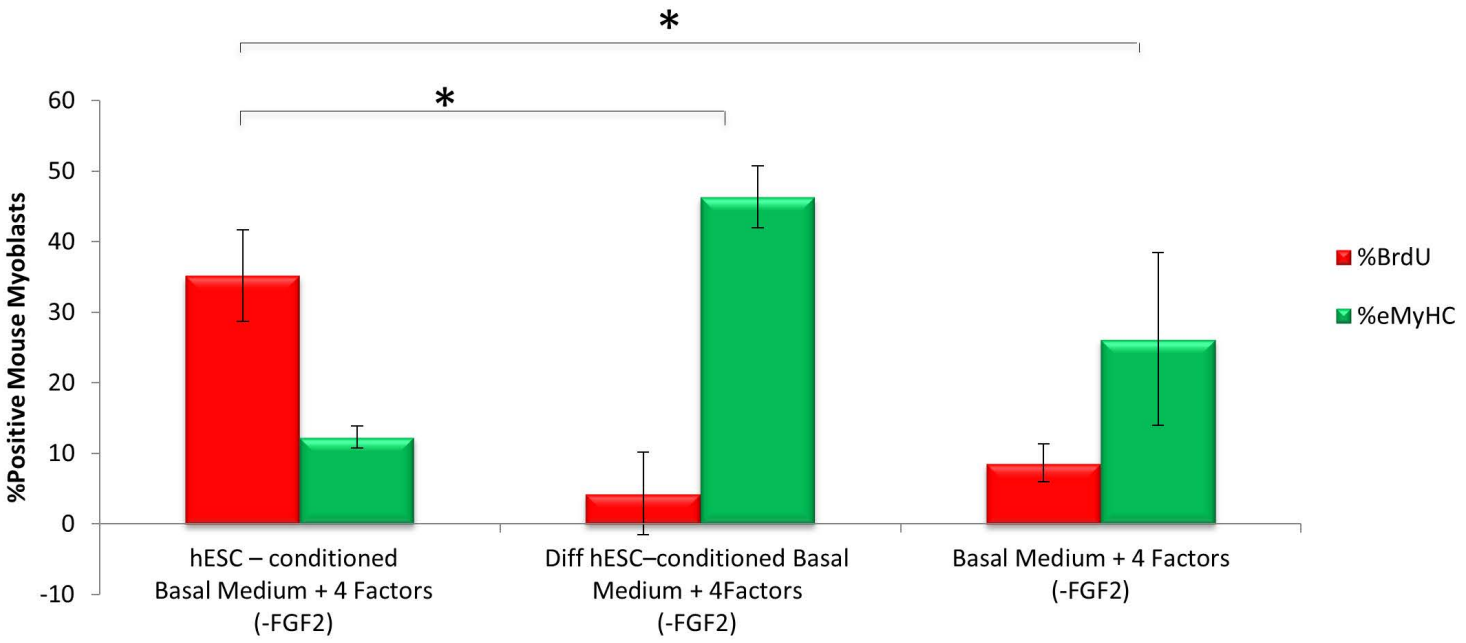

A

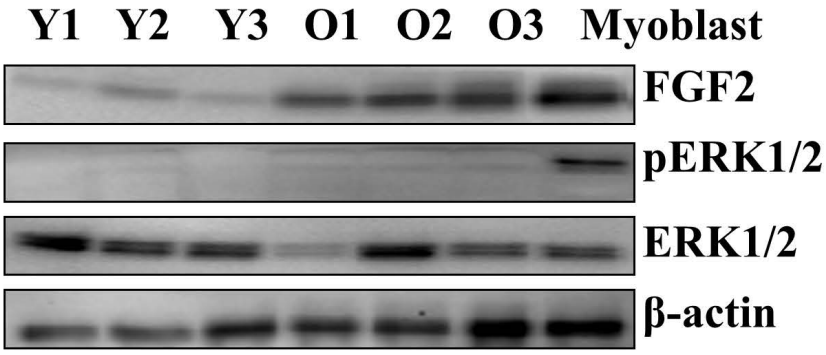
Y1 Y2 Y3 O1 O2 O3 Myoblast
FGF2
pERK1/2
ERK1/2
β-actin

B

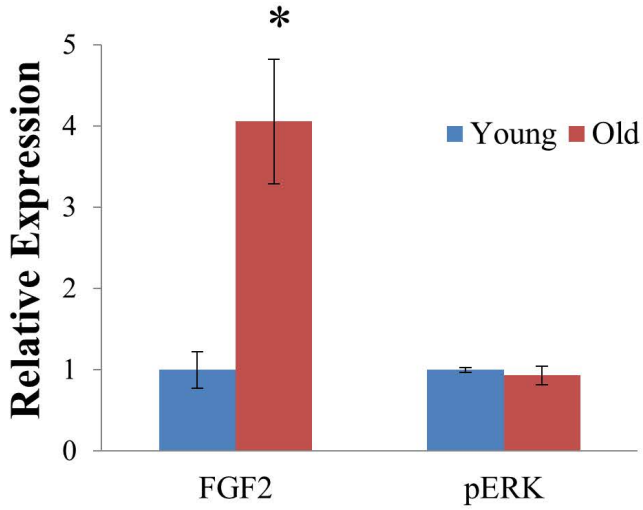
*
Relative Expression
0
1
2
3
4
5
Young
Old
FGF2
pERK

C

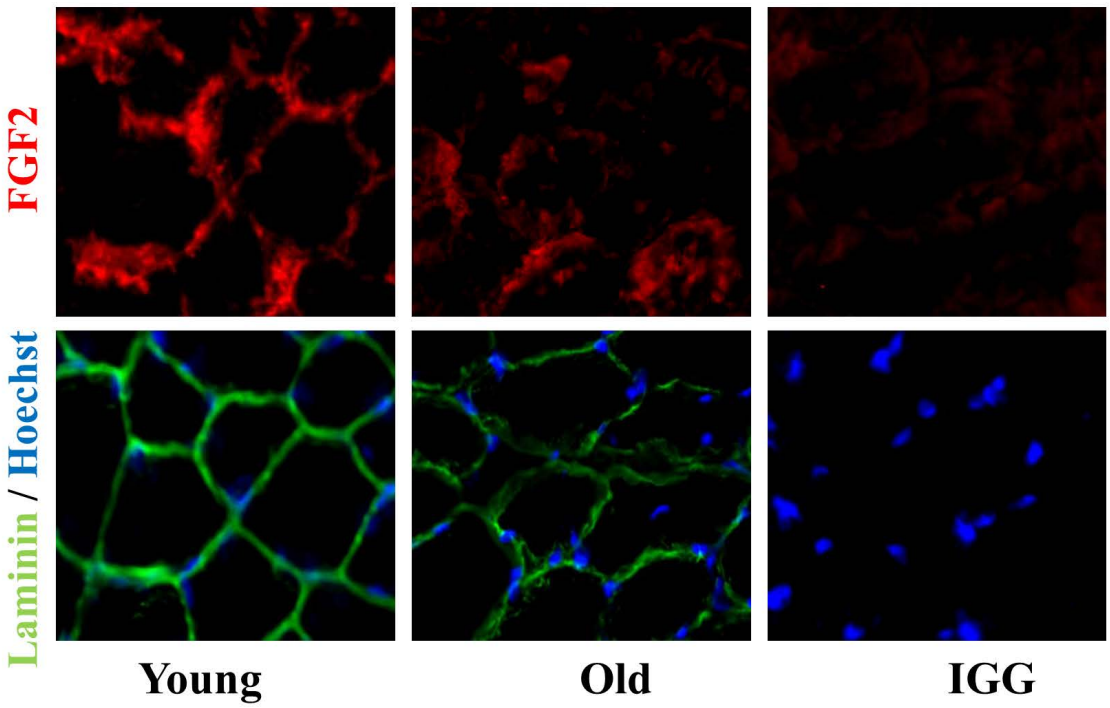
FGF2
Laminin / Hoechst
Young
Old
IGG

D

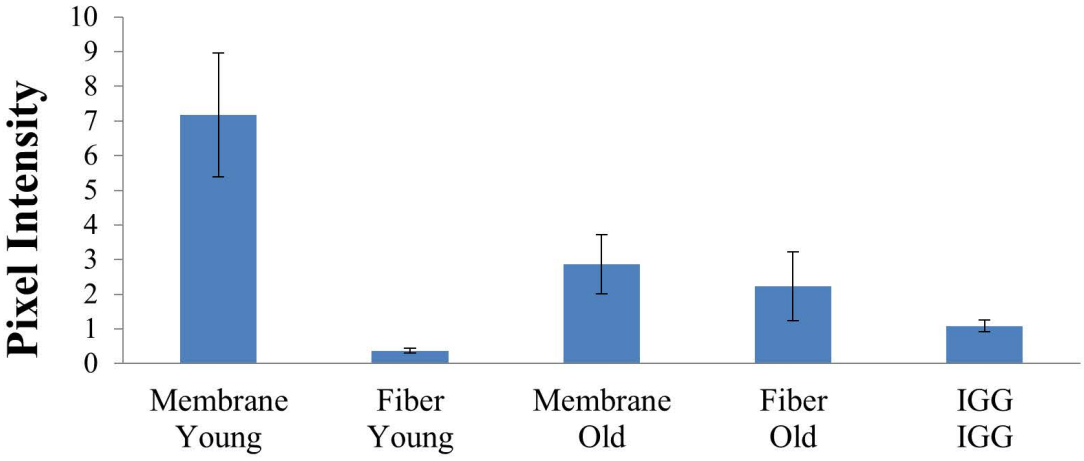
Pixel Intensity
0
1
2
3
4
5
6
7
8
9
10
Membrane Young
Fiber Young
Membrane Old
Fiber Old
IGG IGG

Figure 4

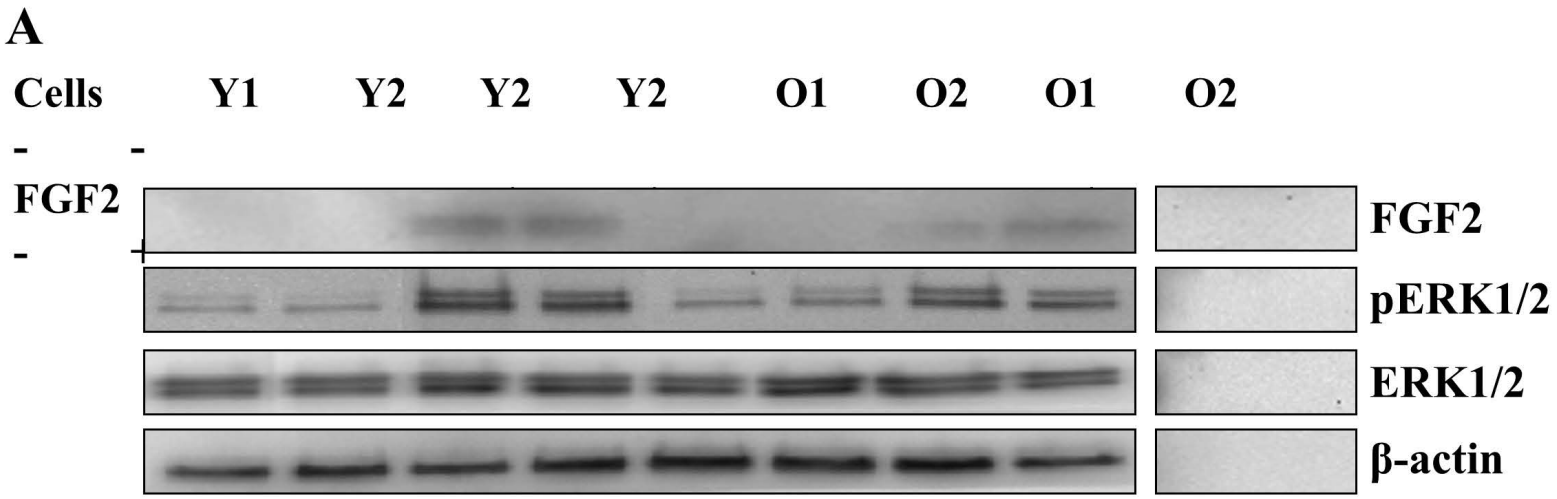
A
Cells
Y1
Y2
Y2
Y2
O1
O2
O1
O2
-
-
FGF2
-
+
FGF2
pERK1/2
ERK1/2
β-actin

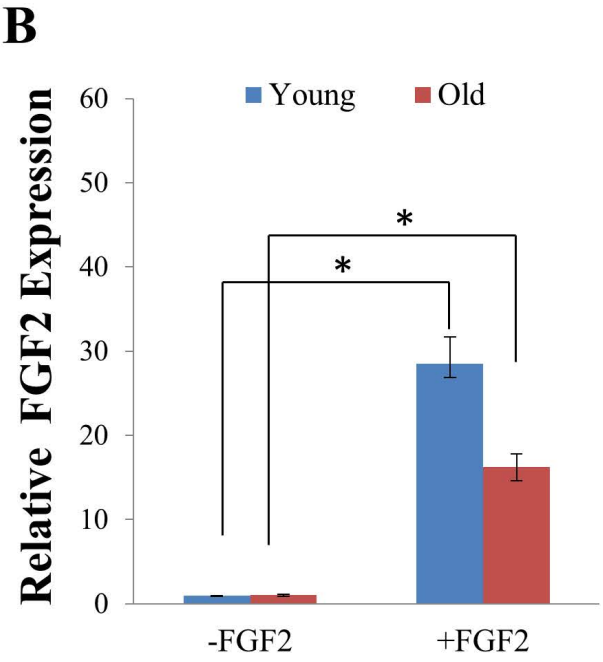
B
Young
Old
Relative FGF2 Expression
60
50
40
30
20
10
0
*
*
-FGF2
+FGF2

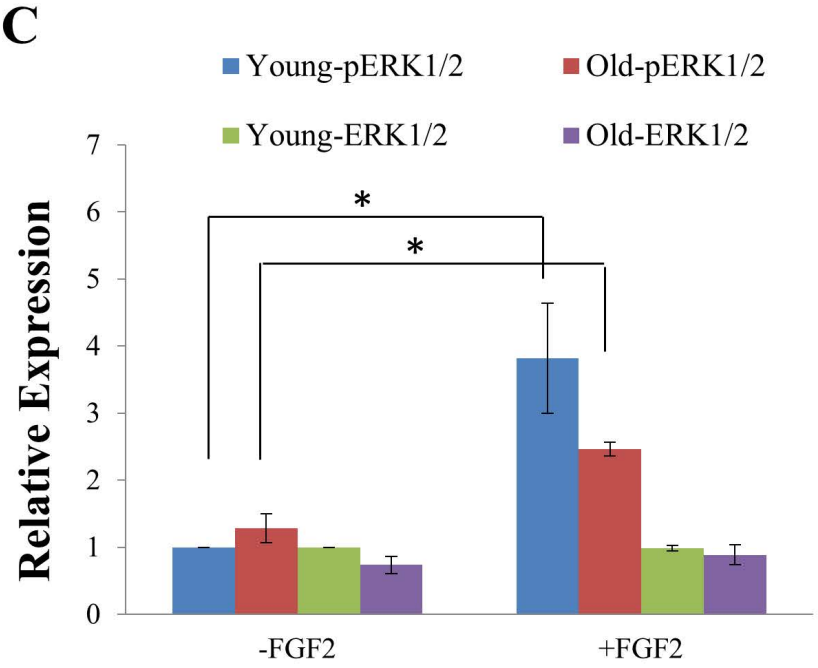
C
Young-pERK1/2
Old-pERK1/2
Young-ERK1/2
Old-ERK1/2
Relative Expression
7
6
5
4
3
2
1
0
*
*
-FGF2
+FGF2

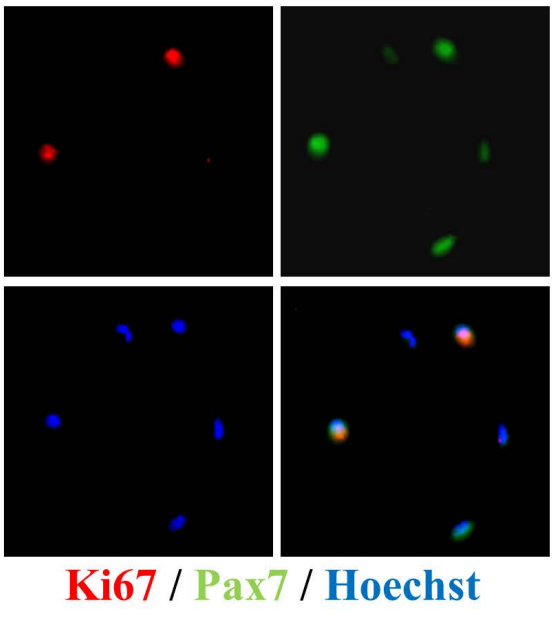
D
Ki67 / Pax7 / Hoechst

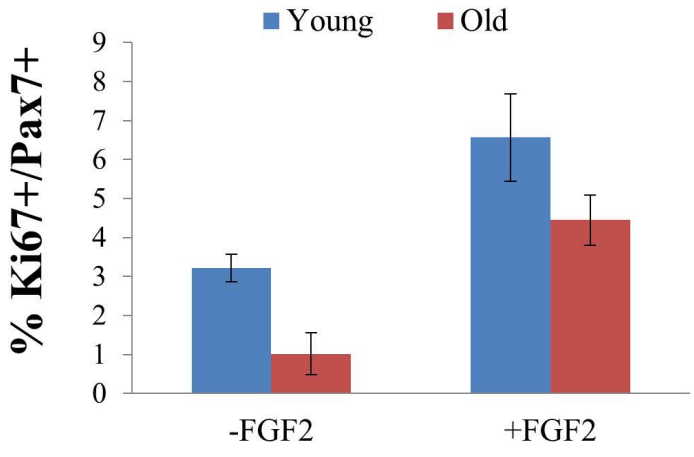
E
Young
Old
% Ki67+/Pax7+
9
8
7
6
5
4
3
2
1
0
-FGF2
+FGF2

Figure 5

A

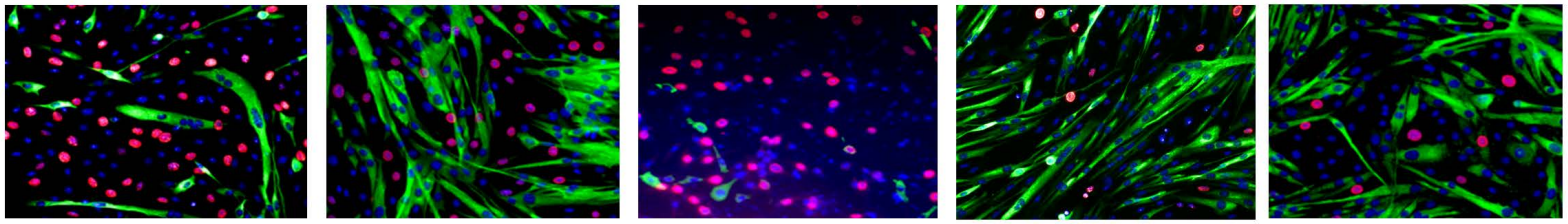

hESC-conditioned OptiMEM | Heparin depleted hESC-conditioned OptiMEM | Eluted Heparin Binding Proteins | OptiMEM | Differentiated hESC-conditioned OptiMEM

Hoechst eMyHC BrdU

B

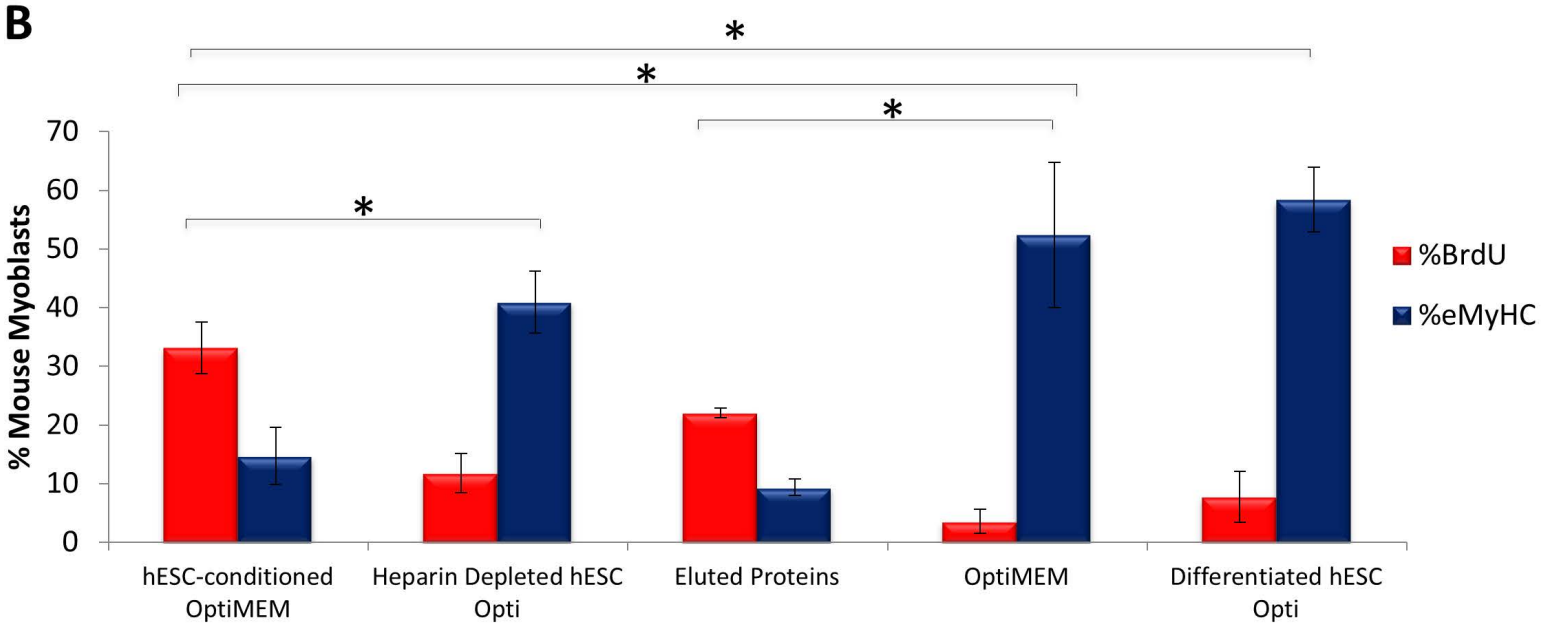

C

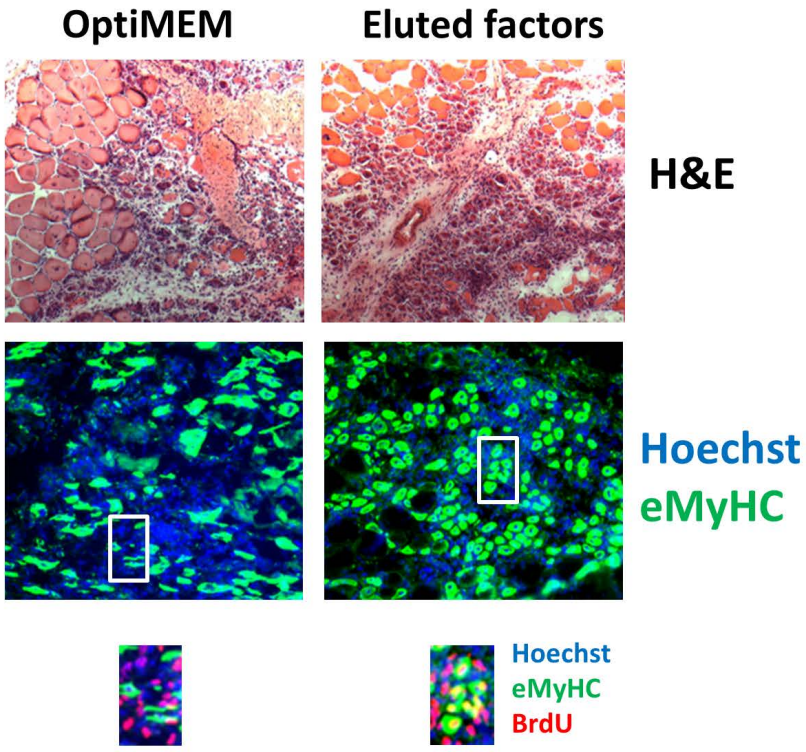

D

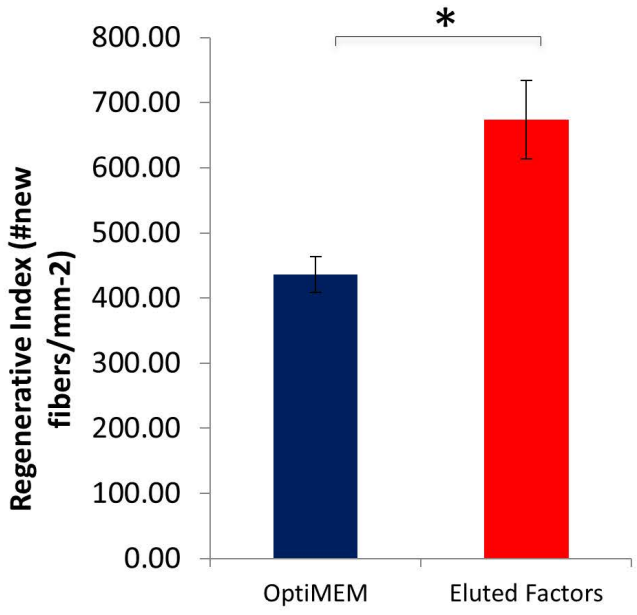

Figure 6

A

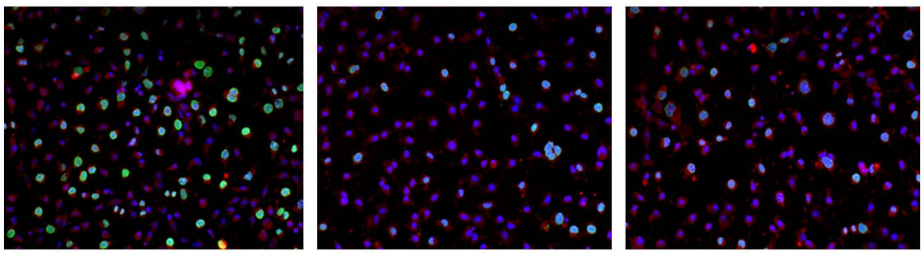

Hoechst
BrdU
Sox2

hESC-Conditioned OptiMEM

Differentiated hESC-Conditioned OptiMEM

OptiMEM

B

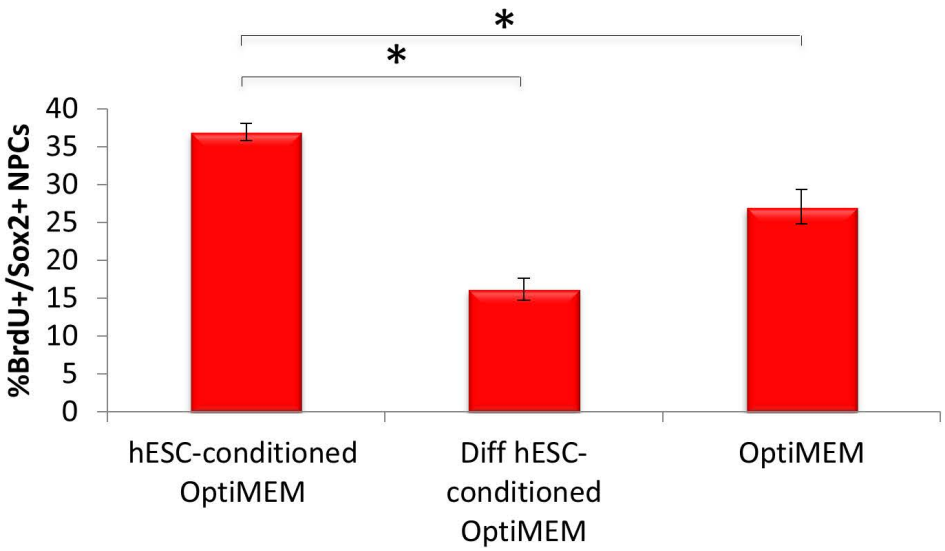

C

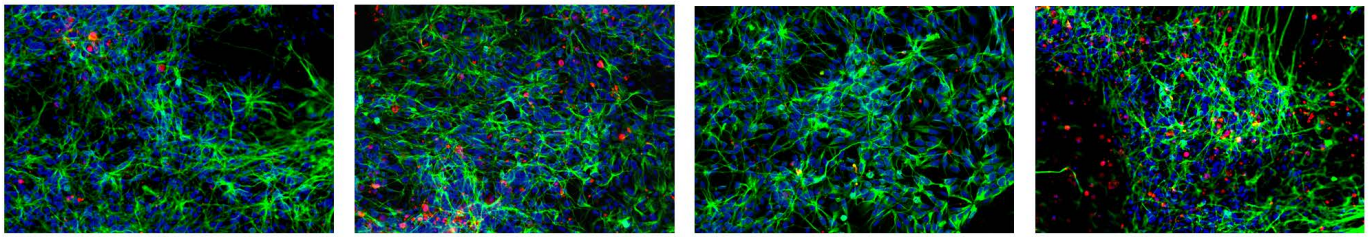

hESC-conditioned OptiMEM

hESC Opti + Aβ

hESC Opti + Aβ Pre-incubation

OptiMEM + Aβ

Hoechst MAP2 Caspase3

D

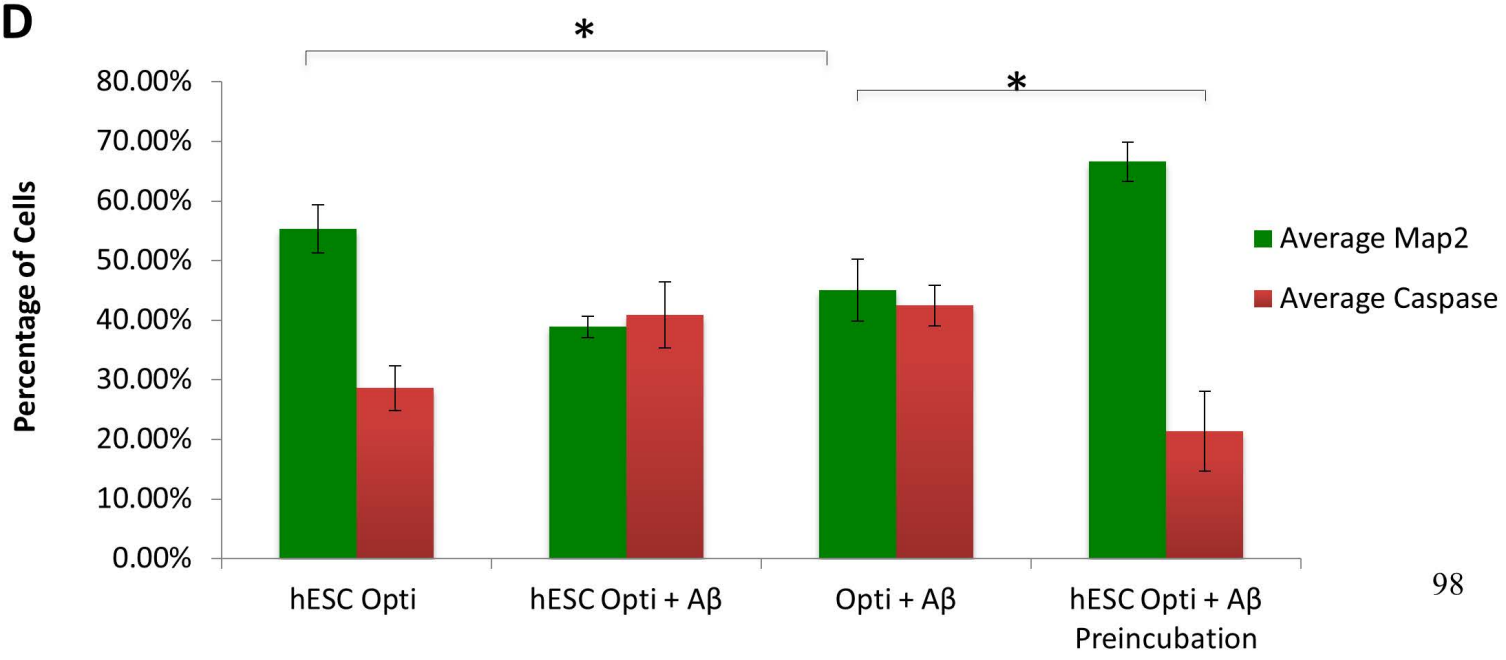

Supplemental Figure 1

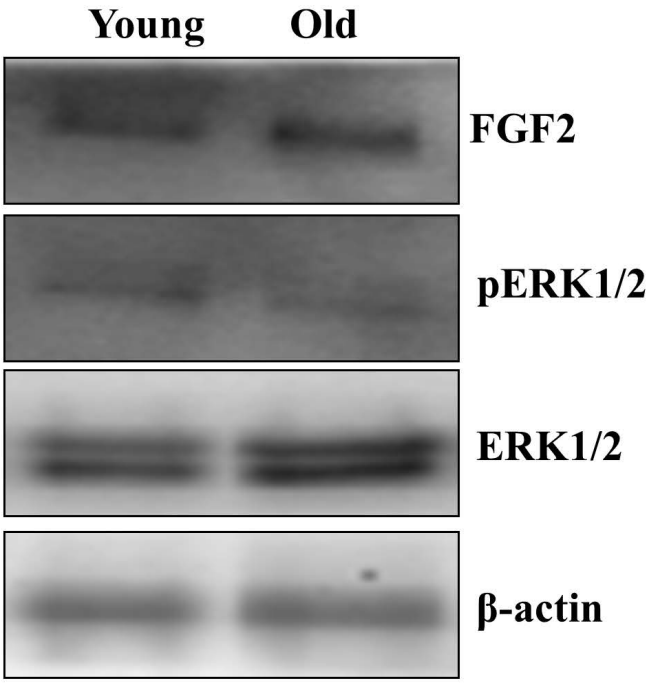

Supplemental Figure 2

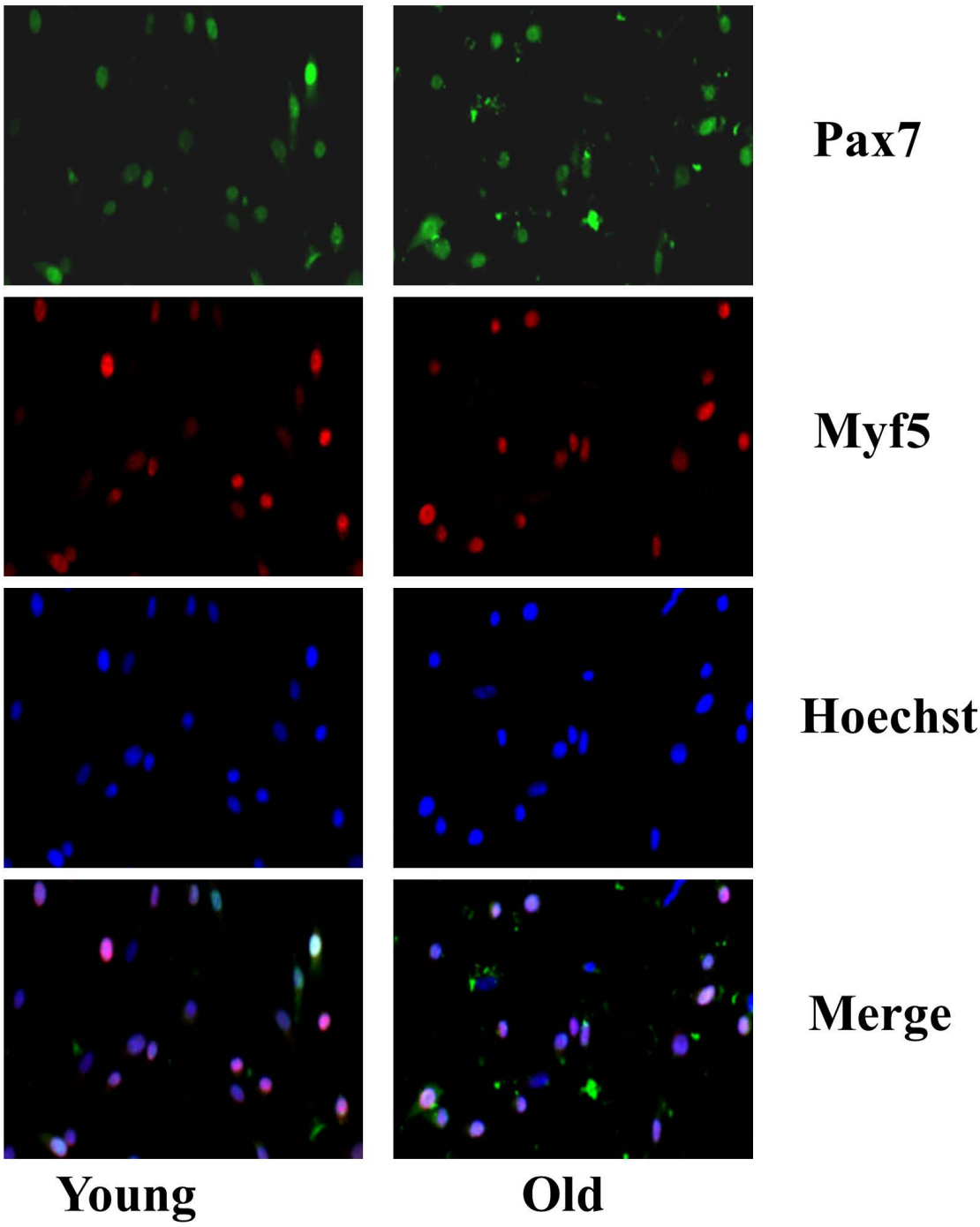

Supplemental Figure 3

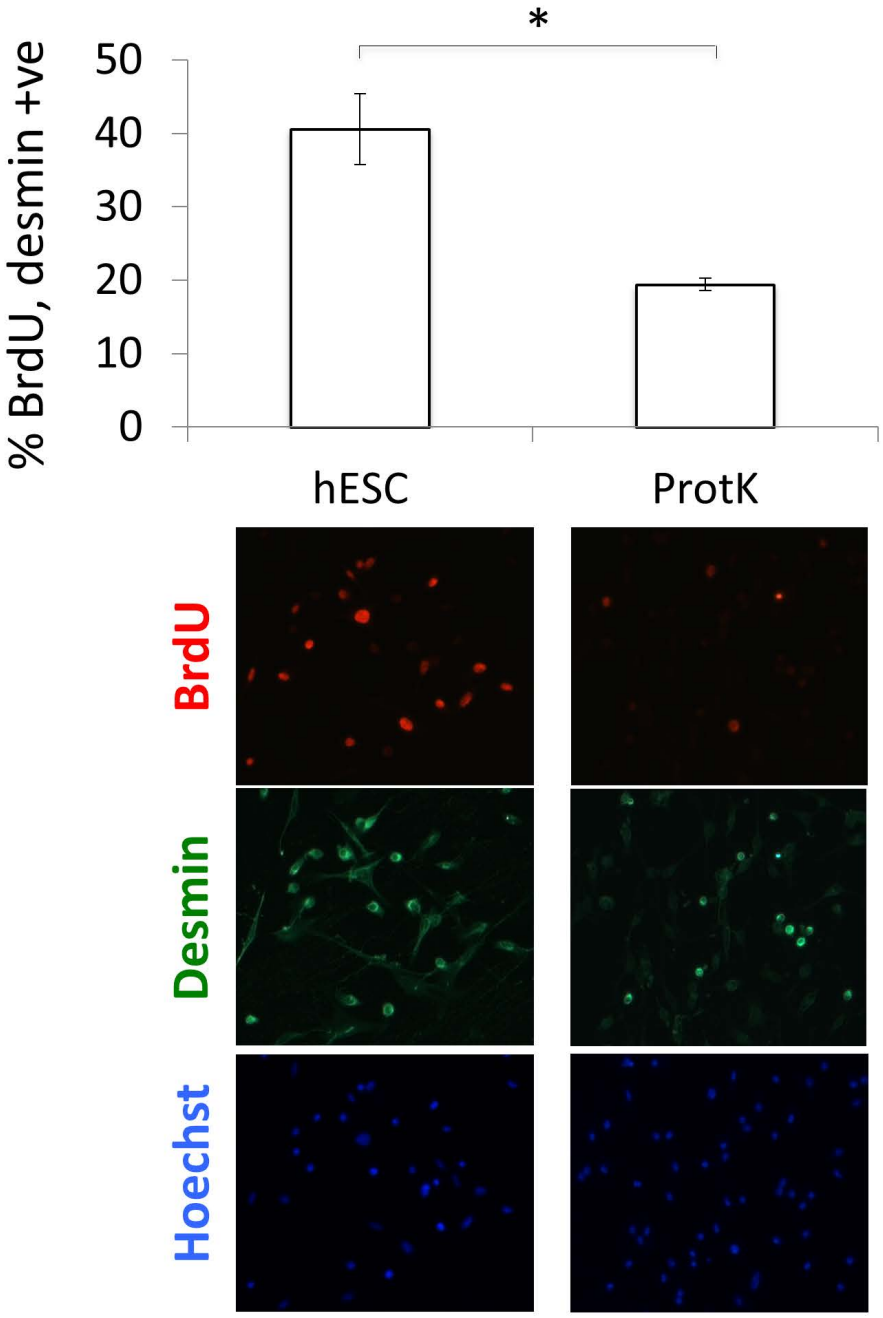

C. Molecular Identity and Mechanisms of Action of hESC-secreted Proteins that Enhance Human and Mouse Myogenesis

Hanadie Yousef[2#], Michael J. Conboy[1#], Hikaru Mamiya[1], Matthew Zeiderman[2], Christina Schlesinger, David V. Schaffer[1,3], and Irina M. Conboy[1]*

1 Department of Bioengineering and California Institute for Quantitative Biosciences (QB3), UC Berkeley, Berkeley, CA 94720, USA

2 Department of Molecular and Cellular Biology, UC Berkeley, Berkeley, CA 94720, USA

3 Department of Chemical and Biomolecular Engineering and Helen Wills Neuroscience Institute, UC Berkeley, Berkeley, CA 94720 USA

co-first authors

* to whom correspondence should be addressed:

email iconboy@berkeley.edu

Summary

Adult stem cells typically grow relatively poorly in vitro compared to embryonic stem cells, and stem cell maintenance and proliferation by tissue niches in vivo progressively deteriorates with age. We have previously reported that factors produced by human embryonic stem cells (hESCs) support a robust regenerative capacity for adult and old mouse muscle stem/progenitor cells. Here we extend these findings to human muscle progenitors and investigate underlying molecular mechanisms. Our results demonstrate that hESC-conditioned medium (but not medium conditioned by their differentiated progeny), enhanced the proliferation of not only mouse but also human muscle progenitors, even under low mitogen conditions. Furthermore, hESC-produced factors activated MAPK and Notch signaling in human myogenic progenitors, and Delta/Notch-1 activation was dependent on MAPK/pERK. Additionally, BMP/pSmad1,5,8 signaling was also high in myogenic cells exposed to culture medium conditioned by both hESCs and differentiated progeny of hESCs, and in primary human muscle progenitor cells this pathway was again dependent on intact MAPK/pERK signaling. Moreover, analysis of downstream cell cycle regulatory proteins demonstrated that c-Myc, p57, and p18 are amongst the key effectors of the enhanced myogenesis promoted by the hECS factors. To identify key hESC-produced proteins responsible for these effects, which may have therapeutic potential, a comparative proteomics array and subsequent functional study identified FGF2, 6 and 19 as key pro-regenerative factors that act via the MAPK pathway to enhance and rejuvenate myogenic capacity. These studies emphasize that the "youthful" signaling intensity of not one but multiple signaling pathways is responsible for the pro-regenerative activity of the hESC factors. Consequentially, the reverse engineering of combinatorial "young" signal transduction in the stem cell niche may avoid side-effects associated with skewing any one key signaling pathway and may thereby promote the long-term enhancement of tissue regeneration.

Introduction

Adult stem cells persist in the body as we age, but their regenerative capacity declines over time, leading to an inability of tissues and organs to maintain homeostasis and repair damage with advancing age. Old skeletal muscle for example loses its regenerative ability due to the failure of satellite cells (muscle stem cells) to divide and generate fusion competent myoblasts and terminally differentiated myofibers in response to muscle injury or attrition [1,2]. Consequentially, the replacement of the damaged tissue with new muscle fibers becomes inefficient with age and instead scarring and inflammation persist [3,4]. This decline in satellite cell proliferation with age results from changes in key cellular signaling that, in turn, are affected by molecular changes in the stem cell niches. Among many other molecular changes, decreased Notch and mitogen-activated protein kinase (MAPK) pathway signaling, as well as mis-regulation of the transforming growth factor-β (TGF-β), tumor necrosis factor-□ (TNF-α), and Wnt molecular pathways, have each been shown to underlie the age-specific decline in muscle regeneration [1, 2].

Notch activation is a key age-specific determinant of satellite cell and myoblast proliferation, and the expression of constitutively active Notch-1 enhances the proliferation of primary myoblasts and delays their differentiation into myofibers [3]. In addition, the level of Notch-1 activation in response to injury decreases with age in satellite cells from C57.B6 mice due to the failure of old damaged muscle fibers to up-regulate the Notch-1 ligand Delta. Forced activation of Notch-1 in old satellite cells restores their proliferation, thereby rescuing the

regeneration of old muscle, while forced inhibition of Notch-1 in young muscle perturbs the activation of young satellite cells and interferes with productive repair of young tissue [4]. During normal adult myogenesis, active Notch served to maintain the pool of proliferating myogenic progenitor cells and prevents their premature differentiation into postmitotic myofibers by antagonism with Wnt/β-catenin [5]. In agreement with this role of Notch, conditional knock-out of RBP-Jκ (one of the main transcriptional effectors that is activating or repressing, depending on the target locus of Notch-1-3 signaling [6], diminishes the ability of satellite cells to self-renew and promotes their precocious differentiation leading to the loss of the satellite cell pool [7, 8].

Interestingly, it has also been shown that MAPK and Notch pathway cross-talk is essential and evolutionarily conserved in the invertebrate embryonic development of *C. elegans* and D. *melanogaster*, where the MAPK pathway positively regulates Delta expression and thus subsequent activation of Notch, in a variety of cell-fate specification processes [10-12]. Furthermore, some evidence also exists for cross-talk between Notch and MAPK in developing and postnatal mammalian tissues [2, 9-11].

Finally, the bone morphogenetic protein (BMP) signaling pathway has been shown to be a critical regulator of various embryonic and adult stem cell niches [14,15]. BMP is a ligand from TGF-β protein superfamily and its signal transduction operates through Smad1, 5 and 8 transcription factors, which become phosphorylated and activated by BMP receptors and form heterodimers with constitutively present Smad4. Such events promote nuclear translocation of these transcriptional regulators causing changes in expression of hundreds of down-stream target genes. In addition to the canonical Smad signaling, the MAPK pathway can also be induced by BMP [12]. In adult myogenesis, BMP signaling is upregulated after satellite cell activation both in vivo and in vitro, and inhibition of BMP signaling promotes myogenic differentiation [16,17]. BMPs may promote satellite cell proliferation by activating their downstream targets, the differentiation-inhibiting Id genes, which inhibit transcription factors that promote cell differentiation [17].

Previous studies have demonstrated that aging of the stem cell niche is responsible for the decline of tissue regeneration and productive homeostasis not only in skeletal muscle but also in a variety of postnatal tissues, and that that old muscle can be rejuvenated to repair almost as well as young through several means [4]. These findings may prove to be important for the development of therapies for age-related tissue degeneration and trauma. However, not all of the factors that influence the niche are known, and the various physiological molecules and balance of signaling crosstalk that modulate healthy regeneration are not well established. In addition, while numerous approaches have been utilized to reverse age-related tissue deterioration in murine models, none are suitable for clinical translation. As one example, skewing the signaling strength of one pathway (either up or down) over a long timespan is likely to be deleterious for cells and tissues, potentially leading to more cellular dysregulation or oncogenic progression [18]. In contrast, a physiological modulation of multiple interactive signaling pathways to their “youthful” levels may have beneficial effects on tissue repair and maintenance.

We previously established that hESC-produced proteins enhance the regenerative capacity of postnatal and old mouse muscle stem/progenitor cells, and that MAPK is indispensable for these pro-regenerative effects [13]. Furthermore, we demonstrated that the heparin-binding fraction of the hESC-produced factors exert the proliferative effects on mouse

muscle progenitor cells and provide regenerative stimulus for old murine muscle rejuvenation [14]. Here, we show that hESC-produced proteins enhance the regenerative capacity of not only mouse but also human muscle progenitor cells, determine the molecular mechanisms by which hESC-produced proteins enhance human myogenic proliferation, and establish the molecular identity of several of these clinically relevant factors.

Results

hESC-produced proteins enhance not only mouse but also human myoblast proliferation

To test the hypothesis that hESC-conditioned medium promotes the proliferation and inhibits the differentiation of both mouse and human muscle progenitor cells, we collected hESC-conditioned medium by incubating hESCs overnight in a serum and growth factor free medium (Opti-MEM). Primary human and mouse myoblasts (muscle progenitor cells) were cultured in a 50/50 mixture of low-mitogen "differentiation medium" (DMEM with 2% horse serum) and hESC-conditioned Opti-MEM, either for 72 hours with daily medium changes (human myoblasts) or overnight (mouse myoblasts). We used two assays of myogenic regenerative activity: the proliferation of human and mouse myoblasts by incorporation of the thymidine analog BrdU, and their resistance to differentiation in this otherwise low-mitogen differentiation medium, as measured by expression of embryonic myosin heavy chain (eMyHC). Proliferation was significantly enhanced and differentiation inhibited in both human and mouse muscle progenitor cells by the hESC-conditioned medium (Figure 1A, B). Analogously, hESC growth medium (mTeSR1) conditioned by hESC culture enhanced myoblast proliferation more effectively than mTeSR1 alone, though mouse myoblasts exhibited significantly enhanced proliferation in both media (Supplementary Figure 1A, B and [14]).

We recently published that in the mouse system, the pro-myogenic activity of hESC-conditioned Opti-MEM is contained in proteins with heparin-binding activity [14]. To explore the evolutionary conservation of this phenomenon in a human system, we cultured primary human muscle progenitor cells in a 50/50 mixture of the low-mitogen differentiation medium plus hESC-conditioned Opti-MEM that was either (1) complete or (2) depleted of heparin-binding proteins. As shown in Figure 1 (C, D), the proliferation of human myogenic cells is greatly enhanced and their differentiation is inhibited by the hESC-conditioned Opti-MEM, but this pro-myogenic effect is lost when heparin-bound proteins are depleted.

To further assess the pro-regenerative activity of hESC supernatants, we assayed the myogenic properties of muscle stem cells derived from old (2 year) mice, using our published methods [18,20]. Gastrocnemius muscles were injured using cardiotoxin (CTX), and muscle tissue collected three days post injury. Activated satellite cells associated with muscle fibers were plated overnight in a 50/50 mixture of Opti-MEM and hESC-conditioned Opti-MEM, with 5% old serum. In agreement with previously published work [13], exposure to hESC-conditioned Opti-MEM more than doubled the percentage of BrdU+/Desmin+, old activated satellite cells, bringing them close to the percentage of young activated satellite cells (Supplementary Figure 2A, B). These data demonstrate that the hESC-conditioned Opti-MEM exerts a strong pro-myogenic activity on not only mouse but also human muscle progenitor cells, as well as positively affects the myogenicity of freshly-isolated muscle stem cells that respond to tissue injury, even in an old environment or when cultured in old serum where their myogenicity is typically suppressed.

Identifying the molecular mechanisms by which hESC-produced factors enhance the regenerative responses of human and mouse muscle progenitor cells

hESC-conditioned medium loses its rejuvenating effect on mouse stem and progenitor cells when the MAPK pathway is inhibited [13]. Considering the evolutionary conservation of the pro-myogenic activity of hESC-produced proteins between mouse and human, we examined the dependence of hESC-produced proteins on MAPK in human muscle progenitor cells. Differentiation medium is extremely low in mitogens such as fibroblast growth factor and quickly (in 48-72 hours) promotes the differentiation of myoblasts into multinucleated myotubes. Based on BrdU incorporation, MAPK inhibition – via incubation of human muscle progenitor cells for 72 hours in a 50/50 mixture of differentiation medium and hESC-conditioned Opti-MEM along with a mitogen-activated protein kinase-kinase inhibitor (MEKi) – drastically inhibited proliferation of primary human muscle progenitor cells (Figure 2A, quantified in B). In this hESC-conditioned Opti-MEM plus differentiation medium, the notable increase of proliferation caused by hESC-produced factors (9.53%) as compared to controls and hESC-conditioned medium with MEK inhibitor (.14%), indicates that the hESC-produced, pro-regenerative proteins signal through the MAPK pathway in human muscle progenitor cells (Figure 2A, B). These results from human muscle progenitor cells are conserved with mouse myoblasts and with old mouse muscle stem cells, as confirmed by incubation of mouse cells in hESC-conditioned Opti-MEM with or without treatment with a MEKi (Figure 2A, B, Supplementary Figure 2B, and as previously published [13]). The negative effect on cell proliferation by pharmacological inactivation of the MAPK pathway in low mitogen-differentiation medium supplemented with the hESC-conditioned medium suggest a vital role of the MAPK signaling pathway in the regenerative capacity of human muscle progenitor cells.

We further pursued the mechanisms by which hESC-produced proteins enhance the regenerative capacity of muscle progenitor cells, with a focus on MAPK signaling. Human and mouse muscle progenitor cells were serum starved for one hour, followed by a 20 minute culture in differentiation medium with 50% of (1) hESC-conditioned Opti-MEM, (2) hESC-conditioned Opti-MEM + MEKi, or (3) Opti-MEM conditioned by differentiated hESCs as a negative control. Immuno-detection by Western blotting was performed using lysates of mouse and human cells, and data were normalized to the levels of housekeeping proteins (GAPDH and cytoplasmic □-actin). The levels of detected phosphorylated-activated proteins (for example, pERK1/2s) were also normalized by the levels of their respective total protein (for example total ERK1/2). As shown in Figure 2C (quantified in D), hESC-produced factors induced higher levels of pERK1 and pERK2 in human and mouse muscle progenitor cells, as compared to the negative control cells cultured in medium conditioned by differentiated progeny of hESCs. As anticipated, MEKi treatment down-regulated pERK1 and pERK2. These data suggest that proteins produced by hESCs, but not by their differentiated progeny, exert a cross-species, conserved activation of the MAPK pathway in myogenic cells.

Several signaling pathways (such as TGF-β/pSmad2,3, BMP/pSmad1,5,8, canonical Wnt and Delta/Notch), have been shown to be crucial for muscle regenerative capacity and to be deregulated with age [2]. When studied by the above described method, the intensities of TGF-β/pSmad2,3, BMP/pSmad1,5,8, and canonical Wnt/β-catenin signaling revealed no significant up or down-regulation in primary human and mouse muscle progenitor cells upon exposure to the hESC-produced factors after 20 minutes or even after 24 hours (Supplementary Figure 3A,

B). In contrast, the Notch ligand Delta-1 and truncated/activated Notch-1 (NICD1) were significantly up-regulated by exposure to the hESC-produced proteins, as compared to the differentiated progeny of these hESCs that lack pro-regenerative activity (Figure 3A, quantified in B). Similar to MAPK/pERK, the induction of Delta/Notch was conserved between human and mouse primary muscle progenitors, although in mouse progenitors there was a more apparent upregulation of NICD1. As compared to mouse cells, basal Notch signaling remained relatively high in human muscle progenitors transferred from highly mitogenic growth medium into the mitogen-low differentiation medium or Opti-MEM, even after serum starvation (Supplementary Figure 3C), suggesting that Notch-1 that has been activated in growth medium persists in human muscle progenitors, thus disguising the effects of hESC-factors and of MAPK on the de-novo activation/inactivation, respectively, of Notch-1 via the up- and down-modulation of its ligand Delta (Figure 3A, B).

Considering the prominent evolutionary-conserved cross talk between MAPK and Notch pathways, we examined whether MAPK/pERK signaling is required for the activation of the key age-dependent pro-myogenic Delta/Notch pathway by the hESC-produced factors [3, 4]. Western blotting was performed on human and mouse muscle progenitors that were serum starved for one hour and then exposed for 20 minutes to hESC-produced proteins in the absence or presence of MEKi. As shown in Figure 3A and B, Delta-1 was up-regulated by the hESC-conditioned medium in both human and mouse primary muscle progenitor cells, and NICD upregulated in mouse cells, but not when MAPK signaling was inhibited. Expression levels of Wnt/□-catenin and TGF-β/pSmad2,3 pathway components, on the other hand, were not regulated by hESC-produced proteins, and not affected by MEKi, as demonstrated with this 20 minute exposure or even a 24 hour exposure (Supplementary Figure 3A, B) to hESC-produced factors in presence/absence of MEKi. These results demonstrate that activation of MAPK by the hESC secretome specifically induced the myogenic Delta/Notch-1 signaling in human myogenic progenitors. Finally, even though BMP/pSmad1,5,8 signaling was not activated by the hESC-conditioned medium in human or mouse primary muscle progenitor cells (Figure 3C, D), this pathway was dependent on intact MAPK signaling in myogenic progenitors of both species, since phosphorylation of pSmad1,5,8 was significantly down-regulated by the MEK inhibitor after just 20 minutes of exposure to hESC-produced factors with MEKi (Figure 3C, D), and remained inhibited even after 24 hours of treatment (Figure 3E); whereas for mouse cells the dependence of BMP/pSmad1,5,8 on intact MAPK was not noticeable at 20 minutes but could be observed after 24 hours of culture (Figure 3C, D and E)

These results suggest that hESC-produced proteins enhance the regenerative capacity of postnatal mouse and human muscle progenitors by quickly activating MAPK/pERK and Delta/Notch signaling, and are suggestive of crosstalk between MAPK and Notch signaling pathways. Also, a BMP/pSmad1,5,8 signal appears dependent on MAPK signaling, though hESC produced proteins do not appreciably change that signal.

Identity of the downstream effectors of signaling induced by hESC-produced factors in human myogenic progenitors

To further understand the mechanisms by which hESC-produced factors enhance the regenerative responses of muscle progenitor cells, gene expression analysis was performed on the downstream targets/effectors of the above signaling pathways, with a specific focus on the regulators of cell cycle progression. Human myoblasts were cultured for 72 hours in a 50/50

mixture of differentiation medium plus medium conditioned by either hESCs or differentiated hESCs, or in 100% of differentiation medium, followed by mRNA expression analysis. As shown in Figure 4A-C, hESC-produced factors induced expression of c-Myc and down-regulated the levels of p57 and p18 cyclin dependent kinase (CDK) inhibitors. Interestingly, as compared to the low-mitogen differentiation medium, the level of another CDK inhibitor p27 was down-regulated by both pro-myogenic medium conditioned by hESCs and control medium conditioned by their differentiated progeny (Figure 4D). However, the expression of an additional regulator of cell cycle progression, cdc25a, was not influenced by either hESC or differentiated hESC-conditioned medium (data not shown). These results demonstrate that hESC-produced proteins do not down-regulate cell cycle inhibitors broadly, but rather induce a specific subset of the downstream effectors of cell proliferation in human muscle progenitor cells. Considering that these downstream effectors are direct targets of the MAPK/pERK and Delta/Notch pathways, such signaling cascades could interact combinatorially to induce c-Myc and repress p18 and p57 in muscle progenitor cells, promoting their regenerative/proliferative capacity.

Proteomics analysis of hESC-conditioned Opti-MEM suggests the molecular identity of candidate pro-regenerative proteins

Considering that medium conditioned by hESCs, but not their differentiated progeny, has pro-regenerative activity (Figure 1), which is lost upon Proteinase K treatment [13, Yousef Aging 2013, 14], we performed a comparative proteomics antibody array analysis of these two media. Conditioned medium was hybridized to Raybiotech 507 antibody array slides and imaged on a Molecular Devices 4000b scanner and analyzed using Genepix software (Materials and Methods). Replicate experiments indicated specific proteins that were more abundant in the hESC-conditioned medium compared with medium conditioned by differentiated hESCs, and the top candidates are listed in Table 1. Consistently abundant were factors that signal through the MAPK, TGF-β, Interleukin, and apoptosis pathways (Table 1). Given that heparin-binding, hESC-produced factors contained the pro-myogenic and regenerative properties, FGFs bind heparin [15], and that MAPK signaling was crucial for the regenerative effects of hESC-conditioned medium, from among the growth factors and cytokines that were highly up-regulated in the hESC-conditioned medium, we first focused on the FGFs.

hESC candidate proteins FGF 2,6, and 19 enhance myogenesis and old muscle regeneration

We tested the myogenic effects of fibroblast growth factors found to be enriched in hESC-conditioned medium, specifically FGFs 2, 6, and 19, first singly on mouse myoblasts in a dose-dependent manner, and then in combinations. We did so by assaying the cell proliferation (BrdU incorporation) and myogenic differentiation (eMyHC+) of myoblasts conditioned for 24 hours in differentiation medium supplemented with recombinant FGF 2, 6, or 19. FGF2, as expected due to its common use in tissue culture medium for maintaining cell proliferation, enhanced mouse myoblast proliferation in a dose-dependent manner, and FGF6 also enhanced proliferation but to a lesser degree. FGF19 alone, however, had minimal effects on proliferation (Supplementary Figure 4A). Furthermore, both FGF2 and 6 inhibited differentiation, also in a dose-dependent manner (Supplementary Figure 4B). FGF19, on the other hand, did not inhibit differentiation (Suppl. Figure 4B). It is important to note that human FGF19 does not exist in mouse cells, and its closest homologue is FGF15 [16]. Curiously, when added in combination, FGF6 and 19 were pro-proliferative and inhibited differentiation to a degree similar to that of

FGF2 alone (Supplementary Figure 4C, D). Based on the dosage assays, FGF2-induced proliferation was optimal at 30 ng/mL and decreased at higher doses; and FGF6 and 19-induced proliferation plateaued at 30 ng/mL (Suppl. Figure 4).

We next tested the effects of these embryonic candidate factors on human myoblasts to determine whether their activities were evolutionarily conserved. FGF2, 6, and 19 all induced proliferation of human myoblasts in a dose-dependent manner (Supplementary Figure 5A, C). However, similar to mouse cells, FGF19 did not inhibit differentiation, while FGFs 2 and 6 did (Supplementary Figure 5B, C). When tested on freshly isolated, injury-activated old muscle stem cells, each exogenous FGF individually enhanced and rejuvenated myogenesis, based on the numbers of newly generated BrdU+/Desmin+ proliferating muscle progenitors that migrate off their respectively isolated old muscle fibers in culture (Figure 5A, B). Additionally, while FGF19 had very mild effects on the primary cultured mouse myoblasts, this growth factor displayed a potent pro-regenerative activity on freshly isolated muscle stem cells (Figure 5A, B). These results suggest that either FGF19 signaling is different between the muscle stem cells and their more differentiated cultured progeny (progenitor cells), or that a mild activation of cell proliferation without significant inhibition of differentiation is effective for the rejuvenation of the myogenic capacity of old satellite cells.

When tested *in vivo*, a FGF2, 6, and 19 mixture significantly improved the activation of the aged muscle stem cells following injury and rejuvenated the repair of old injured skeletal muscle, based on the numbers of newly-generated proliferating muscle progenitors at 3 days post injury and the robust formation of the de-novo eMyHC+ muscle fibers at 5 days after the injury (Figure 5C-G).

These results demonstrate that FGFs 2, 6, and 19 are not only enriched in serum-free medium conditioned by the hESCs, but are sufficient for pro-myogenic effects in mouse and human systems and additionally in their combination, enhance the repair of old injured muscle.

Discussion

Our initial study demonstrated that embryonic stem cells produce soluble proteins that robustly enhance adult muscle stem cell function even in an aged environment, and that production of such proteins is lost when these cells differentiate [13, 14]. Furthermore, the MAPK pathway was determined to be critical in modulating the activity of these embryonic protein(s) [13]. These findings are supported by microarray analysis conducted on cardiomyocytes subjected to hESC-conditioned medium, demonstrating that MAPK pathway signaling was among the main induced signaling cascades [17]. Here we uncover the molecular identity of active hESC-produced proteins and demonstrate that specific FGFs are sufficient to enhance mouse and human myogenesis.

The FGFs had significant effects on cell proliferation of human and mouse myogenic progenitors. Old muscle stem and progenitor cells fail to break quiescence and proliferate in response to muscle injury largely due to a decrease in Notch signaling, and when down-stream Notch effectors become lacking, muscle stem cell prematurely differentiate into myofibers, both of which interferes with cellular homeostasis resulting in scar tissue formation rather than newly formed muscle fibers [4]. Therefore, the pro-proliferative activities of the heparin-binding, hESC-secreted factors FGFs 2,6, and 19 have clear therapeutic potential for enhancing old

muscle progenitor cell function during muscle injury and repair. While FGF2 and 6 were able to promote proliferation and inhibit differentiation of human muscle progenitors, FGF19 mildly induced proliferation. FGF2, a well-known mitogen and critical component of adult and embryonic stem cell culture medium [18], it is also known to promote angiogenesis, osteogenesis, wound healing, and tumorigenesis [19, 20] and to become deregulated in muscle with age [21]. FGF6, interestingly, is restricted almost exclusively in expression to the myogenic lineage during embryonic development, and at high doses FGF6 activates proliferation of muscle progenitor cells, while at low doses FGF-6 directs cell differentiation [22]. FGF19, unlike the auto-paracrine FGF2 and 6, has both local and systemic endocrine effects [16]. FGF19 acts as a hormone to regulate nutrient metabolism, it is expressed in both neuroectoderm and mesoderm during embryonic development, and is known to induce ear formation [23, 24]. However, a role for FGF19 in muscle regulation is has not been characterized prior to our work. While FGF2 is known primarily to bind FGFR1, FGF6 binds FGFR1 and 4, and FGF19 binds FGFR4, though these ligands they can also induce signaling through other somewhat promiscuous FGF receptors [20, 24, 25]. Overall, the FGFs thus have complex, multifunctional roles in development and tissue regeneration, but we just starting to uncover their influence on rejuvenating the regenerative capacity of adult tissue stem cells. It will be interesting to find out how differences in downstream effectors allow FGFs2 and 6 but not FGF19 to inhibit differentiation and to understand in molecular terms, how FGF19 exerts its robust positive activity on the myogenicity of aged muscle stem cells. While FGF2, 6, and 19 were among the most highly upregulated by hESCs, it is important to note that hESC-produced factors enhanced proliferation and inhibited differentiation to a greater extent than FGFs added alone or in combination at optimal dosage, suggesting that there may be other factors in the conditioned medium that contribute to the observed rejuvenating effect. Deciphering the molecular identity of these boosters of tissue repair is our future interesting goal.

Further analysis revealed that gene expression not of the traditional CDK inhibitors, but a very specific sub-set of cell cycle regulators – p18, p57 and c-Myc – became altered and is thus likely responsible for transducing the pro-regenerative activity of the hESC produced proteins. In agreement with our findings, these molecules have been demonstrated to act downstream of the MAPK, Notch, and TGF-β/BMP signaling pathways in other cell types [26, 27]. c-Myc is a well-known target of MAPK signaling and inducer of proliferation [28, 29]. p18, an INK4 family member, suppresses CDK4 or CDK6 during the G1 stage of the cell cycle, and inhibits the self-renewal of adult stem cells [30]. Therefore, hESC factor-induced downregulation of p18 in adult human myogenic progenitors may enhance their function by enhancing self-renewal. p57, a KIP2 family member, also inhibits proliferation by suppressing several G1 cyclin/CDK complexes [31]. One characteristic of aged muscle is the up-regulation of various CDK inhibitors by increased TGF-β signaling and concurrent lack of Notch-1 activation, leading to the failure of satellite cells to activate/proliferate during injury [32]. hESC-secreted, heparin-binding factors can counteract this effect to enhance old muscle regeneration [14], and we now show this is mediated through downregulation of specific CDK inhibitors via a key evolutionary and developmentally conserved MAPK/Notch signaling cross-talk. Specifically, in the presence of pro-regenerative hESC proteins, MAPK, Notch-1, and BMP are active in mouse and human muscle progenitor cells, and Notch and BMP signaling are dependent on intact MAPK. Two other key morphogenic signaling pathways that are known to regulate adult myogenesis, Wnt and TGF-□[2], do not rely on MAPK signaling and are not up-regulated by the hESC secretome in the studied mouse and human myogenic progenitors. Postnatal myogenic progenitors of both

species that are exposed to the proteins secreted by differentiated hESCs and show no enhancement or rejuvenation of their regenerative capacity, have active BMP/pSmad1,5,8, Wnt and TGF-β pathways, but lack MAPK and Notch signaling. Summarily, combinatorial signaling of specific morphogenic pathways is (1) induced in postnatal myogenic progenitors by the hESC secretome and (2) is critically important for the positive effect of hESC-secreted proteins on robustly engaging mouse and human, young and old muscle stem and progenitor cells with regeneration of this important tissue.

Identifying and reconstructing a "youthful" stem cell niche may thus, have long-term beneficial effects on tissue regeneration, in contrast to the drastic modulation of a single cell-fate regulatory pathway that could have deleterious side effects by promoting oncogenic transformation and/or inducing cellular senescence [13]. In this regard, the composition and concentrations of the defined human FGFs that were determined and investigated in this work may be translatable to the clinic and yield novel strategies for the enhancement of tissue repair in the elderly. These molecules, produced by human cells, do not need to be "humanized" for clinical applications. We thus anticipate that these FGFs in combination (potentially with additional pro-regenerative factors identified by the comparative proteomics and investigated in future work for their positive effects on tissue regeneration) will ultimately lead to a biochemically defined cocktail of physiological molecules that is able to delay and even reverse the onset of human aging.

Figure Legends

Figure 1. Pro-regenerative embryonic factors that enhance human and mouse myoblast proliferation contain heparin binding domains. (A) Primary human or mouse myoblasts were cultured for 24 hours or 72 hours, respectively, in 50% differentiation medium (DMEM, 2% horse serum) plus 50% of the specified medium, with daily medium changes. A 4 hour or 2 hour BrdU pulse on human or mouse myoblasts, respectively, was performed before cell fixation to label proliferating cells. Immunofluorescence was performed for eMyHC (green) and BrdU (red), with Hoechst (blue) labeling all nuclei. Representative images are shown. (B) Proliferation and differentiation of fusion-competent myoblasts were quantified by cell scoring in 25-50 random fields of each condition using a Molecular Devices MetaXpress automated imager and cell scoring software. Results are displayed as the mean percent of BrdU+ or eMyHC+ proliferating or differentiating cells +/-SD, respectively (n=6). Significant differences were identified by Student's t-tests *(*$p<0.004$* for human cells; **$p<8x10^{-19}$* for mouse cells). (C) Primary human myoblasts were cultured for 72 hours in 50% differentiation medium + 50% of the specified medium. A 4 hour BrdU pulse was performed before cell fixation to label proliferating cells. Immunofluorescence was performed for eMyHC (green) and BrdU (red), with Hoechst (blue) labeling all nuclei. Representative images are shown. (D) Proliferation and differentiation of fusion-competent human myoblasts were quantified by cell scoring in 25-100 random fields of each condition using a Molecular Devices MetaXpress automated imager and cell scoring software. Results are displayed as the mean percent of BrdU+ or eMyHC+ proliferating or differentiating cells +/-SD, respectively (n=6). Significant differences were identified by Student's t-tests *(*$p<0.004$).*

Figure 2. hESCs secrete pro-myogenic proteins that act primarily through MAPK signaling. (A) Primary human or mouse myoblasts were cultured for 24 hours or 72 hours, respectively, in 50% differentiation medium (DMEM, 2% horse serum) plus 50% of the

specified medium +/- 10 μM of a MAPK pathway inhibitor (MEKi), with daily medium changes. A 4 hour or 2 hour BrdU pulse on human or mouse myoblasts, respectively, was performed before cell fixation to label proliferating cells. Immunofluorescence was performed for eMyHC (green) and BrdU (red), with Hoechst (blue) labeling all nuclei. Representative images are shown. Proliferation and differentiation of fusion-competent myoblasts were quantified by cell scoring in 25-50 random fields of each condition using a Molecular Devices automated imager and MetaXpress cell scoring software. (B) Results are displayed as the mean percent of BrdU+ or eMyHC+ proliferating or differentiating cells +/-SD, respectively (n=4). Significant differences were identified by Student's t-tests *(*p<0.004* for human cells; **p<2x10^{-20} for mouse cells).* (C) Immunoblotting analysis of the downstream effector pErk1/2 in the MAPK signaling pathway in human and mouse myoblasts serum starved for one hour then treated for 20 minutes with 50% differentiation medium and 50% of the specified medium +/- a MEKi (10 μM). (D) Quantification of pERK1/2 expression in human myoblasts. The relative expression level was normalized by GAPDH and presented as the expression level relative to that of human myoblasts treated with just differentiation medium. Significant differences were identified by Student's t tests (**p<0.02 and **p<0.05).* Error bars indicate standard error of the mean (n=4).

Figure 3. hESC-produced factors act on multiple biochemical pathways. (A) Western immunoblotting analysis of the Notch pathway, specifically Delta-1 (dll1) and active Notch-1 (Nicd1), with GAPDH or β actin as loading controls, from human and mouse myoblasts serum starved for one hour then treated for 20 minutes with 50% differentiation medium and 50% specified medium +/- a MEKi (10 μM) to analyze crosstalk with MAPK pathway. (B) Quantification of Dll1 and Nicd1 expression in human myoblasts. The relative expression level was normalized by GAPDH and presented as the expression level relative to that of human myoblasts treated with just differentiation medium. Significant differences were identified by Student's t tests (**p<0.002 and **p<0.05).* Error bars indicate standard error of the mean (n=3). (C) Western immunobloting analysis of BMP pathway proteins pSmad 1/5/8 with βactin as a loading control, from human and mouse myoblasts serum starved for one hour then treated for 20 minutes with 50% differentiation medium and 50% specified medium +/- a MEKi (10 μM) to analyze crosstalk with MAPK pathway. (D) Quantification of pSmad1/5/8 expression in human myoblasts. The relative expression level was normalized by βactin and presented as the expression level relative to that of human myoblasts treated with just differentiation medium. Significant differences were identified by Student's t tests (**p<0.05).* Error bars indicate standard error of the mean (n=3). (E) Western immunobloting analysis of BMP pathway protein pSmad 1/5/8 with βactin as a loading control, from human and mouse myoblasts treated for 24 hours with 50% differentiation medium and 50% specified medium +/- a MEKi (10 μM).

Figure 4. Expression analysis of MAPK regulated genes. (A-D) Quantification of downstream CDK inhibitor expression genes by qRT-PCR in human myoblasts treated for 72 hours with 50% differentiation medium and 50% medium specified, with daily medium changes. The relative expression level was normalized by GAPDH. Significant differences were identified by Student's t tests *(*p<0.05* for c-Myc, **p<7x10^{-6}* and ***p<0.005* for p57,**p<0.05* and ***p<0.01* for p18, **p<3x10^{-6}* for p27). Error bars indicate standard error of the mean (n=2-4).

Figure 5. hESC candidate factors FGF2, 6, and 19 exhibit a pro-myogenic effect in an old environment and enhance old muscle regeneration *in vivo*. (A) Old injury activated myofiber-associated satellite cells were isolated at 3 days post cardiotoxin-induced muscle

injury, and cultured overnight in DMF12 with 10% of old serum and 10 ng/mL FGF 2, 6, 19, or FGFs6 and 19 in combination, followed by a 2 hour BrdU pulse to label proliferating cells before fixation. Immunofluorescence was performed with Desmin (green) and BrdU (red), with Hoechst (blue) labeling all cell nuclei. Representative images are shown and demonstrate that hESC –produced candidate factors have a pro-myogenic and rejuvenating effect on old activated satellite cells. (B) Proliferating myogenic Desmin+/BrdU+ satellite cells were counted. Results are displayed as the mean percent of BrdU+/Desmin+ proliferating satellite cell cells. Error bars indicate standard error of the mean (n=4). Significant differences were identified by Student's t tests *(*p<0.0004).* (C) Schematic of *in vivo* FGF2, 6, and 19 injection. EdU was injected (intraperitoneal) at Day 4 to label proliferating, fusion-competent myoblasts. (D) Old injury activated myofiber-associated satellite cells were isolated at 3 days post cardiotoxin-induced muscle injury (Day 5 in schematic), and cultured overnight in Opti-MEM with 10% of their respective old serum, followed by cell fixation. Immunofluorescence was performed with Desmin (red) and EdU (green), with Hoechst (blue) labeling all cell nuclei. Representative images are shown and demonstrate that hESC –secreted candidate factors have a pro-myogenic and rejuvenating effect. (E) Proliferating myogenic Desmin+/EdU+ satellite cells were quantified by cell scoring in 25 random fields of each condition using a Molecular Devices automated imager and MetaXpress cell scoring software. Results are displayed as the mean percent of EdU+/Desmin+ proliferating satellite cell cells +/-SD (n=4). Significant differences were identified by Student's t tests *(*p<0.03).* (F) Cryosections (10 μm) of old Tibialis Anterior muscles were analyzed by hematoxylin/eosin (H&E) staining and immunostaining for embryonic myosin heavy chain (eMyHC, shown in green). Hoechst stains nuclei (blue). As shown by representative images, the regenerative outcome of old muscle given hESC-secreted candidate factors FGF 2, 6, and 19 was significantly improved as compared to old muscle given Opti-MEM vehicle control, based on significantly diminished scar tissue formation, larger and more dense *de novo* myofibers and an increase in the numbers of eMyHC+ myofibers with centrally-located nuclei that replaced the damaged tissue. (G) Regeneration of old mice Tibialis Anterior muscle 5 days post injury, that received candidate factors FGF 2,6, and 19 or vehicle, were quantified from muscle sections, and are presented as the number of newly regenerated myofibers per square millimeter of injury site. Error bars indicate standard error of the mean (n=4). Significant differences were identified by Student's t tests *(*p<0.0007).*

Supplementary Figure 1. hESC-Conditioned mTeSR-1, but not mTeSR-1, increases primary human myoblast Proliferation and inhibits Differentiation. (A) Primary human myoblasts were cultured for 72 hours in 50% differentiation medium (DMEM, 2% horse serum) plus 50% of the specified medium. A 4 hour BrdU pulse was performed before cell fixation to label proliferating cells. Immunofluorescence was performed for eMyHC (green) and BrdU (red), with Hoechst (blue) labeling all nuclei. Representative images are shown. (B) Proliferation and differentiation of fusion-competent myoblasts were quantified by using cell profiler cell scoring software. Results are displayed as the mean percent of BrdU+ or eMyHC+ proliferating or differentiating cells +/-SEM, respectively (n=6), Significant differences were identified by Student's t tests (**p< 0.004).*

Supplementary Figure 2. hESC-conditioned medium enhanced old satellite cell activation through inducing MAPK. (A) Young or Old injury activated myofiber-associated satellite cells were isolated at 3 days post cardiotoxin-induced muscle injury, and cultured overnight in 50% Ham's F10 with 5% of their respective young or old serum, and 50% of the medium specified,

followed by a 2 hour BrdU pulse to label proliferating cells before cell fixation. Immunofluorescence was performed with Desmin (green) and BrdU (red), with Hoechst (blue) labeling all cell nuclei. Representative images are shown. (B) Proliferating Desmin+/BrdU+ satellite cells were quantified by cell scoring in multiple random fields of each condition. Results are displayed as the mean percent of BrdU+/Desmin+ proliferating satellite cell cells +/-SD (N=4). Significant differences were identified by Student's t tests (*$p< 0.01$, **$p<0.006$, ***$p<0.002$.)

Supplementary Figure 3. hESC-produced factors Act through MapK and BMP signaling pathways, but not through TGF-β or Wnt Signaling. Western immunoblotting analysis of downstream effectors of BMP and Wnt signaling pathways in human or mouse myoblasts serum starved for one hour followed by treatment for 20 minutes (A) or 24 hours (B) with 50% Differentiation Medium and 50% Specified Medium +/- a MEKi (10 μM) to analyze crosstalk with MAPK pathway. (C) Western immunoblotting analysis of active Notch-1 in human myoblasts treated for 20 minutes with specified medium after 1 hour serum starvation.

Supplementary Figure 4. hESC candidate factors FGF2,6,&19 exhibit a pro-myogenic effect on mouse myoblasts in a dose dependent manner. Primary mouse myoblasts were cultured for 24 hours in differentiation medium (DMEM, 2% horse serum) plus 0, 5, 10, 30 or 100 ng/mL FGF2, 6, or 19. A 2 hour BrdU pulse on mouse myoblasts was performed before cell fixation to label proliferating cells. Immunofluorescence was performed for eMyHC (green) and BrdU (red), with Hoechst (blue) labeling all nuclei (30 ng/ml images shown in C). Proliferation and differentiation of fusion-competent myoblasts were quantified by cell scoring in 25-50 random fields of each condition using a Molecular Devices automated imager and MetaXpress cell scoring software, and results are displayed as the mean percent of (A) BrdU+ or (B) eMyHC+ proliferating or differentiating cells +/-SD, respectively (n=6). (D) Quantification of FGFs added individually at the determined optimal dosage for proliferation (30 ng/mL) or in combination, using Molecular Devices automated imager and MetaXpress cell scoring software as described for (A) and (B). Significant differences were identified by Student's t tests (*$p< 0.0008$ and **$p<0.05$).

Supplementary Figure 5. hESC candidate factors FGF2, 6, 19 exhibit a pro-myogenic effect on human myoblasts in a conserved and dose dependent manner. Primary human myoblasts were cultured for 72 hours in differentiation medium (DMEM, 2% horse serum) plus 0-100 ng/mL FGF2, 6, or 19 with daily medium changes. A 4 hour BrdU pulse on human myoblasts was performed before cell fixation to label proliferating cells. Immunofluorescence was performed for eMyHC (green) and BrdU (red), with Hoechst (blue) labeling all nuclei (Images not shown). Proliferation and differentiation of fusion-competent myoblasts were quantified by cell scoring in 25-50 random fields of each condition using a Molecular Devices automated imager and MetaXpress cell scoring software, and results are displayed as the mean percent of (A) BrdU+ or (B) eMyHC+ proliferating or differentiating cells +/-SD, respectively (n=6). (C) Quantification of FGFs added individually at optimal determined dosage for proliferation (30 ng/mL) or in combination, using Molecular Devices automated imager and MetaXpress cell scoring software as described for (A) and (B). Significant differences were identified by Student's t tests (*$p< 0.005$ and **$p<0.05$).

Experimental Procedures

Animals

Young (2-3 month old) and old (22-24 month old) C57BL6/J mice were purchased from the Jackson Laboratory and the NIH. The animal experimental procedures were performed in accordance with the Guide for Care and Use of Laboratory Animals of the National Institutes of Health, and approved by the Office of Laboratory Animal Care, UC Berkeley.

Muscle fibers and muscle stem cell isolation

Injured TA muscle was dissected from healthy young and old mice and incubated at 37°C in digestion medium (150 U/mL Collagenase type II in DMEM medium with 10% horse serum and buffered with 30 mM HEPES) for 2 hours [33, 34]. Digested muscle was gently triturated and myofibers were collected. To obtain satellite/myofiber associated regenerative cells, myofibers were further digested with 1 U/mL Dispase and 40 U/mL Collagenase type II in DMEM, 2% horse serum, to liberate muscle stem cells [34]. Muscle stem cells were cultured in DMEM with 5% serum from the same age mouse.

Cell Culture

Adult human myoblasts were cultured and expanded in human growth medium: Ham's F-10 (Gibco), 10% Bovine Growth Serum (Hyclone), 30 ng/mL FGF2, and 1% penicillin–streptomycin on Matrigel (BD Biosciences) coated plates (1:100 matrigel:PBS), at 37C and 5% CO2. For experimental conditions involving immunostaining, cells were plated at 10,000 cells/well in Matrigel coated 8-well chamber slides (1:100 Matrigel: PBS), and cultured for 72 hours with daily re-feedings at 37C in 10% CO2 incubator prior to fixation with 70% ethanol at 4°C. Mouse myoblasts were cultured and expanded in mouse growth medium: Ham's F-10 (Gibco), 20% Bovine Growth Serum (Hyclone), 5 ng/mL FGF2 and 1% penicillin–streptomycin on Matrigel coated plates (1:300 matrigel: PBS), at 37°C and 5% CO2. For experimental conditions involving immunostaining, cells were plated at 40,000 cells/well on Matrigel coated 8-well chamber slides (1:100 matrigel: PBS) and cultured for 24 hours at 37°C in 10% CO2 incubator prior to fixation with 70% ethanol at 4°C.

Human embryonic stem cells (H9 and H7 lines), were cultured on diluted Matrigel (1:30), in mTeSR-1 (Stem Cell Technologies), according to manufacturer's recommendations. hESCs were differentiated after plating in mTeSR-1 by changing the medium to DMEM/F12 with 10% Bovine Growth Serum (Hyclone), and culturing for an additional 6-8 days. Cells were washed with Opti-MEM (Gibco) and then cultured in Opti-MEM for 18 hours prior to collection as hESC-conditioned Opti-MEM (hESC-conditioned medium) and stored at -80°C. All experiments using a MEK inhibitor were treated with 10 μM MEK1/2 Inhibitor (U0126, Cell Signaling Technologies).

Heparin Binding of hESC-Produced Proteins from hESC-Conditioned Medium

Heparin-Agarose Type I Beads (H 6508, Sigma Aldrich) were washed with molecular grade water and preconditioned in 1mL Opti-MEM as recommended by manufacturer. hESC-conditioned medium was incubated with Heparin-Agarose Beads for 2 hours shaking at 4°C.

Beads and all medium were separated by centrifugation. Myoblasts were treated with depleted medium after two rounds of centrifugation and separation of beads and medium so as to remove all residual beads from depleted hESC-conditioned medium.

After depleting hESC-conditioned Opti-MEM, the protein bound heparin beads were washed two times for 10 minutes at 4°C in 1ml PBS + .05% Tween-20. Proteins were eluted twice for 15 minutes at 4°C in 400µl of elution buffer (.01M Tris-HCl pH 7.5 +1.5M NaCl + 0.1%BSA) to collect proteins in a total of 800µl of elution buffer. The proteins were purified by dialysis for 2 hours shaking at 4°C in 500ml McCoy's 5A Medium (Gibco) followed by overnight dialysis shaking at 4°C in 200ml Opti-MEM (Gibco). The eluted heparin beads were re-suspended in 800 µl Opti-MEM and stored overnight at 4°C. One hour after plating, human myoblasts were treated with respective mediums for 72 hours with daily medium changes prior to a 4 hour BrdU pulse and fixation in 70% cold ethanol.

Cell-Starvation –Mechanism Analysis

Human myoblasts were plated at 200,000 cells/well in a 6-well plate. Mouse myoblasts were plated at 300,000 cells/well in a 6-well plate. Plate wells were coated at 1:100 ECM: PBS. Cells were allowed to stick in human growth medium and mouse growth medium, respectively, for 1 hour at 5% CO_2 at 37°C prior to 2 washes in serum-free medium (DMEM (Gibco) + 1% sodium pyruvate + 1% penicillin streptomycin). Cells were then treated 10 seconds in serum-free medium with 10µg/mL protamine sulfate for 10 seconds in order to remove any remaining bound ligands, followed by 2 more washes in serum-free medium and a one hour incubation in serum-free medium. Cells were then treated for 20 min. in 10% CO_2 at 37°C in 50% Differentiation Medium (DMEM + 2%HS + 1% penicillin streptomycin) and 50% specified medium. Cells were washed with PBS and cell lysates collected and analyzed for western blot using above mentioned western blot analysis method. Human and mouse myoblasts treated with a MEK inhibitor received 10µM MEK1/2 Inhibitor (U0126, Cell Signaling Technologies).

Immunocytochemistry and Quantification

For immunoflourescence assays, human or mouse stem and progenitor cells were given a 4 hour or 2 hour, 3 µM BrdU pulse, respectively. Cells were fixed with 70% ethanol 30 minutes to overnight before 3, 5 minute PBS washes, 10 minute 4N HCl treatment, permeablization with PBS + 0.25% Triton X-100 for 15 minutes, 3 PBS washes, and blocking one hour in PBS + 2% FBS. The cells were then incubated with primary antibodies overnight at 4C in PBS + 2% FBS. Cells were immunostained for eMyHC (Hybridoma Bank), Desmin (Sigma-Aldrich**),** or BrdU (Abcam). If stained for EdU (Invitrogen), the HCl antibody retrieval method was not performed. Tissue sections were fixed with 70% ethanol 30 minutes to overnight before 3, 5 minute PBS washes, 2N HCl treatment for 20 minutes, permeablization with 0.25% Triton-X 100 for 30 minutes, 3 PBS washes followed by blocking 1 hour with PBS + 2% FBS. The sections were then stained for eMyHC (Hybridoma Bank).

Secondary staining with fluorophore-conjugated, species-specific antibodies (Donkey anti-Rat-488, #712-485-150; Donkey anti-Mouse-488, #715-485-150; Donkey anti-Rat-Cy3 #712-165-150; or donkey anti-Mouse-Cy3 #715-165-150; all secondary antibodies from Jackson ImmunoResearch) was performed for 1 hour at room temperature at a 1:500 dilution in PBS

+2%FBS. Nuclei were visualized by Hoechst stain, and samples were analyzed at room temperature with a Zeiss Axio Imager A1, and imaged with Axiocam MRm or MRc cameras and AxioVision software. Mouse myoblasts were imaged at 10X and 20X magnification, respectively. For cell quantification, 25-50 20x images per replicate were taken on the Molecular Devices ImageXpress Micro automated epifluorescence imager, followed by automated cell quantification using the multiwavelength cell scoring module within the MetaXpress analysis software.

Western blotting

Human or mouse primary muscle progenitor cells were lysed in RIPA buffer (50 mM Tris, 150 mM NaCl, 1% NP40, 0.25% sodium deoxycholate and 1 mM EDTA, pH 7.4) containing 1X protease inhibitor (Roche), 1 mM Phenylmethylsulfonyl fluoride (PMSF), 1 mM sodium fluoride and 1 mM sodium orthovanadate. The protein concentration was determined by Bradford assay (Bio-Rad). Cell lysates were resuspended in 1X Laemmli buffer (Bio-Rad), boiled for 5 minutes and separated on precast 7.5% or 4-15% TGX gels (Biorad). Primary antibodies were diluted in 5% non-fat milk in TBS + 0.1% Tween-20, and nitrocellulose membranes were incubated with antibody mixtures overnight at 4 °C. HRP-conjugated secondary antibodies (Santa Cruz Biotech) were diluted 1:1,000 in 5% non-fat milk in TBS + 0.1% Tween-20 and incubated for 1 hour at room temperature. Blots were developed using Western Lightning ECL reagent (Perkin Elmer), and analyzed with Bio-Rad Gel Doc/Chemi Doc Imaging System and Quantity One software. Results of multiple assays were quantified by digitizing the data and normalizing pixel density of examined protein bands by glyceraldehydes-3-phosphate dehydrogenase-specific pixel density.

Proteomic analysis

Medium conditioned by hESCs or control differentiated hESCs, in duplicate, was labeled and hybridized to Raybiotech 507 antibody array slides according to the manufacturer's protocol. Briefly, conditioned Opti-MEM medium containing extracellular proteins was dialyzed against phosphate buffered saline, biotinylated, dialyzed again, hybridized to the array, washed, labeled with streptavidin-Cy3, washed, dried and the fluorescent features imaged on a Molecular Devices 4000b scanner. Data were analyzed using Genepix and Microsoft Excel software to determine relatively enriched signal in the hESC versus differentiated samples.

Antibodies

Antibodies for phospho-ERK1/2, ERK1/2, pSmad1,5,8 and β-Actin**,** pGSK3β Y216, and Total GSK3β, were purchased from Cell Signaling. pSmad3 was purchased from Epitomics. Desmin was from Sigma-Aldrich**.** FGF2,6,&19, Smad2/3, and Dll1 antibodies were from Santa Cruz. eMyHC antibodies was from Hybridoma Bank. BrdU, GapDH and Nicd1 antibodies were from Abcam, EdU Click-It staining kit was from Invitrogen. pSmad2 and β-Catenin were from Millipore.

RNA extraction, RT-PCR and real-time PCR

Total RNA was extracted from primary human muscle progenitor cells using Trizol reagent (Invitrogen) according to manufacturer's instructions. 1 ug of total RNA was used for

cDNA synthesis with oligo dT primers (Invitrogen). For real-time PCR amplification and quantification of genes of interest, an initial amplification using specific primers to each gene of interest (realtimeprimers.com) was done with a denaturation step at 95°C for 5 min, followed by 40 cycles of denaturation at 95°C for 1 min, primer annealing at 55°C for 30 s, and primer extension at 72°C for 30 s. Real-time PCR was performed using SYBR and an ABI PRISM 7500 Sequence Detection System (Applied Biosystems). Reactions were run in triplicate in three independent experiments. The geometric mean of housekeeping gene GAPDH or β-Actin was used as an internal control to normalize the variability in expression levels and were analyzed using the $2^{-\Delta\Delta CT}$ method described [35].

Muscle Injury and In vivo FGF2,6,&19 Injection

Isoflurane was used to anesthetize the animal during the muscle injury procedure. For bulk myofiber satellite cell activation, gastrocnemius muscles were injected with cardiotoxin 1 (Sigma) dissolved at 100 micrograms per milliliter in PBS, at 4 sites of 10 microliters each for each muscle. Muscles were harvested 3 days later. For focal injury, to assay regeneration *in vivo*, 5 microliters of 0.5 milligram per milliliter CTX was injected at two sites to the middle of the tibialis anterior, and muscle harvested 5 days later. FGFs were administered to the site of injury at the time of injury and again one day later, 5 microliters per site, of 3 nanograms per microliter FGF.

TA and Gastroc hindleg muscles were injured with cardiotoxin as described (see Muscle Injury methods) on Days 0 and 2, and injected with Opti-MEM (vehicle), or FGF 2,6,19 cocktail (100 ng/mL in Opti-MEM) at Days 0 and Day 2 for TA, and Days 2 and 4 for gastroc (See Figure 5C schematic) . Mice received intraperitonial injections of EdU (50 mg/kg) at Day 4 to label proliferating cells, and muscle was harvested at Day 5

Tissue Immunofluorescence and Histological Analysis

Muscle tissue was dissected, flash frozen in OCT compound (Tissue Tek; Sakura) and cryo-sectioned at 10 micrometers. Cryo-sectioning was performed through the entire volume of muscle (typically 50–70 sections total, done at 200 μm intervals), thereby serially reconstituting the entire tissue, ex vivo. Muscle sections were stained with aqueous hematoxylin and eosin (H&E), as per the manufacturer's instructions (Sigma-Aldrich). Regeneration and myogenic potential was quantified by examining injury sites from representative sections along the muscle (spanning the volume of injury), then by measuring the injured/regenerating area using Adobe Photoshop Elements. Myofiber regeneration was quantified by counting total newly regenerated fibers and dividing by the regeneration area. Immunostaining was performed as described [36]. Briefly, after permeabilization in PBS + 1% FBS + 0.25% Triton-X-100, tissues and cells were incubated with primary antibodies in staining buffer (PBS + 1% FBS) for 1 h at room temperature, followed by 1 h incubation fluorochrome-labeled secondary antibodies (ALEXA at 1:1000). BrdU-specific immunostaining required an extra step of 2 M HCl treatment before permeablization.

Quantification and Statistical Analysis

For automated quantification of immuno-fluorescent images, 25-100 20x images per replicate were taken on the Molecular Devices ImageXpress Micro automated epifluorescence imager, followed by automated cell quantification using the multiwavelength cell scoring module within the MetaXpress analysis software. Data was analyzed using Anova and P values equal or lower than 0.05 were considered statistically significant.

Acknowledgements
This work was supported by grants from the National Institutes of Health R01 AG02725201 and California Institute for Regenerative Medicine RN1-00532-1 to IMC, CIRM grant RT2-02022 to DVS, and NSF Pre-doctoral fellowship to HY. We thank Mary West and the CIRM/QB3 Shared Stem Cell Facility at UC Berkeley for use of the Molecular Devices ImageExpress, and Mustafa Alkhouli, Adam Morgenthaler, and George Sun for providing technical assistance with this work. Wendy Cousin provided primary human muscle progenitor cells.

Authors contributions:

HY designed, performed and analyzed the experiments for Figures 1-5 and Supplemental Figures 1-5, interpreted these data and co-wrote the manuscript; MJC designed, performed and analyzed the proteomics (Table 1), performed and designed experiments for Figures 1, 2A-B, 5, S1, S2, S4, S5, interpreted data and co-wrote the manuscript; HM performed experiments for Table 1, Figures 2, 3, and S3; MZ performed experiments for Figure 1-3, S1 and S3-S5; CS performed experiments for Figure 5C-D; DVS participated in the design and interpretation of the experiments and edited the manuscript; IMC designed, guided, and integrated the study, interpreted the data and co-wrote the manuscript.

Table 1, List of most highly enriched proteins in hESC-conditioned medium

Ranking	Protein name	Function/pathway
1	FGF Basic	Growth factor/ MapK
2	FGF-19	Growth Factor/ MapK
3	Angiogenin	Ribonuclease, activates ERK
4	BTC	Betacellulin growth factor
5	IL-13 R alpha 2	Cytokine receptor
6	Siglec-5/CD170	Sialic acid IgG like lectin, recruits phosphatases to attenuate signaling
7	IL-15	Cytokine
8	APJ	Apelin receptor, GCPR signals motility
9	IGFBP-2	Insulin like Growth Factor Binding Protein/ MapK

10	Chordin-Like 1	TGF-β pathway antagonist
11	GASP-1 / WFIKKNRP	TGF-inhibitor, protease inhibitor, binds myostatin
12	MFRP	Membrane Frizzled related protein, Wnt pathway
13	IL-10 R alpha	Cytokine receptor
14	Chem R23	Chimerin receptor 23, chemokine
15	HB-EGF	Growth factor/ MapK
16	FGF-6	Growth factor/ MapK
17	HGF	Hepatocyte Growth Factor-Scatter Factor/ MapK
18	IL-16	Cytokine
19	IL-7 R alpha	Cytokine receptor
20	TRAIL R3 / TNFRSF10C	TNF receptor family, antagonist to apoptosis
21	BMP-6	TGF-β ligand
22	IL-1 F9 / IL-1 H1	Cytokine
23	IL-1 β	Cytokine
24	Kremen-2	Kringle containing membrane protein 2, antagonist to Wnt
25	TRAIL R4 / TNFRSF10D	Antagonist to apoptosis
26	CXCR1 / IL-8 RA	Cytokine receptor
27	Ck β 8-1 / CCL23	Cytokine
28	β-Catenin	Wnt pathway
29	FGF-13 1B	Growth factor/ MapK
30	TRAIL / TNFSF10	Modulates apoptosis
31	CCL14 / HCC-1 / HCC-3	Cytokine
32	FGF-4	Growth factor/ MapK

References

1. Conboy, I.M. and T.A. Rando, *Aging, stem cells and tissue regeneration: lessons from muscle.* Cell Cycle, 2005. **4**(3): p. 407-410.
2. Conboy, I.M. and T.A. Rando, *Heterochronic parabiosis for the study of the effects of aging on stem cells and their niches.* Cell Cycle, 2012. **11**(12): p. 2260-7.
3. Conboy, I.M. and T.A. Rando, *The regulation of Notch signaling controls satellite cell activation and cell fate determination in postnatal myogenesis.* Dev.Cell, 2002. **3**(3): p. 397-409.
4. Conboy, I.M., et al., *Notch-mediated restoration of regenerative potential to aged muscle.* Science, 2003. **302**(5650): p. 1575-1577.
5. Brack, A.S., et al., *A temporal switch from notch to Wnt signaling in muscle stem cells is necessary for normal adult myogenesis.* Cell Stem Cell, 2008. **2**(1): p. 50-9.
6. Tanigaki, K. and T. Honjo, *Two opposing roles of RBP-J in Notch signaling.* Curr Top Dev Biol, 2010. **92**: p. 231-52.
7. Bjornson, C.R., et al., *Notch signaling is necessary to maintain quiescence in adult muscle stem cells.* Stem Cells, 2012. **30**(2): p. 232-42.
8. Mourikis, P., et al., *A critical requirement for notch signaling in maintenance of the quiescent skeletal muscle stem cell state.* Stem Cells, 2012. **30**(2): p. 243-52.
9. Carlson, M.E., et al., *Relative roles of TGF- β1 and Wnt in the systemic regulation and aging of satellite cell responses.* Aging Cell, 2009. **8**(6): p. 676-89.
10. Konishi, J., et al., *Notch3 cooperates with the EGFR pathway to modulate apoptosis through the induction of bim.* Oncogene, 2010. **29**(4): p. 589-96.
11. Chappell, W.H., et al., *Increased protein expression of the PTEN tumor suppressor in the presence of constitutively active Notch-1.* Cell Cycle, 2005. **4**(10): p. 1389-95.
12. Sieber, C., et al., *Recent advances in BMP receptor signaling.* Cytokine Growth Factor Rev, 2009. **20**(5-6): p. 343-55.
13. Conboy, I.M., H. Yousef, and M.J. Conboy, *Embryonic anti-aging niche.* Aging (Albany NY), 2011. **3**(5): p. 555-63.
14. Yousef, H., et al., *hESC-secreted proteins can be enriched for multiple regenerative therapies by heparin-binding.* Aging (Albany NY), 2013. **5**(5): p. 357-72.
15. van Zoelen, E.J., et al., *Identification and characterization of polypeptide growth factors secreted by murine embryonal carcinoma cells.* Dev Biol, 1989. **133**(1): p. 272-83.
16. Potthoff, M.J., S.A. Kliewer, and D.J. Mangelsdorf, *Endocrine fibroblast growth factors 15/19 and 21: from feast to famine.* Genes Dev, 2012. **26**(4): p. 312-24.
17. LaFramboise, W.A., et al., *Proteins secreted by embryonic stem cells activate cardiomyocytes through ligand binding pathways.* J Proteomics, 2010. **73**(5): p. 992-1003.
18. Ludwig, T.E., et al., *Derivation of human embryonic stem cells in defined conditions.* Nat Biotechnol., 2006. **24**(2): p. 185-187.
19. Kottakis, F., et al., *FGF-2 regulates cell proliferation, migration, and angiogenesis through an NDY1/KDM2B-miR-101-EZH2 pathway.* Mol Cell, 2011. **43**(2): p. 285-98.
20. Kuhn, M.C., et al., *Adipocyte-secreted factors increase osteoblast proliferation and the OPG/RANKL ratio to influence osteoclast formation.* Mol Cell Endocrinol, 2012. **349**(2): p. 180-8.
21. Chakkalakal, J.V., et al., *The aged niche disrupts muscle stem cell quiescence.* Nature, 2012. **490**(7420): p. 355-60.

22. Armand, A.S., et al., *FGF6 regulates muscle differentiation through a calcineurin-dependent pathway in regenerating soleus of adult mice.* J Cell Physiol, 2005. **204**(1): p. 297-308.
23. Wu, A.L., et al., *FGF19 regulates cell proliferation, glucose and bile acid metabolism via FGFR4-dependent and independent pathways.* PLoS One, 2011. **6**(3): p. e17868.
24. Wright, T.J., et al., *Mouse FGF15 is the ortholog of human and chick FGF19, but is not uniquely required for otic induction.* Dev Biol, 2004. **269**(1): p. 264-75.
25. Powers, C.J., S.W. McLeskey, and A. Wellstein, *Fibroblast growth factors, their receptors and signaling.* Endocr Relat Cancer, 2000. **7**(3): p. 165-97.
26. Wilkinson, M.G. and J.B. Millar, *Control of the eukaryotic cell cycle by MAP kinase signaling pathways.* FASEB J, 2000. **14**(14): p. 2147-57.
27. Yagi, K., et al., *c-myc is a downstream target of the Smad pathway.* J Biol Chem, 2002. **277**(1): p. 854-61.
28. Bernard, S. and M. Eilers, *Control of cell proliferation and growth by Myc proteins.* Results Probl Cell Differ, 2006. **42**: p. 329-42.
29. Nie, Z., et al., *c-Myc Is a Universal Amplifier of Expressed Genes in Lymphocytes and Embryonic Stem Cells.* Cell, 2012. **151**(1): p. 68-79.
30. Cheng, T., *Cell cycle inhibitors in normal and tumor stem cells.* Oncogene, 2004. **23**(43): p. 7256-66.
31. Matsuoka, S., et al., *p57KIP2, a structurally distinct member of the p21CIP1 Cdk inhibitor family, is a candidate tumor suppressor gene.* Genes Dev, 1995. **9**(6): p. 650-62.
32. Carlson, M.E., M. Hsu, and I.M. Conboy, *Imbalance between pSmad3 and Notch induces CDK inhibitors in old muscle stem cells.* Nature, 2008. **454**(7203): p. 528-32.
33. Bischoff, R., *Proliferation of muscle satellite cells on intact myofibers in culture.* Developmental biology, 1986. **115**(1): p. 129-139.
34. Conboy, M.J. and I.M. Conboy, *Preparation of adult muscle fiber-associated stem/precursor cells.* Methods Mol Biol, 2010. **621**: p. 149-63.
35. Livak, K.J. and T.D. Schmittgen, *Analysis of relative gene expression data using real-time quantitative PCR and the 2(-Delta Delta C(T)) Method.* Methods, 2001. **25**(4): p. 402-8.
36. Conboy, M.J., et al., *Immuno-analysis and FACS sorting of adult muscle fiber-associated stem/precursor cells.* Methods Mol Biol, 2010. **621**: p. 165-73.

Figure 1

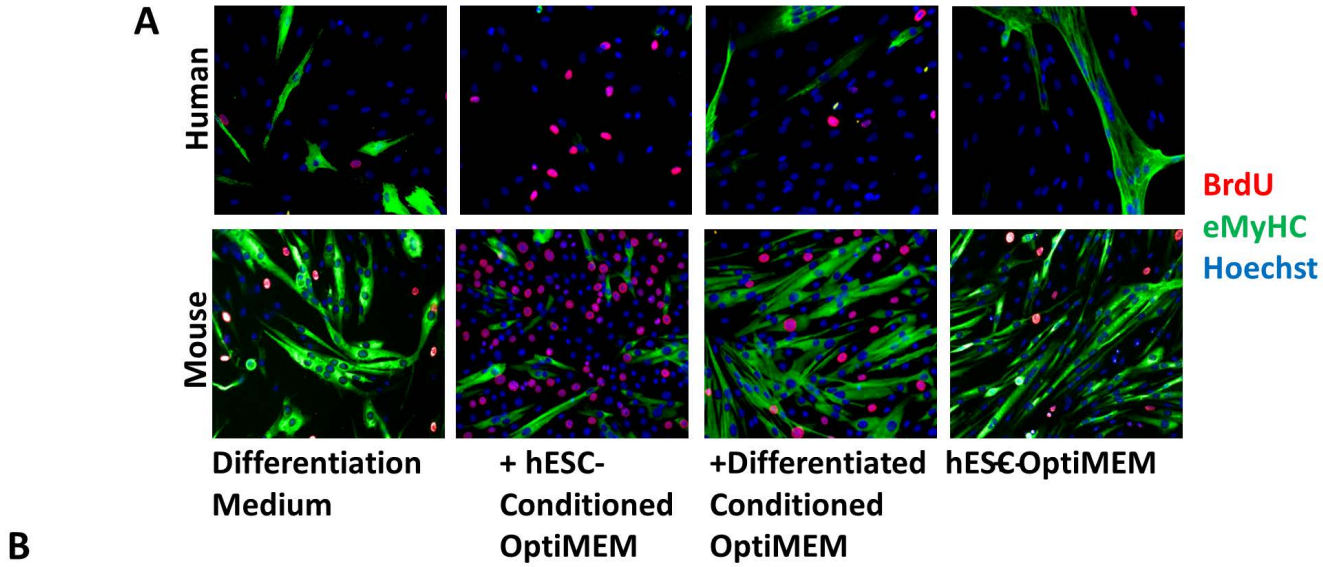
A
Human
Mouse
BrdU
eMyHC
Hoechst
Differentiation Medium
+ hESC-Conditioned OptiMEM
+Differentiated hESC-Conditioned OptiMEM
OptiMEM

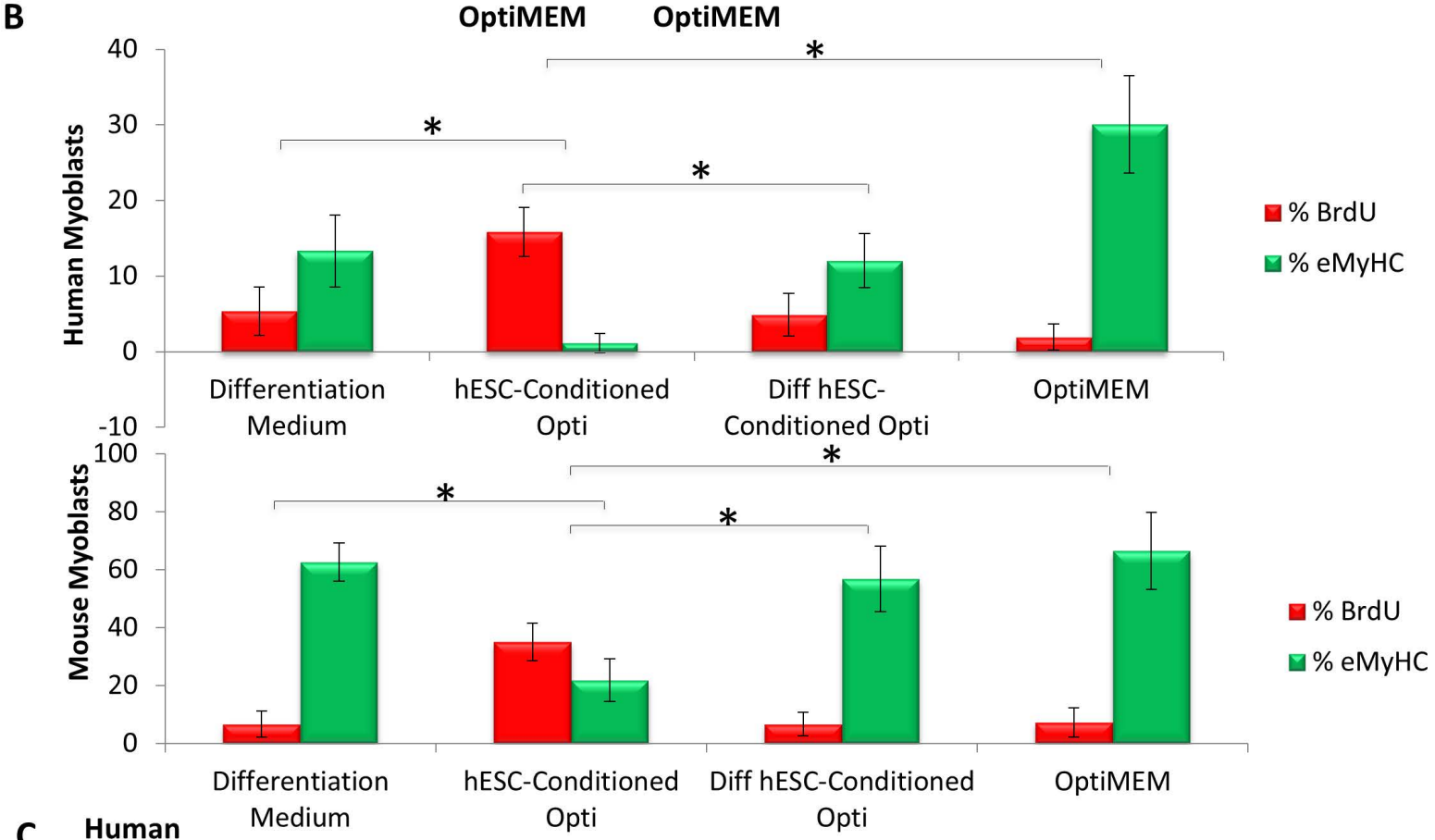
B
Human Myoblasts
40
30
20
10
0
-10
*
*
*
% BrdU
% eMyHC
Differentiation Medium
hESC-Conditioned Opti
Diff hESC-Conditioned Opti
OptiMEM
Mouse Myoblasts
100
80
60
40
20
0
*
*
*
% BrdU
% eMyHC
Differentiation Medium
hESC-Conditioned Opti
Diff hESC-Conditioned Opti
OptiMEM

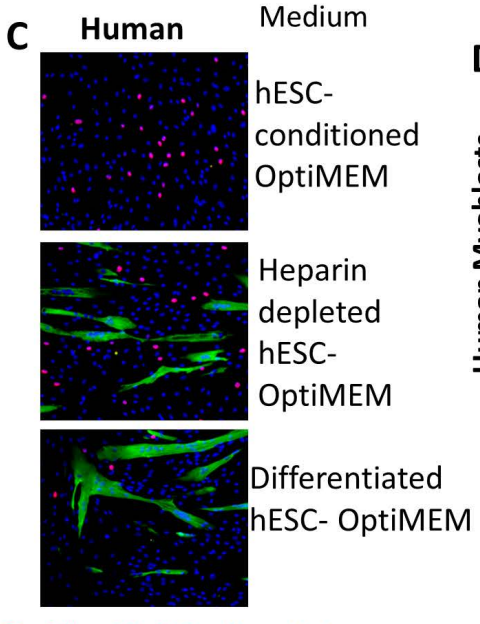
C
Human
hESC-conditioned OptiMEM
Heparin depleted hESC-OptiMEM
Differentiated hESC- OptiMEM
BrdU eMyHC Hoechst

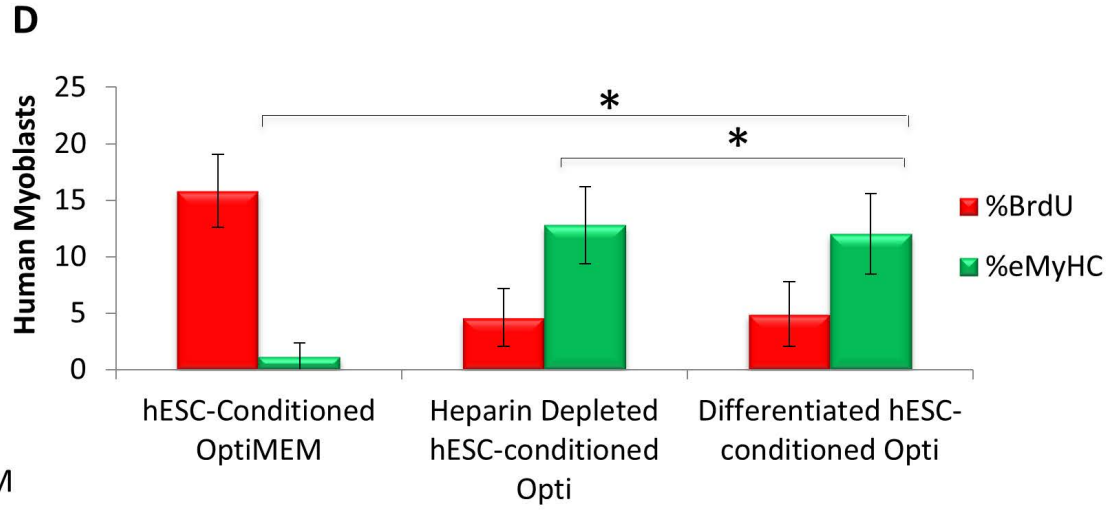
D
Human Myoblasts
25
20
15
10
5
0
*
*
%BrdU
%eMyHC
hESC-Conditioned OptiMEM
Heparin Depleted hESC-conditioned Opti
Differentiated hESC-conditioned Opti

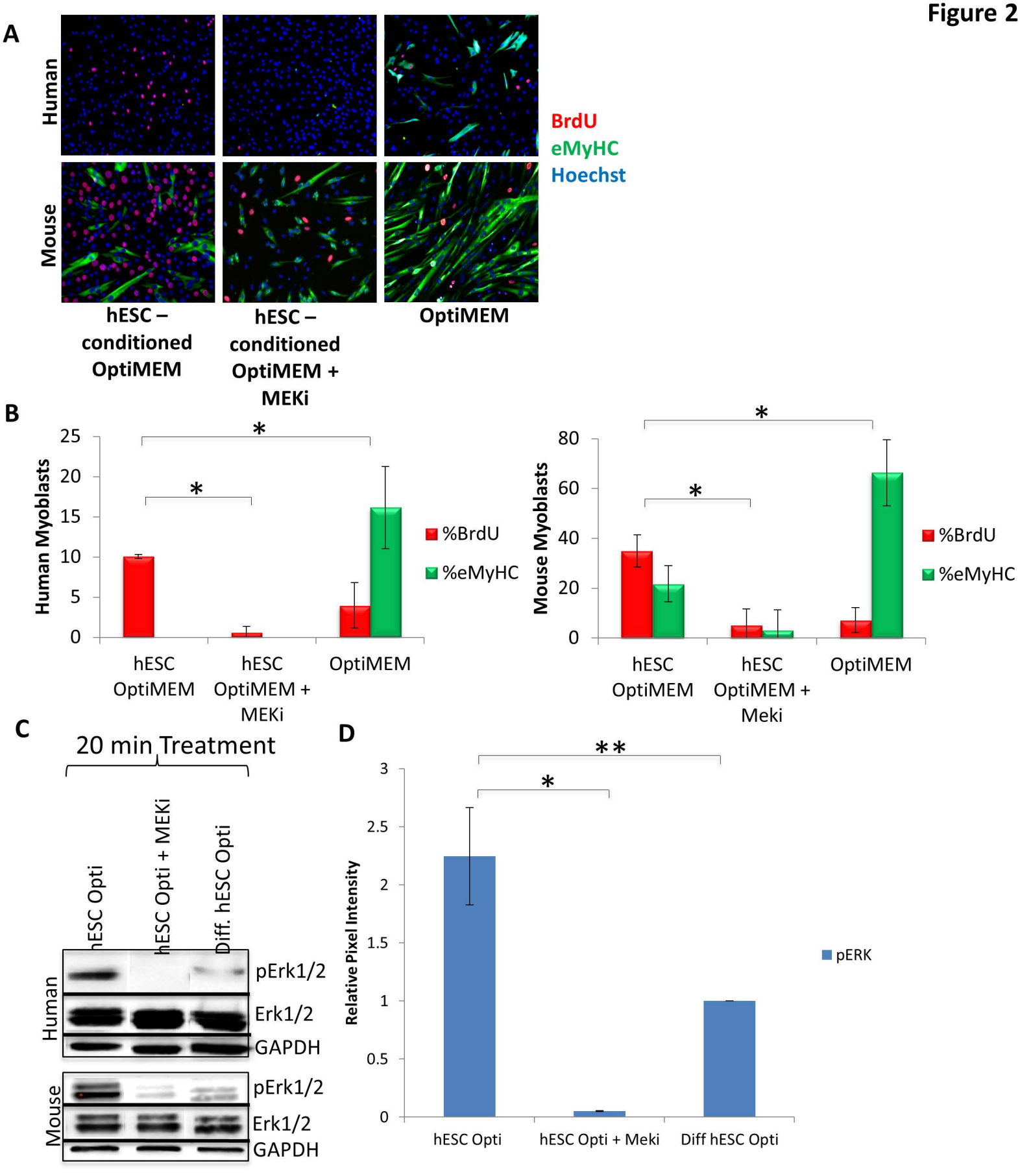
A
Human
Mouse
BrdU
eMyHC
Hoechst
hESC – conditioned OptiMEM
hESC – conditioned OptiMEM + MEKi
OptiMEM
B
Human Myoblasts
%BrdU
%eMyHC
hESC OptiMEM
hESC OptiMEM + MEKi
OptiMEM
Mouse Myoblasts
hESC OptiMEM
hESC OptiMEM + Meki
OptiMEM
C
20 min Treatment
hESC Opti
hESC Opti + MEKi
Diff. hESC Opti
Human
pErk1/2
Erk1/2
GAPDH
Mouse
pErk1/2
Erk1/2
GAPDH
D
Relative Pixel Intensity
pERK
hESC Opti
hESC Opti + Meki
Diff hESC Opti

A

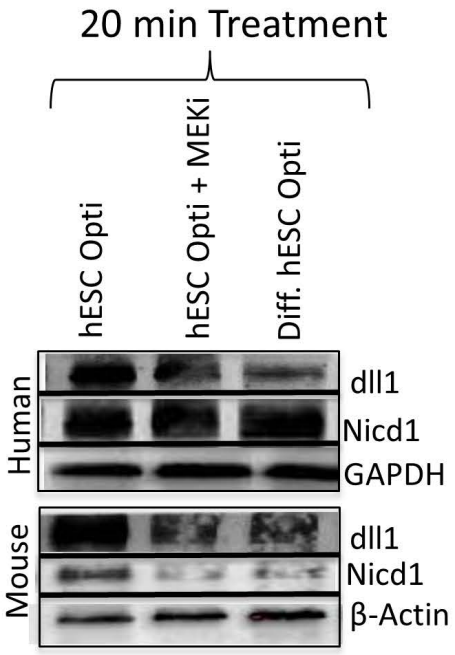
20 min Treatment
hESC Opti
hESC Opti + MEKi
Diff. hESC Opti
Human
dll1
Nicd1
GAPDH
Mouse
dll1
Nicd1
β-Actin

B

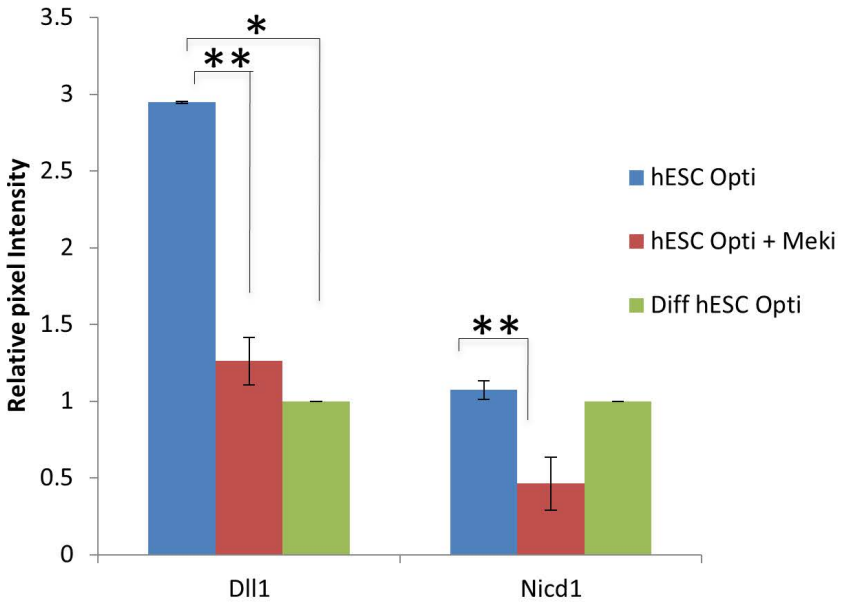
Relative pixel Intensity
3.5
3
2.5
2
1.5
1
0.5
0
*
**
**
hESC Opti
hESC Opti + Meki
Diff hESC Opti
Dll1
Nicd1

C

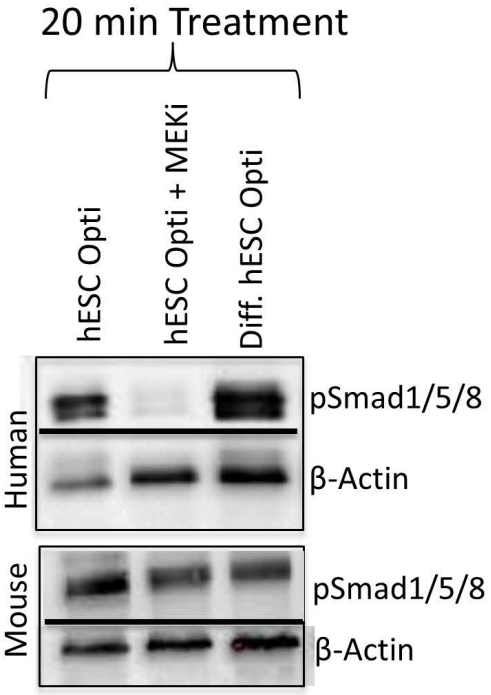
20 min Treatment
hESC Opti
hESC Opti + MEKi
Diff. hESC Opti
Human
pSmad1/5/8
β-Actin
Mouse
pSmad1/5/8
β-Actin

D

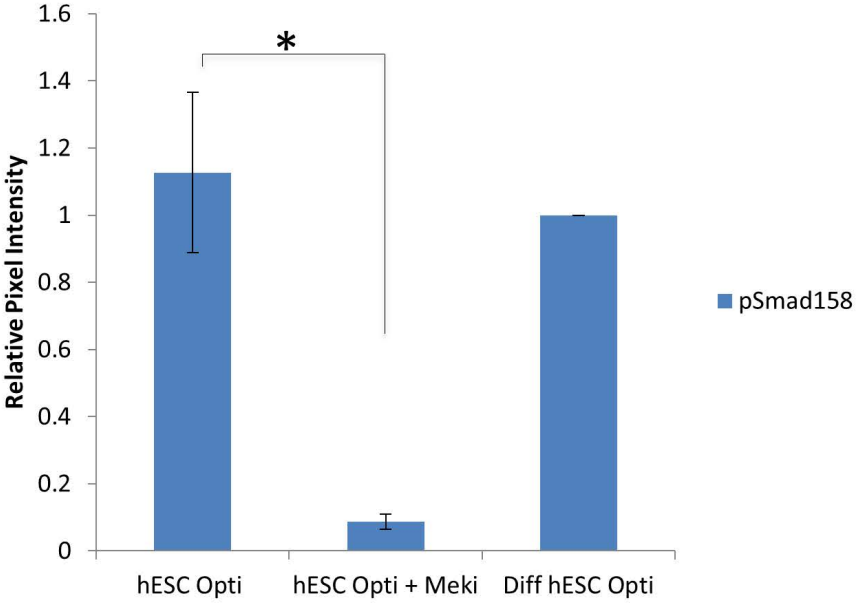
Relative Pixel Intensity
1.6
1.4
1.2
1
0.8
0.6
0.4
0.2
0
*
hESC Opti
hESC Opti + Meki
Diff hESC Opti
pSmad158

E

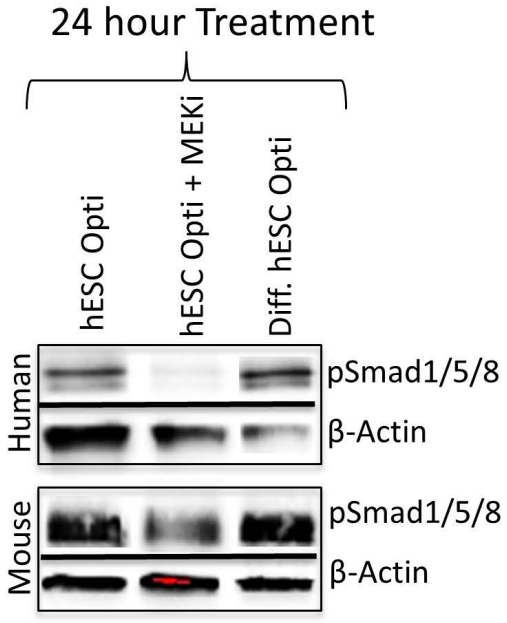
24 hour Treatment
hESC Opti
hESC Opti + MEKi
Diff. hESC Opti
Human
pSmad1/5/8
β-Actin
Mouse
pSmad1/5/8
β-Actin

Figure 4

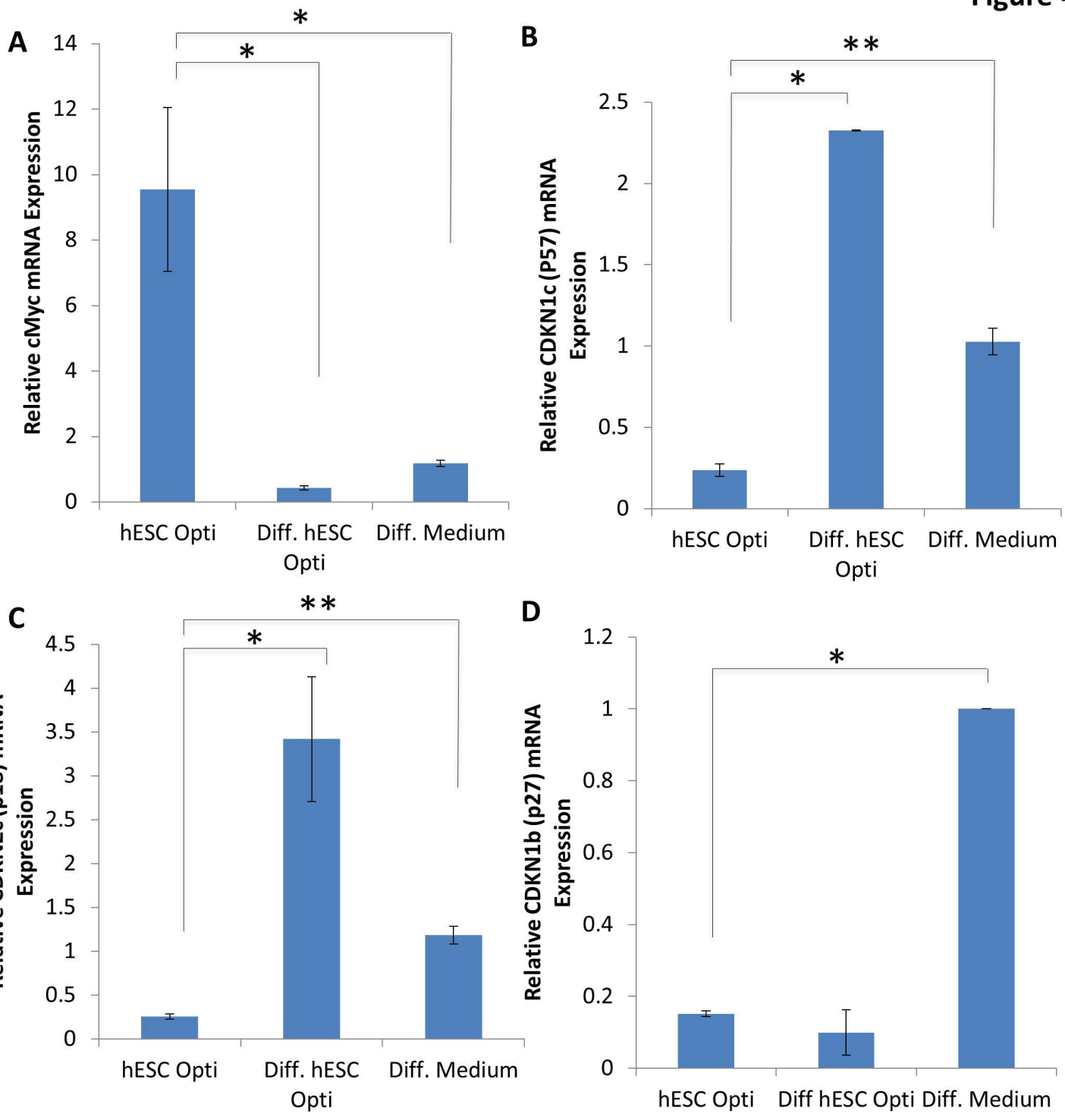
A
Relative cMyc mRNA Expression
14
12
10
8
6
4
2
0
*
*
hESC Opti
Diff. hESC Opti
Diff. Medium
B
Relative CDKN1c (P57) mRNA Expression
2.5
2
1.5
1
0.5
0
**
*
hESC Opti
Diff. hESC Opti
Diff. Medium
C
Relative CDKN2c (p18) mRNA Expression
4.5
4
3.5
3
2.5
2
1.5
1
0.5
0
**
*
hESC Opti
Diff. hESC Opti
Diff. Medium
D
Relative CDKN1b (p27) mRNA Expression
1.2
1
0.8
0.6
0.4
0.2
0
*
hESC Opti
Diff hESC Opti
Diff. Medium

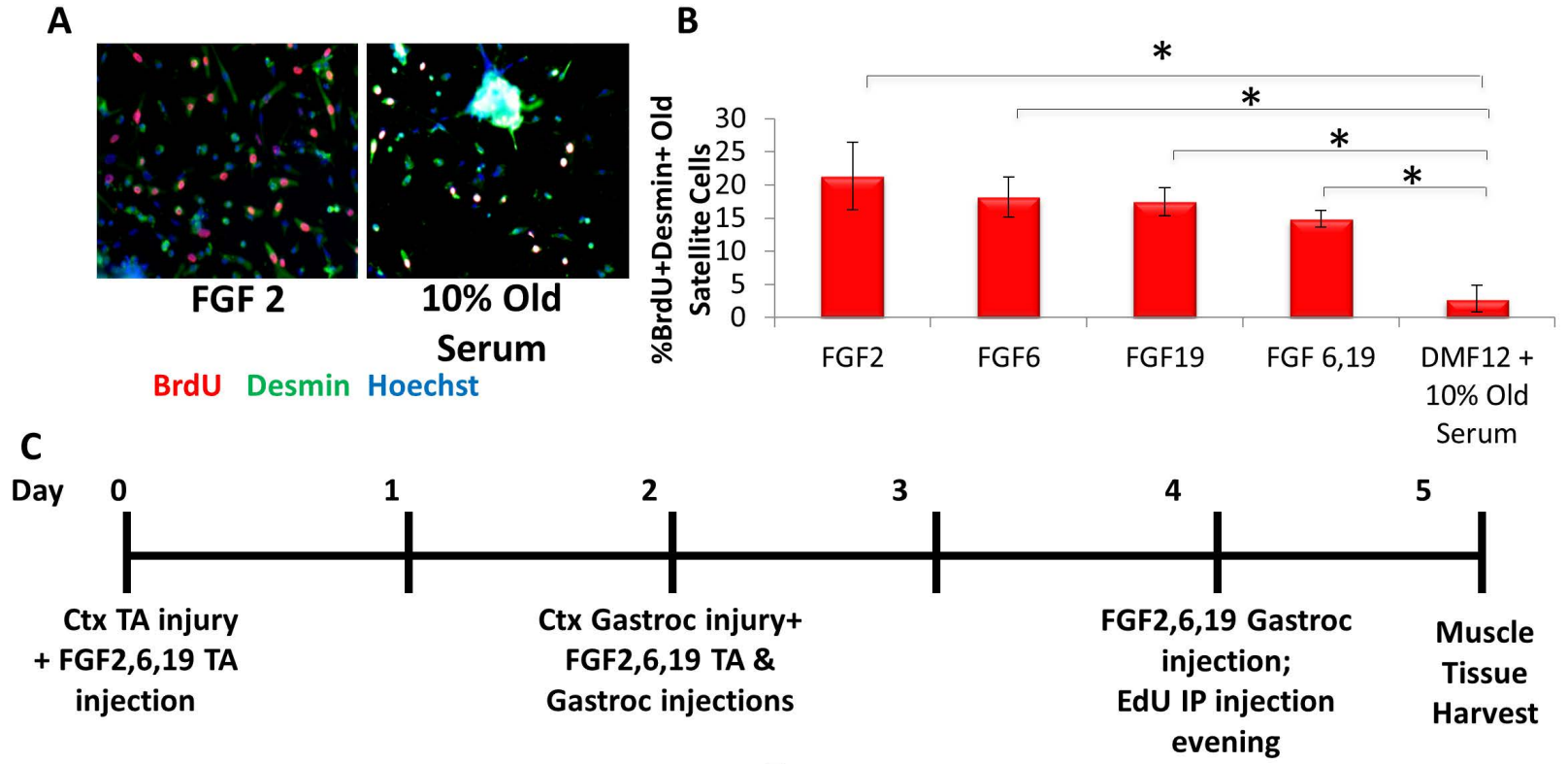
A
FGF 2
10% Old Serum
BrdU Desmin Hoechst
B
%BrdU+Desmin+ Old Satellite Cells
30
25
20
15
10
5
0
*
*
*
*
FGF2
FGF6
FGF19
FGF 6,19
DMF12 + 10% Old Serum
C
Day 0 1 2 3 4 5
Ctx TA injury + FGF2,6,19 TA injection
Ctx Gastroc injury+ FGF2,6,19 TA & Gastroc injections
FGF2,6,19 Gastroc injection; EdU IP injection evening
Muscle Tissue Harvest

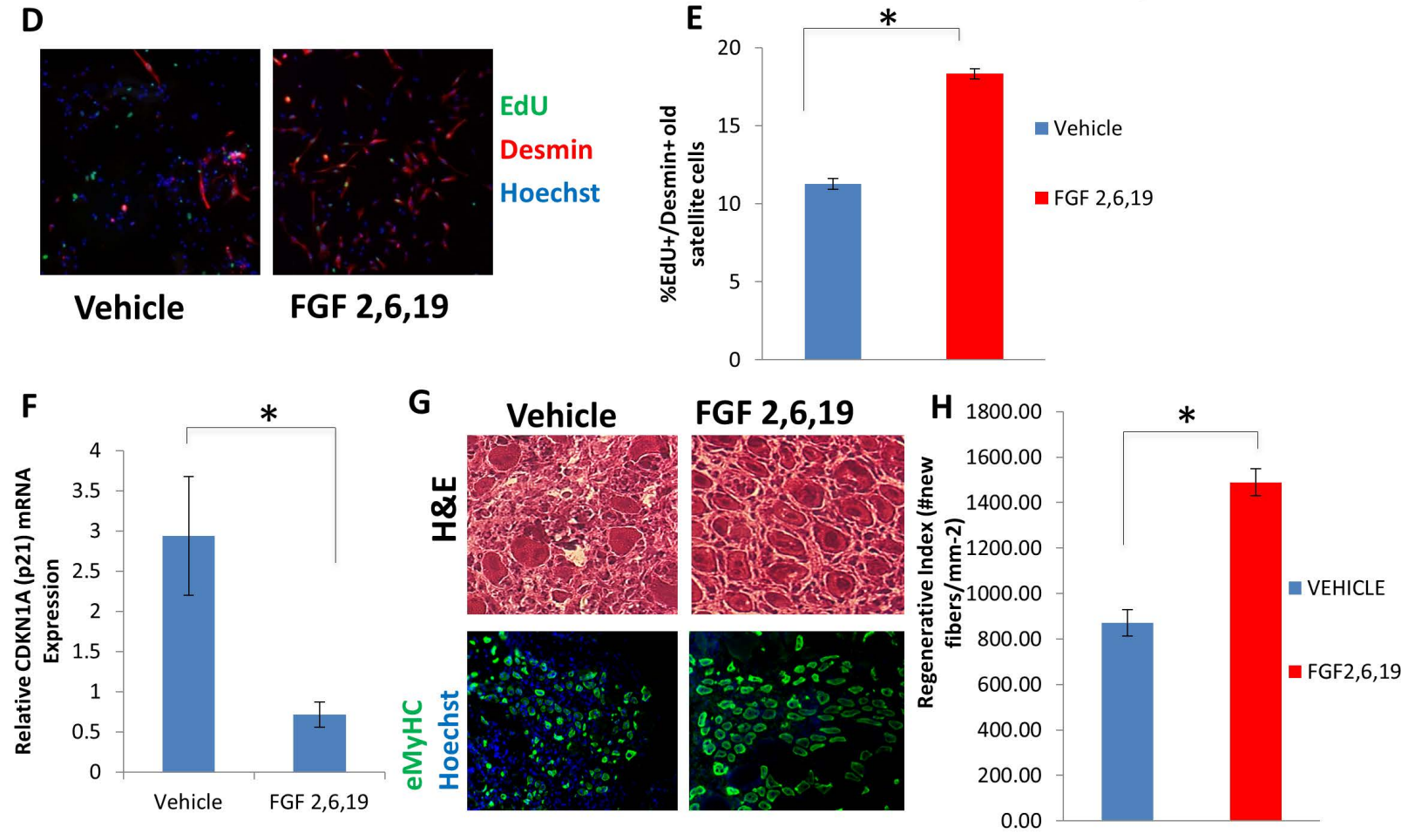
D
EdU
Desmin
Hoechst
Vehicle
FGF 2,6,19
E
%EdU+/Desmin+ old satellite cells
20
15
10
5
0
*
Vehicle
FGF 2,6,19
F
Relative CDKN1A (p21) mRNA Expression
4
3.5
3
2.5
2
1.5
1
0.5
0
*
Vehicle
FGF 2,6,19
G
Vehicle
FGF 2,6,19
H&E
eMyHC Hoechst
H
Regenerative Index (#new fibers/mm-2)
1800.00
1600.00
1400.00
1200.00
1000.00
800.00
600.00
400.00
200.00
0.00
*
VEHICLE
FGF2,6,19

Supplementary Figure 1

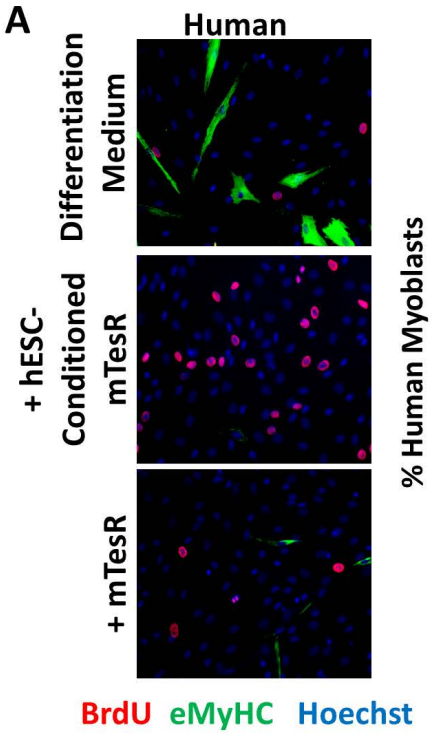

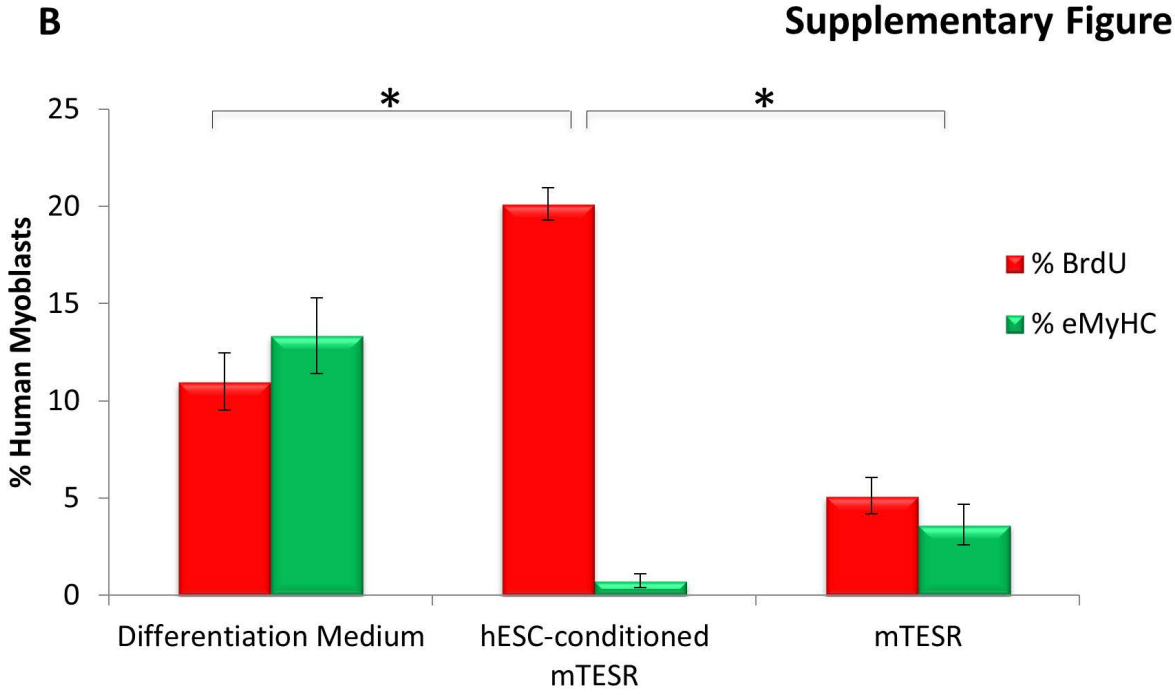

Supplementary Figure 2

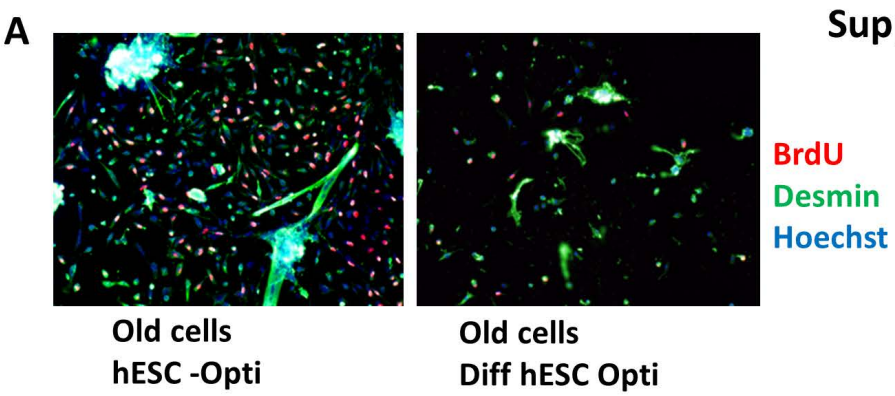

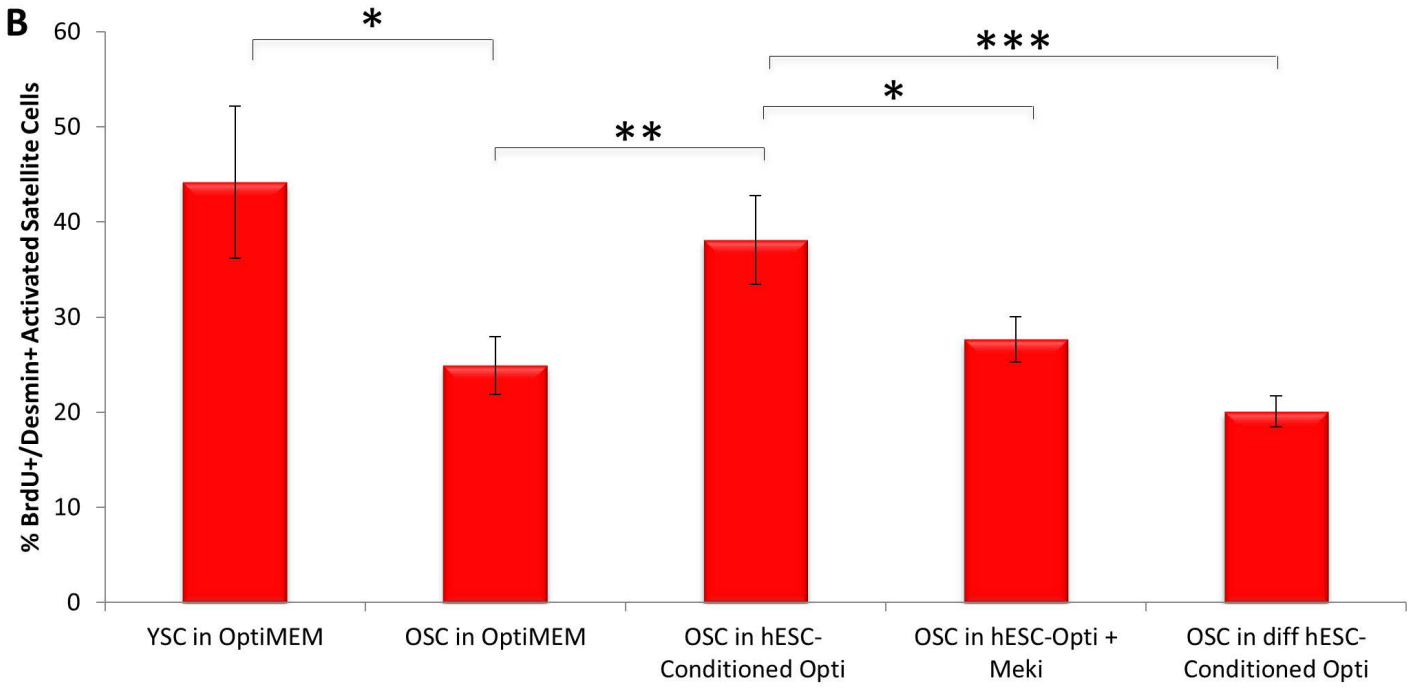

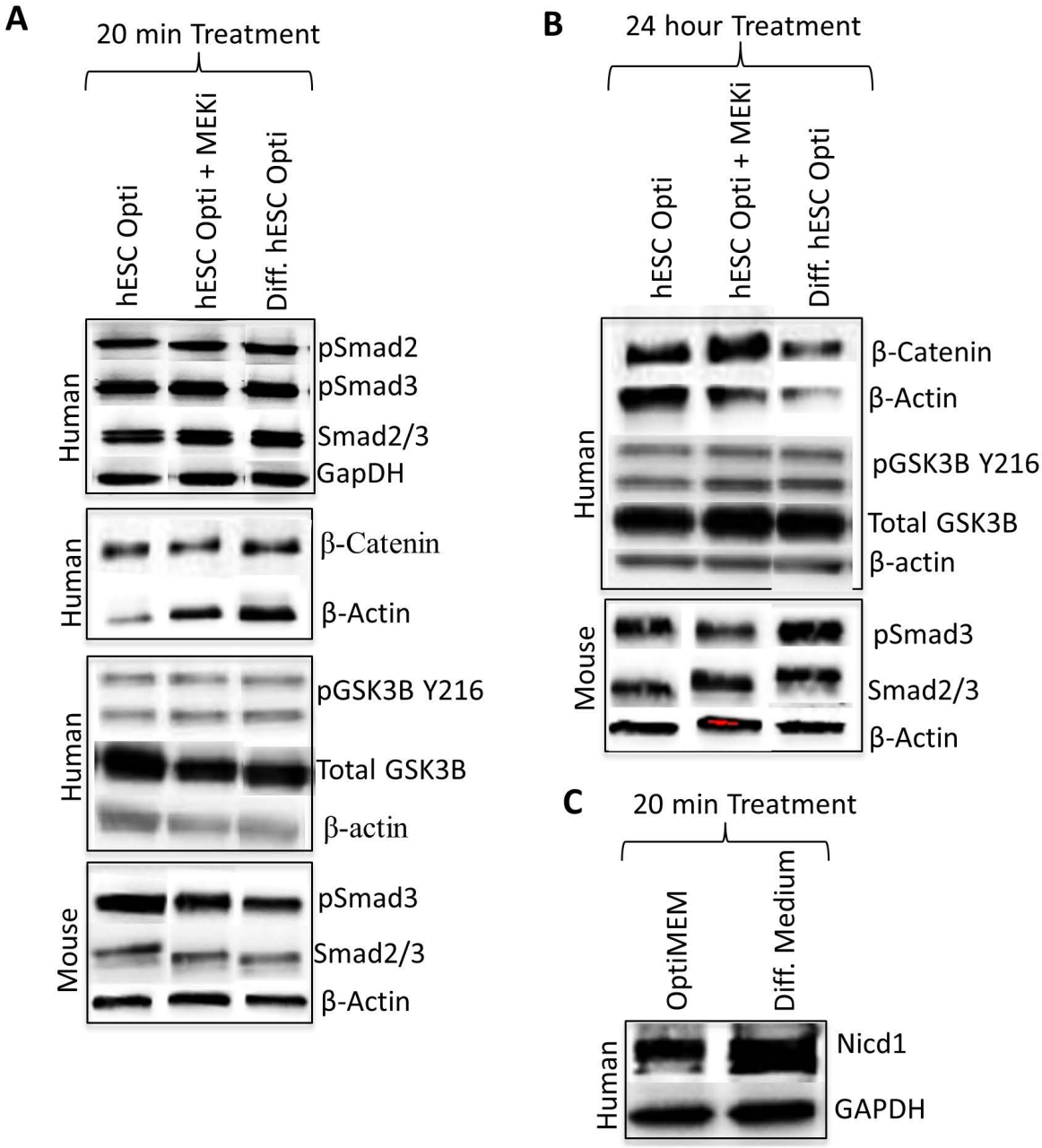
A
20 min Treatment
hESC Opti
hESC Opti + MEKi
Diff. hESC Opti
Human
pSmad2
pSmad3
Smad2/3
GapDH
Human
β-Catenin
β-Actin
Human
pGSK3B Y216
Total GSK3B
β-actin
Mouse
pSmad3
Smad2/3
β-Actin
B
24 hour Treatment
hESC Opti
hESC Opti + MEKi
Diff. hESC Opti
Human
β-Catenin
β-Actin
pGSK3B Y216
Total GSK3B
β-actin
Mouse
pSmad3
Smad2/3
β-Actin
C
20 min Treatment
OptiMEM
Diff. Medium
Human
Nicd1
GAPDH

Supplementary Figure 4

A

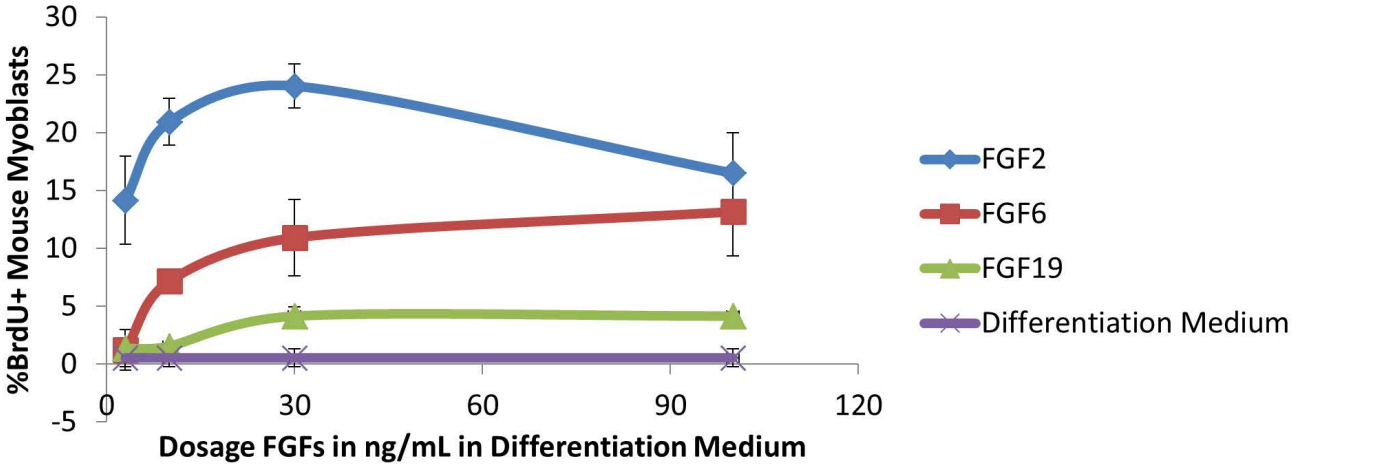

B

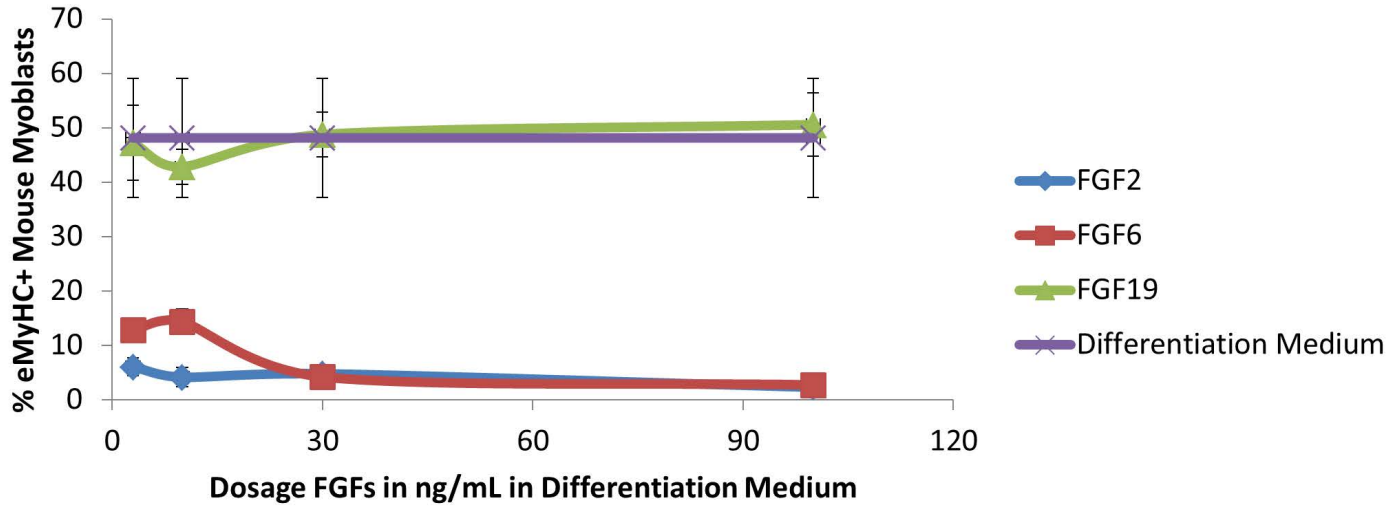

C

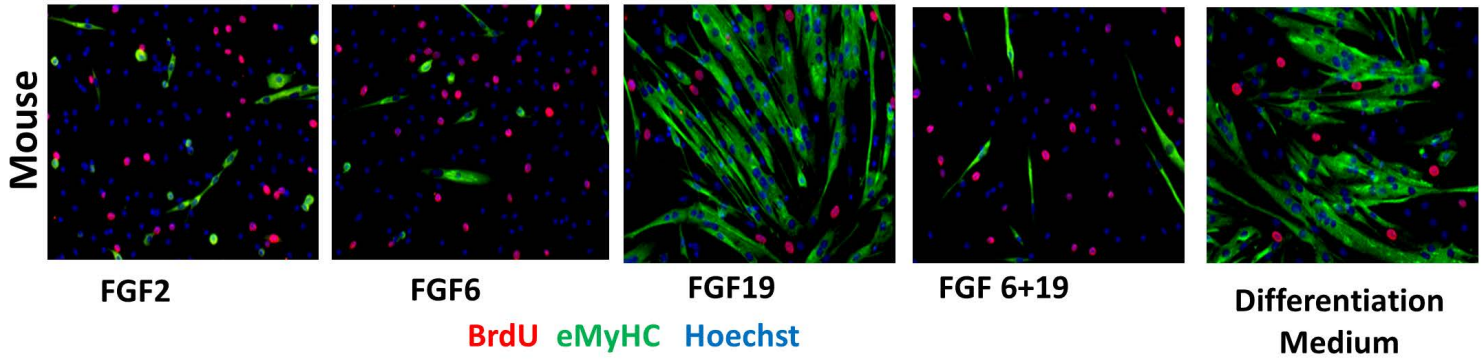

D

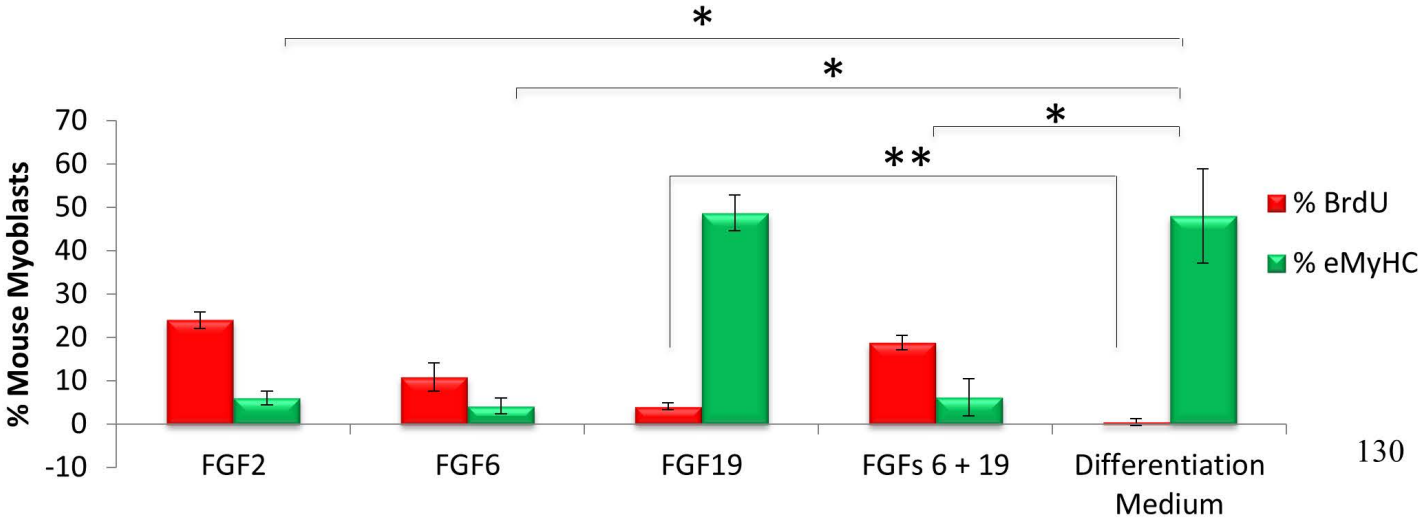

Supplementary Figure 5

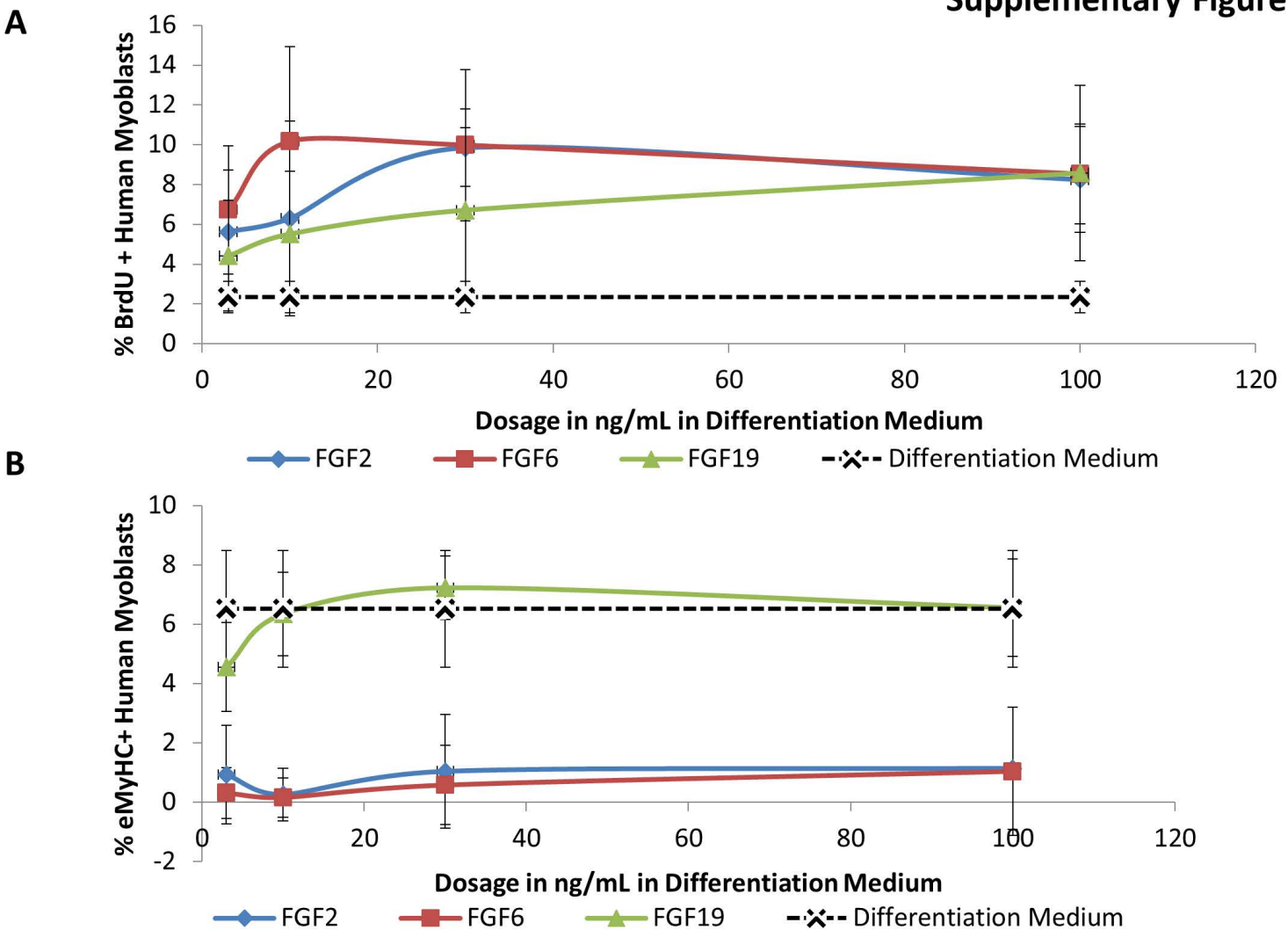

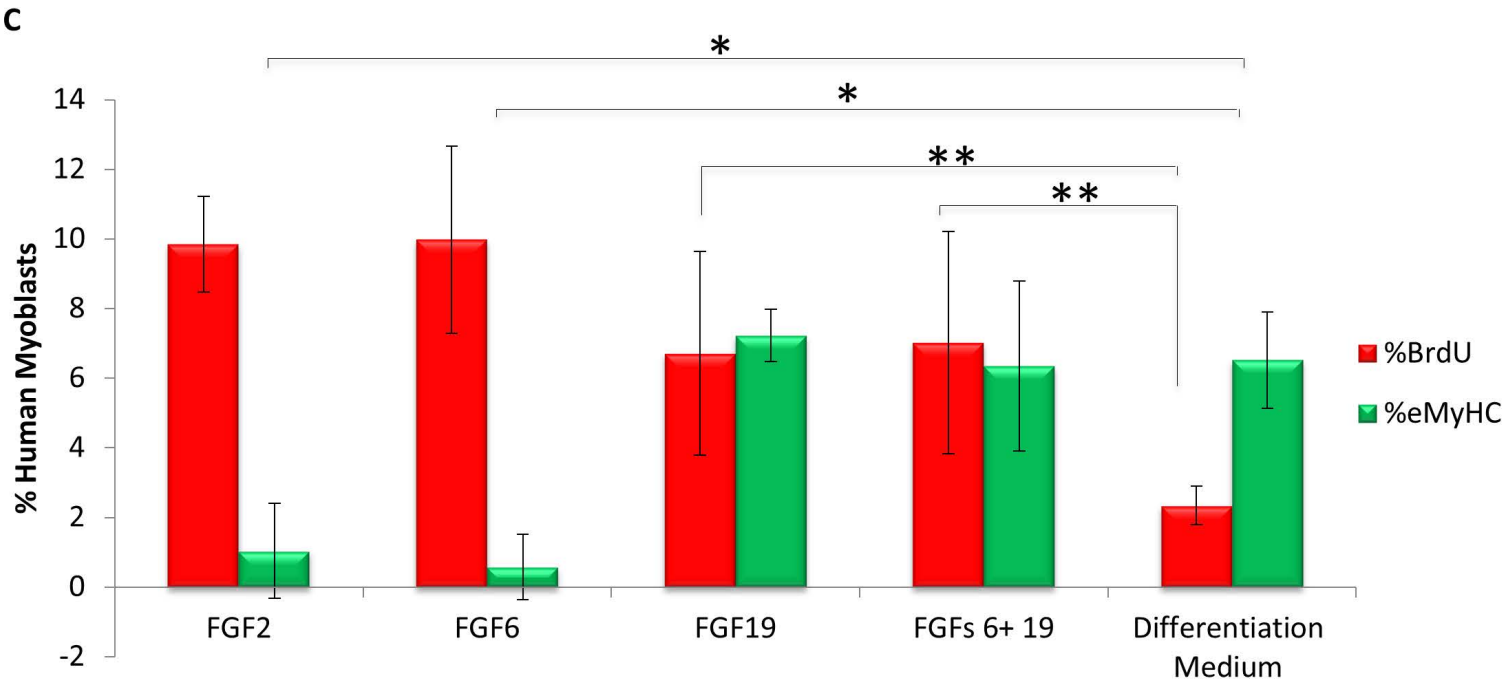

Conclusion

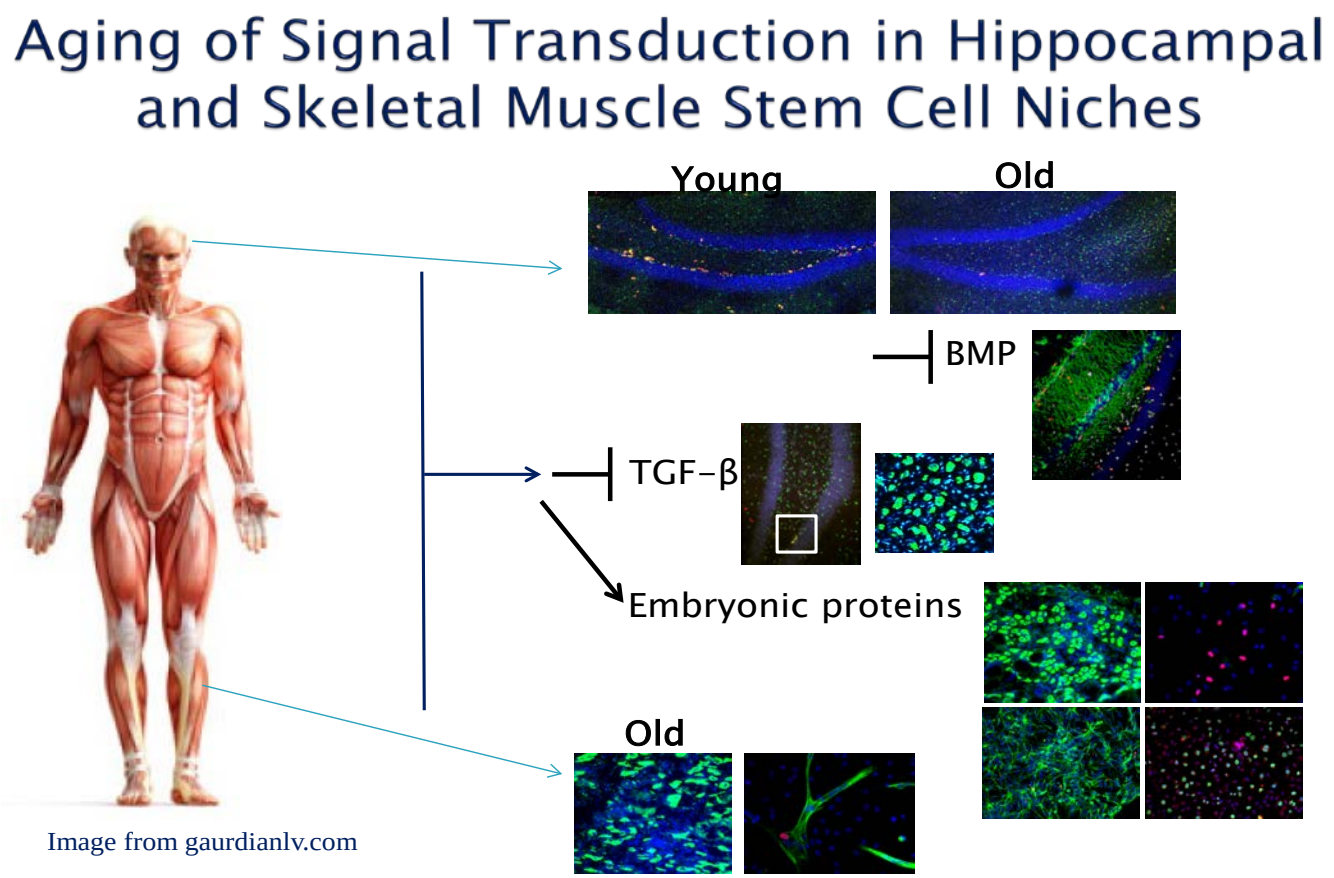

Figure 1. Aging of Signal Transduction in Brain and Muscle Tissue Stem Cell Niches.

In summary, we use young (2-4 month) and aged (18-24 month) mice, the equivalent of humans in their 20s and 80s, as a mammalian model to understand human aging. Specifically, we are interested in understanding the conserved, extrinsic signaling mechanisms that underlie the decline in adult stem cell mediated hippocampal neurogenesis and skeletal muscle regeneration with age. To that end, in this dissertation we elucidated molecular mechanisms that underlie the decline of brain and muscle tissue stem cell function with aging. We discovered that BMP signaling increases in the old hippocampal stem cell niche and inhibits neural precursor cell proliferation and subsequent neurogenesis in the aged brain. Importantly, we demonstrated partial rescue of neurogenesis by inhibiting BMP signaling directly in the aged hippocampus. In our quest to elucidate conserved signaling deregulation in aged tissue stem cell niches, we discovered that TGF-β signaling increases systemically and locally in both brain and muscle stem cell niches. Both hippocampal neurogenesis and myogenesis could be simultaneously enhanced by systemic inhibition of TGF-β signaling, suggesting therapeutic potential for rejuvenating multiple aged organs with a single therapy. Thirdly, we discovered that embryonic stem cells secrete pro-regenerative heparin-binding proteins that act through multiple biochemical pathways- specifically Notch, MAPK, and BMP signaling pathways- to rejuvenate aged skeletal muscle regeneration and provide neuroprotection. Summarily, we have demonstrated that calibration of signal transduction in both brain and muscle stem cell niches can reverse the age-induced regenerative decline.